Security-constrained expansion planning of low carbon power systems

SEBASTIÁN TOMÁS PÜSCHEL LØVENGREEN
ORCID: 0000-0002-0248-9618

Doctor of Philosophy
March 2021

Department of Electrical and Electronic Engineering
Melbourne School of Engineering

Submitted in total fulfilment for the degree of
Doctor of Philosophy

Abstract

Power systems worldwide are experiencing a radical transition from a traditional configuration based on conventional thermal prime movers with synchronous generators to systems increasingly dominated by variable renewable energy sources that are asynchronously connected to the system via power electronic interfaces. Consequently, the level of system synchronous inertia is rapidly decreasing, with potentially severe effects on frequency stability. In Australia, the recent decommission of large coal-fired power plants, recurrent brown-outs over hot summer days, in addition to a major blackout in South Australia in 2016, have thus raised significant concerns as to the capability of the current system and market arrangements to adapt to the varying technical, economic and environmental requirements. Also, Australia's weak grid faces a high risk of separation during extreme weather conditions or in the event of cascading failures. These contingencies may become particularly severe in low-inertia grids, where the subregions resulting after system split need to procure enough resources to respond to low (importing areas) and high (exporting areas) frequency conditions.

In this work, a multi-service frequency response model is developed to represent the frequency behaviour of a system (or subsystems) considering different contingencies, frequency response resources, inertia availability and demand sensitivity to frequency changes. This model is used to build frequency response constraints that guarantee the allocation of the resources necessary to contain frequency deviations after load, generation and transmission contingencies. These frequency response constraints are used to assemble a multi-area security-constrained unit commitment, capable of minimising the total cost of operation considering the technical characteristics of synchronous units, renewable energy resources availability, DC power flows, transmission constraints, and the allocation of reserves (including fast frequency response resources) and inertia to comply with statutory limits for the rate of change of frequency, frequency nadir and zenith, and quasi-steady-state frequency. This unit commitment model, cast as a mixed-integer linear program, is investigated on test systems representing the Australian power system and validated via dynamic simulations. The results show how the system's frequency resilience to extreme events can be effectively enhanced for both high- and low-frequency conditions that arise in different areas after a generation, load or interconnector contingency.

As decreasing inertia levels put pressure on the system frequency security adequacy, investing in technologies to support it becomes necessary. Using the unit commitment model as the framework to study low-inertia power system operation, this work presents an expansion model based on Dantzig-Wolfe decomposition and delayed column generation algorithm that inherently embeds the associated frequency security constraints in the expansion process. As a result, the expansion model guarantees minimum investment and operation cost decisions and frequency security adequacy. A case study application representing the actual characteristics of the Australian power system is presented, using the parameters provided by the Australian Energy Market Operator in the context of the Integrated System Plan. This work studies the optimal development paths for the system under uncertainty, considering the investment in transmission lines, battery energy storage systems, pumped-hydro storage systems, and synchronous condensers. The expansion model is validated and tested using different scenario trees that help identify the investment flexibility provided by various technologies in the presence of uncertainty.

The novelties of this work include a multi-area security-constrained unit commitment model capable of allocating frequency security resources, including fast frequency response to withstand generation and load contingencies, and transmission contingencies leading to system split. Furthermore, the model can co-optimise the largest contingency size and guarantee the feasibility of transmission of contingency reserves through the interconnectors after contingency. It also presents a state-of-the-art security-constrained expansion planning model capable of making investment decisions that consider frequency response constraints and fast frequency response. To the best of the author's knowledge, this is the first time an expansion planning model with these characteristics has been presented and applied on a real system to make investment decisions not only on transmission and storage assets but also on synchronous condensers.

Some of the novel elements presented in this work have had a substantial impact on real-world applications. The frequency response adequacy model has been used to analyse the frequency security of future energy scenarios in Australia in the context of the *Independent Review into the Future Security of the National Electricity Market* conducted by Australia's Chief Scientist. A graphical tool derived from the frequency adequacy model has been used by the Australian Energy Market Operator to analyse the frequency behaviour of the South West Interconnected System in Western Australia. Also, recently, UK's National Grid Electricity System Operator has started applying a new framework to evaluate investment decisions in new transmission assets based on the least worst weighted regret approach presented in this work.

Declaration

This is to certify that

1. the thesis comprises only of my original work towards the degree of Doctor of Philosophy except where indicated in the preface,
2. due acknowledgement has been made in the text to all other material used, and
3. the thesis is less than 100,000 words in length, exclusive of tables, maps, bibliographies, and appendices.

Sebastián Tomás Püschel Løvengreen, March 2021

This page intentionally left blank.

Preface

This thesis has been executed under the supervision of Prof. Mancarella and portions of the work were carried out in close collaboration with Dr Stephen Clegg, Dr Lingxi Zhang, Carmen Bas Domenech, Mehdi Ghazavi Dozein and Prof. Steven Low. These collaborations enabled the timely production of research. The list below identifies the publications (both published and unpublished work) that correspond to each chapter, as well as the contributions of each collaborator.

Chapter 2

1. P. Mancarella, **S. Püschel-Løvengreen**, L. Zhang, H. Wang, M. Brear, T. Jones, M. Jeppesen, R. Batterham, R. Evans, and I. Mareels, "Power system security assessment of the future National Electricity Market", Technical Report, June 2017.

2. **S. Püschel-Løvengreen** and P. Mancarella, "Mapping the Frequency Response Adequacy of the Australian National Electricity Market," in Proceedings of the Australasian Universities Power Engineering Conference, AUPEC 2017.

Chapter 3

3. **S. Püschel-Løvengreen** and P. Mancarella, "Frequency response constrained economic dispatch with consideration of generation contingency size," in 20th Power Systems Computation Conference, PSCC 2018.

4. **S. Püschel-Løvengreen**, M. Ghazavi Dozein, S. Low, and P. Mancarella, "Separation event-constrained optimal power flow to enhance resilience in low-inertia power systems," Electric Power Systems Research, vol. 189, pp. 1–8, 2020.

M. Ghazavi Dozein was involved in the development of the dynamic model and the simulation of the dynamic behaviour of the test system given the operation points defined by the security-constrained optimal power flow presented in the the paper. Dr. S. Low took part in the development of the theoretical analysis of the multi-area frequency response constraints.

5. **S. Püschel-Løvengreen**, and P. Mancarella, "Multi-area frequency response security-constrained unit commitment in low-inertia power systems with risk of separation

events," (in preparation).

Chapter 4

6. P. Mancarella, **S. Püschel-Løvengreen**, C. Bas-Domenech, and L. Zhang, "Study of advanced modelling for network planning under uncertainty || Part 1: Review of frameworks and industrial practices for decision-making in transmission network planning," prepared for National Grid ESO, UK, Technical Report, 2019.

Considering the portions of the work included in this thesis, C. Bas-Domenech was involved in the description of decision making under uncertainty.

7. P. Mancarella, L. Zhang, and **S. Püschel-Løvengreen**, "Study of advanced modelling for network planning under uncertainty || Part 2: Review of power transfer capability assessment and investment flexibility in transmission network planning ," prepared for National Grid ESO, UK, Technical Report, 2020.

Chapter 5

8. **S. Püschel-Løvengreen**, and P. Mancarella, "Security-constrained expansion planning of low-inertia power systems," (in preparation).

"While it's true that someone can impede your actions, they can't impede our intentions and our attitudes, which have the power of being conditional and adaptable. For the mind adapts and converts any obstacle to its action into a means of achieving it. That which is an impediment to action is turned to advanced action. The obstacle on the path becomes the way."

—Marcus Aurelius, Meditations, 5.20

This page intentionally left blank.

Dedication

To my wife, Nicole,
who joined me in this quest and, with love and patience, helped me bear the burden of this project all along the way.

To my mother, Charlotte,
whose selfless support and care once again proved immune to distance.

This page intentionally left blank.

Acknowledgements

I WANT to express my sincere gratitude to Prof Pierluigi Mancarella for taking me on as a student. Without his support, ideas and continuous supervision, the completion of this thesis would not have been possible.

Special thanks also to the group of people who collaborated directly to develop parts of this work, thus allowing the timely delivery of papers and reports. I want to highlight the contributions of Dr Alysson Machado, Dr Steven Clegg, Dr Lingxi Zhang, Dr Han Wang, Carmen Bas Domenech, Mehdi Ghazavi Dozein and Prof Steven Low. Also, a special acknowledgement to the visiting students from the University of Chile, Héctor Otárola and Bastian Moya, whose work supported the development of the chapter on power system planning.

Friendship, as always, played a fundamental role in keeping things in balance. I want to thank my friends within the Power and Energy Systems group at the University of Melbourne for their support and the good times we spent together: Kyriacos, Nando, Dillon, Andreas, Han, Kevin and Carmen. A special mention to the members of the WSC appreciation society for the great food, drinks and conversation. To my family and friends spread around the world who fought the distance, kept in touch, and showed me their love and support throughout this process. Also, to the Chilean diaspora in Melbourne, especially to Paula and Gustavo, for easing off the transition when we moved to this beautiful city, allowing us to recreate a little bit of Chile in Australia. And also to Nata and Woody for always being good friends and so much fun.

Finally and most importantly, I would like to express my deepest and uttermost appreciation and admiration to my wife, Nicole. She had to delay her career, rebuild her life and face many challenges to enable this venture. She provided me with all the support that was so much needed during the completion of this thesis. She always reminded me of the important things in life and helped me reconnect with myself when things were tough. I will never be able to repay her for all that she did for me in Australia.

This work was partially funded by the National Agency for Research and Development (ANID) through its scholarship program Doctorado Becas Chile 2016 - 72170650.

This page intentionally left blank.

Contents

This page intentionally left blank.

List of Tables

List of Figures

This page intentionally left blank.

Glossary of terms, abbreviations and acronyms

AEMO Australian Energy Market Operator.

BESS battery energy storage systems.

BOTN Battery of the Nation.

CBA cost-benefit analysis.

CCGT combined cycle gas turbine.

DER distributed energy resources.

DW Dantzig-Wolfe.

ESS energy storage systems.

FCAS frequency control ancillary services.

FES Future Energy Scenarios.

FFR fast frequency response.

FR frequency response.

FRSM frequency response security maps.

GHG greenhouse gas.

HVAC high-voltage alternating current.

HVDC high-voltage direct current.

ISP Integrated System Plan.

LB lower bound.

LWR least worst regret.

LWWR least worst weighted regret.

MILP mixed-integer linear problem.

MSG minimum stable generation.

NEM National Electricity Market.

NGESO National Grid Electricity System Operator.

NOA Network Options Assessment.

NPV net present value.

NSW New South Wales.

OCGT open cycle gas turbine.

OPF optimal power flow.

PFR primary frequency response.

POE probability of exceedance.

PSS pumped-hydro storage systems.

PV photovoltaic.

QLD Queensland.

QNI Queensland-New South Wales interconnector.

QSSF quasi-steady-state frequency.

RMP restricted master problem.

ROCOF rate of change of frequency.

SA South Australia.

SCOPF security-constrained optimal power flow.

SFR secondary frequency response.

SNSP system non-synchronous penetration.

SO system operator.

SP pricing subproblem.

TAS Tasmania.

TEP transmission expansion planning.

TO transmission owner.

UC unit commitment.

UFLS under frequency load shedding.

UK United Kingdom.

VIC Victoria.

VNI Victoria-New South Wales Interconnector.

VPP virtual power plant.

VRES variable renewable energy sources.

This page intentionally left blank.

Nomenclature

Indices and sets

Ω_a^{SY}	Index, set of synchronous units in area a
$\Omega_b^{LS}, \Omega_b^{LR}$	Set of lines whose sending LS / receiving LR end is connected to bus b
$\psi, \Omega_{s,t}^{nd/zh}$	Index, set of frequency nadir/zenith hyperplanes for subsystem s, time t
Ψ_m	Set of nodes preceding and including node m
a, Ω^A, Ω_s^A	Index, set of areas, set of areas in inertial subsystem s
$Ar/s\,(l)$	Area connected to the receiving/sending end of line l
$b,\ \Omega^{Bus}$	Index, set of buses
$Br/s\,(l)$	Bus at the receiving/sending end of line l
G_C	Set of candidate generation units
$i, \Omega^{RE}, \Omega_b^{RE}$	Index, set of renewable energy sources, on bus b
$j, \Omega^{BS}, \Omega_b^{BS}$	Index, set of battery energy storage systems, on bus b
$k, \Omega^{TH}, \Omega_b^{TH}$	Index, set of thermal/synchronous generators, on bus b
$K_{m,w}$	Set of available columns associated to node m, week w
l, Ω^{LN}	Index, set of lines
L_C	Set of candidate lines
M	Set of nodes in scenario tree
m, μ	Index of nodes in scenario tree
p	Index of column
r	Index of frequency response service (ffr, pfr, sfr)
$s,\ \Omega^S$	Index, set of subsystems
S_C	Set of candidate storage units
T	Time range
ty	Index of type of response up, down = dw
w	Index of representative week
W_m	Set of representative weeks in node m

Parameters

Δf_{min}^n	Frequency nadir limit [Hz]
$\Delta QF^{lw/hg}$	Target quasi steady state frequency low, high events [Hz]

Δ_t	Step duration time t [h]
Δfdb	Frequency response dead-band [Hz]
ΔP_{loss}	Largest generation indeed loss [MW]
$\hat{H}_k$	Inertia constant synchronous unit k [MWs/MVA]
$\omega_{m,w}$	Weight of representative week w in node m
ρ_m	Probability of node m
φ_l	Factor for short term emergency rating line l
$\widehat{i}^{S,p}_{m,w,j}$	Decision on candidate storage unit j in node m, week w, column p
$\widehat{i}^{G}_{m,w,k}$	Decision on candidate generator k in node m, week w, column p
$\widehat{i}^{L,p}_{m,w,l}$	Decision on candidate line l in node m, week w, column p
$\widehat{OP}^{p}_{m,w}$	Operational cost week w, node m associated to column p [$]
$A_{m,w}, \tilde{A}_{m,w}$	Matrix of coefficients associated to continuous variables
adt_i	Activation delay of response source i [s]
$b_{m,w}, \tilde{b}_{m,w}$	Right hand side vector
C_k	Cost function for energy production unit k [$]
$c_{m,w}$	Vector of costs associated to continuous variables [$]
$CH^{\max}_j$	Maximum charge power storage system j [MW]
CLL_b	Cost function for lost load at bus b [$]
CSU_k, CSD_k	Cost functions for start-up and shut-down unit k [$]
D	Composite load damping factor for the system [%/Hz]
D_s	Composite load damping factor subsystem s [pu/Hz]
$DCH^{\max}_j$	Maximum charge power storage system j [MW]
dt_i	Response delivery time for source i [s]
$E^{\min}_j, E^{\max}_j$	Min/Max energy capacity of storage system j [MWh]
E_{sys}	Total kinetic energy stored in synchronous units in the system [MWs]
$F^{fwd}_{l,t}, F^{rev}_{l,t}$	Max. forward and reverse flows of line l, time t [MW]
F_o	Nominal frequency [Hz]
f^{0+}_o	System frequency at the time of the contingency
$FFR^{\max}_j$	Maximum capacity to provide fast FR storage j [MW]
fr_i	Response capacity source i [MW]
frt_i	Full response time source i [s]
$G_{m,w}, \tilde{G}_{m,w}$	Matrix of coefficients associated to integer variables
G_{sys}	Aggregated system PFR provision rate [MW/s]
H_a	Total kinetic energy of area a [MWs]
H^{ch}_j, H^{dch}_j	Charging and discharging efficiency storage j [MW]
H_k	Kinetic energy of unit k [MWs]
$h_{m,w}$	Vector of costs associated to integer variables [$]
I_m	Matrix of coefficients associated to investment variables
IC_m	Investment costs for candidate technologies in node m [$]
$IC^{S}_{m,j}$	Investment costs for candidate storage j in node m [$]
$IC^{G}_{m,k}$	Investment costs for candidate generator k in node m [$]
$IC^{L}_{m,l}$	Investment costs for candidate line l in node m [$]

$LL_{a,t}$	Largest load contingency area a, time t [MW]
N	Number of sources providing response in the system
N_k	Number of units in cluster k
$P(m)$	Preceding node to node m
P^D	Total system demand
$P^L_{b,t}, P^L_{a,t}, P^L_{s,t}$	Load at bus b/area a/subsystem s, time t [MW]
$P^{RN}_{i,t}$	Available renewable resource unit i, time t [MW]
$P^{\min}_k, P^{\max}_k$	Minimum, maximum output unit k [MW]
PF_k	Power factor unit k
PFR	Aggregated system PFR [MW]
$PFR^{\max}_k$	Max. capacity to provide primary FR unit k [MW]
$ROCOF^{lw/hg}$	Rate of change of frequency limit low, high events [Hz/s]
RS_k	Frequency response slope of unit in cluster k
RT	Financial discount rate
T_{pfr}, T_{sfr}	Time window for primary/secondary frequency response provision [s]
X_l	Reactance of line l [pu]
Y_m	Calendar year associated to node m
Y_R	Reference year for financial discounts
Variables and functions	
Δf^n	Function describing frequency nadir
$\Delta f(t)$	Function describing frequency evolution with respect of nominal frequency
$\lambda^p_{m,w}$	Variable to select column p associated to node m, representative week w
$\pi^S_{m,w,j}$	Dual variable investment constraint storage unit j in node m, week w
$\pi^G_{m,w,k}$	Dual variable investment constraint generator k in node m, week w
$\pi^L_{m,w,l}$	Dual variable investment constraint line l in node m, week w
$\sigma_{m,w}$	Dual variable convexity constraint for node m, week w
$\theta_{b,t}$	Voltage angle at bus b, time t [pu]
$c_{i,t}$	Curtailment renewable energy source i, time t [MW]
$ch_{j,t}, dch_{j,t}$	Charging/discharging storage j, time t [MW]
$cl\_on_{k,t}$	On-off state of cluster k
$d^L_{m,l}$	Building decision for line l in node m
$e_{j,t}$	Energy stored in storage j, at the end of time t [MWh]
$ffr^{ty}_{j,t}, ffr^{ty}_{a,t}$	Fast FR service type ty, unit j/area a, time t [MW]
$fl\_r^{ty}_{a,l,t}$	Flow FR service r of type ty through line l at time t when the contingency occurs in area a [MW]
$fl_{l,t}$	Power flow line l, time t [MW]
$fp_{l,t}, fn_{l,t}$	Positive/negative transmission slack line l, time t [MW]
$G(t)$	Aggregated frequency response function
$g_i(t)$	Provision of response by source i
$g_k(t)$	Function describing the provision of response by unit k
$h_{a,t}, h_{s,t}$	Aggregated inertia area a/subsystem s, time t [MWs/Hz]

$i^S_{m,w,j}$	Pricing subproblem investment decision node m, week w for storage j
$i^G_{m,w,k}$	Pricing subproblem investment decision node m, week w for generator k
$i^L_{m,w,l}$	Pricing subproblem investment decision node m, week w for line l
$ll_{a,t}, ll_{s,t}$	Load contingency size in area a/subsystem s, time t [MW]
$n_{k,t}$	Commitment variable unit/cluster k, time t [MW]
$OP_{m,w}$	Total cost of operation of representative week w in node m [$]
$p^R_{i,t}$	Output renewable energy source i, time t [MW]
$p_{k,t}$	Output unit/cluster k, time t [MW]
$pfr^{ty}_{k,t}, pfr^{ty}_{a,t}$	Primary FR service type ty, unit k/area a, time t [MW]
$pl_{a,t}, pl_{s,t}$	Generation contingency size in area a/subsystem s, time t [MW]
$s^L_{b,t}$	Load shedding bus b, time t [MW]
$sfr^{ty}_{k,t}, sfr^{ty}_{a,t}$	Secondary FR service type ty, unit j/area a, time t [MW]
$shdw_{k,t}$	Shut down unit/cluster k, time t
$stup_{k,t}$	Start-up unit/cluster k, time t
$t\_r^{ty}_{a,t}$	Total FR service r of type ty at time t in area a [MW]
$u_{j,t}$	State of operation of battery j
$x_{m,w}$	Vector of continuous variables
$y^S_{m,j}$	Master problem investment decision node m for candidate storage unit j
$y^G_{m,k}$	Master problem investment decision node m for candidate generator k
$y^L_{m,l}$	Master problem investment decision node m for candidate line l
$y_{m,w}$	Vector of investment decisions in node m
$z_{m,w}$	Vector of integer variables

CHAPTER 1

Introduction

THIS chapter gives motivation, context and background to the subject of this thesis. It then presents the key research questions and describes the significant contributions of the work. Finally, an overview of the remaining chapters of the thesis is presented.

1.1 Motivation and context

Power systems around the world (in particular the Australian power system) are experiencing a radical transition from a traditional configuration based on conventional thermal prime movers with synchronous generators to a system increasingly dominated by variable renewable energy sources (VRES) that are asynchronously connected to the system via power electronic interface. As a consequence, the level of system synchronous inertia [1–3] may be rapidly decreasing, with potentially profound effect on system stability and frequency response in particular. In Australia, the recent decommissioning of large coal-fired power plants as well as increasing prices of natural gas, in addition to a major blackout in the South Australia region [4], have thus raised major concerns as to the capability of the current system and market arrangements to adapt to the varying technical, economic and environmental conditions.

In response to these changing conditions and the various questions posed, the Australian government appointed a special panel to review these issues, which resulted in the *Independent Review into the Future Security of the National Electricity Market* [1], commonly known as the "Finkel review". The analysis focused on the security of the system in the future and, amongst other recommendations, advocates for the need to create high security standards to successfully operate the system securely. The report modelled an emissions reduction target of 28% relative to 2005 levels by 2030, with a linear trajectory to zero emissions by 2070. The resulting expansion scenarios were analysed in [5] to as-

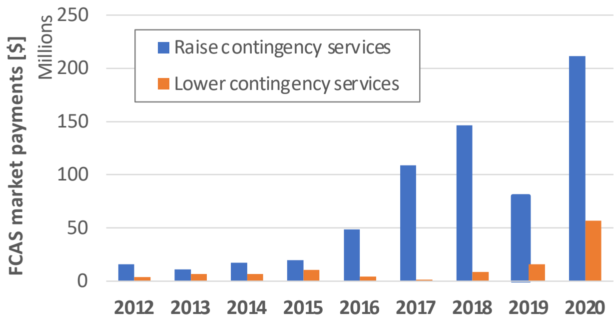

Figure 1.1 Total payments made in the raise and lower contingency FCAS markets in the period 2012-2020 in Australia's NEM [8].

sess the frequency response performance of the future system. The ex-post assessment of the secure operation of a certain expansion scenario is a requirement that has become increasingly necessary because of the growing penetration of technologies connected to the system through power electronics interfaces, which is expected to deepen in the future, leading to even lower levels of inertia available in the system, hence challenging reliability (security).

Since then, the response from stakeholders in the National Electricity Market (NEM) has been to install battery energy storage systems (BESS) [6] and synchronous condensers [7] to deal with the increased need for frequency response reserves and inertia (and also system strength issues, a topic that is not covered in this work). The investment in BESS has been supported by the market price and requirements for frequency control ancillary services (FCAS)[1], which have been increasing substantially since 2014. Figure 1.1 depicts the total payments for raise services in NEM between 2012 and 2020. The new system needs in the context of a renewable energy-dominated future create very challenging conditions to approach an optimal deployment of new assets, which include not only BESS and synchronous condensers, but also large-scale pumped-hydro storage systems (PSS) and transmission lines.

The challenge of understanding the optimal expansion path of the system was addressed in the Finkel review guidelines: recommendation 5.1 instructs that the Australian Energy Market Operator (AEMO) *"... should develop an integrated grid plan to facilitate the efficient development and connection of renewable energy zones across the National Electricity Market"*. This plan is known as Integrated System Plan (ISP), and its purpose is to *"...identify investment choices and recommends essential actions to optimise consumer benefits as Australia experiences what is acknowledged to be the world's fastest energy transition. That is, it aims to minimise costs and the risk of events that can adversely impact future power costs and consumer prices, while also maintaining the reliability and security of the power system."*. The ISP can be understood as an attempt to address what has been called the *energy trilemma*, which corresponds to achieving a secure, low cost and environmentally

[1]The FCAS in Australia are organised as 8 independent markets. Raise primary frequency response (to address low-frequency events) is allocated through two different markets, one in which full activation of the resources has to occur before 6 seconds and another one where resources have to be fully deployed within 60s. Fast frequency response is subject to the same conditions, hence there is no special compensation for a faster response speed. Inertia is not being traded.

sustainable power system; these conflicting objectives give place to a complex problem that connects the short-term operation (security, cost) with the long-term decisions (cost, sustainability).

Recent developments in the modelling of frequency response requirements have opened the possibility to create an expansion model that inherently embeds the associated requirements of the trilemma in the expansion process, in order not only to guarantee minimum cost and sustainability targets but also frequency security requirements. This thesis follows up on these ideas and develops an integrated operation and expansion model that can inform the best paths to develop the system.

1.2 Scope of work

This work will focus on several aspects surrounding the operation and the expansion planning of low-inertia power systems, with a particular focus on the optimal allocation of frequency response (FR) resources. This section presents the scope of the work.

1.2.1 Frequency response adequacy

The cornerstone of this work is developing a single-mass dynamic model capable of integrating multiple frequency response resources with different characteristics. Such a model is built by reasoning from first principles and considers the natural response of demand, the aggregated available inertia after contingency, the size of the contingency, and the attributes of the frequency response resources. These attributes include the delays in the provision of response after an event has occurred, the speed of response of the different technologies and the capacity of the technology to sustain its response in time. The model considers both high- and low-frequency events and the associated response profiles that the system can experience after a contingency.

Such a model enables a streamlined assessment of secure operation points in a given system, which allows determining the system's compliance with frequency security standards. The assessment can be conducted in two different ways:

- **Ex-post approach**: given a system's operation point, the model can be utilised to determine if it complies with the frequency standards or rules that govern its technical performance.
- **Ex-ante approach**: through an adequate sampling of the dynamic model, the requirements can be embedded in a bespoke scheduling model of the system to force it to find optimal points of operation that already comply with frequency security requirements.

In recent years, the Australian power system has experienced a series of frequency events that have led to the loss of interconnection of the system, the activation of substantial low-frequency load shedding, the partial loss of load in some areas and the total loss of load in the South Australian region. The dynamic model has been conceived to help understand these events and to support the optimal allocation of resources to avoid them in the future.

1.2.2 Optimal allocation of frequency response resources

With prices increasing substantially in frequency control ancillary services (FCAS) markets in Australia, the optimal allocation of frequency response resources is becoming a critical task for the efficient operation of the system. In this context, the aforementioned ex-ante approach becomes highly relevant to achieving an adequate economic schedule of the units in low-inertia power systems. The samples obtained from the frequency response model are used to build robust linear approximations that can then be used within an economic dispatch model or a unit-commitment model to determine the optimal operation of the system considering the minimisation of costs and the compliance with frequency security standards.

Embedding the frequency security constraints in a scheduling model allows not only to guarantee compliance with the security standards but also to understand the value that new technologies with flexible operation and fast response time (e.g. battery energy storage system, high-voltage direct-current power transmission) bring to the system. In addition, in systems where synchronous units are being decommissioned due to environmental or economic considerations, the capacity to value fast response resources (even only low levels) is essential to understand the size and distribution of resources to replace the inertia and response capacity of coal- and gas-fired units.

In this work, the scheduling models are also used to study the effect of the contingency size on the allocation of frequency response resources, the resilience of weakly interconnected systems like the Australian power system when facing the loss of interconnection under different levels of penetration of fast frequency response resources, and the effects of decreasing levels of natural response of demand in the requirements for inertia and frequency response, among other aspects.

1.2.3 Investment flexibility in low-carbon power systems

An efficient transition to future low-carbon power systems is challenging because it involves committing today to assets that will still be operational 40 or 50 years from now. The deep uncertainty faced today by decision-makers concerning the technologies that will dominate in the future requires a decision-making framework capable of identifying the value of the investment options (e.g., transmission, storage, synchronous condensers) that can better adapt to the future realisations of the uncertain variables.

Failing to do this could result in stranded assets, higher energy prices, unserved energy, higher greenhouse gas (GHG) emissions or frequency instability.

The scope, in this case, is limited to understand the elements in play when making investment decisions from a centralised point of view. The aim is to determine the optimal combination of technologies that will hedge the system against the uncertain future. The underlying assumption is that the market rules will be timely adapted to avoid the adverse effects of stakeholders engaging in gaming and other non-competitive behaviours, hence observing results close to perfect competition. Alternatively, the results presented here have to be interpreted as the desirable investment trends in the system, which the relevant regulatory body should target when adapting the the system's regulatory framework.

The work focuses on discussing the elements involved in the definition of the framework to evaluate and capture investment flexibility. The countries that show the most advanced methodologies to conduct investment decisions in the realm of transmission assets show a clear tendency towards risk-averse approaches, with a tendency to rely on least worst regret (LWR) to determine the optimal development path for the transmission network. This work dissects the components of the stochastic methodologies used to assess new investment options and presents a critical analysis of the advantages and limitations of selecting a specific set of metrics and indicators to determine the optimal expansion profile.

1.2.4 Modelling security-constrained expansion planning

Combining highly detailed operational constraints (e.g. security constraints), long planning horizons, deep uncertainties, and multiple investment options poses a serious modelling challenge. Industry relies on divide-and-conquer approaches to tackle the size of the problem and produce decisions within the time frames allocated by each regulatory framework. Large teams of people assess the technical implications of deploying different combinations of assets in the system and relay this information to other teams in charge of determining the value of those investments in the future [9, 10]. This work progresses the task of linking the technical and the economic aspects of the problem in a unified model, which is cast as a mixed-integer linear optimisation problem.

From a mathematical modelling perspective, while off-the-shelf mixed-integer linear optimisation solvers are very powerful and robust tools, the security-constrained expansion planning problem introduced here requires additional mathematical modelling efforts to undertake the task in scope. In this context, this work presents the monolithic deterministic equivalent problem that results from the combination of the scheduling model in the context of large scenario trees representing the future uncertainties in the system. Then, it discusses a decomposition approach (Danztig-Wolfe) and solution algorithm (column generation) to address the size of the problem that, in general, cannot be solved as a monolithic problem due to the high requirements on computational resources. The representation of the operation can address different levels of operational details and constraints. Any element that falls within the category of generator, transmission line or storage system qualifies to be considered among the investment options. Finally, the model is used on a real-world case study application based on the information presented in the Integrated System Plan by AEMO, to study the optimal portfolio to be deployed in Australia to address the energy trilemma.

1.3 Research questions

Developing power systems with the objective to reduce costs and emissions while preserving or increasing security, poses several research questions this thesis attempts to answer:

1. **What is the relationship between inertia, frequency response technologies and contingency size to contain high- and low-frequency contingency events?**

   To address this question, a series of elements need to be captured from the point of view of modelling, namely, the frequency response performance of new technologies, the effect of credible and non-credible contingencies in the system, the impact of decreasing levels of natural response from demand to changes in frequency, etc. The model is validated by comparing its results against frequency events experienced in Australia. A graphical representation of frequency security adequacy is introduced to simplify the analysis and convey a clear message. This artefact can illustrate all the elements that enter into play to define the system's secure operation and easily identify if a given operation point is, in fact, secure.

2. **How does the optimal operation of the system change as inertia decreases?**

   Decreasing inertia is a reality across power systems around the world. Isolated countries experiencing a rapid increase of VRES, like Australia, are already facing the challenges of operating their power system within technical requirements. This question is very broad, and it is relevant to clarify the limits of this work through the following set of specific questions:

   (a) What is the impact of the contingency size in the optimal operation of the system?

   (b) What is the effect of fast frequency response resources in the operation of the system?

   (c) How does the allocation of frequency response resources change when separation events are considered?

(d) How does the transmission capacity limit the optimal allocation of frequency response resources?

3. **What is the best framework to evaluate the expansion plan of low-inertia power systems?**

   Power systems need to rely on the deployment of new assets to cope with changing system conditions. In the past, the expansion of the system (generation and transmission) was driven by demand growth. Currently, the expansion of demand is slowing down substantially, and the need for new assets (transmission, storage) is driven by the expansion of utility-scale and distributed VRES, as well as the challenges imposed by lighter systems (e.g. need for synchronous condensers). Since the deployment of new VRES requires shorter planning periods (in comparison to coal and hydro units), the system is subject to larger locational and volumetric supply uncertainties in the scope of the planning periods (20+ years). Also, large-scale and distributed battery storage is playing an essential role as the investment costs of these technologies drop swiftly, and they perform not only arbitrage but also provide fast frequency response and other ancillary services. It is very relevant to determine the proper framework to define the investment needed that can provide the most flexibility across different scenarios.

4. **What is the optimal way to develop the system to cope with decreasing inertia levels and uncertainty about the future flows through the transmission network?**

   Low-inertia power systems face a series of challenges that need to be addressed by a strategic combination of technologies. For example, some technologies provide relief for grids facing transmission congestion (e.g. transmission and storage assets); other elements deliver frequency response capability to the system (e.g. synchronous condensers, storage assets). In addition, investment costs and future uncertainty come into play in an intricate trade-off between investment and operational costs. Some specific questions related to the expansion planning of low-inertia power systems are stated below:

   (a) What are the relevant technologies which need to be considered in the context of the expansion planning of low-inertia power systems?

   (b) How do different storage technologies perform in the context of a security-constrained expansion planning model?

   (c) What are the technologies that provide the most flexibility when more uncertainty is considered?

   (d) What investment strategy reduces the risk of facing high-cost outcomes?

1.4 Aims and objectives

The global objective of this work is to better understand the trade-offs associated with the energy trilemma in low-inertia power systems. The specific objectives are summarised below:

(i) Examine the current state-of-the-art of frequency security-constrained operation in power systems.

(ii) Investigate the factors affecting frequency response adequacy in low inertia power systems.

(iii) Develop a highly detailed security-constrained scheduling model for the Australian power system.

(iv) Investigate the prevailing methods to model the expansion planning of generation, transmission and storage in power systems.

(v) Develop a model of the Australian power system that allows making investment decisions in different assets considering complex scenario trees.

(vi) Integrate the security-constrained scheduling model and the expansion planning model to produce investment decisions that embed frequency security standards.

(vii) Determine the best combination of assets to allow the lowest cost, secure and clean electricity production in low-inertia power systems.

1.5 Novelty and contributions

The outcomes presented in this work contribute to fathom critical aspects of the secure operation of low-inertia power systems and to uncover some of the challenges behind the optimal investment strategy for these systems. Several contributions introduced here have already been published in different articles and reports, as presented in the preface. The summary of the primary novelty and contributions of this work can be summarised as follows.

1.5.1 Assessment framework of frequency response adequacy in low-inertia power systems

This work sets out to describe the relationship between primary frequency response (PFR), fast frequency response (FFR), synchronous inertia and the contingency size to achieve a frequency-secure system. The influence of different levels of load, contingency size and location, frequency response requirements, and other system parameters, is considered to analyse both high- and low-frequency events. This allows performing fundamental frequency response adequacy assessment based on ex-post analysis at the level of the whole National Electricity Market (NEM) as well as individual regions, for example, South Australia. Furthermore, the model considers the traditional frequency security metrics, namely rate of change of frequency (ROCOF), frequency nadir and zenith, and quasi-steady-state frequency (QSSF) to define response requirements to contain frequency events. To this end, the frequency response security maps (FRSM) are introduced, a graphical representation of the relations between relevant frequency response variables, which is derived from first principles on frequency dynamics after contingency.

1.5.2 Comprehensive multi-area security-constrained unit commitment model

This work contributes to developing means to enhance system resilience by understanding the value of co-optimising pre-contingency control variables (e.g. largest contingency size, inertia) and post-contingency response resources (PFR, FFR) in order to limit the costs of a system that faces the risk of loss of generation, load and interconnection. In particular, this thesis extends the recent low-inertia frequency stability works available in the literature not only to be applicable to low-frequency events but also to high-frequency events. The ability to constrain the system against high- and low-frequency events is required to deal with separation events that threaten system resilience. In order to achieve this, a novel UC model is proposed that aims to allocate frequency response resources in individual areas and at system level to face both high- and low-frequency events. The model also considers secondary frequency response (SFR) resources for both types of frequency events. The following novel traits of the model can be highlighted:

1. The capacity to control the maximum generation contingency size, which provides increased flexibility and reduces operation costs. This flexibility is critical to enable a secure operation in low-inertia power systems. The proposed approach does not require the use of bespoke dynamic models to determine the security requirements of the system, decoupling the security-constrained dispatch phase from the dynamic studies.

2. Quantification of the effect of the co-allocation of FR resources, including inertia, PFR and FFR resources both in individual balancing areas and at system level using different ROCOF, QSSF and, frequency nadir/zenith requirements.

3. Consideration of the loss of critical interconnectors in the system to allocate FR resources to improve system's resilience when the risk of separation is high due to extreme weather events (or other system-specific conditions). The set of constraints associated with the separation events can be activated or deactivated in

any given analysis period, depending on the risk assessment conducted by the system operator.

4. The allocation of adequate transmission slacks considering DC power flows, guaranteeing the possibility to transfer PFR and FFR resources between areas after low and high-frequency events (post-contingency feasibility).

1.5.3 Framework to assess the value of investment flexibility and risk in low inertia power systems

This work presents a structure to compare and analyse different objective functions used to evaluate investment options. Using this approach, it discusses the merits of the approaches used by industry and state-of-the-art models to arrive at decisions associated with the deployment of new assets in power systems. The discussion revolves around least worst regret (LWR) and expected cost minimisation, focusing on the practical advantages and disadvantages of each approach when it comes to making decisions in the expansion processes of countries like Australia and the UK. A set of graphical tools are presented to help define the stability of an investment solution and understand its associated risk.

1.5.4 Security-constrained expansion planning of low-inertia power systems

This work presents the first expansion planning model capable of making decisions on new generation, transmission and storage assets, considering frequency security constraints that differentiate between primary frequency response and fast frequency response resources. From the point of view of the operation, the expansion model features all the characteristics of the security-constrained unit commitment model; from the perspective of the expansion process, it allows for the consideration of complex scenario trees, where each node in the tree can be represented by any number of typical days, weeks or months. The scenarios can be built considering different conditions for any element in the system, for instance, varying dates of decommissioning of coal-fired units, the available capacity and output profiles for VRES, the trends in investment costs for each investment option, the demand profile for each load in the system, among other parameters.

Due to the size of the resulting expansion problem, the model is implemented using state-of-the-art decomposition approaches, which enables the use of distributed computing to find the solution. The solution to the problem is found by means of a column generation approach.

1.5.5 Power system operation and expansion modelling tool

Another contribution of this work includes a fully-fledged software package to run power system optimisation studies, which was built from the ground up. The mathematical modelling work conducted in this project was structured as a consistent modelling tool for power systems. The foundation of the tool is a data model capable of storing the parameters and technical data associated not only with the power system but also with the hydro basins, and it has been conceived so that the natural gas system can be readily incorporated. Also, the tool has been designed to cope with multiple study types (economic dispatch, optimal DC-power flow, stochastic expansion planning, etc.), parallel computing, and also includes interfaces for data visualisation. The different studies conducted within this project, whose results are presented in this thesis, were run using the modelling tool. For further information on the tool, see Appendix A.

1.6 Thesis overview

The thesis is structured as follows.

Chapter 2 discusses first principles of frequency response in low inertia power systems, including the current evolution of frequency response adequacy in the Australian power system, modelling of steady-state frequency response constraints considering multiple response resources, and multi-area constraints. Several case study applications are presented to understand the relationship between different technologies and the provision of services to contain frequency after contingency.

Chapter 3 presents a security-constrained unit-commitment and discusses different operational approaches to economically allocate resources to cater for energy and the required reserves to contain frequency events. The analysis includes the influence of the largest generation contingency on operation costs, and studies to understand how to optimally prepare the system for the potential loss of interconnection between areas, which involves allocating upward and downward reserves necessary to contain low- and high- frequency events, respectively.

Chapter 4 discusses investment flexibility. This chapter provides the theoretical framework to understand how to approach the expansion planning problem. Concepts like indicators, metrics, risk are presented, and different methodologies are analysed. The foundations for the planning model used in Chapter 5 are introduced at this stage.

Chapter 5 contains the description of the expansion model and the results of applying a Dantzig-Wolfe decomposition approach. It describes the column generation algorithm utilised to find the solution for the decomposed problem. A series of validation exercises are presented, where a monolithic version of the expansion problem is used to determine the quality of the solution found through the decomposition strategy. Further experiments are presented to understand the value of a higher degree of detail in the operation model, the benefits of relaxing the binary and integer variables, etc. Finally, a case study application on the Australian system based on input data obtained from AEMO's 2020 ISP is used to analyse the consequences of applying frequency security constraints in the expansion problem.

Chapter 6 presents conclusions, recommendations and future work.

CHAPTER 2

First principles of frequency response adequacy in low inertia power systems

2.1 Introduction

Power systems are facing the challenge to provide clean, cheap and reliable energy. The massive deployment of variable speed wind turbines (type III and IV) and, in recent years, photovoltaic (PV) capacity have helped to reduce the greenhouse gas emissions of the sector. With decreasing investment costs and little or no variable costs, these technologies allow envisioning large shares of non-synchronous capacity and energy in future power systems [11]. Reliability is probably the most pressing challenge in both system's operation and expansion, where the smart grid has been called upon to coordinate storage solutions, transmission technologies, distributed resources and demand to cope with renewable energies' variability and uncertainty. One particular aspect of reliability has been central in the discussion: the capability of future portfolios to constrain the frequency excursion following a contingency event, also known as frequency response adequacy [12], in particular for isolated power systems (e.g., Ireland [13]). As the system non-synchronous penetration in isolated system increases, the level of system synchronous inertia will decrease, with potentially severe effects on system stability and frequency response in particular [5]. Load also provides negative feedback against frequency variations, with changes of frequency proportionally changing the load consumption. This innate response is expected to change with the proliferation of loads connected through power electronic converters [14]. The crucial idea behind frequency response adequacy in power systems is to have prompt, coordinated actions to balance energy in order to stabilise frequency before it reaches prohibitive levels, after either generation, load or transmission contingencies.

The Australian National Electricity Market (NEM) is an excellent example of a system experiencing a radical transition from a traditional configuration based on conventional thermal prime movers with synchronous generators to a system increasingly dominated by variable renewable energy sources (VRES) that are asynchronously connected to the system via power electronic interface. As a consequence, the level of system synchronous inertia [1–3] may be rapidly decreasing, with potentially profound effects on system stability and frequency response in particular. Recent decommission of large coal-fired power plants as well as increasing prices of natural gas, in addition to a major blackout in the South Australia region [4], have thus raised significant concerns as to the capacity of the current system and market arrangements to adapt to the varying technical, economic and environmental conditions. In response to these changing conditions and the various questions posed, the Australian government appointed a special panel to review these issues [1]. The analysis focused on the security of the system in the future and, amongst other recommendations, advocates the need for creating an appropriate set of Energy Security Obligations to successfully operate the system within a framework of high security standards. The report modelled an emissions reduction target of 28% relative to 2005 levels by 2030, with a linear trajectory to zero emissions by 2070. The resulting expansion scenarios were analysed in [5] to assess the frequency response performance of the future system.

The increase of VRES and the associated impact on the NEM have already been under discussion for numerous years. For example, some approaches have looked into the 100% renewable scenario for the NEM reviewing system's energy adequacy and policy challenges and solutions, but without studying relevant security issues [15–17].

The security issues arising from changes in the generation mix have been reviewed and analysed in several papers, as presented below. The focus has been on the effects of the reduction of synchronous inertia and its impact on the rate of change of frequency (ROCOF) after generation or transmission contingencies, with a few papers also discussing the minimum frequency level (usually referred to as frequency nadir) after contingency and other transient phenomena. Dynamic studies of several plausible extreme operation conditions (e.g., low demand, high VRES) were carried out for South Australia considering varying levels of wind, inertia and imports, with the loss of the interconnector as the studied contingency (whose size is the import level) [18]. Likewise, [19] included solar PV as an increasing source of displacement of synchronous capacity, with various contingency cases for multiple combinations of load and generation levels and a dynamic model that includes the response of different wind technologies, load relief, synchronous machines dynamics, and under frequency load shedding (UFLS) schemes, among others.

A dynamic assessment assumes certain power flow configurations, potentially coming from economic dispatch or unit commitment (UC) solutions. A few approaches have thus proposed two-stage methodologies that sequentially dispatch the system and check the dynamic behaviour for multiple contingencies. For example, in [20] the 2020 NEM is analysed using proprietary software for both the UC and the dynamic analysis. The latter included not only frequency but also voltage and rotor angle stability considerations. The proprietary UC model is then replaced in [21] with a multi-nodal UC model with minimum synchronous inertia requirements by area. Another stage-wise approach is presented in [2] and tested on a NEM equivalent system for the year 2030. It describes an algorithm that systematically checks the resulting dynamic behavior of an economic dispatch until it converges to a set of online units that can satisfy the frequency limits after the largest generation contingency. The dispatch also considers the possibility to provide inertia from synchronous condensers as well as from wind farms that can deliver an inertial response. Various strategies to improve frequency adequacy, including the pre-curtailment of wind to provide primary frequency response, the deployment of synchronous condensers and the post-retirement operation of thermal units as synchronous condensersan are presented in [12].

Similar to [21], in [22] a UC model is proposed that implements three different strategies to comply with frequency response adequacy, namely, minimum online synchronous capacity, minimum online synchronous output, and minimum amount of inertia. The target values for each requirement are arbitrary, hence yielding results that do not necessarily prove effective in complying with frequency excursion limits in general cases.

A statistical approach to frequency response adequacy is presented in [12]. The authors introduce an estimator of maximum wind penetration level to comply with frequency response adequacy. It relies on historical data to determine inertia and headroom levels for different load levels and systematically calculates regressions to produce a linear relationship between maximum wind penetration and load levels.

Market aspects of the frequency response adequacy have also been discussed. The market for frequency control ancillary services (FCAS) within the NEM is presented in detail in [23]. The authors discuss the appropriateness of fast frequency response (FFR) as well as possible changes in the timing and duration of the current services in the FCAS market. In [24], the characteristics of a market for FFR are further described and analysed as a means to leverage the necessary resources to compensate for the diminishing synchronous inertia level. Different sources for FFR are presented, and conclusions are drawn regarding the market impact of the various options.

The literature that reviews the frequency security aspects of low-inertia systems typically oversights a more accessible presentation of the concepts behind frequency excursion after contingency and its relation with frequency response services and system inertia. In particular, the appropriate graphical representation of these relations can help to comprehend the complexity of a low-inertia power system's secure operation. Also, the presentation of specific case study applications can support not only the technical discussion of this issue but also the debate within a broader audience with less technical knowledge.

The chapter is structured as follows: first, a single-mass model to describe the frequency excursion after contingency is presented considering multiple sources of frequency response, which will be referred to as the multi-service frequency response model. Then, the extension to a multi-bus model is introduced and discussed. The next step corresponds to the introduction of the frequency response security maps (FRSM), a graphical tool to describe frequency response adequacy based on the multi-service frequency response model. The chapter closes with the presentation of three case study applications of the frequency response security maps.

2.2 Single-mass model

Frequency excursion after contingency can be expressed in a simplified way following [25, 26], which have developed allocation strategies of frequency control resources based on the solution of the equation that governs the behaviour of frequency after a sudden disruption in the balance of generation and demand [27]:

$$2\frac{E_{sys}}{f_o^{0+}}\Delta f'(t) + D \cdot P^D \Delta f(t) = \sum_k g_k(t) - \Delta P_{loss} \tag{2.2.1}$$

It is important to highlight that the online synchronous machines store a specific amount of rotational kinetic energy associated with the spin of the rotor; this energy is released to the system whenever a generation contingency arises. The concept of inertia is strictly tied up with the system's rotational kinetic energy E_{sys} as presented in (2.2.2).

$$\frac{E_{sys}}{f_0^{0+}} = H_{sys} = \frac{1}{f_0^{0+}} \sum_{k \in \Omega^{TH}} H_k = \frac{1}{f_0^{0+}} \sum_{k \in \Omega^{TH}} \frac{\widehat{H}_k \cdot P_k^{\max}}{PF_k} \tag{2.2.2}$$

By analysing (2.2.1) for different conditions, it is possible to derive expressions for rate of change of frequency, frequency nadir (Nadir) and the quasi-steady-state frequency as functions of the system inertia, primary frequency response and/or contingency size. More specifically, if at time $t = 0^+$ the system frequency can be assumed to be at nominal level and also that no response activation is present from the set of online generators, then it is possible to derive the following expression:

$$ROCOF := \Delta f'\left(0^+\right) = \frac{\Delta P_{loss}}{2H_{sys}} \tag{2.2.3}$$

Given a ROCOF limit $ROCOF_{lw}$ it is possible to find a relation between the size of the contingency and the inertia after contingency that complies with $ROCOF_{lw}$,

$$H_{sys} \geq \frac{\Delta P_{loss}}{2ROCOF_{lw}} \tag{2.2.4}$$

After the generators allocated to provide PFR have delivered their full response, the frequency stabilises at the QSSF value. The level of frequency in quasi-steady-state depends on the contingency size, the scheduled PFR, and the relief coming from demand due to the change in frequency, modelled through the composite load-damping factor D.

$$QSSF := \Delta f\left(t_\infty\right) = \frac{PFR - \Delta P_{loss}}{DP^D} \tag{2.2.5}$$

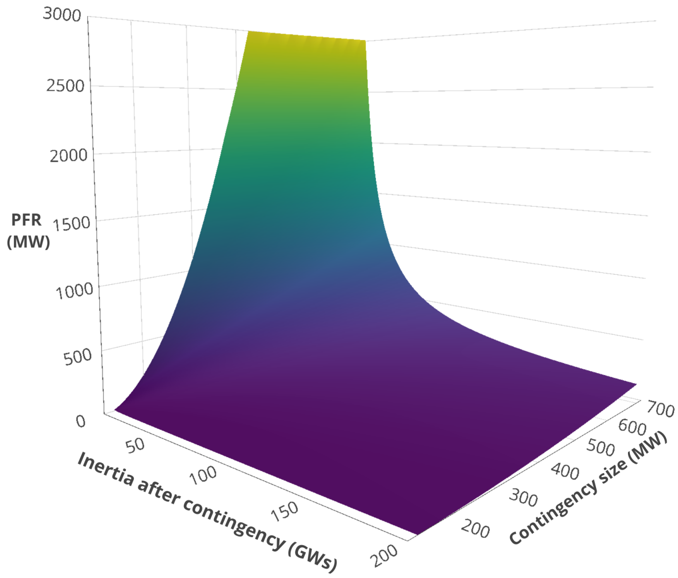

Figure 2.1 Relationship between inertia, PFR and contingency size to comply with nadir. Demand level of 14 GW, composite load-damping factor of 1 %/Hz, nadir limit of 49.0 Hz.

As with the ROCOF limit, by considering a specific quasi-steady-state frequency target ΔQF_{lw} it is possible to determine a condition on the minimum PFR amount that is required by the system to ensure that particular quasi-steady-state frequency. This condition may also be referred to as static requirement since it is independent of the inertia level.

$$PFR \geq \Delta P_{loss} - DP^D \Delta QF_{lw} \tag{2.2.6}$$

The lowest frequency level following a contingency event is known as frequency nadir. By minimising the solution of the differential equation (2.2.1), it is possible to calculate a nonlinear expression for frequency as a function of inertia, contingency size, primary frequency response, PFR duration, demand level, composite load damping factor, control dead-bands and delays, among others [25]. A concise version of the frequency nadir expression without the consideration of delays or dead-bands is presented in (2.2.7).

$$Nadir := \Delta f^n = \frac{\Delta P_{\text{loss}}}{D \cdot P^D} + \frac{2G_{\text{sys}} \cdot H_{\text{sys}}}{(D \cdot P^D)^2} \ln \left(\frac{2G_{\text{sys}} \cdot H_{\text{sys}}}{D \cdot P^D \cdot \Delta P_{\text{loss}} + 2G_{\text{sys}} \cdot H_{\text{sys}}} \right) \tag{2.2.7}$$

By establishing a limit for the frequency nadir, Δf^n_{min}, it is possible to derive a third condition on PFR, inertia and the contingency size, for a given set of parameters and demand level. By defining the target, and solving (2.2.7) for the product $G_{sys} \cdot H_{sys}$, where G_{sys} corresponds to the aggregated PFR provision rate, and also for several contingency sizes, it is possible to calculate the PFR requirement as a function of inertia and contingency size, as presented in Figure 2.1.

$$\Delta f^n_{min} \leq \Delta f^n \left(G_{sys}, H_{sys}, \Delta P_{loss} \right) \tag{2.2.8}$$

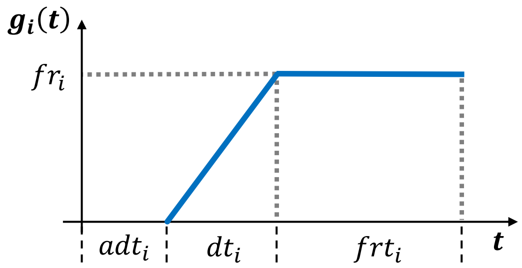

Figure 2.2 Generalised frequency response provision profile from synchronous technologies and fast frequency response technologies.

2.3 Multi-service frequency response

The evolution of frequency after contingency results from a set of inherent physical processes that take place in the system along with exogenous control strategies. The control schemes to keep frequency within boundaries after contingency have latency associated with measuring, identification, communication and activation delays [14], resulting in periods without activation of exogenous correction actions. At any point in time, the difference between load and generation is compensated using the rotating energy –inertia– of the system's synchronous machines (generators and motors), which leads to the deceleration (load > generation) or acceleration (generation > load) of the machines. The contribution of loads to inertia is generally neglected, although it can account for significant amounts of rotational energy in the system (e.g. in average 20% for the UK [28]). The aggregated inertia in a general isolated area a corresponds to the sum of the inertia provided by each generator that is online in the area and by subtracting the inertia lost in the contingency. The calculations consider the power factor of each generator, their inertia constant relative to their apparent power, and their installed capacity.

$$H_a = \sum_{k \epsilon \Omega_a^{SY}} H_k = \sum_{k \epsilon \Omega_a^{SY}} \frac{\widehat{H}_k P_k^{max}}{PF_k} \tag{2.3.1}$$

In parallel to the inertial response, there is a second inherent mechanism that counterbalances any frequency excursion: the self-regulating effect of the load. The energy that passive loads draw from the system depends on the frequency; an increase (decrease) in system frequency, e.g., sudden load (generation) disconnection, leads to a proportional increase (decrease) in power consumption, which counteracts the initial load (generation) loss. This effect is represented as a factor of the demand level of the system or area under analysis.

The frequency response dynamics after a contingency event is governed by (2.2.1) in the presence of synchronous inertia, frequency-dependent loads and resources providing frequency response.

The resources providing frequency response can be divided into two categories: synchronous technologies providing PFR and the technologies providing FFR. In this work, both types of responses will be represented through a generalised response function

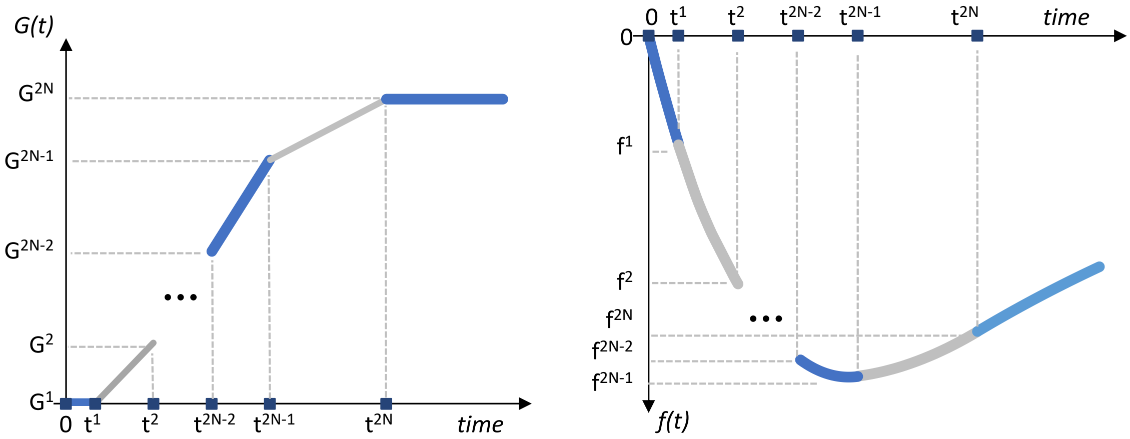

(a) Aggregated frequency response $G(t)$ **(b)** Frequency excursion with response $G(t)$

Figure 2.3 Generalised aggregated frequency response provision profile and resulting frequency excursion profile.

$g_i(t)$. This response function is modelled through the following parameters: an activation delay adt_i, delivery time dt_i, full response time frt_i, and frequency response capacity fr_i as shown in Figure 2.2. In general, the time in which the sources deliver full response frt_i is long enough to consider that they will be active for the entire window of primary frequency response provision in place in a given ancillary market.

The derivation of results in this work will be done by considering frequency response after generation contingency events. Results for load contingency events can be derived in a similar fashion. The formulation stems from the previous analysis presented in [25, 26].

The aggregated frequency response at time t coming from N sources providing PFR or FFR, $G(t) = \sum_i^N g_i(t)$, can be represented by a piece-wise linear function which can be further characterized by a series of $2N$ tuples $\{t^k, G^k\}$, as presented in Figure 2.3a. This frequency response profile will impact frequency excursion after contingency in a way that can be represented by the piece-wise functions in Figure 2.3b. Let us derive a formal expression for the frequency excursion after contingency considering a frequency response profile composed by multiple sources.

Considering that each of the N sources of frequency response has an activation delay time adt_i and also a time to reach full deployment, represented by $adt_i + dt_i$, by aggregating these two time-steps for every resource i and then sorting them in ascending order, it is possible to define the set of time steps t^k, with $k = 1 \; to \; 2N$.

On the other hand, the G^k components of the tuples can be expressed as a function of the parameters defining each of the N individual sources of frequency response (fr_i, adt_i, dt_i) and the corresponding time step t^k, as shown in the following equation:

$$G^k = \sum_{i=1}^{N} \left[\beta_i^k fr_i + \alpha_i^k \left(1 - \beta_i^k\right) \frac{t^k - adt_i}{dt_i} \right] \tag{2.3.2}$$

Auxiliary binary parameter α_i^k describes if source i-th has been activated or not at time step t^k ($\alpha_i^k = 1$ if $adt_i \leq t^k$). Binary parameter β_i^k describe if source i-th has reached

full activation or not at time step t^k ($\beta_i^k = 1$ if $adt_i + dt_i \leq t^k$).
The aggregated frequency response rate at time t, $frr(t) = \frac{d}{dt}G(t)$, can also be represented by a series of tuples $\left\{t^k, frr^k\right\}$, in which frr^k corresponds to the aggregated frequency response rate in the interval $\left[t^k, t^{k+1}\right)$. Following a similar reasoning as with (2.3.2), the frr^k components of the tuples are

$$frr^k = \sum_{i=1}^{N} \left[\alpha_i^k \left(1 - \beta_i^k\right) \frac{fr_i}{dt_i}\right] \tag{2.3.3}$$

With the description of the aggregated frequency response and aggregated frequency response rate it is easier to derive expressions describing the frequency excursion $\Delta f^k(t)$ after contingency ΔP_{loss} based on the differential equation presented in (2.2.1), for each time interval $\left[t^k, t^{k+1}\right)$. Solving (2.2.1) using the method of the integration factor returns:

$$\Delta f^k(\tau) = \frac{G^k + frr^k(\tau - t^k) + \Delta P_{loss}}{DP^D} - \frac{2frr^k H_{sys}}{\left(DP^D\right)^2} - A\exp\left(-\frac{DP^D}{2H_{sys}}\tau\right) \tag{2.3.4}$$

In (2.3.4), A corresponds to an integration constant. For $\tau \in \left[0, t^1\right)$ no PFR or FFR resources are active and the integration constant can be determined by the condition $\Delta f(0) = 0$. This yields:

$$\Delta f(\tau) = \frac{\Delta P_{loss}}{DP^D}\left(1 - \exp\left(-\frac{DP^D}{2H_{sys}}\tau\right)\right) \quad \forall \tau \in \left[0, t^1\right) \tag{2.3.5}$$

Then, solving (2.3.4) for $\tau \in \left[t^k, t^{k+1}\right)$ results in the expression presented in (2.3.6).

$$\begin{aligned}\Delta f(\tau) =& \Delta f\left(t^k\right)\exp\left(-\frac{D\cdot P^D}{2\cdot H_{sys}}\left(\tau - t^k\right)\right) + frr^k\frac{\left(\tau - t^k\right)}{D\cdot P^D} \\ &- \left(1 - \exp\left(-\frac{D\cdot P^D}{2\cdot H_{sys}}\left(\tau - t^k\right)\right)\right)\left(-\frac{\Delta P_{loss} + G^k}{D\cdot P^D} + \frac{2\cdot H_{sys}\cdot frr^k}{\left(D\cdot P^D\right)^2}\right)\end{aligned} \tag{2.3.6}$$

With the expressions derived so far, it is possible to determine the values of the three metrics for frequency excursion after contingency:

Rate of change of frequency [Hz/s] which corresponds to the initial slope of the frequency change immediately following the contingency event, i.e., the derivative of frequency deviation at $t = 0^+$. The derivative of (2.3.5) evaluated at $\tau = 0$ allows finding the following expression for ROCOF, which is dependent on system inertia and the size of the contingency. If the contingency ΔP_{loss} corresponds to a generation loss, $\Delta C < 0$, hence yielding a negative ROCOF. The opposite happens with a load contingency.

$$ROCOF := \Delta f'\left(0^+\right) = \frac{\Delta P_{loss}}{2H_{sys}} \tag{2.3.7}$$

Quasi Steady-State frequency [Hz] is the frequency that is reached after generators have provided the scheduled PFR, before automatic generation control or other similar scheme brings the frequency back to the nominal level. Considering (2.3.6) evaluated for $k = 2N$ ($frr^{2N} = 0$ and $G^{2N} = \sum_{i=1}^{N} fr_i$) and taking the limit $\tau \rightarrow \infty$, an expression for QSSF can be derived, as presented in (2.3.8). Its magnitude depends on the size of the contingency, the total scheduled capacity of response, and the natural response coming from demand.

$$QSSF := \Delta f\left(t_\infty\right) = \frac{G^{2N} + \Delta P_{loss}}{DP^D} \tag{2.3.8}$$

Frequency Extremum [Hz] is the maximum deviation of frequency that is reached following the contingency event and after the frequency arrest mechanisms have been activated. It is generally known as frequency nadir in low-frequency events or frequency zenith in high-frequency events. The mathematical expression for frequency extremum depends –among others– on inertia, allocated response levels, contingency size, load frequency damping factor, demand level, activation delays, etc.

In order to derive an expression for the third metric considering multiple frequency response sources, further conditions need to be studied. Let's start by differentiating (2.3.6) and establishing the condition to find the extrema of $\Delta \mathrm{f}(\tau)$:

$$\begin{aligned}\frac{d\Delta f(\tau)}{d\tau} = \frac{frr^k}{DP^D} - \left(\Delta f\left(t^k\right) - \frac{\Delta P_{loss} + G^k}{DP^D} + \frac{2H_{sys} frr^k}{\left(DP^D\right)^2}\right)& \\ \cdot \exp\left(-\frac{DP^D}{2H_{sys}}\left(\tau - t^k\right)\right)\frac{DP^D}{2H_{sys}} = 0&\end{aligned} \tag{2.3.9}$$

By rearranging (2.3.9), for any given time range $\left[t^k, t^{k+1}\right)$, condition (2.3.10) can be derived.

$$\mathrm{t}^{\mathrm{k}+1} - t^k = \frac{2 \cdot H_{sys}}{D \cdot P^D} \cdot \ln\left(1 + \frac{\left(\Delta f\left(t^k\right) \cdot D \cdot P^D - \Delta P_{loss} - G^k\right) \cdot D \cdot P^D}{2 \cdot H_{sys} \cdot frr^k}\right) \tag{2.3.10}$$

Then, it is possible to replace the time variable in (2.3.6) by means of (2.3.10), in order to find an expression for the frequency extrema in any time range $\left[t^k, t^{k+1}\right)$. (2.3.11) presents an expression for the exponential terms in (2.3.6).

$$\exp\left(-\frac{D \cdot P^D}{2 \cdot H_{sys}}\left(t^{k+1} - t^k\right)\right) = \frac{\frac{2 \cdot H_{sys} \cdot frr^k}{\left(D \cdot P^D\right)^2}}{\Delta f\left(t^k\right) + \frac{\Delta P_{loss} + G^k}{D \cdot P^D} + \frac{2 \cdot H_{sys} \cdot frr^k}{\left(D \cdot P^D\right)^2}} \tag{2.3.11}$$

Replacing (2.3.11) in (2.3.6) generates a general expression for the frequency extrema in time range $\left[t^k, t^{k+1}\right)$, presented in (2.3.12).

$$\begin{aligned}\Delta f_k^{ext} = \frac{\Delta P_{loss} + G^k}{D \cdot P^D} - \frac{2 \cdot H_{sys} \cdot frr^k}{\left(D \cdot P^D\right)^2}& \\ \cdot \ln\left(\frac{2 \cdot H_{sys} \cdot frr^k}{\left(\Delta P_{loss} + G^k - \Delta f\left(t^k\right) \cdot D \cdot P^D\right) \cdot D \cdot P^D - 2 \cdot H_{sys} \cdot frr^k}\right)&\end{aligned} \tag{2.3.12}$$

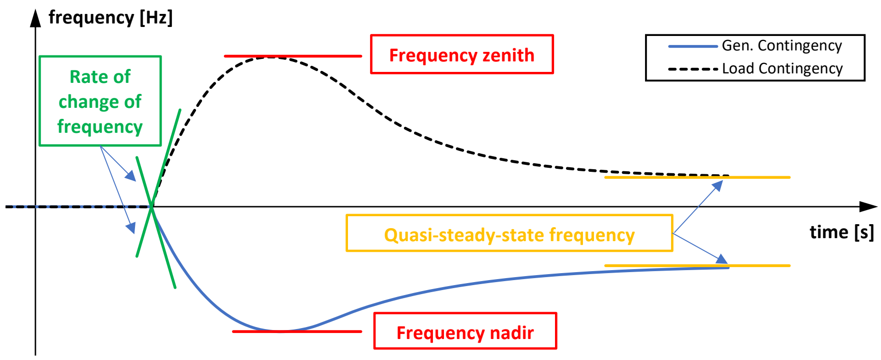

Figure 2.4 System frequency excursion and recovery after a generation/transmission contingency, highlighting the three key metrics describing the transient behaviour.

By analysing (2.3.12) it is possible to appreciate that frequency extrema in time range $\left[t^k, t^{k+1}\right)$ depends on the conditions at a given time range, for instance, the initial level of frequency excursion $\Delta f\left(t^k\right)$, the aggregated level of frequency response rate frr^k and the level of accumulated frequency response G^k. On the other hand, inertia level H_{sys}, demand level P^D, composite demand damping factor D and contingency size ΔP^C also influence the frequency extrema, and they are time-independent.

Thus, any condition on the frequency extrema will require the use of (2.3.12) which also requires considering (2.3.2), (2.3.3) and (2.3.6) recurrently. (2.3.12) is then formed by nesting (2.3.6) $k-1$ times. This creates a cumbersome non-linear expression for nadir that cannot directly be used to establish a condition on the amount of frequency response resources to comply with nadir or zenith; however, (2.3.12) is an expression that is easy to evaluate numerically to determine values for inertia and frequency response resources to comply with targets for frequency extrema in a given time range $\left[t^k, t^{k+1}\right)$. For instance, by fixing the amount of FFR, it is possible to determine the minimum amount of frequency response coming from synchronous technologies that comply with a given nadir level in a specific time range.

Expressions (2.3.7), (2.3.8) and (2.3.12) allow describing and measuring the characteristics of frequency excursion after contingency with consideration of multiple sources of frequency response after contingency, as presented in Figure 2.4. As it will be presented in Chapter 3, they can be used within economic dispatch and unit commitment models to guide the simultaneous allocation of frequency response resources and inertia in order to guarantee that the frequency excursion after contingency will comply with given requirements for ROCOF, frequency extrema, and QSSF level that are allowed in the system.

2.4 Multi-bus extension of the single mass model

In the following sections and chapters, this work discusses the effects of separation events in low-inertia power systems, among other topics. In this section, the frequency response model and the associated constraints introduced before are extended to be applied to analyse the loss of interconnection in a system like the NEM, as presented in [29]. The main focus is put on ROCOF and QSSF requirements per balance area, while for nadir/zenith requirements a single mass model like the one presented in [25, 30] and in Section 2.3. The network model captures the spatial dynamics during transient and can be used to derive requirements on both system ROCOF and local ROCOF before local frequencies synchronise for both load/generation contingencies and separation contingencies. Here, however, the aim is to derive requirements to mitigate separation events.

Consider a connected network with buses $b \in \Omega^{Bus}$ and lines $l \in \Omega^{Line}$. Suppose there is a load/generator contingency or a separation contingency right before time $t = 0$. Let the operating point just before the contingency event be described by $(f_b^0,\ g_b^0,\ fl_l^0)$ for all buses k and lines l where

- f_b^0 is the angular frequency at bus b;
- g_b^0 is the power injection from bus b to the rest of the network;
- fl_l^0 is the power flow one line l;

Denote by $f^0 := (f_b^0, \forall b)$ without subscript the vector of local bus frequencies f_b^0, and similarly for other variables such as $g^0,\ fl^0$. Post contingency, for $t \geq 0$, the system dynamics are described by the state at time t:

$$f^0 + f(t); g^0 + g(t); fl^0 + fl(t) \tag{2.4.1}$$

where $(f(t),\ g(t), fl(t))$ are perturbations around the operating point $\left(f^0,\ g^0,\ fl^0\right)$.

The network dynamics [31] are modeled by:

$$2H_b^B \dot{f}_b(t) + D_b P_b^L f_b(t) = \left(g_b^0 + g_b(t)\right) - \sum_l C_{bl} \left(fl_l^0 + fl_l(t)\right) \tag{2.4.2}$$

$$\dot{fl}_l(t) = \frac{\left(f_{Bs(l)}(t) - f_{Br(l)}(t)\right)}{X_l} \tag{2.4.3}$$

where $f_{Bs(l)}(t)$ and $f_{Br(l)}(t)$ are the bus angular frequencies at the sending and receiving end of line l respectively. Here $C_{bl} = 1$ if the graph orientation is such that line l leaves bus b, $C_{bl} = -1$ if line l enters bus b and $C_{bl} = 0$ if line l is not connected to bus b. H_b, P_b^L refer to the total inertia and total load connected to bus b, respectively, and D_b represent the demand damping factor in bus b. It is assumed that the operating point $\left(f^0,\ g^0,\ fl^0\right)$ is in steady state so that, from (2.4.2), it satisfies

$$0 = g_b^0 - \sum_l C_{bl} fl_l^0 \tag{2.4.4}$$

2.4.1 Network dynamics post separation contingency

Suppose at time $t = 0^-$, line/interconnector $\widetilde{l}$ (connecting buses β and γ) is disconnected and the disconnection partitions the system into two subsystems with two disjoint set of buses. Let Ω_β^{Bus} be the set of buses that are connected to bus β (including β) and Ω_γ^{Bus} be the other buses connected to bus γ (including γ). Consider first the subsystem Ω_β^{Bus}. From (2.4.2), the post-contingency network dynamics for $t \geq 0$ are given by:

$$2H_b\dot{f}_b(t) + D_bP_b^L f_b(t) = \left(g_b^0 - \sum_{l \neq \tilde{l}} C_{bl}fl_l^0\right) + \left(g_b(t) - \sum_{l \neq \tilde{l}} C_{bl}fl_l(t)\right) \tag{2.4.5}$$

For buses $b \in \Omega_\beta^{Bus}$, $b \neq \beta$, $\sum_{l \neq \widetilde{l}} C_{bl}fl_l^0 = \sum_l C_{bl}fl_l^0$ holds and hence the equilibrium condition (2.4.4) implies

$$g_b^0 - \sum_{l \neq \widetilde{l}} C_{bl}fl_l^0 = 0 \tag{2.4.6}$$

For bus β, the equilibrium condition (2.4.4) implies

$$g_b^0 - \sum_{l \neq \widetilde{l}} C_{bl}fl_l^0 = fl_{\widetilde{l}}^0 \tag{2.4.7}$$

Substituting these into (2.4.5) and combining with (2.4.3), the post-contingency network dynamics for $t \geq 0$ are given by:

$$2H_b\dot{f}_b(t) + D_bP_b^L f_b(t) = \begin{cases} g_\beta(t) - \sum_{l \neq \tilde{l}} C_{\beta l}fl_l(t) + fl_{\tilde{l}}^0 & \text{if } b = \beta \\ g_b(t) - \sum_{l \neq \tilde{l}} C_{bl}fl_l(t) & \text{if } b \neq \beta, b \in \Omega_\beta^{Bus} \end{cases} \tag{2.4.8}$$

$$\dot{fl}_l(t) = \left(f_{Bs(l)}(t) - f_{Br(l)}(t)\right)/X_l \quad \forall l \mid Br(l), Bs(l) \in \Omega_\beta^{Bus} \tag{2.4.9}$$

Similarly, for subsystem Ω_γ^B the post-contingency dynamics for $t \geq 0$ are given by:

$$2H_b\dot{f}_b(t) + D_bP_b^L f_b(t) = \begin{cases} g_\gamma(t) - \sum_{l \neq \tilde{l}} C_{\gamma l}fl_l(t) + fl_{\tilde{l}}^0 & \text{if } b = \gamma \\ g_b(t) - \sum_{l \neq \tilde{l}} C_{bl}fl_l(t) & \text{if } b \neq \gamma, b \in \Omega_\gamma^{Bus} \end{cases} \tag{2.4.10}$$

$$\dot{fl}_l(t) = \left(f_{Bs(l)}(t) - f_{Br(l)}(t)\right)/X_l \quad \forall l \mid Br(l), Bs(l) \in \Omega_\gamma^{Bus} \tag{2.4.11}$$

2.4.2 Rate of Change of Frequency

By definition of the perturbation variables, $f_b(0) = g_b(0) = fl_l(0) = 0$ at $t = 0$. Substituting this into (2.4.8)-(2.4.9):

$$2H_\beta \dot{f}_\beta(0) = fl_{\tilde{l}}^0 \tag{2.4.12}$$

$$2H_\gamma \dot{f}_\gamma(0) = -fl_{\tilde{l}}^0 \tag{2.4.13}$$

$$2H_b \dot{f}_b(0) = 0 \quad b \neq \beta, \gamma \tag{2.4.14}$$

therefore, the *local* ROCOFs at each bus at time $t = 0$ are:

$$\dot{f}_\beta(0) = fl_l^0 / 2H_\beta \tag{2.4.15}$$

$$\dot{f}_\gamma(0) = -fl_i^0 / 2H_\gamma \tag{2.4.16}$$

$$\dot{f}_b(0) = 0 \quad b \neq \beta, \gamma \tag{2.4.17}$$

This means that when interconnector $\tilde{l}$ is disconnected, the local ROCOFs at buses β and γ are proportional to the line flow $F_{\tilde{l}}^0$ on the interconnector right before the disconnection with opposite signs. The local ROCOFs at all other buses are zero at time $t = 0$. The impact of the separation event will propagate to other buses and areas in the subsystems Ω_β^B and Ω_γ^{Bus} through power flows $fl(t)$ according to the network dynamics (2.4.8)-(2.4.9) and (2.4.10)-(2.4.11) respectively. Note, however, that while there is discontinuity in $\dot{f}_\beta(t)$ and $\dot{f}_\gamma(t)$ at time $t = 0$ due to the disconnection of the interconnector $\tilde{l}$, $\dot{f}_b(t)$ at all other buses $b \neq \beta, \gamma$, will evolve smoothly according to (2.4.8)-(2.4.9) and (2.4.10)-(2.4.11) without discontinuity at $t = 0$.

Define the system frequency (perturbation) for each of the subsystems Ω_β^{Bus} and Ω_γ^{Bus} as the weighted average of local frequencies, weighted by the local inertias:

$$\bar{f}_\beta(t) := \frac{1}{\sum_{b \in \Omega_\beta^{Bus}} H_b} \sum_{b \in \Omega_\beta^{Bus}} H_b f_b(t) \tag{2.4.18}$$

$$\bar{f}_\gamma(t) := \frac{1}{\sum_{b \in \Omega_\gamma^{Bus}} H_b} \sum_{b \in \Omega_\gamma^{Bus}} H_b f_b(t) \tag{2.4.19}$$

This corresponds to the classical notion of center of inertia [32]. Informally, $\bar{f}_\beta(t)$ and $\bar{f}_\gamma(t)$ represent the voltage frequency perturbations, not necessarily at any bus in the network, but at a fictitious bus at the center of inertia of the subsystems Ω_β^{Bus} and Ω_γ^{Bus} respectively. From (2.4.12)-(2.4.14), the system ROCOFs for each subsystem are:

$$\dot{\bar{f}}_\beta(0) := \frac{1}{\sum_{b \in \Omega_\beta^{Bus}} H_b} \sum_{b \in \Omega_\beta^{Bus}} H_b \dot{f}_b(0) = \frac{fl_l^0}{2 \sum_{b \in \Omega_\beta^{Bus}} H_b} \tag{2.4.20}$$

$$\dot{\bar{f}}_\gamma(0) := \frac{1}{\sum_{b \in \Omega_\gamma^{Bus}} H_b} \sum_{b \in \Omega_\gamma^{Bus}} H_b \dot{f}_b(0) = \frac{-fl_l^0}{2 \sum_{b \in \Omega_\beta^{Bus}} H_b} \tag{2.4.21}$$

For ROCOF security, one can require that the system ROCOFs $\dot{\bar{f}}_\beta(0)$ and $\dot{\bar{f}}_\gamma(0)$ stay within a range. This constrains the total inertia in each subsystem after the separation contingency, as well as the scheduled line flow $\left|fl_{\tilde{l}}^{0}\right|$ on the interconnector $\tilde{l}$. Note that the system ROCOFs are larger than the local ROCOFs $\dot{f}_{\beta}(0)$ and $\dot{f}_{\gamma}(0)$ which depend only on the local inertias H_{β} and H_{γ} respectively. Therefore, a separation security constraint based on local ROCOFs represents a more stringent inertia requirement.

2.4.3 Quasi-Steady-State Frequency

Consider first the subsystem Ω_{β}^{Bus}. From the post-contingency dynamics (2.4.9), the quasi-steady state frequencies in Ω_{β}^{Bus} are synchronised, i.e., $f_{\beta}(t) = f_{\text{qss},\beta}$ for all $\beta \in \Omega_{\beta}^{Bus}$ where $f_{\text{qss},\beta}$ denotes the QSSF in the subsystem Ω_{β}^{Bus}. Under droop control, the generation (perturbation) in the quasi-steady state is

$$g_{qss,b} = -\rho_b f_{qss,\beta} \quad b \in \Omega_{\beta}^{Bus} \tag{2.4.22}$$

Expression (2.4.22) assumes that the generator response is droop control. Other generator response can also be modelled and that amounts to replacing (2.4.22) by an appropriate quasi steady state behaviour. Let $fl_{\text{qss},l}$ denote the quasi-steady state line flows on for lines $l \neq \tilde{l}$. Then (2.4.8) in quasi-steady state becomes:

$$D_b P_b^L f_{qss,\beta} = g_{qss,b} - \sum_{l \neq i} C_{bl} fl_{qss,\beta} + fl_{l}^{0} 1(b = \beta) \quad b \in \Omega_{\beta}^{Bus} \tag{2.4.23}$$

where the indicator function $1(b = \beta) = 1$ if bus $b = \beta$ and 0 otherwise. Substitute (2.4.22) and sum over $b \in \Omega_{\beta}^{Bus}$ to get:

$$f_{qss,\beta} \sum_{b \in \Omega_{\beta}^{Bus}} \left(D_b P_b^L + \rho_b \right) = - \sum_{b \in \Omega_{\beta}^{Bus}} \sum_{l \neq i} C_{bl} fl_{qss,\beta} + fl_{l}^{0} \tag{2.4.24}$$

But $\sum_{b \in \Omega_{\beta}^{Bus}} \sum_{l \neq \tilde{l}} C_{bl} fl_{\text{qss},\beta} = 0$ post contingency and hence the QSSF in subsystem Ω_{β}^{Bus} is:

$$f_{qss,\beta} = fl_{\tilde{l}}^{0} / \sum_{b \in \Omega_{\beta}^{Bus}} \left(D_b P_b^L + \rho_b \right) \tag{2.4.25}$$

A similar analysis shows that the QSSF in subsystem Ω_{γ}^{Bus} is:

$$f_{qss,\gamma} = fl_{\tilde{l}}^{0} / \sum_{b \in \Omega_{\gamma}^{Bus}} \left(D_b P_b^L + \rho_b \right) \tag{2.4.26}$$

Hence, if $fl_{\tilde{l}}^{0} > 0$, i.e., power flows from bus β to bus γ before the separation contingency, then the quasi-steady state frequency (deviation) $f_{\text{qss},\beta} > 0$ and hence the frequency in subsystem Ω_{β}^{Bus} will increase above the pre-contingency frequency f^0 while $f_{\text{qss},\gamma} < 0$ and hence the frequency in subsystem Ω_{γ}^{Bus} will decrease, as it would be expected.

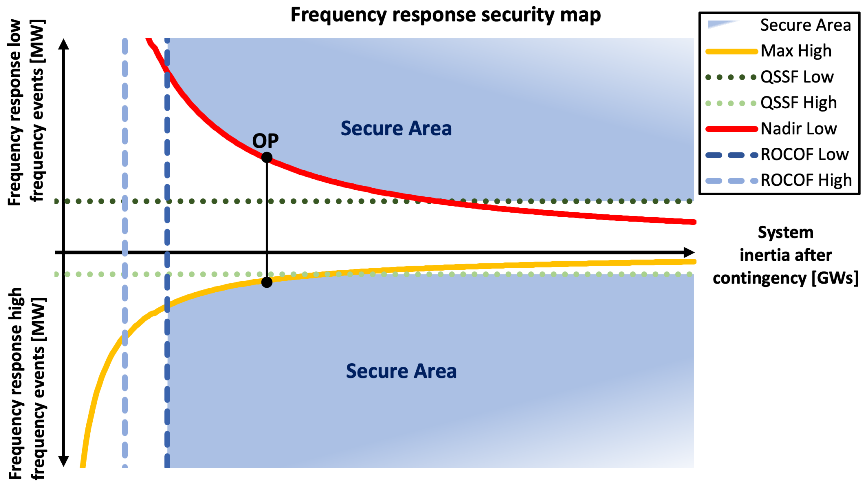

Figure 2.5 Illustration of frequency response security map: Frequency response vs Inertia chart representing constraints to comply with desired nadir/zenith, ROCOF and QSSF limits for load and generation contingencies of specific characteristics.

2.5 Frequency response security maps

In this section, the frequency response security maps (FRSM) are introduced, which correspond to a graphical representation of the limits for the combination of FR resources and inertia available in the system to keep frequency excursion within boundaries. Since its first introduction [5], the FRSM have been used by industry [33] and academia [34] as a mean to describe frequency response adequacy.

The limits of the FRSM are set by an adequate use of expressions (2.3.7), (2.3.8) and (2.3.12) and by considering the allowed values for frequency excursion after load and generation contingencies. For the sake of generality, in this work, six different limits for the frequency excursion metrics are used, namely frequency zenith and nadir limit, and maximum and minimum ROCOF and QSSF for high- and low-frequency events, respectively.

Let us start by considering the ROCOF limits, represented in this case by (2.3.7). For a low-frequency event, the desired operation behaviour is that the ROCOF does not get steeper than $ROCOF_{low}$, while for a high-frequency event, ROCOF can be as high as $ROCOF_{high}$. This translates into the following conditions on system inertia after contingency:

$$H_{sys} \geq \frac{\Delta P_{loss}}{2 \cdot ROCOF_{low/high}} \qquad \begin{array}{l} \Delta P_{loss} < 0 \wedge ROCOF_{low} < 0 \\ \Delta P_{loss} > 0 \wedge ROCOF_{high} > 0 \end{array} \tag{2.5.1}$$

Since the ROCOF limits for both low- and high-frequency events create a constraint over the system inertia after contingency, the most stringent condition in (2.5.1) will define the minimum acceptable level of inertia for the system, according to (2.3.1), as it is depicted in Figure 2.5 (vertical dashed lines).

The QSSF requirement for low and high frequency events is represented by (2.3.8).

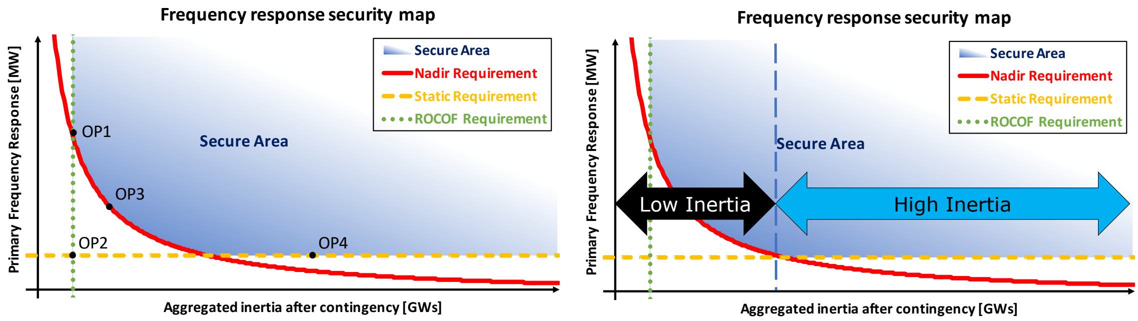

(a) Relevant operation points for frequency analysis. **(b)** Low-inertia power system definition.

Figure 2.6 Frequency response security map applications.

By using that expression, it is possible to derive constraints for the minimum amount of frequency response capacity (after full deployment of PFR and FFR resources) necessary to comply with the requirement for QSSF after low and high frequency events. These expressions are presented in (2.5.2) and depicted in Figure 2.5 as two horizontal dotted lines.

$$\begin{array}{ll} G^{2N}_{low} \geq \Delta QSSF_{low} \cdot D \cdot P^{D} - \Delta P_{loss} & \Delta P_{loss} < 0 \wedge QSSF_{low} < 0 \\ G^{2N}_{high} \leq \Delta QSSF_{high} \cdot D \cdot P^{D} - \Delta P_{loss} & \Delta P_{loss} > 0 \wedge QSSF_{high} > 0 \end{array} \tag{2.5.2}$$

Finally, the conditions to limit the frequency extrema can be imposed utilising expression (2.3.12). As it was already pointed out, the nested nature of expression (2.3.6) leads to a large non-linear expression for (2.3.12). In order to find the relation between frequency response and inertia after contingency that complies with the target for frequency extrema, the resulting non-linear expression is solved for a set of inertia values in the time range of interest. This time range is defined by the maximum time T_{FR} at which the frequency response can be delivered in a given market. This can be defined by including that particular time sample in the analysis $\left[t^{k}, t^{k+1} = T_{FR}\right)$. Algorithm 2.1 presents the set of steps that produce the non-linear constraints associated with frequency extrema in Figure 2.5. This algorithm focuses on identifying the occurrence of the activation of the frequency dead-band F_{DB} of the droop control of synchronous units based on the aggregated behaviour of FR resources (as depicted in Figure 2.3a). After determining the activation time of the droop control, it builds the piece-wise representation of the frequency evolution (as in Figure 2.3b) by evaluating (2.3.6). Using (2.3.12) allows to find the required PFR to comply with the frequency extrema requirement.

$$\begin{array}{ll} f_{nadir} \geq \overline{f_{nadir}} & \Delta P_{loss} < 0 \\ f_{zenith} \leq \overline{f_{zenith}} & \Delta P_{loss} > 0 \end{array} \tag{2.5.3}$$

The frequency response security maps help the analysis of a large variety of system operating conditions. The frequency adequacy requirements of power systems have been addressed by ensuring a minimum level of inertia to comply with ROCOF limits (OP2 in Figure 2.6a). This approach can be effective for particular conditions that can lead to a frequency nadir requirement that is not active. However, as it will be shown in

Algorithm 2.1: Calculating frequency extrema requirements

Data: D,P^D,ΔP_{loss},F_{DB},$\{dt,adt,frt,fr\}_{(i|i\in 1,...,N_{fr})}$,$\overline{f_{ext}}$
Result: Array sol_h with PFR values that guarantee compliance with frequency extrema requirement $\overline{f_{ext}}$

```
Initialise Ho with NH samples;
Initialise vector f_hk to store frequency values for each inertia level h and time
  step k;
Initialise vector T_h to store NT_h time values for each inertia level h, add relevant
  time steps for N_fr FR sources for all h;
Initialise vector FRR_h to store aggregated FR rate for each inertia level h, add
  aggregated response at each time step in T_h ;
Initialise vector G_h to store total FR for each inertia level h, add total response at
  each time step in T_h ;
for h = 1 to NH do
    for k = 1 to NT_h do
        Evaluate Δf_k(τ) in (2.3.6) using Ho(h), T_h(k), FRR_h(k), G_h(k);
        if |Δf_k(T_h(k))| ≤ |F_DB| and |Δf_k(T_h(k+1))| ≥ |F_DB| then
            Determine t̄_DB by solving |Δf_k(T_h(k))| = |F_DB|;
            Add t̄_DB to T_h;
            Update FFR_h, G_h to include a variable x_pfr representing the unknown
              total synchronous PFR ;
            Evaluate and store Δf_k̃(τ, x_pfr) in f_hk̃ for all k̃ ≥ k ;
        else
            Store Δf_k(τ) in f_hk ;
        end
    end
end
for h = 1 to NH do
    for k = 1 to NT_h do
        if dΔf_k(τ)/dt = 0 for τ ∈ [t^k, t^(k+1)) then
            Evaluate (2.3.12) using f_hk and solve Δf_k^ext(x_pfr) = f̄_ext for x_pfr;
            Store solution x_pfr into sol_h ;
        else
            continue ;
        end
    end
end
```

the next section, there may be many operational settings in which the nadir requirement is conditioning the combined amount of PFR, FFR and inertia necessary to stop the frequency excursion (OP1 and OP3 in Figure 2.6a), which neither the ROCOF constraint nor the QSSF constraint can adequately address.

In general, the FRSM allow categorising a low-inertia power system in a very straightforward way. High inertia systems are typically constrained by the QSSF requirements that are independent of the system inertia, i.e. the secure area is bounded by the horizontal line (OP4 in Figure 2.6a). However, when transitioning towards lower inertia systems, both the frequency nadir limit (the red curve) and the ROCOF limit (the vertical line) may become binding (see Figure 2.6b). Since the secure area for low inertia systems is bounded by both the frequency nadir and ROCOF requirements, the scheduled FR must therefore be higher than the QSSF requirement whilst also taking into account the current system inertia.

2.6 Case study applications

To demonstrate the graphical approach to frequency security illustrated above, three case studies are presented in this section. In particular, the first case will be based on the whole National Electricity Market (NEM) to exemplify one type of analysis that can be conducted on the maps and highlight the effect of specific parameters. Then, the specific case of South Australia will be presented to explain the critical impact of the available level of system inertia, the contingency size, and the minimum frequency nadir requirements on the secure operation of the system.

2.6.1 Case study I: Low-frequency events in the National Electricity Market

The first case study application focuses on the NEM before the deployment of the large battery energy storage systems (BESS) in South Australia, hence no fast frequency response (FFR) is available to support a contingency event. This case study was presented in [35]. The NEM operates in a system that stretches from the northeast to the south side of Australia, a distance of over 5000 km. It includes several interconnected states, namely Queensland (QLD), New South Wales (NSW), Tasmania (TAS), Victoria (VIC) and South Australia (SA), supplying ca. 9 million customer points and generating over 200 TWh in 2016. In particular, South Australia (SA) is characterised by a large penetration of wind and solar PV technologies, with more than 2200 GW of aggregated installed capacity and a peak demand close to 2800 GW [36–38]. South Australia is connected to the rest of the NEM system through two interconnectors, a 650 MW high-voltage alternating current (HVAC) link (Heywood) and a 220 MW high-voltage direct current (HVDC) link (Murraylink).

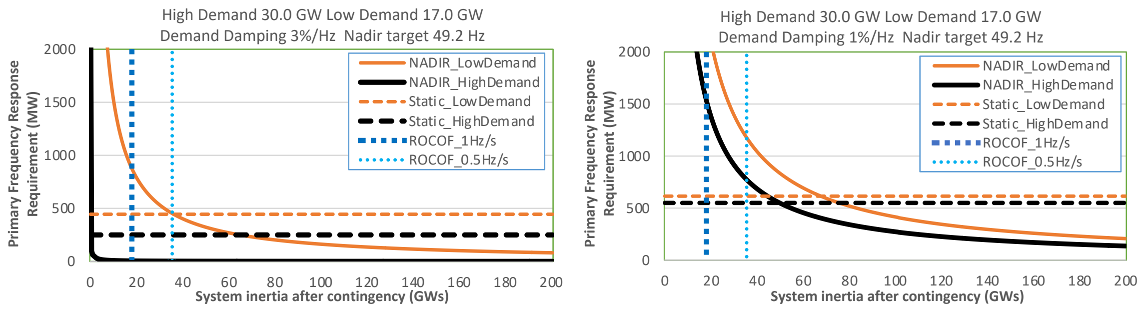

(a) Load damping factor 3%/Hz.

(b) Load damping factor 1%/Hz.

Figure 2.7 Frequency response security map for the NEM for high and low demand levels and a nadir target of 49.2 Hz.

2.6.1.1 NEM-level frequency response security maps

In this case, the minimum information necessary to represent constraints (2.5.1) and (2.5.2) in a security map for the NEM is the level of demand, contingency size, load frequency damping factor, as well as the maximum level of ROCOF and desired QSSF target. Then, the nadir constraint (2.5.3) requires a frequency nadir target an also specific information regarding the control characteristics and types of generators providing the PFR. In the NEM, the PFR requirements for the frequency nadir effectively correspond to the 6 seconds raise FCAS, while it is assumed that the PFR requirements for QSSF correspond to the 60 seconds raise FCAS [39, 40].

The largest generation contingency considered for the NEM is the outage of the Kogan Creek Power Station, which consists of one coal-fired unit of ca. 700 MW. This unit is reported to have very low variable cost of operation [9], supporting the assumption that it will likely be online and operating at full capacity in both high- and low-demand periods.

The FCAS presented in Figure 2.7a and Figure 2.7b consider a frequency nadir limit of 49.2 Hz and QSSF target of 49.5 Hz. Two ROCOF limits are considered, namely, equal to 1 Hz/s and 0.5 Hz/s. It is also assumed that the frequency control scheme has an activation dead-band of 150 mHz. As reported by AEMO, the NEM has a load damping factor of 3%/Hz [41]. This is the parameter used to plot Figure 2.7a. However, the load damping factor, which expresses the dependence of the active power demand on the frequency, may be expected to decline over the next years due to more and more power electronic-connected devices. Hence, a case of load damping factor equal to 1%/Hz was also considered in Figure 2.7b.

In Figure 2.7a, the frequency response security map for NEM for high and low demand levels (the corresponding loads are 30 and 17 GW, respectively) is presented. It can be seen that during high demand periods, the nadir requirement does not get active under any condition of PFR and inertia; for that load level, the ROCOF limit and the static frequency requirement define the (synchronous) resources required to provide secure operation. The inertia requirements for a contingency of 700 MW due to a ROCOF limit of 0.5 and 1 Hz/s are 35 and 17.5 GWs, respectively. The static requirement is 250 MW during periods of demand close to 30 GW. If the demand level decreases, the relief coming from the load also decreases, which leads to higher requirements for inertia and PFR to ensure the excursion of frequency after contingency is contained within the predefined limit. In Figure 2.7a it can thus be observed that the nadir and static requirements for low demand periods increase substantially. If the ROCOF limit is set at 1 Hz/s, keeping the frequency nadir above the limit would require 17.5 GWs of inertia (complying with the ROCOF constraint) and 870 MW of PFR to be delivered within 6 seconds after the contingency. On the other hand, if the ROCOF limit is set to 0.5 Hz/s, a PFR-inertia combination that can prevent the frequency from dropping below 49.2 Hz could be to allocate 35 GWs of inertia and 445 MW of PFR. This operational point is also at the intersection with the PFR requirement for QSSF.

The security requirements change radically if, *ceteris paribus*, the load damping factor decreases, as can be appreciated in Figure 2.7b. In this case, a less frequency-responsive load can have a substantial impact on the frequency response requirements. For example, considering the low demand case again, for a ROCOF limit of 0.5 Hz/s, the inertia level has to stay above 35 GWs, as before. However, now the corresponding PFR requirement to also meet the 49.2 Hz nadir limit increases to above 1100 MW. Alternatively, a larger inertia level could be scheduled in the system in order to decrease the PFR requirement to comply with frequency nadir. For example, for a system inertia level of about 50 GWs, the nadir-driven PFR requirement is about 750 MW.

2.6.1.2 South Australia frequency response security maps

Let us now analyse an example for SA. The objective here is to ensure its secure operation either under two conditions: the loss of a generator while SA is islanded from the NEM and following the loss of the Heywood interconnector while it is transferring energy from Victoria to SA. The case under analysis refers to 2035 with a contingency of 200 MW, which corresponds to:

- the approximate loading level of the largest synchronous generation unit during low demand level (which is set at 1.2 GW for this analysis [42]) and high levels of VRES, while SA is disconnected from the NEM. This may, for example, correspond to night-time periods with high wind generation output, or
- the maximum import (SA usually exports energy to VIC) level through the Heywood interconnector expected for that year [42].

For a contingency of 200 MW, the frequency response security map for South Australia, considering a load damping factor of 2%/Hz, target nadir levels of 48.8 and 49 Hz, and ROCOF of 1 Hz/s and 0.5 Hz/s, are presented in Figure 2.8a. As a reference of the resources potentially available in South Australia, let us consider the current generation fleet and corresponding level of available synchronous inertia. Using again average inertia constant and power factors equal to 5 s and 0.85, respectively, and considering a total installed capacity of 2.8 GW of either combined cycle gas turbine (CCGT) or open cycle gas turbine (OCGT) units, the inertia currently available in SA totals about 16.5

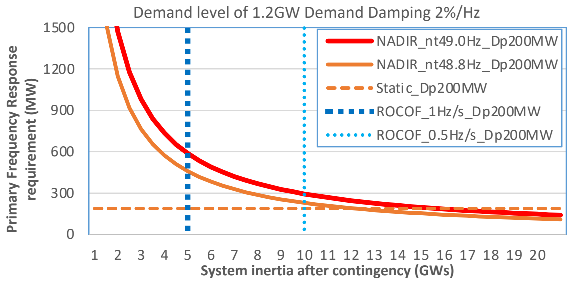

(a) Contingency (Dp) 200 MW
nadir (nt) 48.8/49.0 Hz and ROCOF 0.5/1.0 Hz/s.

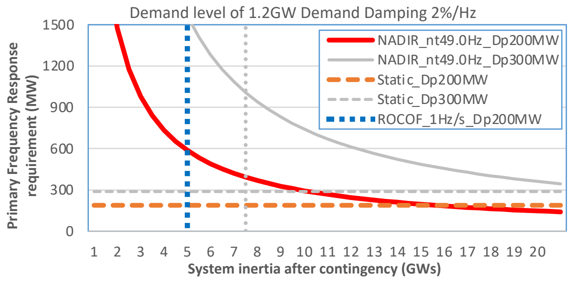

(b) Contingency (Dp) 200-300 MW
nadir (nt) 49 Hz - ROCOF 1 Hz/s.

Figure 2.8 Frequency response security map for South Australia for a demand level of 1200MW and a load damping factor of 2%/Hz.

GWs. Considering the synchronous inertia provided by type I and II wind turbines within the subsystem [19], the aggregated inertia in SA could rise over 20 GWs.

As an example of possible operational arrangement, let us now consider the case, during low demand condition and equivalent wind availability of 650 MW or more, in which, after the contingency, there are two CCGT and two OCGT units online operating at an aggregate minimum stable generation level equal to 350 MW. The corresponding aggregated inertia would be close to 5.5 GWs, which would lead to a PFR requirement of around 530 MW for a nadir limit of 49.0 Hz. This figure is larger than the idle spinning capacity available from the four online synchronous units. Hence, it would not be possible to meet the security constraints under these conditions securely. A possible mitigation option could, for example, be to bring online another synchronous unit in order to increase inertia and decrease the PFR requirements, at the cost of either decreasing the import or curtailing some wind energy. Another option could be to relax the nadir requirement down to 48.8 Hz, aiming for 420 MW of PFR. However, the actual feasibility of the considered synchronous generator to provide that level of PFR would need to be assessed further. If type I and type II wind turbines were present at this period of low demand, the online inertia might increase up to 9.5 GWs, which makes the PFR requirements for 49.0 Hz and 48.8 Hz nadir drop to 310 and 240 MW, respectively. These PFR levels appear more achievable for the four online synchronous machines that were assumed online. Such inertia level would also allow keeping ROCOF closer to 0.5 Hz/s.

In order to study the significant effect of the contingency size on the frequency response adequacy of the system, Figure 2.8b shows the SA security map for a nadir limit of 49.0 Hz and the same demand and load damping levels as before, with nadir, static and ROCOF constraints for contingency levels of 200 MW (as before) and 300 MW. It is straightforward to appreciate that for the 300 MW contingency case, the secure region moves towards the upper right side, increasing the requirements on PFR and inertia for all constraints. The ROCOF and static constraint increase proportionally to the contingency size (50%). On the other hand, the nadir-driven PFR requirement for a given level of inertia become much more demanding, with an increase in the order of 130% with respect to the 200 MW contingency. For example, to meet all the frequency

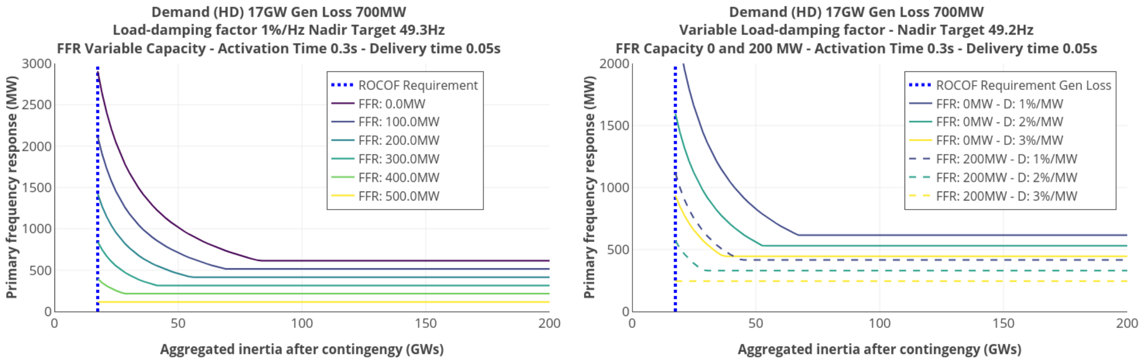

(a) FFR response capacity.

(b) Demand damping effect.

Figure 2.9 Frequency response security maps for the NEM considering a maximum generation loss of 700 MW and different availabilities of FFR and demand damping.

stability requirements with a contingency of 300 MW, not only the minimum inertia level due to a ROCOF limit of 1 Hz/s needs to increase from 5 GWs to 7.5 GWs, but also the nadir-driven PFR increases from 580 MW to a potentially prohibitive level of more than 1100 MW. Under these conditions, either the contingency size is decreased (for example, by reducing the import level through the interconnector), or other means need to be sought, such as synchronous condensers, FFR, etc.

2.6.2 Case study II: Effects of fast frequency response parameters on frequency security adequacy

The impact that fast frequency response sources like the Hornsdale BESS [6] has on the allocation of inertia and frequency response from synchronous units can be conducted in a systematic way based on the model presented on equations (2.5.1), (2.5.2) and (2.5.3). Hong et al. [43] present a similar analysis of FFR parameters on frequency control. By looking only at generation contingencies and condensing the nadir and QSSF requirements in one series of data, it is possible to plot the changes in the aggregated synchronous headroom for different amounts of FFR available capacity, as seen in Figure 2.9a. This considers an activation time of 300 ms and a delivery time of 50 ms, which is in line with the parameters presented in [14] for FFR coming from a BESS system, and in general, for any FFR source with similar activation and delivery times.

It is interesting to highlight that the available FFR capacity has a great impact on the allocation of frequency response resources, in particular during periods of low inertia, where 100 MW of FFR can replace up to 800 MW of PFR. In high inertia regimes, the effect of 100 MW of FFR on FCAS allocation is the equal reduction of synchronous PFR resources, as it can be expected from equation (2.5.3).

It is also relevant to provide a reference to the effect on the system's frequency response of demand's natural response to frequency changes. As stated before, this characteristic is expected to reduce in the future as more demand is connected to the grid through power electronic interfaces. As the natural response reduces, the required

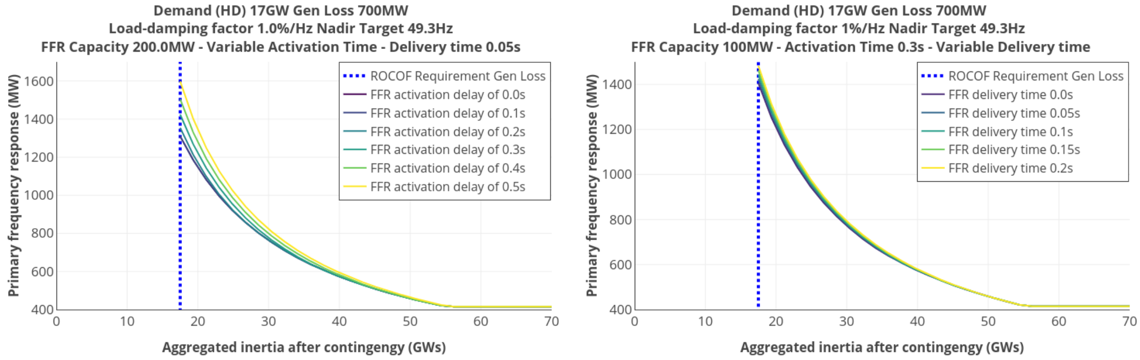

(a) FFR activation time. **(b)** FFR delivery time.

Figure 2.10 Frequency response security maps depicting the effects of the activation delay and the activation speed.

amount of synchronous PFR increases, both with and without FFR resources available to provide frequency response, as shown in Figure 2.9b.

There is an ongoing discussion about the extent to which FFR sources can replace the inertial response of synchronous machines to avoid nadir problems. The ability of FFR sources to inject a large amount of energy in an opportune fashion into the system is directly linked to its ability to measure frequency and ROCOF. Measuring these quantities with precision is not a trivial problem [44], and it is critical to be capable of identifying real events in a well-timed manner. The effect on the activation delay of FFR resources (which includes the measuring delay) is depicted in Figure 2.10a, for a range of delays between 0 and 500 ms. The difference between PFR allocation for the inertia level of the ROCOF requirement (17.5 GWs) varies up to 300 MW only due to an activation delay of 500 ms.

The same exercise is conducted for the delivery time, for a fixed activation delay and FFR capacity. After activation, BESS systems are capable of delivering all its capacity in a short period, reported to be circa 40 ms [14]. Figure 2.10b depicts the effects of delivery times between 0 and 200 ms on PFR allocation. It can be seen that the delivery times considered do not radically impact the allocation of PFR, with a difference of about 80 MW between the fastest and slowest delivery time under consideration, for the minimum inertia level of the system.

2.6.3 Case study III: August 2018 separation event analysis

The following section describes the application of the frequency response security maps to understand the sequence of events that led to the separation of the NEM into three different islands. NEM spans over the states of Queensland (QLD), New South Wales (NSW), Victoria (VIC), South Australia (SA) and Tasmania (TAS), as depicted in Figure 2.11. The different states are connected through a radial network of HVAC and HVDC interconnectors. In August 2018 [45], the interconnector between Queensland (QLD) and New South Wales (NSW) tripped after being hit by lightning, leading to an

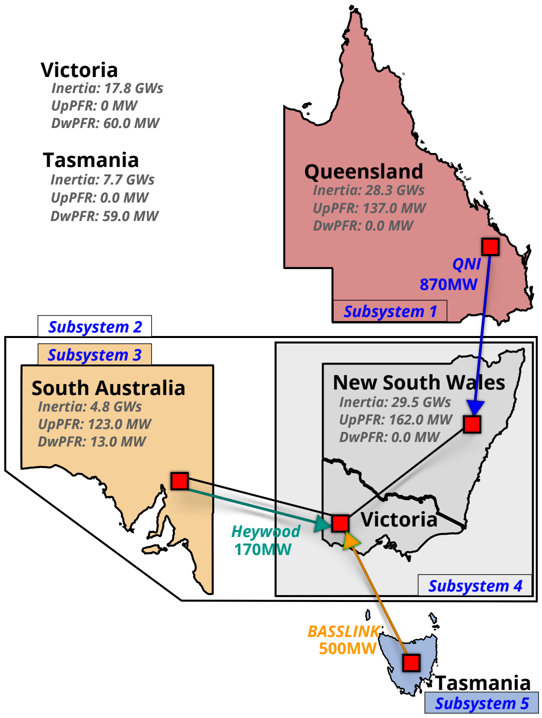

Figure 2.11 Australian NEM map displaying pre-event estimated inertia, PFR allocation per area and relevant interconnector flows.

imbalance of 870 MW in the sending area (QLD) and 857 MW in the receiving subsystem. The resulting equivalent load and generation contingencies in the sending and receiving ends, respectively, were larger than the expected maximum contingencies for the intact system. On top of that, inertia in each subsystem was smaller than in the intact system creating the conditions for large frequency deviations. As a matter of fact, the separation event under analysis triggered the activation of load shedding in various areas of the system and the subsequent tripping of the interconnector between South Australia (SA) and Victoria (VIC), which at the time was transferring 430 MW.

In this case study application, the event's conditions, responses activated, and frequency behaviour are used to show the flexibility of the frequency response security maps (FRSM) and their potential not only to understand the system limits and requirements from the point of view of frequency response but also to help the ex-post analysis of events. The system dispatch by area and technology before the event is presented in Table 2.1. This dispatch can be translated to inertia per area using referential values by technology, resulting in the values presented in the last row of the table.

The inteact system's pre-event frequency response security map considers that the largest generation and load contingencies are 750 MW and 500 MW, respectively. The resulting requirements are presented in Figure 2.12. The aggregated frequency response allocated for generation events (raise) and load contingencies (lower) is determined to comply with quasi-steady-state frequency requirements. The FRSM is calculated considering a system-wide demand damping factor of 3%/Hz (this value might be slightly overestimated because Tasmania has a demand damping factor of 2%/Hz [46]). QSSF requirements are set to 49.5 Hz and 50.5 Hz for low- and high-frequency events, re-

Table 2.1 August 2018 pre-event dispatch (power in MW, inertia in GWs)

Technology	QLD	NSW	SA	VIC	TAS	Total NEM
Black Coal	5690.1	5919.5				11609.6
Brown Coal				3777		3777
Gas	215.1	0.21	807.8	0.24	202	1225.4
Wind	1.7	94.2	129.2	7.7	43.5	276.3
Hydro	52.1	343.2		0.12	1386.4	1781.9
*Other	0.22	0	0.02			0.24
Utility scale PV	286.1	96.96	88.65	38.4		510.1
Rooftop PV	1043	526	600	862	65	3096
Total (MW)	7288.3	6980.1	1625.7	4685.5	1696.9	22276.5
Inertia (GWs)	28.29	29.47	4.75	17.78	7.71	88

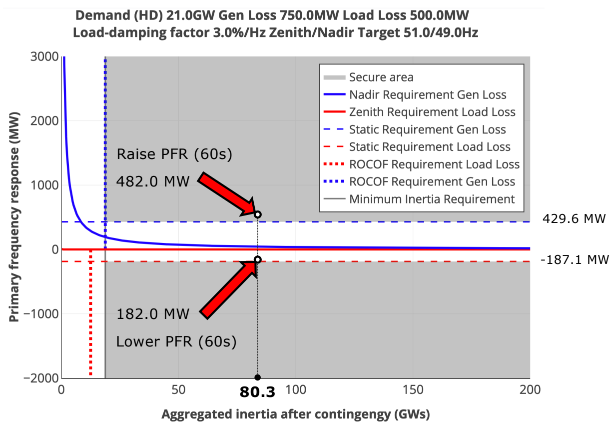

Figure 2.12 FRSM for the system considering maximum load and generation contingencies.

spectively. The system's frequency control ancillary services for containment (6 seconds window) and recovery (60 seconds window), known as fast and slow services in Australia, at the time of the event were allocated as presented in Table 2.2.

As it can be seen in Table 2.1, right before the event, the output coming from non-synchronous technologies was only 17% due to low wind at that time, giving space to relatively high levels of inertia (over 80 GWs). From Table 2.2, it is possible to confirm that the allocated frequency response varies largely between areas and it is allocated based on the system's requirements and not on potential local issues. In the following sections, the loss of the interconnectors is analysed, to explain how the different areas were able to keep operating despite the fact that there were not nearly enough market-enabled resources to respond to the massive equivalent contingencies produced by the disconnection events. It is relevant to point out that inertia calculations are not precise due to the lack of access to unit's parameters and the neglect of inertia coming from demand; however, the majority of the assumptions behind this study are supported by official reports produced by AEMO [45].

Table 2.2 Frequency control ancillary services allocated before the event (in MW)

Service	QLD	NSW	SA	VIC	TAS	Total NEM
Lower 6s	0	0	13	0	59	82
Raise 6s	137	162	123	60	0	482
Lower 60s	0	10	59	40	73	182
Raise 60s	155	150	128	49	0	482

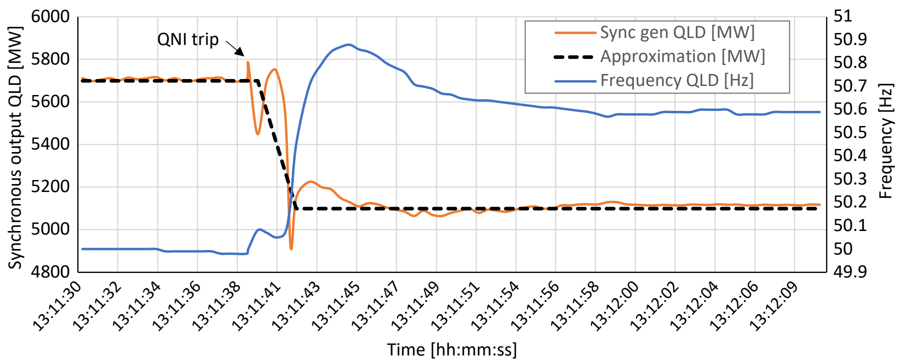

Figure 2.13 Non market-enabled lower synchronous response in QLD (Source [45]).

2.6.3.1 Queensland-New South Wales interconnector - QNI

At the time of the weather event that led to the loss of QNI, Queensland, labelled as Subsystem 1 (S1) in Figure 2.11, was exporting 870 MW to New South Wales. Subsystem 2 (S2) was, in turn, receiving 857.0 MW due to active losses in the transmission lines. The loss of the interconnector represented an equivalent load contingency in S1 and a generation contingency in S2.

S1 had no fast or slow market-enabled lower frequency response resources in place. Despite this, the area was able to control frequency excursion, leading to a frequency zenith of 50.9 Hz and a QSSF of 50.6 Hz[2]. This was possible due to the governor-based response coming from synchronous technologies (units with active droop control settings that did not participate in the FCAS market) and active power control response in place in gird-connected PV and rooftop PV systems. As presented in Figure 2.13 for the synchronous lower response in QLD, the responses coming from different technologies can be approximated as linear ramps with corresponding delays and speeds of response, hence making it possible to use the multi-service frequency response modelling presented in Section 2.3. The response developed by rooftop PV systems is not straightforward to be described since it can only be deduced from the change in demand, and, considering the information available, it is not possible to isolate it from other phenomena affecting demand at the time of the event (e.g. changes in demand due to changes in frequency).

Figure 2.14a shows the effect of the two responses described here. It is easy to see that the surprisingly quick governor-based response coming from synchronous technologies

[2]It is important to highlight that this QSSF is higher than 50.5 Hz, which is the target frequency after containment.

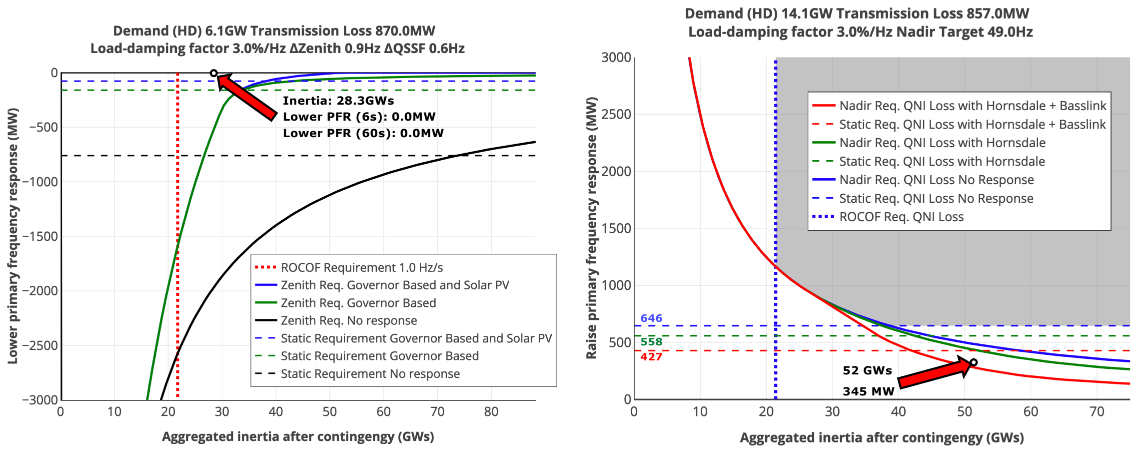

(a) FRSM Queensland. **(b)** FRSM Subsystem 2.

Figure 2.14 Frequency response security maps (FRSM) for the loss of Queensland-New South Wales interconnector (QNI).

had a tremendous impact in allowing the subsystem to control frequency. The role of PV enabled response was not relevant for the level of inertia at the time of the event, given its significant activation delay. The area's inertia level led to a frequency excursion with a rate of change of frequency lower than 1 Hz/s.

Considering the errors in the calculation of inertia, it is possible to use the FRSM of Figure 2.14a to highlight the influence of rooftop PV response during the event, which certainly had an effect on controlling frequency. Preliminary estimations of AEMO point to a response capacity between 200 and 250 MW coming from these systems, which is in line with the FRSM.

The loss of QNI also produced a major deviation of frequency in S2. The FRSM for that area is presented in Figure 2.14b. Subsystem 2 is composed by NSW, VIC and SA; TAS could be considered as part of any subsystem that contains VIC because, during this event, it never becomes isolated. However, here it is modelled as a separate subsystem because it is connected through an HVDC link that decouples inertial response. However, the HVDC link, known as Basslink, does provide frequency response to mainland Australia. At the time of the dismembering of QLD there were two responses of interest reacting to S2's frequency deviation, namely Hornsdale battery and Basslink responses.

Although the responses from Basslink and Hornsdale battery[3] were relatively slow (delays close to 3 seconds), the high inertia levels generated a lower rate of change of frequency and allowed more of the response to impact frequency excursion. Frequency in Subsystem 2 never stabilised because the subsystem split again before frequency could reach nadir, let alone quasi-steady state. Hence, the map is built considering a frequency nadir of 49.0Hz, and it shows that the allocated raise response (345 MW) within the sub-

[3]This delay in response after the loss of QNI results from measurement delays and, more importantly, from the interaction of high inertia conditions and the battery's frequency dead-band (150 mHz). The effect of the amount of inertia on the activation delay can be compared in Figure 2.16 for the response of the battery at the time of the trip of QNI and Heywood. The ROCOF in the second trip is substantially more pronounced, which takes the frequency outside of the dead-band faster, which leads to a short activation delay.

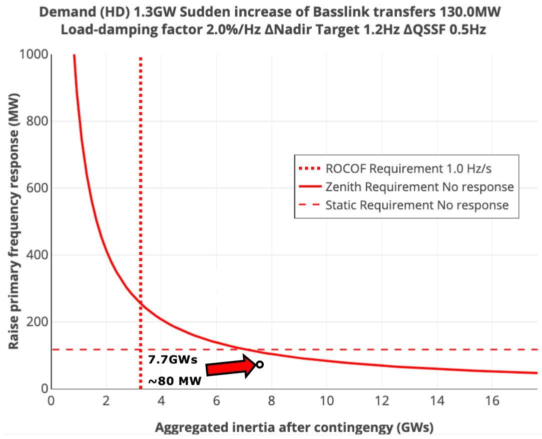

Figure 2.15 FRSM Subsystem 5 after the loss of QNI.

system was enough to comply with it but not enough to bring the frequency back to 49.5 Hz, which required 427 MW.

Given the sudden increase of the transfers through Basslink (speed of provision of the 130 MW was very high), this generated an imbalance in Tasmania or Subsystem 5, equivalent to the sudden loss of a generator (more load than generation). The frequency in Tasmania started to drift down, up to the activation of under frequency load shedding (UFLS) at a frequency level of 48.8 Hz. The FRSM for S5 after the contingency is presented in Figure 2.15, which considers a nadir of 48.8 Hz and a load damping factor of 2%/Hz, as reported by AEMO [46]. No market-enabled raise frequency response capacity was present in Tasmania at the time of the increase of transfers through Basslink. To avoid triggering UFLS over a 100 MW of raise FCAS would have been necessary, but the subsystem was able to activate only around 80 MW of governor-based raise response, which led to the activation of 81 MW of UFLS, stopping the frequency drift and allowing it to get back to the vicinity of the nominal band.

2.6.3.2 South Australia-Victoria interconnector – Heywood

The frequency excursion in Subsystem 2 put pressure on the Heywood interconnector, which started experiencing oscillations in its power flow, to a point where the protection system of Heywood deemed that the transfer was insecure and disconnected the line. South Australia is also connected to Victoria through an HVDC link, Murraylink; this interconnector did not play any role during the events of August 25th since it was transferring 18 MW and did not provide any response to frequency changes in the interconnected areas. For the sake of the analysis presented here, the loss of Heywood created two new subsystems, Subsystem 3 (S3, South Australia) and Subsystem 4 (S4, VIC-NSW).

At the time of the disconnection of Heywood, the frequency in South Australia was 49.15 Hz, as seen in Figure 2.16. South Australia was exporting 430 MW at that point, which had the equivalent effect of a load contingency within S3, producing a new imbalance that led to a rise in frequency that reached a zenith of 50.45 Hz. This corresponds

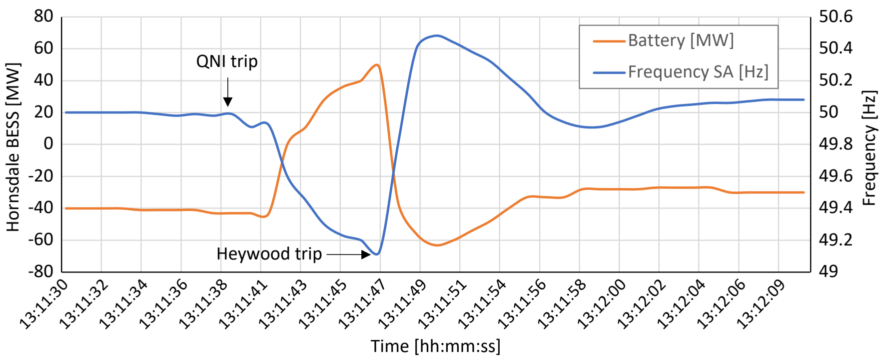

Figure 2.16 South Australia frequency and Hornsdale BESS response [45].

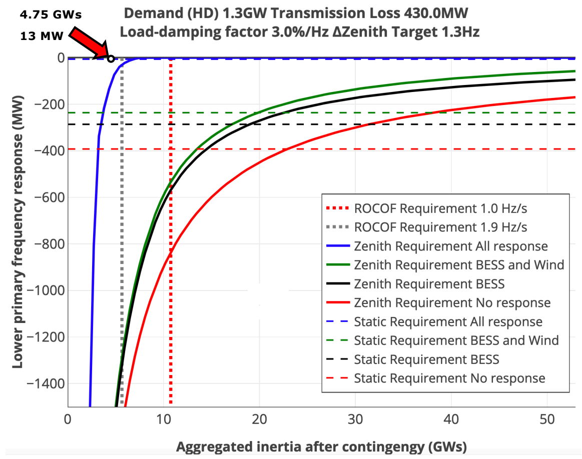

Figure 2.17 FRSM Subsystem 3 after the loss of Heywood.

to a change of 1.3 Hz in the local frequency due to the loss of interconnection. After reaching the zenith, the frequency stabilised around 50.1 Hz, that is at 0.95 Hz from the initial frequency. With this information it is possible to build the FRSM for South Australia to review the effects of different responses experienced after the disconnection. This information is presented in Figure 2.17.

Three primary responses explain the containment of the high-frequency event that was triggered by the loss of Heywood: non-market-enabled governor-based synchronous response, the response of Hornsdale battery, and unintended wind turbines response. In addition, the subsystem experienced the response of transmission connected PV, but it was slow, and it did not impact frequency excursion, therefore it has not been considered in the FRSM. Also, rooftop PV responded to the event, but as with distributed PV in Queensland, it is not possible to isolate the actual response to assess its effect on frequency.

It is important to highlight that the inertia in South Australia was low at the time of the event. This led to a rate of change of frequency (ca. 1.9 Hz/s) after the event that was higher than the 1.0 Hz/s that is usually deemed the maximum allowable ROCOF.

It can be seen that the effect of the wind response on frequency is rather low. On the other hand, the Hornsdale battery is responding by changing from charging to discharging mode, with an equivalent response capacity of -106 MW. The synchronous units reduce their output quickly, reaching an aggregated reduction of 330 MW and rapidly increasing 100 MW again. This response is modelled as the superposition of lower and raise responses, and it has a great impact on frequency control after a contingency which is large for a relatively small subsystem like SA. The aggregated effect of all the responses yields a requirement on lower primary frequency response which closely matches the available inertia and allocated FR[4].

This case study application has shown how the FRSM can be utilised to analyse complex frequency events. The disconnections of QNI and Heywood show how the FCAS allocation at system level was not prepared to cope with large equivalent contingencies associated with the dismembering of the system. However, despite these contingencies, the different subsystems did not suffer blackouts (only relatively small amounts of load were lost due to frequency load shedding activation). This shows that many synchronous units responded to the event without being FCAS market participants at the time of the event; this situation is explained because of the existence of many units around Australia that have not modified their old droop control settings since the creation of the market.

2.7 Chapter summary

This chapter presented the theoretical foundations necessary to study the frequency response characteristic of a system. A single-mass multi-service frequency response model was introduced, and a set of conditions were presented to guarantee frequency security in low-inertia power systems; these conditions can be translated into what this work calls the frequency response security map, an artifact that allows to graphically analyse frequency security by comparing different operation points for the system. Finally, several study cases on frequency response adequacy using frequency response security maps were also presented.

[4] If the effect of rooftop PV is considered and inertia was slightly underestimated, the requirements and available resources could match.

CHAPTER 3

Security-constrained operation of weakly interconnected low-inertia power systems

3.1 Introduction

This chapter presents a scheduling model in the form of a unit commitment (UC) that integrates the necessary elements to support the ex-ante consideration of the frequency response constraints presented in the previous chapter. The model has been conceived to be able to analyse the effect of frequency response resources (with different response speeds) not only to cope with the largest load and generation contingencies at system level but also for a system with different inertial subsystems (subsystems connected only through HVDC lines), and the potential for the system to split into multiple subsystems after the loss of interconnection, which in turn can become the largest load or generation contingency in the subsystem.

The current trends in power system operation around the world [7, 44, 47], indicate that containing frequency deviations is becoming increasingly challenging, in particular for isolated power systems. This reality is putting pressure on frequency control markets, which have seen a substantial increase in payments in recent years (see Figure 1.1). As inertia decreases, the largest contingency a given system can experience does not necessarily reduce, requiring larger shares of frequency response to stop frequency events. Although balancing and frequency control reserves have been considered in UC models [48, 49] before VRES dominated low-inertia power systems were a subject of interest in research [50–52], in recent years, the interest in this problem has seen a substantial increase due to the economic impact of doing a conservative allocation of FR and the security implications of not allocating the right amount of response. On top of this, the emergence of FFR resources [14] has created an additional layer of complexity in the economic allocation of frequency control ancillary services. In order to cover the current state-of-the-art in security-constrained scheduling of low inertia power systems, the literature review is split into three categories, namely, frequency extrema constraints, the role of fast frequency response, and multi-area considerations.

Finally, it is essential to highlight that this UC model will become an integral part of the expansion model presented in Chapter 5. The different features of the UC model are implemented through purely linear expressions so that they can be used in economic dispatch engines like the one used by AEMO to clear the market in every trading period.

3.1.1 Frequency extrema constraints in scheduling models

The integration of large shares of wind and solar power in various power systems worldwide is impacting the levels of inertia, who have the mandate to operate the system within strict boundaries for frequency and under cost minimisation targets. The portfolio of dispatchable resources that can respond to frequency events includes synchronous units providing an inertial response, units providing PFR and technologies capable of delivering FFR. As inertia decreases, the allocation of FR resources is transiting from being based on balancing back [46] the system after the contingency to being calculated on other metrics such as the ROCOF [53] and frequency nadir or zenith [54]. This requires finding adequate models to represent those metrics as a function of the different FR resources and other variables determining frequency excursion after contingency.

Historically this topic of research has relied on dynamic simulations of the system to derive requirements on frequency response at scheduling level [55–57]. Recently, there have been various efforts to derive expressions for frequency nadir independent of system-specific dynamic simulations; [58] presented a conservative approximation for the requirements on frequency response to limit frequency nadir that neglected demand damping and also uses a predefined operation point that fixes the available inertia in the system (also similar to [59]). Ahmadi et al. [60] included the effects of demand-damping and represented the non-linear constraint for frequency nadir through a piecewise linear approximation in a mixed-integer linear problem. The work in [25] introduced a modelling approach to assess PFR requirements and inertia to limit frequency nadir in low-inertia systems, based on the analytic solution of the equivalent single-mass model of the synchronous units in the system and considering demand damping, all of this in the context of a stochastic unit commitment model. A more detailed representation of the dynamic parameters of the units providing reserve is introduced in [61] to improve the quality of the frequency response constraints. Recently, [62] presented a computationally efficient approach to introduce the nadir constraint in the stochastic unit commitment without the need to approximate the surface using multiple linear constraints.

These works on frequency response constraints representation and security-constrained scheduling of power systems enabled further studies into different aspects of frequency response in low-inertia systems. Already introduced in the previous chapters [5, 35] studied the frequency response adequacy of the NEM in future scenarios. References

[63, 64] assess the impact of the electrification of transport on the provision of ancillary services in power systems with a high share of renewable energy sources. A broader look into the benefits of demand-side response (electric vehicles and heat pumps) from the point of view of flexibility considering frequency response constraints is presented in [65]. An initial assessment of the value of storage systems from the point of view of frequency security is presented in [66], however, this approach does not capture the fast response that batteries (and other technologies) can provide. Since the FFR feature is so relevant, the different works that have addressed this challenge are presented in the next section.

3.1.2 The role of fast frequency response

Fast frequency response is becoming a critical service in systems like the NEM, so the UC model has to incorporate this feature to represent system operation more accurately. FFR has been leveraged by the deployment of battery energy storage systems. On top of their inherent flexible nature that allows them to create value by charging and discharging energy to cover generation and load energy surpluses, their inverters and control strategies allow providing faster response than conventional synchronous units can due to their mechanical limitations. Representing this capability in a scheduling model is critical to achieving an efficient dispatch that will use the quick response capacity of BESS, pre-curtailed PV or any other technology capable of producing a rapid response when the system is subject to frequency deviations.

The UK recently introduced the market for enhanced (fast) frequency response, which triggered the development of different approaches to account for two different contingency services in the unit commitment problem [67, 68]. Both approaches consider two frequency response speeds and include the effect of the load damping factor. Zhang et al. [26] considers multiple response speeds for adequacy studies, but the solution is found iteratively rather than in a single problem cast as a MILP. Multi-service frequency response has been considered in [69] through a conservative approach ignoring demand damping. More recently, [70] presented a set of constraints to represent a finite portfolio of frequency response services, also neglecting the effect of demand damping under the assumption that the frequency responsive demand will reduce drastically in the future.

In this context, the focus of this work requires the FFR modelling to be able to consider the impact of demand-damping. At the same time, it has to be flexible enough to represent multiple frequency response characteristics. Also, it is required (as it will be described in the following chapters) that the solution can be found through the use of a single MILP problem; hence no iterative procedures can be used. The existing literature previously presented here do not fully provide a solution for these requirements since it has focused only on finding closed-expressions considering only two sources of response (slow and fast). The approach taken in this work is to use the multi-service frequency response model presented in the previous chapter to sample a range of operating conditions of interest. Using those samples, a set of linear approximations is created, which then is used in the UC to constrain the frequency nadir/zenith requirements. Also, this approach allows to replace the multi-service frequency response model by any source of operation points of interest (e.g., either the results of a comprehensive dynamic model of the system or a database with historic frequency response performance of the system) that a system operator would like to use to represent the frequency response profile of the system.

3.1.3 Multi-area frequency response modeling

Since this model focuses on the behaviour of a system with multiple balancing areas that might become isolated, it is necessary to introduce the literature that has covered the topic of constraining a system to withstand frequency events affecting multiple areas. Isolated systems like Australia have been experiencing particularly tight operation conditions due to the relative reduction of inertia and FR resources becoming very limited, not only at system level but in particular in specific areas [1]. As presented in Section 2.6.3, recent contingencies involving interconnectors in the eastern Australian power system (NEM) have exposed the degradation of frequency response adequacy for both high- and low-frequency events, activating under frequency load shedding, and resulting in two or more islands. In this case, the resulting equivalent load and generation contingencies in the sending and receiving ends, respectively, were larger than the expected maximum load and generation contingencies for the intact system; furthermore, the inertia level in each of the two separated areas was of course less than in the whole system, thus potentially causing FR issues. The allocation of frequency response resources in low inertia systems that might split has not been widely studied. For the specific event experienced in Australia in 2018, [71] introduces the dynamic assessment of the dismembering of the system and an analysis of the role played by BESS to support the system during cascading events. Recently, [72] studies the over- and under-frequency dynamics after a system split where inverter-based generation dominates. However, these studies consider a predefined operation point, and they ignore the economics of the allocation of frequency response resources.

The groups that have been developing most of the research on frequency response constraints for scheduling purposes are now concentrated in the multi-area modelling of frequency response constraints but always assuming that the system remains intact. The focus is then put on modelling how the frequency evolves in each area individually to derive the constraints that can command the economic allocation of resources. The evolution of frequency after contingency in a multi-area system with a heterogeneous distribution of inertia and frequency response resources has been studied in various works, for instance, [73–75]. At the time of development of this literature review, the first attempts to develop constraints for scheduling purposes aiming to limit frequency

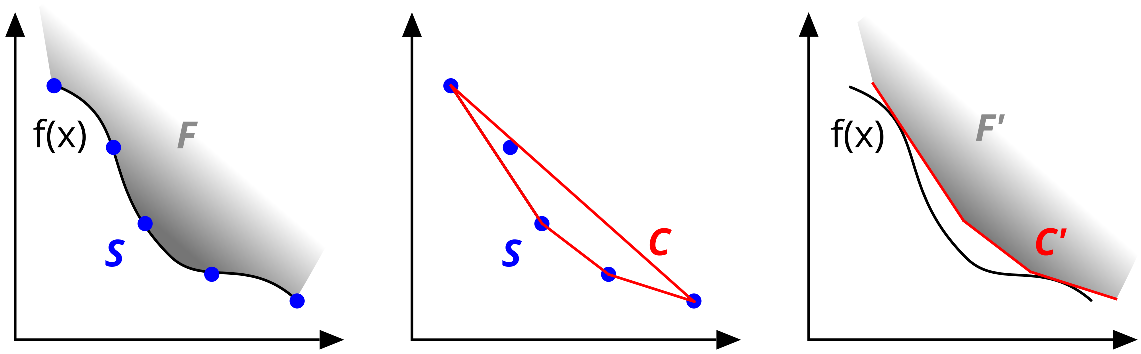

(a) Sampling. **(b)** Convex hull calculation. **(c)** Robust convex approx.

Figure 3.1 Linearisation strategy for the frequency nadir/zenith constraints.

evolution in each area to the technical requirements are still undergoing peer review [76, 77].

Recently, [29] presented an optimal power flow model capable to allocate inertia and PFR to contain frequency after isolation events. Püschel-Løvengreen et al. [29] introduces many of the features of the model presented in the following sections, and its case study application is included in Section 3.4.2.

3.2 Linear approximation of frequency extrema constraints

The security-constrained unit commitment model introduced in this chapter is cast as a mixed-integer linear problem. As presented in the previous chapter in Section 2.3, the derivation of frequency response constraints for multiple sources of FR provision results in strictly linear formulations for ROCOF and QSSF, but frequency extrema requirements yield convoluted expressions that result in a non-linear function of inertia, contingency size and frequency response services. Therefore, before introducing the UC model itself, the linearisation of the frequency extrema constraint is discussed. The general strategy to calculate a set of robust linear constraints to be used in a mixed-integer linear problem (MILP) such as the UC problem is presented in Figure 3.1. The generalised expression to determine the amount of FR resources necessary to contain frequency extrema is used to create a sample S (Figure 3.1a) of the combination of resources that stops frequency right at the target, hence defining the frontier of the set of points F that result in a secure operation of the system. Next, the set of points is used to calculate the convex hull [78] that encloses the sampled set S (Fig. 3.1b).

The convex hull C contains several dominated hyperplanes that cut through the set F that need to be eliminated in order to get it to approximate the frontier represented by samples S. After eliminating the dominated hyperplanes, the remaining cuts are displaced independently until they robustly approximate the frontier of set F (Figure 3.1c), creating the new set of secure points F'. The resulting set of hyperplanes C' is then used to determine the schedule of resources that constraint frequency extrema for a given op-

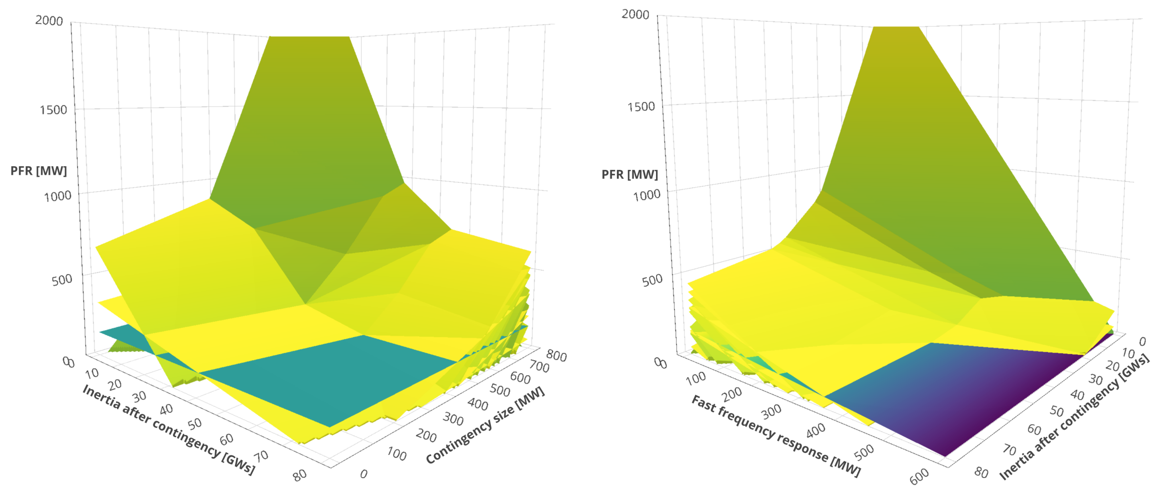

(a) FFR = 0 MW

(b) Contingency = 700 MW

Figure 3.2 Nadir surface robust convex approximation with 23 hyperplanes for mainland Australia.

erational condition. Each hyperplane ψ in the set is described by its coefficients (in this case 4 given the 4 dimensions: inertia, contingency size, PFR and FFR); this is defined for frequency nadir or zenith, as presented in (3.2.1). The underlying assumption for this approximation is that all fast responses (FFR) can be characterised with a similar activation delay and speed. Therefore all responses can be clustered together, being the total response capacity the only unknown. Similarly, all slow frequency responses will be clustered as PFR.

$$\{A, B, C, D\}_{\psi}^{nd/zh} \tag{3.2.1}$$

Figure 3.2 presents the results of applying the approximation methodology for mainland Australia (QLD, NSW, VIC, SA), considering a total demand of 20.18 GW, a demand-damping factor of 1 %/Hz and a nadir target of 49 Hz. The FFR sources are assumed to operate with the same type of response, namely 400 ms activation delay, 20 ms activation speed and up to 10 min of sustained response after reaching full deployment. In this particular case, the approximation results in 23 hyperplanes; this aspect of the methodology cannot be completely controlled, the number of resulting hyperplanes depend on the samples taken of the original surface, and the internal workings of the convex hull calculation [78], hence reducing the samples is the only way to reduce the number of hyperplanes (in this case, 18 samples entered the convex hull calculation engine). The same set of 4-dimensional (PFR, FFR, inertia and contingency size) hyperplanes is used to plot both Figure 3.2a and Figure 3.2b. Figure 3.2a shows the piecewise linear surface that results if no FFR is available to respond to a contingency. On the other hand, Figure 3.2b displays the hyperplanes that result from fixing the contingency size to 700 MW. Table 3.1 presents the numerical results for frequency nadir values for the convex hull approximation (see Figure 3.1b) and the results after displacing the hyperplanes to achieve a robust approximation (as seen in Figure 3.1c).

The strategy to approximate the frequency extrema surface can be extended in case more dimensions are considered, for instance, if there are two different FFR sources

Table 3.1 Frequency nadir (Hz) approximation (target 49.0 Hz)

	Initial convex hull approx.	Robust Hyperplanes
Min	48.8982	48.9991
Mean	49.0668	49.1545
Max	49.3279	49.3849

that are worth differentiating; this will lead to higher-dimensional hyperplanes, and it is likely to introduce more error in the linear approximation.

3.3 Security-constrained unit commitment model

The challenging aspect of modelling the secure operation of a system with interconnected areas is not only to build the functions to comply with frequency response requirements; the determination of available FR resources in each area to subsequently schedule them is not straightforward. For instance, HVDC interconnectors do not transfer inertial response from synchronous units and, depending on the control strategy, they may or may not be able to respond to imbalances by increasing or decreasing their transfers. On top of this, if interconnections are prone to fail during specific conditions, the transfer can become the largest equivalent load or generation contingency in the corresponding sending or receiving subsystem respectively, thus increasing the FR requirements in them.

The system-wide allocation of FR resources to cope with the contingencies in the system assumes that the deployment of response is feasible from the point of view of transmission. Although a thorough assessment of transient power flow feasibility requires to conduct a full dynamic simulation – which is what this steady-state model aims to avoid – in this work, this step is simplified by aiming to guarantee that the FR resources required in the area where the contingency is located can be transferred from the areas where the resources are available. To achieve this, the interconnectors' operation is constrained to maintain a short-term headroom equal to the amount of FR resources to be transferred. This requires determining the largest load and generation contingency in each area and allocate resources accordingly, considering the transfer capabilities of each interconnector.

The model description is split into four sections, namely, the base structure of the UC problem with the models for the provision of reserves for the different units, description of inertia and reserve transmission constraints, contingency definition, and description of frequency adequacy constraints.

3.3.1 Base unit commitment model

For a detailed description of the symbols used in this section, refer to the Nomenclature. The objective of the UC model is to minimise the total cost of operation, including generation costs, start-up and shut-down costs of thermal units, and also a penalty for lost load in each bus. The resulting objective function is presented below, and the UC variables are presented in (3.3.53) and (3.3.54). Although (3.3.1) introduces the different costs as generic functions of the unit's output, start-ups and shut-downs, as well as the lost load, this work considers only linear costs.

$$\begin{aligned}\min_{\vec{x},\vec{y}} \sum_{t} \Bigg(\sum_{k\in\Omega^{TH}} C_k\left(p_{k,t}\right) + \sum_{k\in\Omega^{TH}} CSU_k\left(stup_{k,t}\right) \\ + \sum_{k\in\Omega^{TH}} CSD_k\left(shdw_{k,t}\right) + \sum_{b\in\Omega^{Bus}} CLL_b\left(s^{L}_{b,t}\right)\Bigg)\end{aligned} \tag{3.3.1}$$

A central aspect of the model proposed here is the description of transmission constraints. At least the interconnectors between balance areas have to be considered in the model. In general, the approach allows for a full description of transmission based on DC power flow equations. Depending on the degree of detail of the network, clustering of units might be possible to reduce the number of binary variables and take advantage of the relaxation of integer variables, as presented in [79], where the authors show that clustering units and relaxing the integer variables greatly enhance the model's performance with a loss of precision capped at maximum 2.2%.

Every node of the system will consider a balance equation for power to cover demand, considering injections from thermal units, renewable sources, transmission exchanges, load shedding, as well as charging and discharging of storage systems as presented in (3.3.2). The DC approximation to AC transmission lines flow is determined through equation (3.3.3). The forward and reverse maximum capacity of transmission lines are modelled as presented in (3.3.4). In order to determine the transmission headroom in each direction, (3.3.5) uses explicit variables for forward and reverse transmission slack using factor φ to model the short-term emergency rating of the transmission lines.

$$\begin{aligned}\sum_{k\in\Omega_b^{TH}} p_{k,t} + \sum_{i\in\Omega_b^{RE}} p^{R}_{i,t} + \sum_{j\in\Omega_b^{BS}} \left(dch_{j,t} - ch_{j,t}\right) + \sum_{l\in\Omega_b^{LR}} fl_{l,t} - \sum_{l\in\Omega_b^{LS}} fl_{l,t} \\ = P^{L}_{b,t} - s^{L}_{b,t} \quad \forall b,t\end{aligned} \tag{3.3.2}$$

$$fl_{l,t} = \left(\theta_{Bs(l),t} - \theta_{Br(l),t}\right) / X_l \quad \forall l,t \tag{3.3.3}$$

$$-F^{rev}_{l,t} \leq fl_{l,t} \leq F^{fwd}_{l,t} \quad \forall l,t \tag{3.3.4}$$

$$fl_{l,t} + fp_{l,t} = F_{l,t}^{fwd}\varphi_l \text{ and } fl_{l,t} + fn_{l,t} = -F_{l,t}^{rev}\varphi_l \quad \forall l,t \tag{3.3.5}$$

The balance for each VRES is presented in (3.3.6), with the available resource at time t, $P_{i,t}^{RN}$ being balanced between injections $p_{i,t}^{R}$ and the curtailment $c_{i,t}$.

$$p_{i,t}^{R} + c_{i,t} = P_{i,t}^{RE} \quad \forall i,t \tag{3.3.6}$$

Each thermal unit (or cluster of units) is modelled through the same set of equations (3.3.7)-(3.3.9). Thermal units are capable to provide PFR and secondary frequency response (SFR) during high- and low-frequency events. Downward reserves are presented in (3.3.7) with the minimum stable generation (MSG) as the physical limit for their provision, whereas upward reserves are described in (3.3.8) and (3.3.9), where the headroom and the operation point [79] determine the limit for the allocation of reserves. (3.3.10) limits the number of units that can be committed to the number of available units.

$$n_{k,t} \cdot P_k^{\min} \leq p_{k,t} - pfr_{k,t}^{dw} - sfr_{k,t}^{dw} \quad \forall k,t \tag{3.3.7}$$

$$\frac{pfr_{k,t}^{up}}{RS_k} + sfr_{k,t}^{up} + p_{k,t} \leq n_{k,t} \cdot P_k^{\max} \quad \forall k,t \tag{3.3.8}$$

$$pfr_{k,t}^{up} \leq n_{k,t} \cdot PFR_k^{\max} \quad \forall k,t \tag{3.3.9}$$

$$n_{k,t} \leq N_k \quad \forall k,t \tag{3.3.10}$$

The operation of energy storage systems (ESS) is described in equations (3.3.11)-(3.3.19). In general, this model can be used for battery energy storage systems (BESS) or pumped-hydro storage systems (PSS). The main difference between the model for each type of system is associated to variable $ffr_{j,t}^{up/dw}$ in equations (3.3.13)-(3.3.15), (3.3.18) and (3.3.19) which corresponds to the case of Li-Ion BESS. For PSS these variables have to be replaced by the corresponding $pfr_{j,t}^{up/dw}$ and inertia has to be considered. An integer variable u_j is used to determine if the ESS is operating in charging ($u_j = 0$) or discharging mode ($u_j = 1$), with corresponding variables to define the total power injection or consumption, as presented in equations (3.3.11) and (3.3.12), respectively. The provision of frequency response is presented for upward reserves in (3.3.13) and downward reserve in (3.3.14), also the maximum level of FFR can be set through (3.3.15) for each ESS. The modelling assumes the possibility to provide reserves in both directions either in charging or discharging modes [80]. The energy balances of the ESS are described in equations (3.3.16) and (3.3.17). (3.3.18) and (3.3.19) guarantee the storage has the capacity to provide FR for the time required in each service.

$$ch_{j,t} \leq \left(1 - u_{j,t}\right) \cdot CH_j^{\max} \quad \forall j,t \tag{3.3.11}$$

$$dch_{j,t} \leq u_{j,t} \cdot DCH_j^{\max} \quad \forall j,t \tag{3.3.12}$$

$$ffr_{j,t}^{up} + sfr_{j,t}^{up} \leq u_{j,t}\, DCH_j^{\max} - dch_{j,t} + ch_{j,t} \quad \forall j,t \tag{3.3.13}$$

$$ffr_{j,t}^{dw} + sfr_{j,t}^{dw} \leq \left(1 - u_{j,t}\right) CH_j^{\max} + dch_{j,t} - ch_{j,t} \quad \forall j,t \tag{3.3.14}$$

$$ffr_{j,t}^{dw}, ffr_{j,t}^{up} \leq FFR_j^{\max} \quad \forall j,t \tag{3.3.15}$$

$$e_{j,t} = \left(H_j^{ch} \cdot ch_{j,t} - \frac{dch_{j,t}}{H_j^{dch}} \right) \Delta_t + e_{j,t-1} \quad \forall j,t \tag{3.3.16}$$

$$E_j^{\min} \leq e_{j,t} \leq E_j^{\max} \quad \forall j,t \tag{3.3.17}$$

$$ffr_{j,t}^{up} \cdot T_{pfr} + sfr_{j,t}^{up} \cdot T_{sfr} \leq e_{j,t} - E_j^{\min} \quad \forall j,t \tag{3.3.18}$$

$$ffr_{j,t}^{dw} \cdot T_{pfr} + sfr_{j,t}^{dw} \cdot T_{sfr} \leq E_j^{\max} - e_{j,t} \quad \forall j,t \tag{3.3.19}$$

To finalise the description of the base UC model it is necessary to introduce the standard UC constraints as presented in [79, 81]. The online number of units in each period and the transitions (units start-up/shut-down) is described by (3.3.20). Consider that when the time subindex t equals 0, the corresponding value is defined by a preexisting state or it is treated as a slack variable in the problem. The minimum up-times (T_k^{up}) and down-times (T_k^{down}) are represented by (3.3.21) and (3.3.22), respectively. Also, (3.3.22) integrates the times it takes the units to start-up (T_k^{su}) and shut-down (T_k^{sd}).

$$n_{k,t} - n_{k,t-1} = stup_{k,t} - shdw_{k,t} \quad \forall k,t \tag{3.3.20}$$

$$n_{k,t} \geq \sum_{\tau \in [1, t-(T_k^{up}-1)]} stup_{k,\tau} \quad \forall k,t \tag{3.3.21}$$

$$n_{k,t} \leq N_k - \sum_{\tau \in [1, t-(T_k^{sd}+T_k^{su}+T_k^{down}-1)]} shdw_{k,\tau} \quad \forall k,t \tag{3.3.22}$$

Each cluster of units will change its output between successive periods limited to the unit's ramping ability and the units that might become active and inactive in the interval. (3.3.23) represents the upward change in output for a given cluster k, which considers the ramping capability of the units times the duration of the scheduling interval Δ_t and the units that become active in that period. Similarly, (3.3.24) describes the maximum

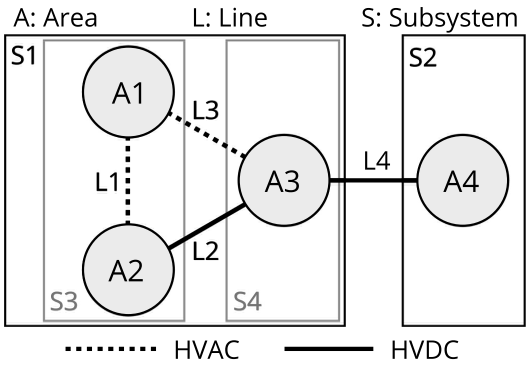

Figure 3.3 Example of a system, its areas and inertial subsystems.

downward change in output for the cluster based on the units' ramping and shut-downs.

$$p_{k,t} - p_{k,t-1} \leq n_{k,t-1} \cdot R_k^{up} \cdot \Delta_t + stup_{k,t} \cdot P_k^{min} \quad \forall k,t \tag{3.3.23}$$

$$p_{k,t-1} - p_{k,t} \leq n_{k,t-1} \cdot R_k^{down} \cdot \Delta_t + shdw_{k,t} \cdot P_k^{min} \quad \forall k,t \tag{3.3.24}$$

In order to limit the computational burden associated to the MILP search, the integer variables $n_{k,t}$, $stup_{k,t}$ and $shdw_{k,t}$ can be relaxed for large clusters without introducing substantial errors in the results as shown in [79].

3.3.2 Inertia and reserves definition

In this section, the expressions associated with inertia and aggregated reserves per area are defined since this information is essential to build the frequency security constraints. The definition of inertial subsystems is at the centre of this work because frequency behaviour will be strictly connected to the amount of inertia an area can access. Figure 3.3 exemplifies the concept of inertial subsystem. If no lines are in danger of tripping, the inertial subsystems are S1 and S2, considering that line L4 is an HVDC link. If line L3 is in danger of tripping, subsystem S1 can further split into subsystem S3 and S4 considering that L2 is also an HVDC link that will isolate A2 and A3 from the inertial response.

First, the inertia per area for each time step is defined in (3.3.25) as a function of the online synchronous units in that period (including PSS in charging and discharging modes). (3.3.26) describes the total inertia accessible in the areas comprising inertial subsystem s, at time t. This set is time dependant due to the periods where there is high risk of separation. Equations (3.3.27)-(3.3.29) describe the local allocation of FFR, PFR and SFR in area a, respectively.

$$h_{a,t} = \frac{1}{F_o} \left[\sum_{k \in \Omega_a^{SY}} \hat{H}_k \cdot \frac{n_{k,t} P_k^{\max}}{PF_k} \right] \quad \forall a,t \tag{3.3.25}$$

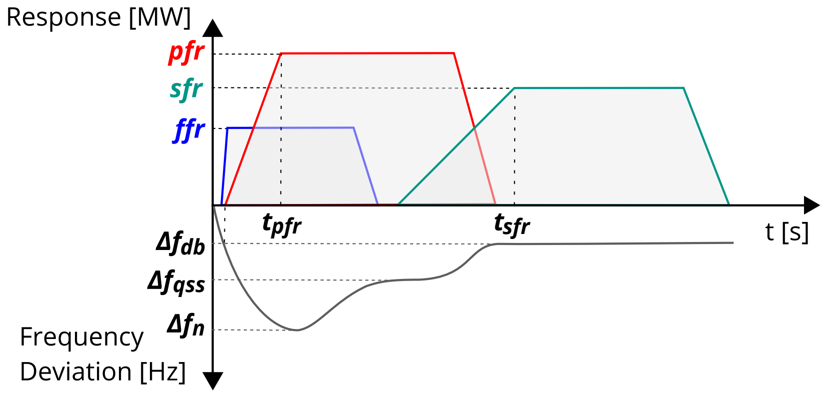

Figure 3.4 Idealised response delivery and frequency excursion after contingency.

$$h_{s,t} = \sum_{\alpha \in \Omega_s^A} h_{\alpha,t} \quad \forall s \in \Omega^S, t \tag{3.3.26}$$

$$ffr_{a,t}^{ty} = \sum_{j \in \Omega_a^{BESS}} ffr_{j,t}^{ty} \quad \forall\ a, ty, t \tag{3.3.27}$$

$$pfr_{a,t}^{ty} = \sum_{k \in \Omega_a^{TH}} pfr_{k,t}^{ty} \quad \forall\ a, ty, t \tag{3.3.28}$$

$$sfr_{a,t}^{ty} = \sum_{k \in \Omega_a^{TH}} sfr_{k,t}^{ty} + \sum_{j \in \Omega_a^{BESS}} sfr_{j,t}^{ty} \quad \forall\ a, ty, t \tag{3.3.29}$$

The expression for the total availability of reserves in each area are described in (3.3.30)-(3.3.33). A set of auxiliary variables is defined to determine the total available reserve r $(r \in ffr, pfr, sfr)$ $t\_r_{a,t}^{ty}$ in area a to withstand a potential contingency there (3.3.30). $fl\_r_{a,l,t}^{ty}$ denotes the flow of reserve service r of type ty through line l when the contingency occurs in area a during period t. These flows are calculated for the lines connecting each area a considering the local reserve allocation and the location of the contingency being each area a. The maximum up- and downward FFR and PFR reserve flows are constrained by the short term transmission slacks in the corresponding transmission lines using (3.3.32) and (3.3.33), respectively. (3.3.34) and (3.3.35) do the same for the case of the SFR, which is assumed not to stack up (see Figure 3.4).

$$t\_r_{a,t}^{ty} = r_{a,t}^{ty} + \sum_{Ar(l)=a} fl\_r_{a,l,t}^{ty} - \sum_{As(l)=a} fl\_r_{a,l,t}^{ty} \quad \forall a, t, ty, r \tag{3.3.30}$$

$$r_{a,t}^{ty} = \sum_{As(l)=a} fl\_r_{\bar{a},l,t}^{ty} - \sum_{Ar(l)=a} fl\_r_{\bar{a},l,t}^{ty} \quad \forall \bar{a}, a, t, ty, r;\ \bar{a} \neq a \tag{3.3.31}$$

$$-fn_{l,t} \leq fl\_ffr_{a,l,t}^{up} + fl\_pfr_{a,l,t}^{up} \leq fp_{l,t} \quad \forall\ a, l, t \tag{3.3.32}$$

$$-fp_{l,t} \leq fl\_ffr_{a,l,t}^{dw} + fl\_pfr_{a,l,t}^{dw} \leq fn_{l,t} \quad \forall\ a, l, t \tag{3.3.33}$$

$$-fn_{l,t} \leq fl\_sfr^{up}_{a,l,t} \leq fp_{l,t} \quad \forall\ a,l,t \tag{3.3.34}$$

$$-fp_{l,t} \leq fl\_sfr^{dw}_{a,l,t} \leq fn_{l,t} \quad \forall\ a,l,t \tag{3.3.35}$$

In those cases where the link $\hat{l}$ between two areas is considered to be at risk in time range $\hat{T} \subseteq T$, reserve flows are not allowed by imposing (3.3.36). This can also be imposed for HVDC links that do not have the capability to react to frequency changes in the areas they interconnect.

$$fl\_r^{ty}_{a,\hat{l},t} = 0 \quad \forall a,r,ty,t \in \hat{T} \tag{3.3.36}$$

3.3.3 Contingency definition

The determination of the largest contingency, both for load and generation, has to be conducted for each area rather than for the system. The reason for this approach is twofold: on the one hand, allocating system-level resources for the largest contingency does not guarantee that the reserves will be able to reach the location of the imbalance; on the other hand, the same variable can be used to account for the loss of imports/exports for inter-area transmission contingencies. (3.3.37) allows defining the largest loss in each subsystem, assuming no clustering of units. The largest load contingency for each area for each period has to be determined as an input parameter for the problem (3.3.38) since the UC model does not consider demand dispatch. (3.3.39) and (3.3.40) extend those definitions to the largest generation and load contingency within each inertial subsystem, respectively.

$$pl_{a,t} \geq p_{k,t} \quad \forall a,k \in \Omega^{TH}_{a},t \tag{3.3.37}$$

$$ll_{a,t} \geq LL_{a,t} \quad \forall a,t \tag{3.3.38}$$

$$pl_{s,t} \geq pl_{a,t} \quad \forall s,t,a \in \Omega^{A}_{s,t} \tag{3.3.39}$$

$$ll_{s,t} \geq ll_{a,t} \quad \forall s,t,a \in \Omega^{A}_{s,t} \tag{3.3.40}$$

When a link $\hat{l}$ between two areas is deemed likely to trip in time range $\hat{T} \subseteq T$, the associated areas get additional constraints for the largest generation (3.3.41) and load (3.3.42) contingency.

$$pl_{Ar(\hat{l}),t} \geq fl_{\hat{l},t} \wedge pl_{As(\hat{l}),t} \geq -fl_{\hat{l},t} \quad \forall t \in \hat{T} \tag{3.3.41}$$

$$ll_{Ar(\hat{l}),t} \geq -fl_{\hat{l},t} \wedge ll_{As(\hat{l}),t} \geq fl_{\hat{l},t} \quad \forall t \in \hat{T} \tag{3.3.42}$$

In a similar fashion to [30, 68], equations (3.3.37)-(3.3.42) allow for the largest contingency to be co-optimised to reduce the FR requirements. This approach is different from the current dispatch practices around the world, but in future low-inertia systems, this might be the only efficient way to deal with requirements on ROCOF, frequency nadir and frequency zenith. In case some generators are clustered, the largest contingency can be determined conservatively by adding (3.3.43) and (3.3.44)[5].

$$pl_{a,t} \geq cl\_on_{k,t} \cdot P_k^{\max} \quad \forall a,k \in \Omega_a^{TH}, t \tag{3.3.43}$$

$$n_{k,t} \leq cl\_on_{k,t} \cdot N_k \quad \forall k \in \Omega^{TH}, t \tag{3.3.44}$$

3.3.4 Frequency response constraints

The ROCOF requirement is set for each inertial area considering the largest positive and negative imbalances that can be experienced by the system based on the parameter $ROCOF^{lw}$ for low frequency events (3.3.45) and $ROCOF^{hg}$ for high-frequency events (3.3.46). The ROCOF constraint for each inertial area can be expressed as a function of the contingency sizes to establish a requirement on the inertial area s inertia $h_{s,t}$:

$$h_{s,t} \geq \frac{-pl_{s,t}}{2 \cdot ROCOF^{lw}} \quad \forall s,t \tag{3.3.45}$$

$$h_{s,t} \geq \frac{ll_{s,t}}{2 \cdot ROCOF^{hg}} \quad \forall s,t \tag{3.3.46}$$

The requirements on reserves to comply with QSSF can be fulfilled by local PFR and FFR providers and imports of reserves depending on transmission conditions determined by (3.3.30). Given the fact that transmission might play an important role in balancing the contingency, this balance is imposed for each area, which is presented for low- and high-frequency events in (3.3.47) and (3.3.48)[6], respectively.

$$t\_pfr_{a,t}^{up} + t\_ffr_{a,t}^{up} \geq pl_{a,t} + D_{s(a)} P_{s(a),t}^{L} \Delta QF^{lw} \quad \forall a,t \tag{3.3.47}$$

$$t\_pfr_{a,t}^{dw} + t\_ffr_{a,t}^{dw} \geq ll_{a,t} - D_{s(a)} \left(P_{s(a)}^{L} - ll_{a,t} \right) \Delta QF^{hg} \quad \forall a,t \tag{3.3.48}$$

In a similar fashion, secondary frequency response reserves are allocated for each

[5]Having a variable representing the output of one unit in the cluster involves the use of bilinear terms formed by integer and continuous variables, whose linearisation is possible but it defeats the purpose of the cluster representation by adding as many binary variables as the original representation.

[6]For load contingencies the lost load is discounted for the consideration of the natural response coming from demand. When the load contingency is loss of export-related, this subtraction will produce a conservative approximation of demand damping.

area and frequency event type considering imports from other balance areas, aiming to bring the frequency back to the dead band, as shown in (3.3.49) and (3.3.50).

$$t\_sfr^{up}_{a,t} \geq pl_{a,t} - D_{s(a)} P^{L}_{s(a)} |\Delta fdb| \quad \forall a,t \tag{3.3.49}$$

$$t\_sfr^{dw}_{a,t} \geq ll_{a,t} - D_{s(a)} \left(P^{L}_{S(a)} - ll_{a,t} \right) |\Delta fdb| \quad \forall a,t \tag{3.3.50}$$

The coefficients necessary to build the constraints to comply with frequency nadir (3.3.51) and zenith (3.3.52) can be calculated ex-ante as presented in Section 3.2. Since this constraint mixes PFR, FFR, contingency size and inertia, it has to be defined for each area of the system to capture limits on PFR and FFR, and the set of hyperplanes have to be calculated for the same inertial area to capture limits on natural response of demand.

$$\begin{aligned} t\_pfr^{up}_{a,t} - A^{nd}_{\psi,s(a),t} \cdot h_{s(a),t} - B^{nd}_{\psi,s(a),t} \cdot pl_{a,t} & \\ - C^{nd}_{\psi,s(a),t} \cdot t\_ffr^{up}_{a,t} - D^{nd}_{\psi,s(a),t} \geq 0 \quad \forall a,t,\psi \in \Omega^{nd}_{s(a),t} & \end{aligned} \tag{3.3.51}$$

$$\begin{aligned} t\_pfr^{dw}_{a,t} - A^{zh}_{\psi,s(a),t} \cdot h_{s(a),t} - B^{zh}_{\psi,s(a),t} \cdot ll_{a,t} & \\ - C^{zh}_{\psi,s(a),t} \cdot t\_ffr^{dw}_{a,t} - D^{zh}_{\psi,s(a),t} \geq 0 \quad \forall a,t,\psi \in \Omega^{zh}_{s(a),t} & \end{aligned} \tag{3.3.52}$$

3.3.5 Variables

All variables (3.3.53)-(3.3.54) are positive except $fl_{l,t}$ and $fl\_r^{ty}_{a,l,t}$.

$$\begin{aligned} \overrightarrow{x} =&(p_{k,t}, p^{R}_{i,t}, c_{i,t}, s^{L}_{b,t}, dch_{j,t}, ch_{j,t}, fl_{l,t}, fp_{l,t}, fn_{l,t}, \theta_{b,t}, ffr^{ty}_{j,t}, ffr^{ty}_{a,t}, \\ & pfr^{ty}_{k,t}, pfr^{ty}_{a,t}, ll_{a,t}, ll_{s,t}, pl_{a,t}, pl_{s,t}, e_{j,t}, t\_r^{ty}_{a,t}, fl\_r^{ty}_{a,l,t}, sfr^{ty}_{k,t}, \\ & sfr^{ty}_{a,t}, h_{a,t}, h_{s,t}) \in R \end{aligned} \tag{3.3.53}$$

$$\overrightarrow{y} = \left(u_{j,t}, n_{k,t}, shdw_{k,t}, stup_{k,t}, cl\_on_{k,t} \right) \in Z_{\geq 0} \tag{3.3.54}$$

3.4 Case study applications

In this section, the security-constrained scheduling model is applied to three different instances of the Australian power system. The first two studies correspond to an economic dispatch application (only a single snapshot is considered) only considering PFR and inertia. Firstly, the model is used to determine the value of optimising the contingency size for the whole NEM and SA. Secondly, the focus is put on the analysis of improved resilience in weakly interconnected power systems by co-optimising frequency response resources to withstand separation events. The third case study extends the separation event constrained economic dispatch to a unit-commitment scheduling approach with all the features of the model presented in Section 3.3, including fast frequency response resources. Appendix A presents the description of the software and input data structure used to run the case study applications.

3.4.1 Case study I: contingency size optimisation

This case study was presented in [30]. The co-optimisation of the maximum contingency size can have a tremendous impact on the allocation of FCAS in a power system; moreover, in some cases, it might be the only way to provide secure operation against low-frequency events. UK's power system operator National Grid [82] in relation to the services the grid will need in the future to provide a secure operation, has stated: *"Increasing the level of inertia on the system would reduce ROCOF, however, this option is less efficient than reducing the largest loss. Adding 3 GW of synchronous generation to increase inertia will have approximately the same effect on ROCOF as reducing the largest loss by 100 MW"*. Thus, it seems a sensible strategy to embed this capability within the dispatch models and study its effect on systems experiencing difficulties in meeting the security criteria determined in their reliability standards.

The case study considers a single snapshot allocation (no inter-temporal constraints), hence locating the exercise in the realm of optimal power flow rather than unit commitment. To achieve this, the underlying model was similar to the one introduced in Section 3.3, using constraints (3.3.2)-(3.3.10) to model the basic power system constraints, the inertia expressions (3.3.25)-(3.3.26) and the FR balances (3.3.28)-(3.3.29). The contingency size control constraints considered in this case study application correspond to (3.3.37)-(3.3.39) and (3.3.43)-(3.3.44); frequency response constraints include the set (3.3.45)-(3.3.52). The exercise is restricted only to low-frequency events and no FFR.

The purpose of the case study is twofold; by testing the centralised dispatch model on a strong system without problems to comply with the frequency security constraints, it is possible to show the effects of allowing the system to reduce the contingency size in order to reach a more efficient dispatch of resources. The second test is performed in a system with limited resources to provide adequate frequency response to show that limiting the contingency size is an effective measure to solve the issue. Figure 3.5 shows the frequency response security maps when the contingency size can be co-optimised for the low-demand case. In particular, Figure 3.5b depicts the case where the nadir surface has been approximated by a bespoke set of linear hyperplanes (i.e. not using the methodology presented in Section 3.2) which correspond to the linear constraints that are included in the MILP that finds the optimal power flow for the system.

This case study considers the NEM to analyse the effects of dispatching the system

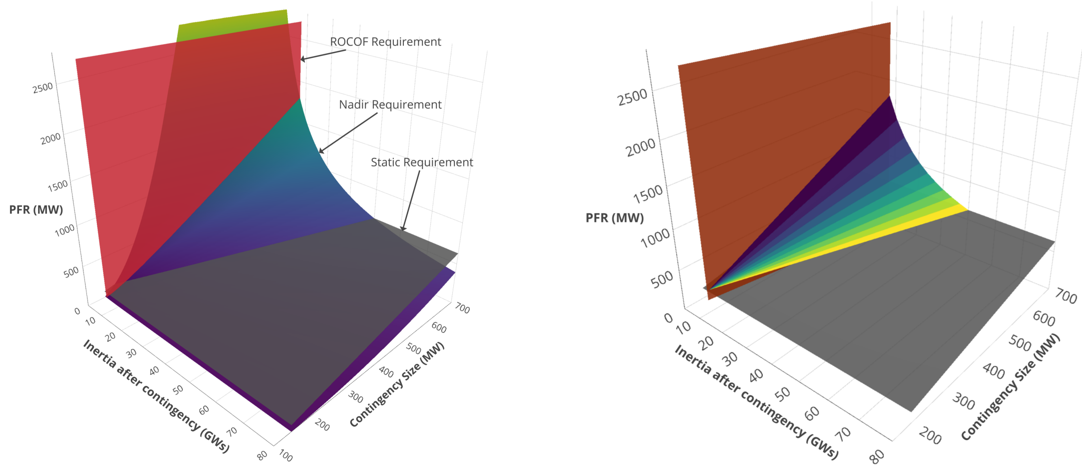

(a) Non-linear nadir surface. **(b)** Linearised nadir surface.

Figure 3.5 Frequency response security map for a demand level of 14GW, considering a composite load-damping factor of 1%/Hz, nadir limit of 49.0 Hz.

with security considerations and variable contingency size. The case studies include the whole system as well as one particular state, South Australia. The input data to run this study was obtained from [42, 83]. Figure 3.6 presents the topology of the system under consideration, where interconnectors are represented as solid lines and two transmission segments are represented in QLD to account for local bottlenecks. The figure also presents the installed capacity by technology by state in 2017.

South Australia is characterised by a large penetration of wind and solar PV technologies, with a ratio of VRES to thermal generation capacity close to one and a peak demand of around 2800 MW [37, 84]. South Australia transfers electricity to and from the rest NEM through interconnectors with the state of Victoria: a 650 MW HVAC link (Heywood) and a 220 MW HVDC link (Murraylink).

3.4.1.1 National Electricity Market

Currently, the NEM hydro-thermal generation fleet has units ranging from 20 to 700 MW of installed capacity, with ca. 92% of the units concentrated in the range 20 to 500 MW and ca. 75% in the range 20 to 200 MW. The largest unit is a relatively new (2007) coal-fired generator of almost 700 MW located in QLD, with a particularly low cost of operation; hence, the unit is usually committed at full capacity both during high and low demand conditions, even during periods of high renewable energy availability.

The current situation of the NEM presents a good case study to understand the impact of the contingency size on relatively strong systems. Assuming a system's nadir limit of 49.2 Hz, a composite load-damping factor of 2 %/Hz and a QSSF after contingency of 49.5 Hz, it is possible to analyse the NEM's frequency security adequacy[7] for conditions of low and high demand, 14 and 32 GW respectively, for different scenarios of hydro and renewable energy availability. The time of delivery of PFR in NEM is 6 seconds. Figure 3.7 presents the dispatch of NEM for low demand levels and a

[7]There is a frequency dead-band of ±150 mHz in place for the activation of generators providing PFR.

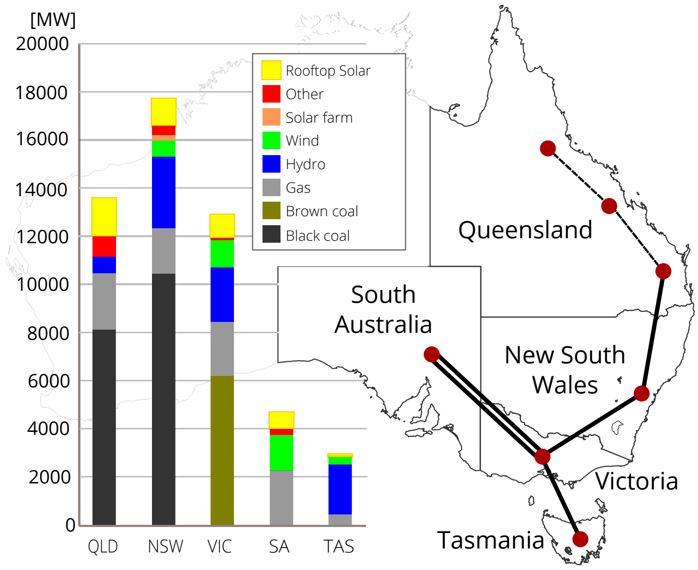

Figure 3.6 System under consideration and installed capacity by technology by state by January 2017. Interconnectors are represented as solid lines.

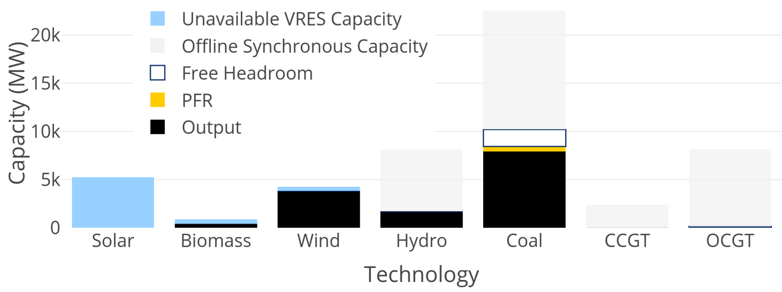

Figure 3.7 NEM dispatch profile by technology for a low demand scenario (night time) with high wind and low hydro availability in 2017.

fixed contingency of 700 MW, where coal and one open cycle gas turbine (OCGT) unit are providing PFR. Due to MSG constraints, coal units operate with considerable free headroom. There are over 350 units in the system represented through 42 clusters. Each snapshot results in a problem with 384 constraints and 421 variables. All available VRES output is integrated into the dispatch.

In Figure 3.8 the results for the cases (low and high demand, various levels of VRES availability) under analysis for NEM in 2017 are presented. The figure depicts requirements and results for a fixed contingency size of 700 MW and the results when the contingency size is co-optimised. Clearly, the current state of the system allows providing enough inertia to guarantee adequate frequency response both during periods of low and high demand, either with high or low renewable output. The static requirement is the security constraint that is active for all conditions, defining the same amount of PFR for every scenario with the same demand level, independent of the inertia available after contingency.

As it can be observed in Figure 3.8, contrasting the resulting sets of combinations of inertia and PFR for the cases with and without variable contingency, it is possible to see that for the variable contingency case, the PFR requirements are reduced up to 23%,

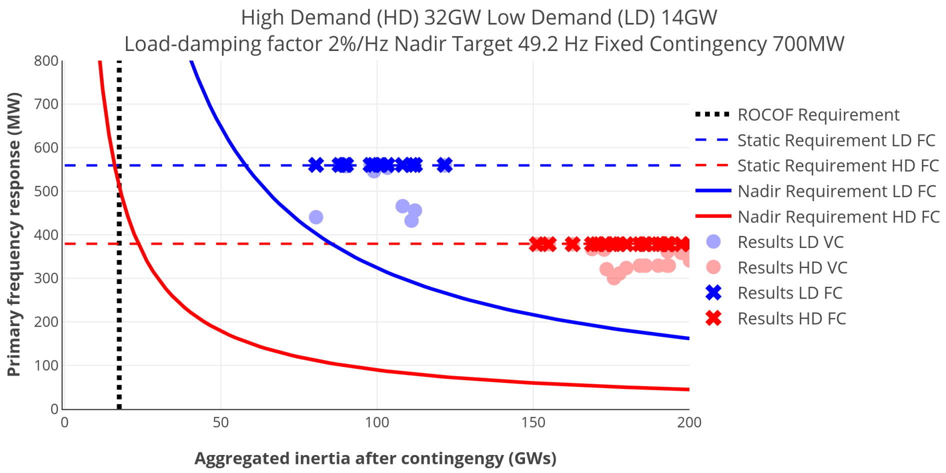

Figure 3.8 Frequency response security map for NEM in 2017 for high demand (HD) and low demand (LD) levels and various conditions of renewable output. Results for fixed (FC) and variable (VC) contingency strategies.

producing a drop in the costs of operation up to 0.62%. The maximum cost reduction also corresponds to the case where the contingency size was reduced the most, from 699.36 MW down to 571.3 MW, during low demand conditions. The cost reduction induced by this operational strategy will depend on the availability and operation costs of flexible and synchronous resources.

3.4.1.2 South Australia

There are particular conditions where SA may operate isolated from the rest of the NEM. It constitutes an interesting case study due to its high level of VRES penetration, which is expected to continue growing in the future [42]. The largest unit in SA is a combined cycle gas turbine (CCGT) with 463 MW of installed capacity. Its variable cost of operation has been reported to be ca. 40 $/MWh [83] and it usually operates partially loaded; the accepted contingency size considered for the allocation of FCAS in SA is 250 MW [85].

The test is conducted on SA in 2030, with a nadir target of 49 Hz, composite load-damping factor of 2 %/Hz and QSSF target of 49.5 Hz. Under the formulation of the model described in Section 3.4.1 and considering a maximum contingency of 250 MW, none of the scenarios yields a feasible, secure dispatch[8]. One of the reasons for this result is the fact that the demand level is below 2.5 GW, so the net reduction of load due to the frequency drop is very low. The aggregated set of units in SA by 2030 is not able to provide inertia and PFR to comply with the requirements depicted in Figure 3.9.

By considering a variable contingency size, the model finds feasible, secure operation points for all the scenarios under consideration, with a maximum contingency level reaching up to 112 MW and relying on VRES output curtailment in most of the cases. Under the proposed dispatch scheme, South Australia can be operated within

[8]This corresponds to a worst-case scenario condition since inertia coming from Type 1 and Type 2 wind turbines present in the system is not being considered in the model.

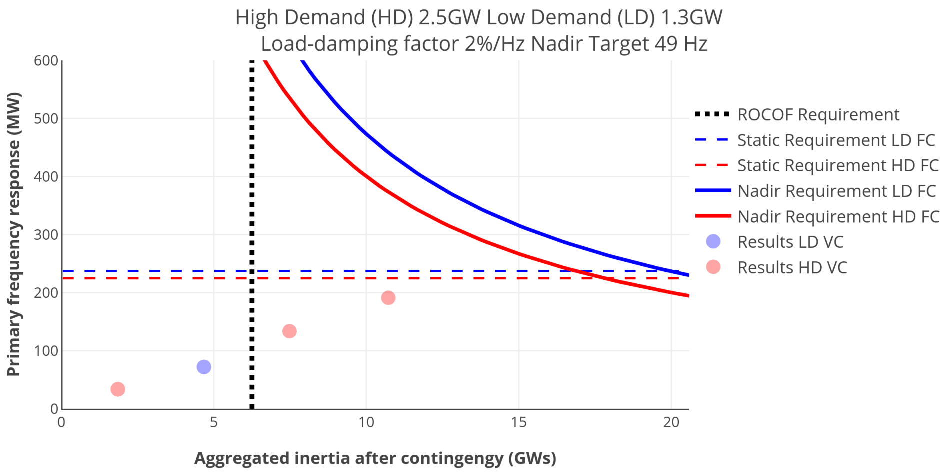

Figure 3.9 Frequency response security map for SA in 2017 for high demand (HD) and low demand (LD) levels and various conditions of renewable output. Results for fixed (FC) and variable (VC) contingency strategies.

frequency security limits without implementing any ex-ante measures such as imposing a discretionary minimum level of synchronous capacity.

3.4.1.3 Discussion

Allowing the dispatch models to determine the optimal contingency size that defines the FCAS requirements exhibits relevant effects on the resulting dispatches and costs of the system. In low inertia power systems with limited response capability, it allows finding feasible dispatch points that enable an operation within frequency control boundaries. The transition to low inertia power systems will include the development of multiple strategies and further investment to deal with the security requirements. For systems experiencing a rapid penetration of low inertia technologies, controlling the contingency size might be the most straightforward and efficient way to operate the system economically and securely. This operational strategy has a straightforward impact on isolated systems with high penetration of VRES, but it can also be applied on any system dominated by VRES, or on systems with areas dominated by VRES that might become isolated due to transmission contingencies. In general, considering transmission networks is of the essence in this type of problem, given the differences between DC and AC links regarding the transference of inertia and PFR between areas and neighbouring systems, and due to the impact of transmission contingencies in the allocation of reserves. This is why future work aims to include the loss of interconnectors as credible contingencies for reserve calculations, as well as the effect of the availability of FFR resources in the system.

In many markets implementing such an operational strategy is not straightforward because it goes against the basic principle of economic merit behind the energy product, and it might impact the economics of cheap, large units operating as baseload. For instance, the market rules in Australia provide the capability to the market operator to reduce the contingency size in case the supply of FCAS is below the requirement for a given level of contingency, but it does not allow the market operator to reduce the contingency size based on cost minimisation arguments. Other markets organised as centralised pools aiming to minimise overall operation costs based on each unit's incremental cost of operation might be able to implement such a mechanism in a more straightforward manner.

3.4.2 Case study II: separation event analysis

The frequency constrained studies available in the literature have not paid major attention to load contingencies to limit the frequency zenith or to transmission contingencies that may lead to system split, which, as it has been the case for NEM, could have devastating effects. This case study application aims to present means to enhance system resilience by understanding the value of co-optimising pre-contingency control variables and post-contingency response resources in order to limit the costs of a system that faces the risk of splitting. In order to achieve this, an optimal power flow (OPF) model aims to allocate inertia and PFR resources in individual areas and at the system level to face both high- and low-frequency events as a result of load, generation and, interconnector contingencies. When the system faces a low-frequency event, raise (upward) PFR resources are activated, whereas when a load contingency event happens, lower (downward) PFR resources are triggered to contain the associated high-frequency event. The model also considers secondary frequency response (SFR) resources for high- and low-frequency events. The allocation of resources is performed using the model presented in Section 3.3, with the exception of constraints (3.3.30)-(3.3.35) to secure transmission slacks to transfer reserves after contingency and the use of fast frequency response resources. The resulting optimal power flow (OPF) is referred to as security-constrained optimal power flow (SCOPF). This case study application was presented in [29].

The system under analysis is the NEM in 2018, aiming to mimic the conditions the system underwent during the separation event in August 2018 [45]. According to [86], the system had an installed capacity of 50.5 GW and committed projects of 2.6 GW of utility solar photovoltaic (PV) and 3.1 GW of wind, and also 4.8 GW of rooftop PV systems [87]. The different states are connected through a radial network of HVAC and HVDC interconnectors, whose transfer limits are specified in Table 3.2.

Table 3.2 Studied interconnectors. Current [88] and future [83] ratings.

Interconnector	State A	State B	Rating A to B (MW)	Rating B to A (MW)
Heywood	VIC	SA	600 {650}	500 {650}
Basslink	TAS	VIC	594 {630}	478 {480}
QNI	NSW	QLD	300-600 {1055}	1078 {1658}

This case study analyses the resilience threats to the system when losing the interconnectors highlighted in blue in Figure 3.10, that is, Heywood and QNI (HVAC), and Basslink (HVDC). For each operating condition, the base case corresponds to the one in

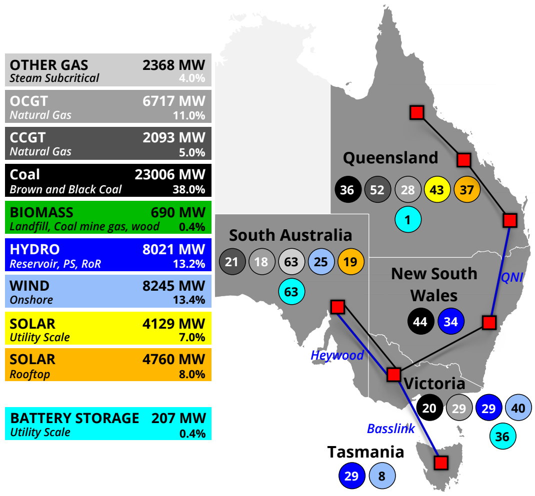

Figure 3.10 NEM multi-area interconnected system. Circles contain the percentage of overall installed and committed capacity by technology in each state by October 2018 (when the capacity is over 10% of the total installed capacity of the state). The interconnectors under analysis are highlighted in blue. The utility BESS capacity is presented for each state [86, 87].

which the interconnectors are not considered credible contingencies[9]. Then, three cases are run, each considering one of the three interconnectors as a credible event, on top of the largest generation and load contingencies, and resources are scheduled using the security-constrained optimal power flow model. Also, to provide a clearer context for analysis, the generation contingency is fixed instead of optimised by considering the largest infeed loss to be the coal-fired unit Kogan Creek located in QLD, whose output is slightly below 700 MW. The largest load contingency is set at 350 MW to approximate the loss of a section of the Portland aluminium smelter in Victoria. Flows are defined positive when they are leaving node A in Table 3.2 (for instance, for Heywood a flow of 300 MW means that 300 MW are being exported from SA to VIC, while -100 MW would represent a flow of 100 MW from VIC to SA). The cases are based on future operating conditions expected for the system based on the data presented in [83, 89].

3.4.2.1 Base case results

The results for the base case are presented in Table 3.3, for low and high demand conditions (17.2 and 34 GW, respectively) and raise and lower PFR services (labelled *up* and *dw*, respectively). The table also presents the value of the aggregated inertia in each area of the system for each demand condition (1 hour dispatch snapshot). Table 3.4 shows the base case flows through the interconnectors under analysis for each demand level. In order to facilitate the analysis, the frequency deviations must be limited to -1 Hz/s for ROCOF, 49.5 Hz for QSSF and 49 Hz nadir limit for low-frequency events, and

[9]From a practical point of view, limiting the flow in the transmission lines for security reasons (when the loss of the line is deemed a credible contingency) is an action performed by system operators worldwide, so this type of dispatch decision can be readily implemented. If a given interconnector displays a high likelihood of tripping at any given time, the systematic reduction in transfers through it may affect its economics and potentially its rated capacity (if this situation is identified at the interconnector design stage).

1 Hz/s for ROCOF, 50.5 Hz for QSSF and 51 Hz zenith limit for high-frequency events.

Table 3.3 Base case results for PFR (in MW) and inertia (in GWs).

Dem	Resource	SA	VIC	TAS	NSW	QLD
High	Inertia	9.6	34.3	8.5	61.2	52.2
	PFR-dw	0	13.3	0	0	0
	PFR-up	117.3	90.9	35.9	41.5	73.6
Low	Inertia	0.1	29.4	11.9	10.6	27.1
	PFR-dw	0	181.3	0	0	0
	PFR-up	2.3	61.9	48.5	129.6	284.8

Table 3.4 Base case results for interconnector flows (in MW). Negative flows represent reversed flows (from node B to node A).

Dem	Heywood (VIC to SA)	Basslink (TAS to VIC)	QNI (NSW to QLD)
High	142.5	-423.1	-727.7
Low	77.2	515.9	-857.4

The PFR resources and inertia allocated in the base case are based on recovering from the largest generation and load contingencies assuming the system remains intact. However, those dispatch conditions will not allow withstanding the loss of interconnectors. For instance, in low demand conditions, SA does not have enough inertia to keep ROCOF within limits for the loss of imports of 77.2 MW through Heywood. Similarly, TAS would experience large ROCOF both in high- (-1.24 Hz/s) and low-demand (-1.07 Hz/s) conditions considering the level of imports/exports and inertia allocation.

The QSSF requirements will be violated in the individual areas if any of the three interconnectors fails. Finally, for the eventual loss of studied interconnectors, frequency extrema are not identified for QLD or TAS due to the very large frequency excursion in both cases and low local response resources. SA complies with frequency nadir in the high demand case (49.01 Hz) and does not in the low demand case (47.18 Hz). Mainland (the areas that remain interconnected) is in general compliant when losing any interconnector, except for QSSF when QNI trips with frequency stabilising at 49.1 Hz/47.58 Hz for high/low demand; also, mainland frequency stabilises at 50.63 Hz after the loss of Basslink on high demand conditions.

3.4.2.2 Security-constrained optimal power flow results

Next, the system is studied under the same demand and renewable energy conditions as the base case but in this case each interconnector is considered as a separate credible contingency. The results for SA-separation constrained operation, i.e., if Heywood trips, yield the PFR resources and inertia presented in Table 3.5[10].

As seen in Table 3.5 applying the SCOPF to the loss of Heywood has the effect of reducing the flows in the interconnector and increasing the inertia and upward PFR resources in SA in the low demand case. This makes SA compliant for ROCOF and

[10] The HVDC link between SA and VIC is assumed not to respond to changes in frequency.

Table 3.5 SCOPF results for PFR (in MW) and inertia (in GWs) for loss of Heywood.

Dem	Flow [MW]	Resource	SA	VIC	TAS	NSW	QLD
High	102.8	Inertia	**9.6**	34.4	8.8	61.2	51.1
		PFR-dw	**0**	0	13.3	0	0
		PFR-up	**112.7**	113.2	68.2	41.5	23.6
Low	11.9	Inertia	**0.7**	28.9	11.9	10.6	26.3
		PFR-dw	**0**	181.3	0	0	0
		PFR-up	**11.4**	85.1	16.2	132.2	282.3

QSSF targets for both demand levels. The loss of the interconnector acts as an equivalent generator contingency in SA; in the high demand case, the resulting nadir is 49.37 Hz, whereas the low demand case does not display a frequency nadir. No FR constraint is binding in SA due to the MSG limit of the gas units in the area. It is important to highlight that the levels of inertia in SA are very low and the SCOPF model can find feasible and secure operation points by controlling the flows through Heywood.

Similarly, when the loss of Basslink is a credible contingency, the most cost-effective way to operate the system while avoiding frequency issues in TAS is to reduce the interconnector flows (keeping flow directions for each case, as seen in Table 3.6). Considering the new transfers and allocation of FR resources, the QSSF requirement becomes binding in TAS for the low demand case and the zenith reaches 50.71 Hz. In the high demand case, the nadir constraint is binding considering the loss of 281 MW being transferred through Heywood with an inertia level of 13.8 GW and local upward PFR of 416 MW.

Table 3.6 SCOPF results for PFR (in MW) and inertia (in GWs) for loss of Basslink.

Dem	Flow [MW]	Resource	SA	VIC	TAS	NSW	QLD
High	-280.5	Inertia	8.3	34.3	**13.8**	61.2	50.8
		PFR-dw	13.3	0.0	**0.0**	0.0	0.0
		PFR-up	0.0	0.0	**416.0**	0.0	0.0
Low	102.8	Inertia	0.1	28.1	**11.9**	14.4	24.0
		PFR-dw	0.0	89.7	**91.5**	0.0	0.0
		PFR-up	2.3	0.0	**0.0**	275.4	249.4

Table 3.7 presents the results for the interconnector between QLD and NSW. In this particular case, the OPF again reduces the flows through the interconnector, but given the large transfers exhibited in the base case, the reduction of the flow to levels closer to zero is not as cost-effective as in the other cases due to the presence of cheap generation in QLD. In this particular case, the binding constraints correspond to the zenith limit in QLD after the trip of QNI for both demand levels. The QSSF in the mainland is also binding during low demand.

It is worth highlighting that the linear hyperplanes used to approximate frequency extrema, represented by (3.3.51) and (3.3.52), are calculated to be robust (following the convex hull methodology presented in this chapter). This can be seen, for example, in Figure 3.11, showing that for the high demand case in QLD the zenith approximation curve is effectively the binding constraint (consistently above the QSSF requirement

Table 3.7 SCOPF results for PFR (in MW) and inertia (in GWs) for loss of QNI.

Dem	Flow [MW]	Resource	SA	VIC	TAS	NSW	QLD
High	-551.0	Inertia	9.6	35.3	8.5	62.7	**50.8**
		PFR-dw	0.0	0.0	0.0	0.0	**655.5**
		PFR-up	98.8	105.9	38.0	66.5	**50.0**
Low	-371.3	Inertia	0.1	29.4	11.9	14.4	**22.5**
		PFR-dw	0.0	0.0	0.0	0.0	**684.1**
		PFR-up	2.3	0.0	16.2	225.3	**283.4**

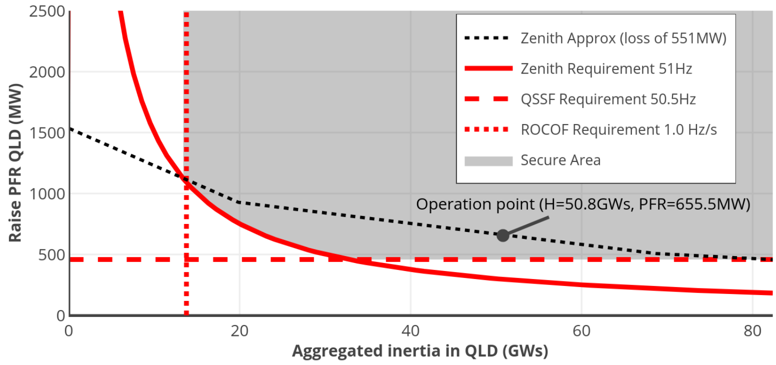

Figure 3.11 QLD frequency response security map for the loss of 551 MW transferred through QNI, with 9224 MW of demand in QLD.

curve) and is also conservative (always above the imposed 51 Hz zenith requirement curve). In other words, the approximated security map is always smaller than the formally calculated one. How conservative this approximation is will depend on the range of potential contingencies considered (in this case, 100 to 800 MW, this range is relatively large) and the number of hyperplanes used (in this case, limited to 4). This result would be improved by a better knowledge of the operation point of the SCOPF (e.g., via iterative calculation of the operation point) or by adding more linear approximations for the zenith constraint. In this example, the resulting frequency zeniths are 50.63 and 50.67 Hz for high and low demand cases, respectively.

3.4.2.3 Validation of SCOPF results via dynamic simulations

A frequency dynamics system model (Figure 3.12) in s-domain [27] is proposed to investigate whether the obtained SCOPF results can meet the frequency stability requirements (i.e., ROCOF, nadir/zenith, and QSSF limits) for each a-th separated area following an interconnector outage. Each area model includes aggregated simplified dynamic models of coal and gas units, consistently with the area-level aggregations in the SCOPF. It is assumed that there is no FR provision from other resources (e.g., renewables). The aggregated coal unit dynamic model consists of droop controller, governor, and turbine models, while its thermal energy system model is ignored [27]. As for gas units, OCGT and CCGT plants are aggregated and represented by one simplified dynamic model, which includes droop controller, governor, and gas turbine transfer functions [90]. Considering the simulation time horizon of interest (i.e., a couple of

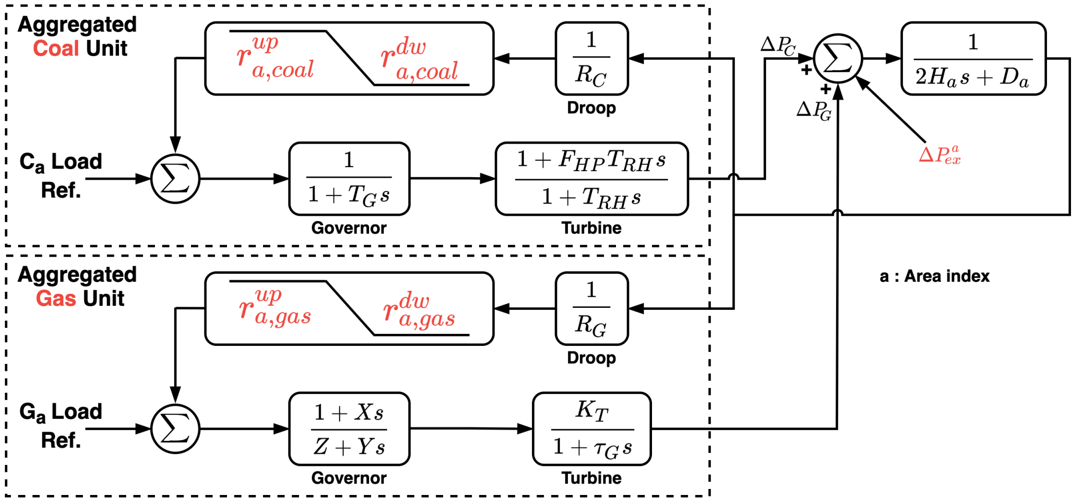

Figure 3.12 Dynamic model of the a-th area for separation event studies.

seconds after separation), the dynamics of temperature control loops in the gas unit dynamic model is ignored since it has slow dynamics in the order of several minutes [90]. Assuming gas turbine operation outside the over-speeding region [90], the acceleration control loop is also omitted. The reader can refer to [27, 90] for further information on generating unit transfer functions and their associated parameters (e.g., R_G, τ_G, etc.).

Following a separation event, each generation technology aggregation in the a-th area ($a \in \{1,2\}$) partake in PFR provision up to the allocated upward/downward PFR. For under-frequency conditions in the a-th area, coal and gas units deliver upward PFR up to, $r^{up}_{a,coal}$ and $r^{up}_{a,gas}$, respectively. Similarly, coal and gas units provide downward PFR up to $r^{dw}_{a,coal}$ and $r^{dw}_{a,gas}$, respectively, for over-frequency conditions in a given area. Furthermore, the effect of the a-th area demand is lumped into a single damping factor (D_a). The inertia level of the a-th area is also modelled by inertia constant (H_a) which is equal to the sum of inertia constants of generating units, neglecting for simplicity the demand-side inertia. Finally, the effect of separation event in the a-th area is represented by ΔP^a_{ex} separation signal. The ΔP^a_{ex} magnitude is equal to the exchanged power between the areas under study before their separation. The ΔP^a_{ex} sign is negative in the dynamic model of the area experiencing generation deficit following the separation and positive for the area with generation surplus.

Considering the QNI outage at $t = 50$s, the proposed dynamic model is constructed for two separated areas (i.e., QLD grid and the rest of NEM) using the parameters given in Table 3.8, while considering PFR allocations from the SCOPF results presented in Table 3.7 (Case-1), and the base case presented in Table 3.3 (Case-2). These parameters have been tuned so that steady-state and dynamic models are consistent with each other.

Table 3.8 Parameters used in the dynamic model of the two separated areas.

Param.	R_C	T_G	F_{HP}	T_{RH}	R_G	X	Y	Z	K_T	τ_G
Value	3%	0.3s	0.3	5s	5%	0	0.05	1	1	0.1s

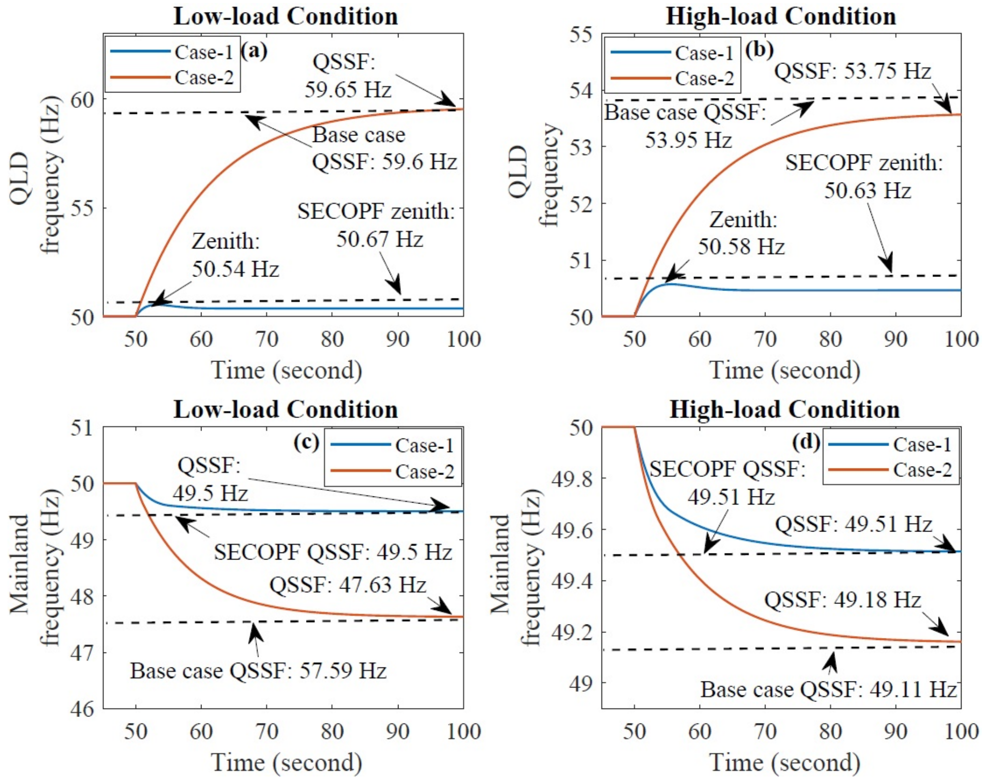

Figure 3.13 Dynamic simulation frequency curves in QLD and mainland grid for SCOPF (Case-1) and base case (Case-2) PFR and inertia allocation methods.

Figure 3.13 shows the frequency curves in QLD and mainland following the QNI outage in low and high loading conditions. The dynamic results (solid lines) match very closely the targets resulting from SCOPF analysis (dashed lines). QSSF after the loss of interconnectors as credible contingency is always within the range 49.5 and 50.5 Hz (not binding when zenith constraint is binding). Furthermore, since the SCOPF is relatively conservative, as mentioned above, in the cases where zenith constraints are active, the corresponding dynamic results are also conservative. ROCOF results are not presented because they are always compliant with the limit of ±1 Hz/s for all cases in both models, with differences between SCOPF and dynamic models below 0.06 Hz/s.

3.4.3 Case study III: role of fast frequency response and impact of reserve transmission

The previous case study applications have already analysed the effects of co-optimising the contingency size and considering separation events, here the focus is put on understanding the role of FFR and the effects of considering transmission limitations to transport FFR, PFR and SFR after a potential contingency event.

This case study aims to represent a week of operation of the Australian system in the year 2040 as described in the Integrated System Plan (ISP) presented by AEMO [9]. The specific conditions of the study case correspond to the Fast Change scenario of the

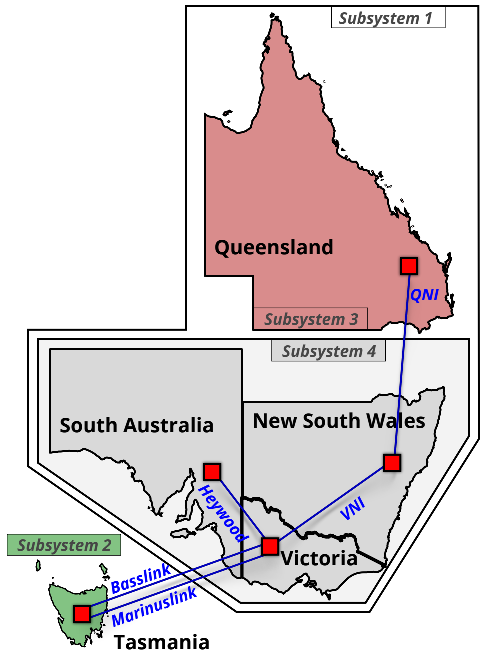

Figure 3.14 NEM diagram, emphasising nodes, areas and inertial subsystems.

ISP, specifically the week from Jan 7th to Jan 13th, 2040 (168 hourly dispatch intervals). A simplified structure of the system is presented in Figure 3.14, describing five balance areas, SA, VIC, NSW, QLD, and Tasmania (TAS). Interconnectors are all HVAC, except for the two HVDC lines connecting VIC and TAS. Also, four inertial subsystems are depicted, with mainland Australia (SA, VIC, NSW, QLD) being labelled as subsystem 1; TAS is interconnected through 2 HVDC interconnectors (existing Basslink and future Marinuslink), and therefore, it can be considered inertia-isolated (subsystem 2). For the discussion presented here, the other subsystems associated with the loss of QLD are not relevant.

The synchronous technologies and their parameters are presented in Table 3.9. Also, variable renewable energy availability like wind and solar PV in represented in each state as depicted in Figure 3.15.

In the ISP, dispatchable[11] energy storage systems include three storage categories, namely shallow (up to 2-hours utility-scale storage and dispatchable aggregated distributed storage up to 3-hours), medium (4 to 12 hours storage) and deep (24 to 48 hours storage). Table 3.10 presents different storage technologies and their aggregated rated capacity and energy for each depth category.

For the sake of simplicity, that the load damping factor is set to 1%/Hz in all the areas [91]. The dead-band for droop control is assumed to be ± 0.15 Hz, ROCOF limits are ± 1 Hz/s, frequency extrema are limited to ± 1 Hz, and QSSF is set to ± 0.5 Hz (limits for frequency nadir and QSSF refer to the nominal frequency of 50 Hz). The sources of FFR are assumed to activate 400 ms after the event, with an activation speed of 20 ms [14].

[11] The impact of non-scheduled behind-the-meter storage is reflected in the demand profile.

Table 3.9 Parameters of synchronous units.

Technology	Coal	Hydro	OCGT	CCGT
Number of units	12	114	49	6
Variable cost [$/MWh]	12 – 42	7.3	114 – 423	65 – 104
Rated Power [MW]	426 – 744	15 – 250	21 – 283	84 – 644
MSG [MW]	121 – 300	3 – 50	7 – 93	15 – 190
Ramp rate [MW/min]	1 – 9	–	3 – 160	2 – 10
Inertia constant [s]	4	2.5	4	4
Min up time[h]	8 – 16	–	–	3 – 6
Max PR headroom	10%	10%	10%	10%
PR slope factor	0.3	0.6	0.6	0.4

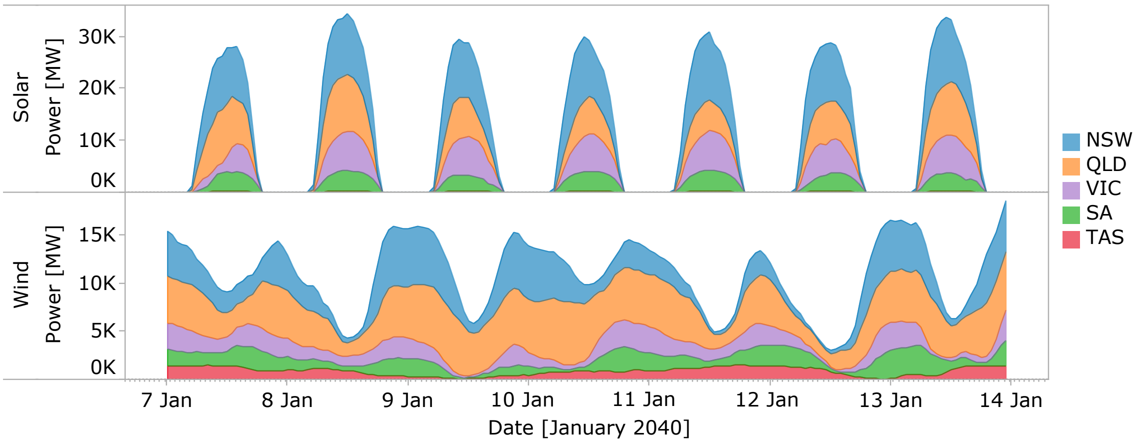

Figure 3.15 Distribution of dispatchable renewable energy resources by area.

The methodology to determine the hyperplane sets to represent frequency extrema requirements on inertia, PFR, FFR and contingency size (see Section 3.2) is run for all the corresponding inertial areas (also for those defined by potential isolation of areas) and time periods. Table 3.1 presented in Section 3.2 contains the numerical results for frequency nadir values for the convex hull approximation and the results after displacing the hyperplanes violating the requirement to make a robust approximation (subsystem 1, first time period, demand 20.1 GW).

Table 3.10 Aggregated storage by technology and depth.

Technology	Depth	Capacity [MW]	Energy [GWh]
Battery Energy Storage Systems (BESS)	Shallow	5941.2	14.9
	Medium	2110.5	8.4
Pumped Hydro Storage (PS)	Medium	2920.5	19.98
	Deep	3063.3	110.28

All simulations presented in this section are run using Gurobi 9.1.1 with a MIP gap target of 0.1% using a 2.9 GHz Quad-Core Intel Core i7. The model has been developed in Julia v1.5.3 and JuMP v0.21.5.

The set of simulations only consider the intact system to show the effects of intro-

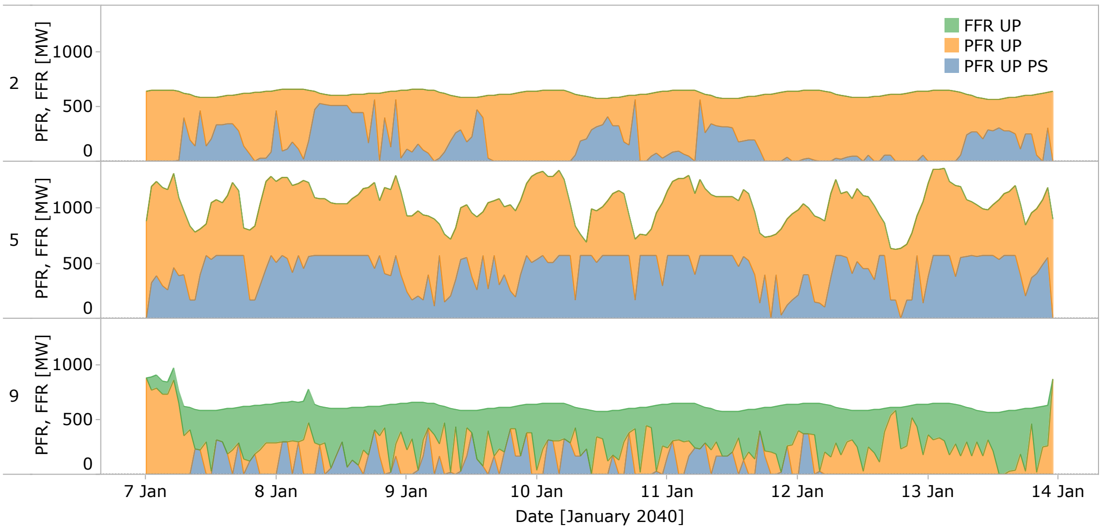

Figure 3.16 Difference in reserve allocation when batteries can provide FFR.

ducing different frequency response constraints in subsystems 1 and 2 (mainland NEM and Tasmania). In general, it is worth noticing that the intact system does not display issues associated with frequency zenith due to the relatively small size of load blocks (max. 400 MW) that could be lost in one event. Ten different case studies are run, all of which have the standard UC constraints [79] activated. The different constraints that are active in each case are presented in Table 3.11. The solution times for the different problems range from 3.2 to 331 s, with case 1 being the fastest and case 9 being the slowest. The size of each problem is different due to the activation of different variables and constraints; as a reference, case 9 contains over 110000 constraints and about 7000 variables, of which over 2000 are integer.

Table 3.11 Constraint activation.

Case ID	1	2	3	4	5	6	7	8	9	10
FFR							1	1	1	1
QSSF		1	1	1	1	1	1	1	1	1
ROCOF			1	1	1	1		1	1	1
Nadir					1	1			1	1
Reserve transmission				1		1				1

One interesting result corresponds to the comparison of time series of allocation of upward reserves in the system with the nadir constraint active without FFR (case id 5), and with FFR (case id 9). For comparison purposes in Figure 3.16, also case 2 is added to provide a reference for the allocation of reserves due to QSSF requirements. It is evident that the adequate consideration of the benefits of FFR in the dispatch of the system produces a substantial reduction of FR requirements (almost following QSSF requirements) associated with the nadir constraint during low demand periods. Figure 3.16 can be seen that over the first few hours of operation, FFR is not available because the BESS (and also PSS) are assumed to start at minimum energy level; this translates into the inability of the storage systems to provide FR due to the lack of energy to

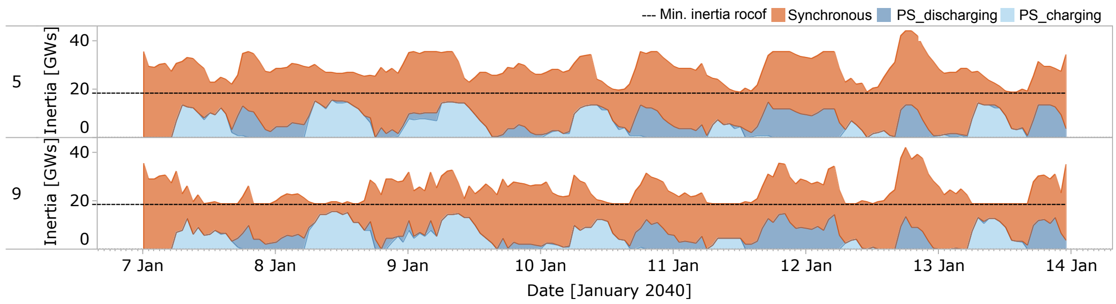

Figure 3.17 Inertia for mainland Australia with and without FFR.

deliver the response effectively if needed. The economic effects of considering FFR are substantial: the total cost of operation of the system over a week is reduced 0.6%, savings that stem from the reduction in the number of units scheduled to be online to provide inertia. The behaviour of inertia hour by hour is presented in Figure 3.17, where it is clear (see dashed line depicting the minimum inertia requirement - 18.6 GWs - due to a ROCOF limit of -1 Hz/s for a contingency of 744 MW) that less synchronous units are needed online when FFR is considered.

The relationship between inertia, PFR and FFR for the different cases under consideration is seen in Figure 3.18, where the box plots have been sorted in a way that adjacent cases correspond to the same active constraints with the exception of the activation of FFR (e.g., cases with ids 2 and 7 present the results of activating the QSSF constraints, with case 2 only considering PFR and case 7 considering both PFR and FFR. The vertical axis of Figure 3.18 shows the total inertia in subsystem 1, and the allocation of FR resources in the whole system because the HVDC links between TAS and the rest of the system have the capacity to transfer reserves. Case 1 shows that no reserves are scheduled in the case where QSSF requirements are not active. The inertia distribution corresponds to the activation of synchronous machines to cover the load. Cases 2 and 7 show how the system benefits from the existence of FFR even in the case of only activating the QSSF constraints, because it can use the headroom of batteries to share the need of reserves with synchronous units, slightly decreasing the median inertia level in the system. Cases 2, 7, 3 and 8 allocate the same level of total reserves (PFR+FFR) because the QSSF requirements are the same in all the cases. Cases 3 and 8 compare the distribution of FR resources when the ROCOF constraints are also active, which has a clear impact on the distribution of inertia (see inertia distribution in cases 2 and 7) bring up the level of inertia to the minimum requirement of 18.6 GWs. Naturally, this minimum level of inertia is also complied with for the distribution of cases 5 and 9 (as previously seen in Figure 3.17) since that constraint is also active. The effect of protecting a low-inertia power system like the NEM against off-limit frequency nadir is highlighted when comparing case 5 with cases 3 and 8. The system has to deviate greatly in terms of the allocation of inertia and PFR, which leads to additional costs (ca. 0.6% increase) and GHG emissions (ca. 1.12%). By introducing FFR, the system manages almost to go back to the allocation of FR resources (as well as costs and emissions) associated to only constraining the system to comply with QSSF and ROCOF.

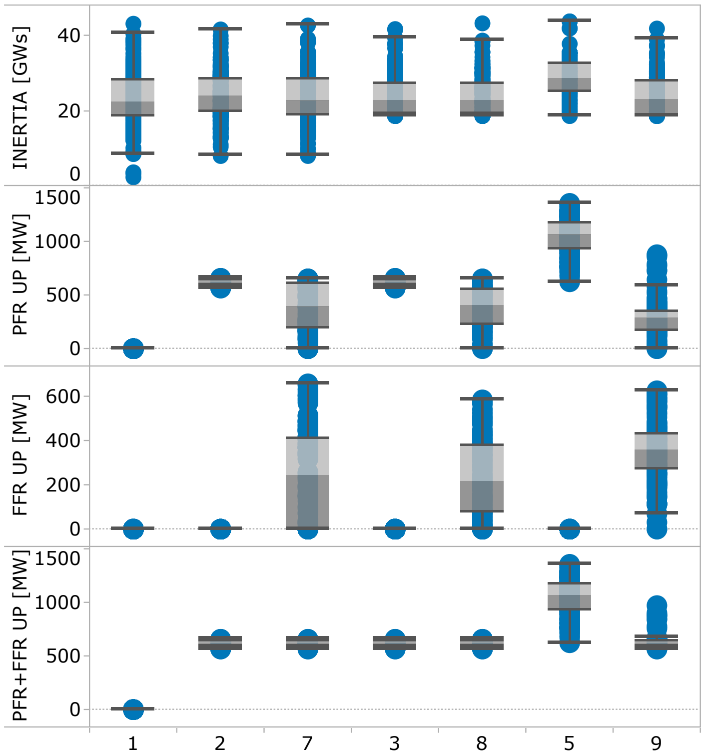

Figure 3.18 Distributions of inertia, PFR and FFR for cases under consideration.

This case study application also allows analysing the effect of transmission limits on the post contingency feasibility. The core idea behind the modelling approach presented in (3.3.30)-(3.3.35) is to provide enough headroom in the transmission lines to transfer the contingency reserves after contingency. The nature of these reserves is transitory, hence approaches like [92][12] are not suitable. The problem with the transitory post-contingency flows in low-inertia power systems is that the volume of reserves can be very large due to the nadir requirement (see Figure 3.18, case 5 shows a PFR allocation that almost doubles the contingency size of 744 MW). The approach here is to consider the largest contingency in each area and, considering the volumes of contingency reserves allocated in each area, force a tight headroom in the corresponding interconnectors to transfer the reserves between adjacent areas.

The effects of activating the reserve transmission constraints can be seen in Figure 3.19, for the set of transmission lines connecting NSW to QLD (positive flows correspond to power transferred to QLD). Case 9 displays several periods where the interconnector is at capacity transferring power to NSW. A large fraction of the contingency reserves is allocated in QLD, while the largest potential contingency in NSW is close to the largest contingency in the system. In the event that a large block of generation is lost in NSW, the imbalance will draw energy to NSW, which will cause the newly injected energy in QLD to flow to the neighbouring area. Without the appropriate headroom in the inter-

[12]In [92] all combinations of contingencies associated with $n-k$ security are considered to define the reserve margins needed to re-balance the system. These reserve margins are calculated to enable a feasible post-contingency re-dispatch for all the combinations of imbalances included within the $n-k$ security criterion.

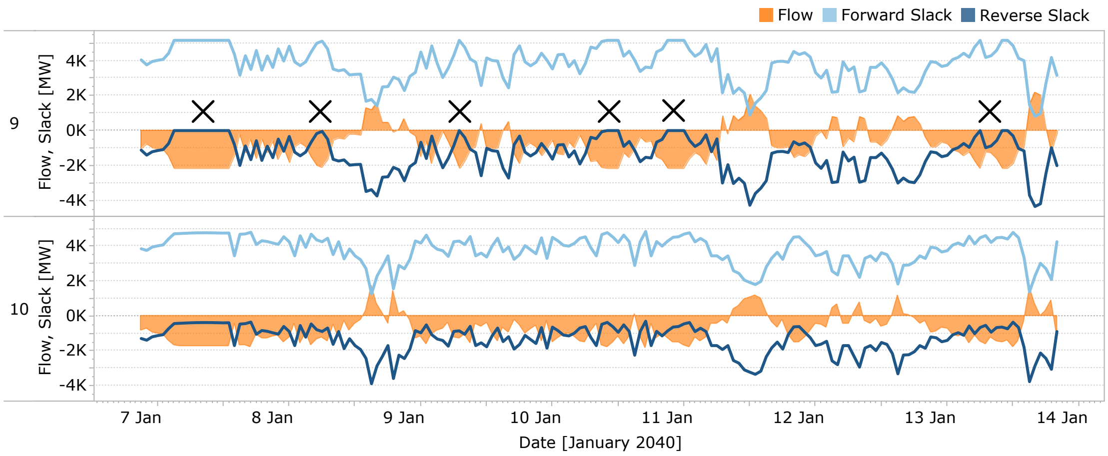

Figure 3.19 Transmission flows and slacks from NSW to QLD with and without reserve transmission constraints. The × highlights the periods where reserve transfers would violate the thermal ratings.

connector, the transient transfer of reserves could cause the trip of the interconnector, as it has been experienced in the recent events in 2016 [4] and 2018 [45].

3.5 Chapter summary

This chapter presented a security-constrained unit-commitment model. The model features the capacity to schedule inertia, which enables the use of inertia-related constraints, like ROCOF, and frequency nadir and zenith. Also, the model considers three types of frequency response services: fast frequency response, primary frequency response and secondary frequency response. Another trait of the model is that it can schedule transmission slacks between areas to cope with post-contingency transfers of reserves, preventing transmission line overloads (and potential cascading events). In order to quantify the effects of each of these features, a set of three case study applications was presented, which covered both schedulings in the form of optimal power flows and unit commitment. The results show the importance of a flexible operation in future low-inertia power systems, enabled by the control of the largest contingency (generation, load and transmission) and the use of fast frequency response resources.

CHAPTER 4

Investment flexibility

THIS chapter discusses the elements involved in making investment decisions in power systems, with the specific aim to understand the role of flexible investment options and risk. The topics covered in this chapter include a review of the theory on investment flexibility and the elements that affect the assessment of the flexibility provided by different assets in the power system. This chapter is independent of the contents presented in Chapter 2 and Chapter 3. Instead, it discusses theoretical foundations necessary to support the expansion planning model presented in Chapter 5, which also uses the operational model introduced in Chapter 3. It has been assembled using the contents of two reports prepared for the system operator (SO) National Grid Electricity System Operator (NGESO) [93, 94], which investigate their transmission expansion methodology framework [95, 96] and pathways to capture more flexibility in it.

4.1 Introduction

Let us start by providing a clear definition of investment flexibility. The literature has addressed this topic in multiple instances [97, 98] referring to concepts like investment flexibility and compromise solutions in a variety of ways, but without a clear and unified definition. Based on these elements, the concept of flexible investment options will be used to refer to investments options (single or multiple assets) whose technical, locational, operational, or procurement characteristics allow them to act as compromise solutions capable of adapting and providing value in a wide variety of scenarios, thus intrinsically hedging against planning uncertainty; these scenarios can describe changes to endogenous system characteristics (e.g. demand growth, renewable energy variability, etc.) and exogenous system characteristics (e.g. technological development, market conditions, etc.).

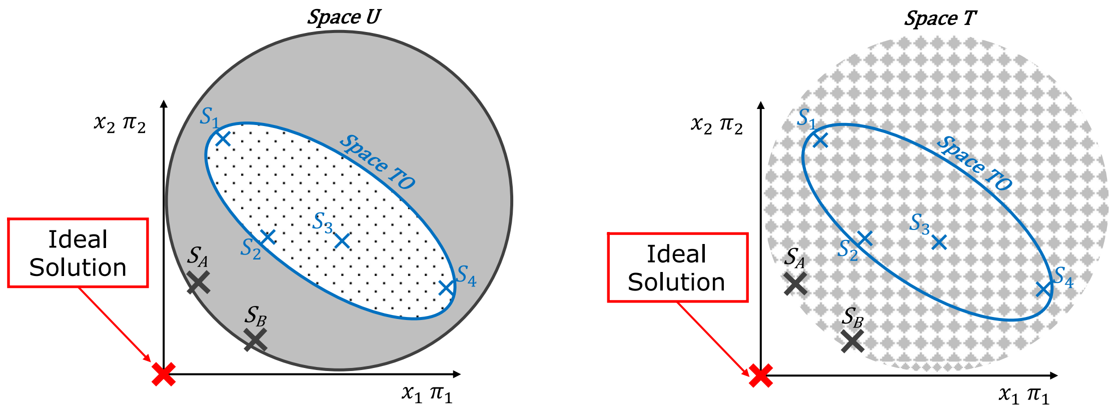

(a) Global set of options **(b)** Set of transmission options

Figure 4.1 Interaction of the solution space associated with options proposed by transmission owners (Space TO), (a) the global set of solutions (Space U) and (b) the global set of transmission solutions (Space T).

The assessment of the flexibility associated with a given investment option must be conducted employing a suitable stochastic methodology [97, 99, 100], where decisions are made here-and-now assuming uncertainty regarding the unfolding of the future (e.g. start the procurement of permits to deploy a transmission line or to build a battery energy storage system) and other decisions are made in the future when more information is available; these decisions are known as wait-and-see decisions (e.g. start construction, decisions on transfers through a HVDC link, etc.). The more wait-and-see decisions are available for an investment option, the more flexible the option is. In some cases, the benefits associated with the flexibility of an option can be balanced out by high investment costs, which can render one particular investment strategy more or less attractive depending on the pool of options against which it is simultaneously being compared. Without a suitable stochastic methodology, it is impossible to effectively discriminate the best investment plan from a flexibility point of view.

Figure 4.1 presents the different spaces of search that a system planner can consider. The set of options presented by the transmission owners (TOs, also known as transmission network service providers, TNSP) is labelled Space TO and is depicted as the area bounded by the dashed line that encloses all the strategies presented by the TOs. Space TO is not a continuous set, it is composed of a limited number of strategies, considering that each reinforcement presented by the TOs has well-defined characteristics (e.g., the capacity of a proposed transmission line reinforcement is fixed). The universe of potential solutions, labelled Space U, is much larger than Space TO. It can be approximated as a continuous set considering all the combinations of solutions (and possible sizes), like transmission, storage, demand response, intertrips, etc. If only transmission options are considered, but all potential combinations of transmission links and sizes, which this work refers to as Space T, it would still be much larger than Space TO, and although still disjoint, it would also be much denser. Space T would offer strategies like S_A and S_B, which can be missed by the TOs because they can only search a finite amount of options and, more importantly, they are blind to the options being considered by other

TOs and therefore by networked effects (impacts and benefits) that only a system-level view can capture.

As technology develops, the number of options available to provide solutions for the reliable operation of power systems is pushing SOs (like AEMO or NGESO) to step into the realm of decisions linked to what can be described as a system architect approach (equivalent to exploring the search Space U in Figure 4.1). In general, however, SOs are limited to select only the best transmission options among a set of reinforcements proposed by the transmission owners.

Current state-of-the-art models can efficiently search a vast portion of Space U, conducting a cost-benefit analysis with optimality assurance and risk aversion control through risk constrained stochastic approaches using DC power flow [97, 101]. For example, the model presented in the following chapter can consider an investment horizon of 20 or more years (sampled every five years) and the operation represented by typical weeks within each year (e.g., one week per month). It also considers a pool of investment options - including transmission, pumped-storage and battery energy storage systems – yielding a combination of over $3x10^{12}$ investment strategies in a given year. With those conditions and considering a specific uncertainty structure, it currently takes around 1-2 days to find the optimal solution depending on various modelling considerations and available computational resources (in that case, ca. 100 parallel CPUs). Although the SO might not be allowed to drive decisions on transmission investment using a system architect approach, these models can be of interest for the determination of signals to send to the system stakeholders (transmission owners included) regarding other products and services that the SO is in charge of securing. In this sense, these models can be used to narrow down the interesting areas of Space T, if co-optimising for other technologies is not in scope. Also, by using only the set of reinforcements presented by the TOs, the Space TO can be explored using the same models to find the optimal strategy, either under deterministic or stochastic conditions.

For the sake of clarity, in the coming sections, the approach based on suitable stochastic methods to search the space will be called *integrated approach*; on the other hand, *sequential approaches* correspond to methods that contain a series of steps that aim to find an optimal solution by reducing the search space through heuristics, which may or may not contain probabilistic considerations.

4.1.1 Introductory example

To allow for a more straightforward way to examine all the elements involved in capturing investment flexibility, this section introduces an example that will provide context and highlight the relevant factors affecting flexible investment decisions.

Let us consider the 3-bus system presented in Figure 4.2, which consists of one generator connected to bus 1 and two loads, one connected to bus 2 and the other to bus 3. The scenarios are given by the values of the load at bus 2 (2 per unit [pu] in scenario

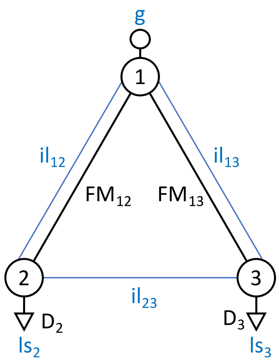

Parameters:	**Value:**
FM_{12}: maximum flow line 12	[1.5pu]
FM_{13}: maximum flow line 13	[1.5pu]
D_2: demand bus 2	[SC1: 2pu SC2: 1pu]
D_3: demand bus 3	[SC1: 1pu SC2: 2pu]
Variables:	**Associated information:**
g: generation bus 1	[unconstrained, \$1 pu output pu time]
ls_2: load shedding bus 2	[unconstrained, \$30 pu lost pu time]
ls_3: load shedding bus 3	[unconstrained, \$30 pu lost pu time]
il_{12}: reconductor line 12, binary	[FM_{12}+0.5pu, \$4]
il_{13}: reconductor line 13, binary	[FM_{13}+0.5pu, \$4]
il_{23}: build line 13, binary	[FM_{23}=0.5pu, \$6]

Figure 4.2 3-bus system.

Scenario 1		
Inv	**OF value**	**Non-zero variables**
-	0 + 17.5 = 17.5	g=2.5, ls_2=0.5
il_{12}	4 + 3 = 7	il_{12}=1, g=3
il_{13}	4 + 17.5 = 21.5	il_{13}=1, g=2.5, ls_2=0.5
il_{23}	6 + 3 = 9	il_{23}=1, g=3

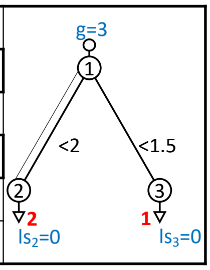

Scenario 2		
Inv	**OF value**	**Non-zero variables**
-	0 + 17.5 = 17.5	g=2.5, ls_3=0.5
il_{12}	4 + 17.5 = 21.5	il_{12}=1, g=2.5, ls_3=0.5
il_{13}	4 + 3 = 7	il_{13}=1, g=3
il_{23}	6 + 3 = 9	il_{23}=1, g=3

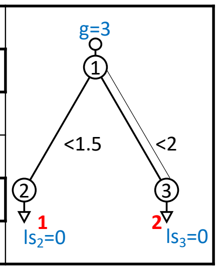

Figure 4.3 Deterministic results.

1, 1 pu in scenario 2) and bus 3 (1 pu in scenario 1, 2 pu in scenario 2). Initially, lines 1-2 and 1-3 have a transfer capacity of 1.5 pu, and there is no line between nodes 2 and 3. The generator can produce energy at a cost of \$1 (per unit of output per unit of time). The value of lost load is \$30. The investment options are 3: reconductoring existing lines to increase transfer capacity in 0.5 pu at a cost of \$4 and to build line 1-3, at a cost of \$6, resulting in a transfer capacity of 0.5 pu between bus 2 and 3. For the sake of simplicity, Kirchhoff's voltage law is ignored; while this approximation has substantial effects on the physical results, it helps to readily understand the principles that are being depicted through this example. Let us start by solving the deterministic cases. As the network is entirely symmetrical, the solutions are also symmetrical, as shown in Figure 4.3. The objective function (OF) of the problem, shown in (4.1.1), considers the investment and operation costs:

$$OF = \overbrace{[4 \cdot (il_{12} + il_{13}) + 6 \cdot il_{23}]}^{\text{Investment cost}} + \overbrace{[1 \cdot g + 30 \cdot (ls_2 + ls_3)]}^{\text{Operation cost}} \tag{4.1.1}$$

In scenario 1 it is beneficial to proceed with the reconductoring of line 1-2, hence increasing the capacity of that link to cover all the demand in node 2 and avoid any load shedding. Similarly, in scenario 2 the optimal deterministic decision is to reinforce line 1-3 to cover the demand on bus 3. Investing in line 2-3, which is more expensive than reconductoring any of the lines, naturally yields a worse result. Not investing in any line produces load shedding in both scenarios, and investing in the reconductoring of the wrong line produces the highest cost (investment and load shedding).

		Non-zero Variables		
Inv	OF value	Inv	Scenario 1	Scenario 2
-	0 + 0.5 · 17.5 + 0.5 ·17.5 = 17.5	-	g^1=2.5, ls^1_2=0.5	g^2=2.5, ls^2_3=0.5
il_{12}	4 + 0.5 · 3 + 0.5 · 17.5 = 14.25	il_{12}=1	g^1=3	g^2=2.5, ls^2_3=0.5
il_{13}	4 + 0.5 · 17.5 + 0.5 · 3 = 14.25	il_{13}=1	g^1=2.5, ls^1_2=0.5	g^2=3
il_{23}	6 + 0.5 · 3 + 0.5 · 3 = 9	il_{23}=1	g^1=3	g^2=3

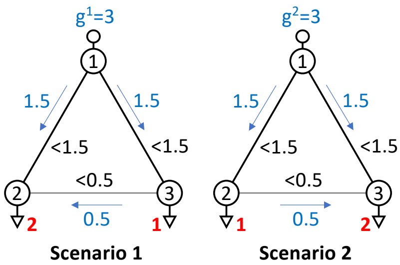

Figure 4.4 Stochastic results.

It is important to highlight that the combination of investment options (for example, the simultaneous consideration of the investment in line 1-2 and line 1-3 as one investment decision) in this example will always yield substantially higher costs with no additional benefits, so they are not analysed. This simplification can only be done because of the size and simplicity of the example; formally, seven different investment combinations should be analysed[13] on top of not investing in new assets.

The version of this problem that minimises the expected cost solves the same two scenarios simultaneously, looking to making investment decisions that can find *compromise* results across the multiple possible futures [97, 98]. The stochastic problem is modelled as a two-stage problem, where the investment decisions are the same as before, but the operation is modelled separately for each scenario (variable superscript denotes scenario in the objective function (4.1.2), where the subscript S stands for stochastic). This example considers equal probabilities for both scenarios.

$$OF_S = \overbrace{[4\,(il_{12} + il_{13}) + 6il_{23}]}^{\text{Investment cost}} + \frac{1}{2}\overbrace{\left[g^1 + 30\left(ls_2^1 + ls_3^1\right)\right]}^{\text{Operation cost scenario 1}} + \frac{1}{2}\overbrace{\left[g^2 + 30\left(ls_2^2 + ls_3^2\right)\right]}^{\text{Operation cost scenario 2}} \tag{4.1.2}$$

When solving this problem, the solution is now to build line 2-3, which allows covering both loads in both scenarios, as shown in Figure 4.4. This is by definition and as from practical evidence a *compromise* solution, which, as it can be seen, may also be completely different from what was suggested by the solution of each deterministic scenario. This compromise solution also intuitively corresponds to the concept of *flexibility* as it allows navigating across uncertain scenarios simultaneously.

This example shows the value of considering all potential scenarios and assessing all compromise solutions in a single problem, which emerges from a stochastic version of the original (scenario-based, deterministic) problem formulation. A few interesting points can be highlighted further based on this example.

Firstly, the integer nature of this problem does not allow for an "average" solution based on the independent solutions of the deterministic cases. Also, even if such a solution were to be feasible, it would not necessarily produce a solution close to the optimal compromise solution obtained by a formal stochastic approach [102, 103].

[13]Considering the effect of Kirchhoff's voltage law in this example would completely change the dynamic of the decisions because, in order to unlock transfer capacity in one link, additional transfer capacity would need to be available in the other links.

Second, the integer nature of the investment decisions in the transmission expansion problem generates, in principle, the possibility to recreate the stochastic solution by ideally listing all the deterministic solutions for the different investment options. Such comprehensive analysis of all options could then be carried out by running an exhaustive search of all ex-post combinations of deterministic solutions to work out the best compromise option. In this simple example, this can be checked for the case of the stochastic option by inspecting the deterministic results in the tables of Figure 4.3 and comparing them with the stochastic results in Figure 4.4. It is possible to see that the stochastic operation in each scenario is the same as the deterministic operation for the corresponding scenario. Since the investment option is the same in both deterministic scenarios, and the sum of probabilities equals 1, the results will match. However, this is only true in the case of integer investment decisions because it is possible to list all potential solutions. Also, although possible in this example, listing all conceivable investment options can be infeasible in most real cases due to the combinatorial explosion of the number of possible integer decisions, in particular if the investment options are more complex: this is, for example, the case when the investment decisions can be made not only now but in the future too and also when a given investment decision can be retracted or delayed.

The value of this simple example is that it highlights the role of compromise solutions in the presence of uncertainty; this, in turn, reinforces the relevance of the way information is used to arrive at a decision, which will be discussed in the following sections. Also, the advantage of having the possibility to list all independent solutions associated with the integer nature of the decisions in the TEP is limited to the practical capacity to cover all options effectively. Any attempt to proceed by listing a subset of options without a clear understanding of what is being left out of the analysis can lead to a substantial loss of efficiency associated with the decision that will be made.

4.2 Decision making methodology

When an entity faces different scenarios to model uncertain future conditions, the transmission expansion planning (TEP) problem effectively becomes a decision-making problem. However, most countries do not include advanced methodologies to model decision-making problems. In most cases, the planner only assesses the net present value (NPV) for individual scenarios, without combining scenarios in any (at least publicly clear) way. Different rules, often based on practical experience, are likely to be used to select the reinforcement options that may perform best across multiple scenarios.

Nevertheless, in the literature, there are several examples of applications where transmission (and distribution) expansion planning under uncertainty could be treated as a decision-making problem. The most relevant and well-known methodologies are probabilistic assessment (which may be seen as a relatively simple version of the more general field of stochastic programming) and min-max (or minimax), applied to both costs (min-max-cost, MMC) and regrets (min-max-regret), commonly referred to as least worst regret (LWR). Robust programming, min-min cost, and real options are other methodologies potentially available to solve transmission expansion planning problems with uncertainty, while certain applications of these methodologies also include specific risk measures that may be relevant for the TEP. These methodologies will be briefly reviewed in the following subsections.

4.2.1 Probabilistic assessment/stochastic programming

Probabilistic assessment (also referred to as "probabilistic choice") falls within the more general stochastic programming/stochastic optimisation framework, which may also include multi-stage decisions. This is the somehow intuitive development of a deterministic approach whereby uncertainty is introduced through scenario analysis. It has a flexible formulation that has drawn much attention, including efforts to develop a canonical framework equivalent to the one found in deterministic optimisation [104, 105].

The most straightforward formulation of probabilistic assessment/stochastic programming problems is based on probabilities applied to different scenarios to select the "statistically" best solution. It originated from assessing the uncertain outcome of a significant number of experiments, in which the frequency of occurrence is close to the probability value assigned. These experiments would typically be carried out in fixed conditions under the same set of laws. The formulation of a probabilistic approach can be readily adapted to the transmission expansion planning problem, in which a limited number of scenarios are assigned (probability) weights and the best investment strategy is selected to optimise (e.g., minimise, in the case of cost) a given attribute (e.g., net present cost) across scenarios through a linear composition of its values weighted with the respective scenario probabilities [106, 107].

4.2.2 Min-Max

This general methodology, much used in the field of game theory, uses two nested optimisations (minmax) to model the decision-making problem under uncertainty. It requires a more complex formulation than stochastic programming, but in principle, does not require the explicit assignment of weights for each scenario, which is considered an advantage by system planners. However, adequate scenario definition may become critical because there might be "no compensation" among scenarios, as generally implied in stochastic programming. In a TEP problem, these two nested optimisations are most commonly used with two attributes, namely, cost (min-max cost) and regret (min-max regret).

- **Min-max cost (MMC)**

  In min-max cost (MMC), the two nested optimisations use cost as the value attribute. This is intuitively a very conservative approach undertaken by a (most) risk-averse decision-maker[14], whereby a high-cost scenario, and the desire to hedge against its consequences, will eventually define the selection of the optimal investment strategy.

- **Min-max regret**

  Min-max regret or least worst regret is a version of the general nested min-max optimisation where the value attribute is now a regret. Regrets are based on an ex-post evaluation of the decision maker's perception regarding its decisions, usually expressed in monetary terms. The selected option is the one that minimises the regret felt by a decision-maker after verifying that the decision he had made was not optimal given the future that would have eventually actually occurred [105].

  Regret functions can be built with different levels of risk-aversion, including non-linear functions to model unacceptable outcomes for the decision-makers (e.g., "vetoes" and "absolute preferences").

  It has been pointed out that by shifting the focus on the decisions rather than the solutions (as in the probabilistic approach), LWR may reflect better the actual decision making process [106, 107]. Furthermore, when regret is used rather than cost (as in min-max cost), a high-cost scenario does not necessarily trigger the strategy selection because regret compares the relative performance of strategies within each scenario. This is a considerable drawback of min-max cost when compared to LWR. On the other hand, it has been discussed that the use of LWR may also have drawbacks. For example, while LWR may not be directly sensitive to the highest-cost scenario, it may still be sensitive to the relationship between "worst" and "best" scenarios, so that it is again possible that extreme (and particularly high-cost) scenarios may somehow drive the results. Furthermore, the methodology may not be robust to the inclusion of "irrelevant" investment options, leading to "spurious" decisions. In contrast, a min-max cost approach does not suffer from the latter issue

  It is also important to notice that, as discussed in [108], and as in classical literature on decision making under uncertainty [109, 110], regrets can be used as a measure of risk (see also below for other risk measures). A methodology such as LWR that aims to minimise regrets (and therefore risk) is therefore intrinsically risk-averse.

[14] MMC can be considered the approach traditionally used by system planners worldwide, particularly when considering the expansion of the system solely based on the expansion of demand.

4.2.3 Robust programming

In robust programming or robust optimisation, the decision-maker imposes feasibility for all possible scenarios, even if only the boundary scenarios are explicitly modelled. Since the worst-case scenario must also be feasible, it effectively becomes the scenario driving the decision. Therefore, the risk aversion of this methodology is again highly dependent on the scenario definition. Robust optimisation can implicitly account for all scenarios within the uncertainty set through efficient search algorithms, an advantage when dealing with large sets of scenarios compared to the previous methodologies [97].

4.2.4 Min-min cost

Min-min cost has a similar formulation to min-max cost, that is, a nested optimisation that does not require the explicit assignment of weights. Conceptually, it is opposite to min-max cost since it aims to obtain the highest benefits by minimising the cost in the lowest-cost scenario. In the context of a decision-making problem, it is used when a risk-seeking decision-maker is willing to obtain the maximum benefits from uncertain scenarios, essentially regardless of risk.

4.2.5 Real options

Real options analysis is a methodology coming from financial options theory. Its application comes from the belief that evaluating investment options using the traditional indicators such as net present value (NPV), net present cost or the discounted cash flow is not adequate in a number of investment problems, including for TEP. This belief mainly comes from the assumptions regarding the irreversibility of investments that these metrics make, which cannot capture the flexibility of the decision-making process realistically. In this light, the framework proposed by Real Options Analysis allows a better quantification of the benefits of flexible investments [111]. However, most proposed real options models are not adequate for transmission expansion planning problems. For example, analytical models using the Black-Scholes formulas only account for two correlated uncertainties, modelled assuming certain distributions and making several other questionable assumptions. On the other hand, lattice models cannot consider multiple interactions between options. Furthermore, concepts such as volatility or the effect of competition need to be carefully considered in real options, as the original settings in the field of finance are inherently very different. Schachter and Mancarella thus concluded that rather than real options models from financial mathematics, it is better to introduce a "real options framework" or "real options thinking" to deal with electricity system investment decision making, which can indeed deploy methodologies such as multi-stage stochastic programming or LWR [99].

4.2.6 Measuring risk in decision making: VaR and CVaR

The previously presented methodologies are used for making a decision according to a value attribute (e.g., cost) in an uncertain environment. Regardless of the methodology used, decisions will eventually have an associated distribution of expected consequences (e.g. costs). The decision will lead to a different outcome in each scenario, and it may be the case that for a given scenario, the outcome is not acceptable for the decision-maker. Therefore, when uncertainty is involved, any such problem is intrinsically related to a decision's risk. Approaches from risk management may therefore be incorporated in the decision-making process to avoid unacceptable decisions.

The most common way to handle risk when making decisions is to include a risk measure. For example, Conejo et al. review different risk measures in [112], namely, variance, shortfall probability, expected shortage, Value-at-Risk (VaR) and Conditional Value-at-Risk (CVaR). In particular, our view is that VaR and CVaR may be most suitable for applications that include risk management in transmission expansion planning problems.

Given a loss function (i.e. a cost function) for an $\alpha \in (0,\ 1)$ the VaR answers the question: "Given an investment decision, what is the highest cost I might experience with a probability of α x 100% ?" Other interpretations of VaR can be found in [113]:

- The maximum costs that will not be exceeded with a given probability α x 100%;
- The α-quantile of the cost distribution;
- The smallest cost in the $(1-\alpha)$x100% of worst cases;
- The highest cost in the α x100% of best cases.

On the other hand, the CVaR answers the question of "Given an investment decision, what will be the average value of costs in the $(1-\alpha)$x100% worst cases?" This risk measure is also known as mean excess loss or average value-at-risk [112]. Another interpretation is:

- The average cost in the $(1-\alpha)$x100% of worst cases.

CVaR is often the preferred risk measure to manage risk in decisions. From the previous interpretations of both measures, VaR informs about the cost when the worst cases start (worst cases are defined by the selection of α) while CVaR informs what is the average cost of those worst cases, providing information about their distribution. Therefore, CVaR can better recognise scenarios with low probability incurring very high costs (which will substantially increase the average cost of the worst scenarios). This is an attractive attribute for a risk measure in transmission expansion planning problems, where these low probability and high-cost scenarios can take place. Figure 4.5 illustrates in a cost distribution function the definitions of VaR and CVaR for an α=0.95:

CVaR mathematical properties are also more attractive than VaR. For example, reference [112] defines specific properties that are desirable for any risk measure, namely,

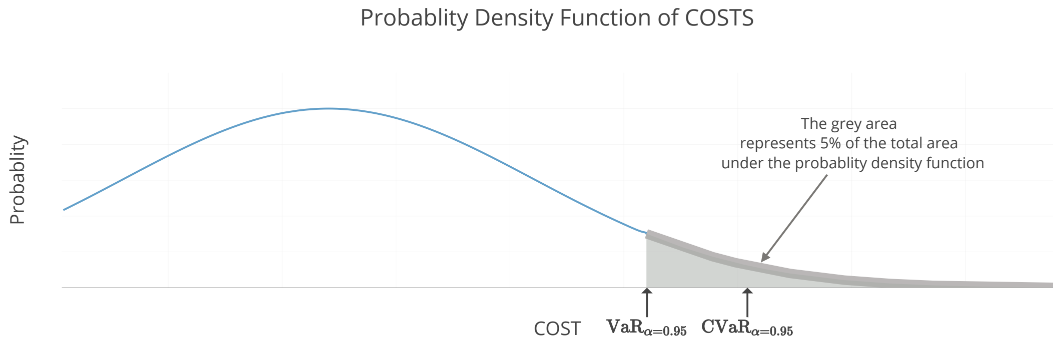

Figure 4.5 Example of cost distribution function showing VaR and CVaR for α=0.95.

monotonicity, translation equivariance, subadditivity and positive homogeneity, so that it is possible to talk about coherent risk measures. VaR does not meet the subadditivity characteristic, while CVaR meets all criteria of a coherent risk measure.

The abovementioned reasons make CVaR an interesting candidate to measure and manage risk in transmission expansion planning problems with uncertainty. For example, it may be used as an ex-post analysis of the result distribution of a decision-making problem or included in the problem formulation [112]. For instance, a decision-making problem may be modelled by using stochastic programming, whose aim is to maximise expected profits, and CVaR may then also be included in the formulation of the objective function. In this case, weights between the expected value and CVaR are applied to represent the decision maker's attitude towards risk. A more risk-averse decision-maker will increase the relative weight of the CVaR in the objective function, while a risk-seeking decision-maker will use a higher relative weight to maximise of expected profits.

4.2.7 Decision making framework

In the previous section, different methodologies to model decision making under uncertainty have been described. While a significant number of applications use these methodologies to solve different decision-making problems related to electrical power systems, there is a general lack of research that aims to systematically assess and compare the implications of selecting one methodology over another. For instance, [106, 107] are some of the few studies that compare methodologies (i.e., probabilistic assessment and LWR) and draw relevant conclusions.

One of the main reasons is the absence of a unified framework that enables such methodology comparison. In particular, most works consider stochastic programming, LWR and min-max cost (which are the most common methodologies used in decision making) as different frameworks, which hinders the possibility of carrying out a systematic comparison. However, these three "most common" methodologies (namely stochastic programming, LWR and min-max cost) do belong within the same same unified framework. Our framework development is supported by concepts from multi-objective decision making and is inspired by Starr and Zeleny's work in [114] and follows closely the work of Miranda and Proenca in [106, 107].

The first step to building this unified framework is to realise that non-trivial decision-making takes place when facing multiple attributes or objectives that may be in conflict with each other. As presented in [114], when facing a decision, typically, the decision-maker has a view on the relative importance of each of the objectives. Therefore, each objective or attribute can be assigned a weight and be referred to as a weighted criterion. In a decision-making problem with a set X of $n = 1, \ldots, N$ weighted criteria[15], each objective or attribute x_j has an assigned weight λ_j

$$X = \left(\lambda_1 x_1, \ldots, \lambda_j x_j, \ldots, \lambda_N x_N\right) \tag{4.2.1}$$

The analogy with a planning-under-uncertainty problem across multiple scenarios characterised by an attribute x_j (for example, cost or regret) and probability weight λ_j in the scenario j, which is explored further below, should have by now become evident.

For each of the weighted criteria (or weighted scenario, in our case), there is at least one value preferred to all the remaining ones. A solution that has the preferred value for all the weighted criteria is referred to as the *ideal solution*. The ideal solution is intrinsically a virtually infeasible solution in any non-trivial problem, firstly introduced as a technical artefact in decision-making problems in [115]. If it were feasible, the problem would be trivial, and the ideal solution would be the obvious choice for the decision-maker, and there would be no decision-making problem.

Evolving from the concept of ideal solution, Zeleny defined compromise solutions as the feasible solutions to a decision-making problem that are closest to the ideal one. These compromise solutions cannot be improved in any objective without losing in another objective. Intuitively, this is the set of solutions that the decision-maker shall explore to select the final decision. This set is also referred to as Pareto-Optimal and a more detailed analysis regarding their role in planning problems can be found in [116].

Using the previous concepts, it is intuitive that a multi-criteria decision-making problem's objective will be looking for which of these feasible compromise solutions are closest to the ideal solution. A more formal definition of that intuitive decision-making objective is to minimise the distance from the ideal solution. Therefore, the formulation of the decision making becomes a distance minimisation problem. Figure 4.6 depicts a simple example to illustrate the concepts discussed above. The figure represents a decision-making problem considering two weighted criteria ($x_1\lambda_1$ and $x_2\lambda_2$). In the problem presented, both weighted criteria can only take positive values, and the best possible desired value for both is zero (the similarities between this generic problem and a cost minimisation problem can again already be perceived and will be further discussed). However, such an *ideal solution*, as aforementioned, is generally not feasible, and the set of feasible solutions for the problem is explicitly shown in the figure. The figure also illustrates the intuitive distance between a feasible solution and the ideal in

[15]The criteria under analysis are assumed to be commensurable. In general, in the planning problem the criteria correspond to the costs or regrets by scenario.

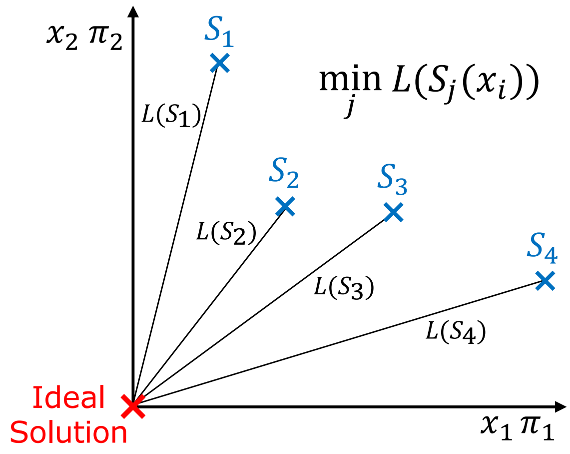

Figure 4.6 Multi-criteria decision making as a distance minimisation problem.

a two-dimensional space, represented by $L(y_i)$, where i is the index for the different feasible solutions in the set $k = 1, \ldots, K$.

To formulate the problem in the most general way, the general Minkowski metric formulation to "measure distance" in an N-dimensional vector space is used, where $y_i j$ now refers to the value of the feasible solution i in the weighted criteria j defined by $x_i j \lambda_j$:

$$L_p = \sqrt[p]{\sum_j^N \left(|y_{ij}|\right)^p} \quad p = 1, \ldots, \infty \tag{4.2.2}$$

Using the Minkowski metric formulation thus allows to formally define the objective function of a multi-criteria decision-making problem in a generic way, where $y_i j$ represents the candidate solution i for the criterion j with its associated weight λ_j and the distance of a candidate solution to the ideal solution is to be minimised in N dimensions:

$$\min_i L_p\left(y_{ij}\right) \tag{4.2.3}$$

By evaluating the general Minkowski metric for $p \in \{1, 2, \infty\}$ it is possible to discuss three metrics of interest. The Manhattan metric is defined when $p = 1$, which determines the distance of a feasible solution to the ideal solution by adding the components in each dimension, as shown in Figure 4.7a. When $p = 2$ the so-called Euclidean metric is defined, which corresponds to the geometric distance to the ideal solution (see Figure 4.7a). The case for $p = \infty$ produces the Chebyshev metric, which determines the distance by selecting the largest of the component for each feasible solution, as presented in Figure 4.7c.

These metrics intuitively resemble the concepts used in decision making under uncertainty, when uncertainty is modelled through scenarios. A parallel can be drawn between the weighted criterion $x_{ij}\lambda_j$ in the multi-criteria decision-making framework and the probability-weighted scenario cost (or regret) in scenario-based decision-making under uncertainty. Also, the objective functions of both approaches are equivalent, hence the metrics presented before can also be used in the context of scenario-based deci-

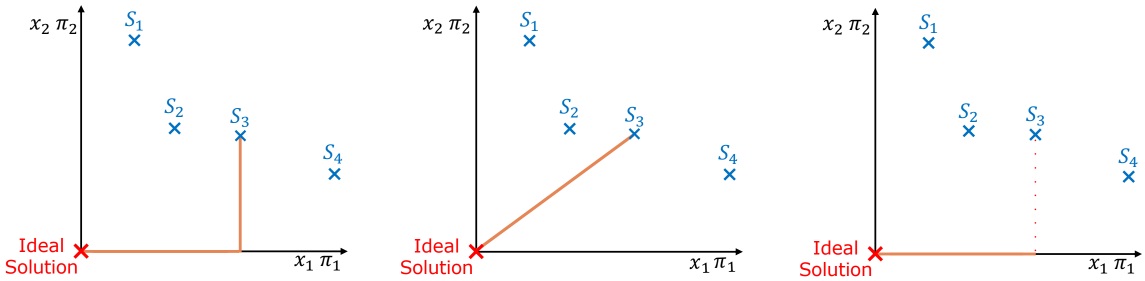

(a) Manhattan metric ($p = 1$) **(b)** Euclidean metric ($p = 2$) **(c)** Chebyshev metric ($p = \infty$)

Figure 4.7 Example of metrics used to determine distance to the ideal solution.

sion making. Table 4.1 summarises the details of equivalency using the terminology of electrical power systems planning problems.

Table 4.1 Parallel between metrics and decision making under uncertainty.

Formulation	Multi-criteria decision making	Decision making under uncertainty
$L_{1,i} = \sum_j^N \lvert y_{ij} \rvert$	Manhattan metric	Probabilistic assessment
$L_{2,i} = \sqrt[2]{\sum_j^N \left(y_{ij}\right)^2}$	Euclidean metric	Euclidean distance
$L_{\infty,i} = \max\left(\lvert y_{ij} \rvert\right) \quad j = 1, \ldots, N$	Chebyshev metric	Min-max cost and LWR

In a decision-making under uncertainty problem in power systems, where a value attribute such as cost or regret is minimised, the ideal solution will have a value equal to zero (e.g., zero costs or regrets) for all the weighted scenarios. However, different constraints make this ideal solution infeasible, and investment strategies that involve some costs and regrets must be pursued. Therefore, the objective is to find the investment strategy that satisfies such constraints minimising the selected attribute. This is equivalent to finding the solution "closest" to the ideal. Different metrics have been introduced in order to find the closest solution in N-criteria problems. If these apparently different approaches are just different metrics to solve the same problem within the same unified framework, they can be systematically compared to discuss their suitability in terms of what is the most suitable metric to address the specific planning problem under consideration.

4.2.7.1 Assigning probabilities to scenarios

In stochastic programming, the weights or probabilities assigned to each scenario must be explicitly stated, as the strategy selection is based on a probabilistic approach (for example, select the strategy that performs best when averaging scenario-specific costs or regrets by their relevant probability weights). This has led to system operators [9, 117] to prefer approaches that avoid the explicit assignment of probabilities, like LWR, over stochastic programming, especially when assigning such probabilities may be considered controversial.

In the previous section, when defining our proposed unified framework, weights were embedded in the definition of scenarios and, accordingly, the Chebyshev metric was also formulated with weights. Now, in the LWR formulation, there is no weight (at least explicitly), and as such, it is considered a "weight-agnostic" approach, as discussed. However, not including weights does not mean that these are not implicit in the formulation and, in fact: when no weights are assigned,LWR (and in general any min-max approach) is implicitly considering all scenarios equiprobable.

To demonstrate this, take the following simple example where the Chebyshev distance metric minimisation problem is presented as an equivalent weighted version of LWR. The indexing is coherent with what was previously presented.

$$\min_i \max_j \left(\lambda_j \text{regret}_{ij}\right) \tag{4.2.4}$$

If the general formulation is specified for a case of equiprobable scenarios with a probability (λ), that is:

$$\lambda_j = \lambda = \frac{1}{N} \quad \forall j \tag{4.2.5}$$

Then the common weight or probability associated with all scenarios becomes a common factor that can be brought outside the minimisation function, where effectively "the decisions are made", yielding:

$$\min_i \max_j \left(\lambda \text{regret}_{ij}\right) = \lambda \cdot \min_i \max_j \left(\text{regret}_{ij}\right) \tag{4.2.6}$$

This simple example thus proves that a LWR weighted formulation including equiprobable scenarios is equivalent to a LWR formulation not considering probabilities. The weighted formulation of LWR is referred to as least worst weighted regret (LWWR). Considering the elements presented in this section, different decision-making frameworks can now be consistently compared by assigning relevant probability weights, and the implications of adopting one approach/metric or another can be assessed.

Selecting an appropriate decision-making methodology is very relevant both to capture flexibility and to control risk. Any framework based on the metrics presented in Table 4.1 will be capable of capturing flexibility since they simultaneously consider multiple scenarios to make investment decisions. However, selecting a particular metric and indicator (cost, regret) will impact the final decision and the risk associated with the resulting investment plan. The following section presents an example that illustrates the differences when using specific combinations of metrics and indicators.

4.2.8 Illustrative case study application

In order to illustrate some of the concepts presented in the previous sections and the potential applications and implications of the proposed unified decision-making framework and relevant weighted decision metrics, a simple TEP problem is considered, namely, the 3-bus system whose topology is depicted in Figure 4.8 and the parameters of the generators are presented in Table 4.2.

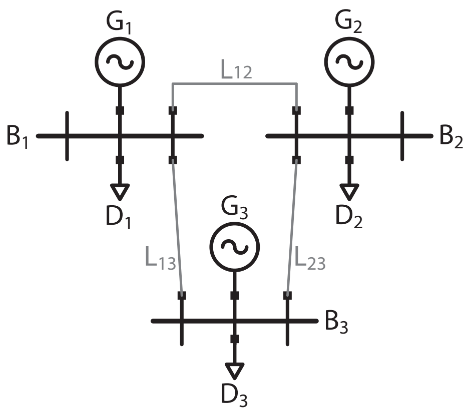

Figure 4.8 3-bus system.

Table 4.2 Parameters of generation units.

Generator	Pmax [pu]	Cost [$/MWh]
G1	0.8	100
G2	0.8	60
G3	0.6	40

The model to calculate the optimal investment simplistically considers the operation of one day only. The stochastic variable is the demand in each node, whose hourly time series for three different scenarios (labelled low, medium and high) are depicted in Figure 4.9.

For simplicity and given the illustrative nature of the example, the power flows in the transmission lines are not subject to Kirchhoff voltage law (transport model only). All existing transmission lines have a maximum transfer capacity of 0.1 pu. Six investment strategies are considered, as presented in Table 4.3. The investment cost IC is the same for all the options (that is, 100% expansion costs IC for each line and 50% expansion costs IC/2 again for each line); the value for IC was chosen aiming to create interesting numerical outcomes, resulting in a value of $1385 per line per day. The ID for each strategy is relevant to interpreting the results in the following figures since the colours are normalised to identify each strategy. Table 4.3 also shows the results for the deterministic assessment of costs for each strategy in all scenarios, highlighting in bold the least cost strategies for each scenario. Table 4.4 presents the results for the regrets calculated

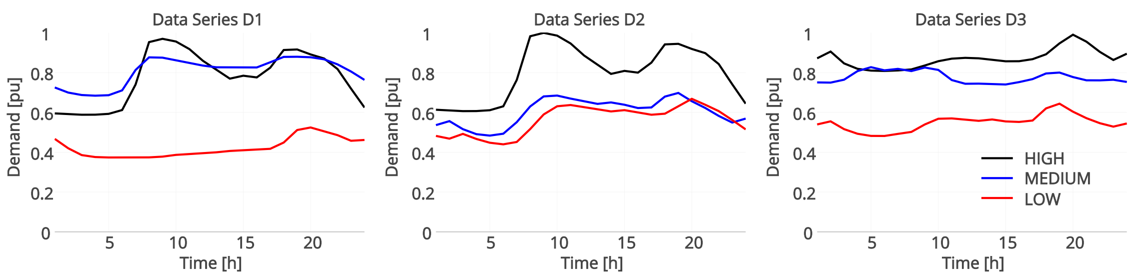

Figure 4.9 Hourly values of load for each demand in each of the three scenarios under consideration.

based on the results presented in Table 4.3. It also shows the maximum regrets for each strategy, and the LWR for the unweighted case is highlighted in bold.

Table 4.3 Investment strategies, investment costs and deterministic results.

Strategy ID	Action	Investment Cost [$/Line/day]	Costs in each scenario [$]		
			High	Medium	Low
0	Not to expand	0	610602.54	426307.07	247709.93
1	Expand Line 1 in 100%	IC	611987.72	426089.73	**246452.39**
2	Expand Line 2 in 100%	IC	**604949.16**	424769.84	249082.63
3	Expand Line 3 in 100%	IC	**604949.16**	426752.31	246882.11
4	Expand Line 1 in 50%	IC/2	611295.13	425793.43	246804.09
5	Expand Line 2 in 50%	IC/2	606601.92	**424473.54**	248390.04
6	Expand Line 3 in 50%	IC/2	606601.92	426059.72	246846.25

Table 4.4 Regrets calculated based on deterministic results.

Strategy ID	Action	Regrets in each scenario [$]			Max regret [$]
		High	Medium	Low	
0	Not to expand	5653.39	1833.53	1257.54	5653.39
1	Expand Line 1 in 100%	7038.56	1616.2	0	7038.56
2	Expand Line 2 in 100%	0	296.31	2630.23	2630.23
3	Expand Line 3 in 100%	0	2278.77	429.71	2278.77
4	Expand Line 1 in 50%	6345.97	1319.89	351.69	6345.97
5	Expand Line 2 in 50%	1652.76	0	1937.65	1937.65
6	Expand Line 3 in 50%	1652.76	1586.19	393.85	**1652.76**

The next step involves using the previous results to determine the optimal strategy based on the weighted metrics presented in Table 4.1. Using the data in Table 4.3 (costs) and Table 4.4 (regrets) it is possible to build these metrics for different weights λ_j for the scenarios. The resulting heatmaps presented in Figure 4.7 use the y-axis to represent the weight of scenario LOW (λ_L) and the x-axis for the weight of scenario HIGH (λ_H); considering that there are only three scenarios, the weight of scenario MEDIUM (λ_M) is implicit in each chart by considering that $\lambda_M = 1 - (\lambda_L + \lambda_H)$. By analysing a range of weights, it is possible to determine the strategy that the different approaches would select for each weight combination, which then can be plotted using the associated ID (first column of the tables with costs and regrets). This graphical approach also clearly visualises the scenario weight ranges for which the same decisions are recommended by different methodologies.

As it can be seen in Figure 4.10a, the probabilistic approach never finds strategy four to be optimal under any choice of weights; furthermore, the resulting areas are convex (the line formed by any two points in the area is contained in the area itself), and the transition from a strategy to another across scenario weights is smooth. As soon as a non-linear metric is used, strategy id 4 appears too in the optimal solution set, as can be seen for the Euclidean distance (Figure 4.10b) and LWWR (Figure 4.10c). These findings are all in line with the theoretical considerations discussed above.

There is a further relevant consideration that can be derived from Figure 4.10: by

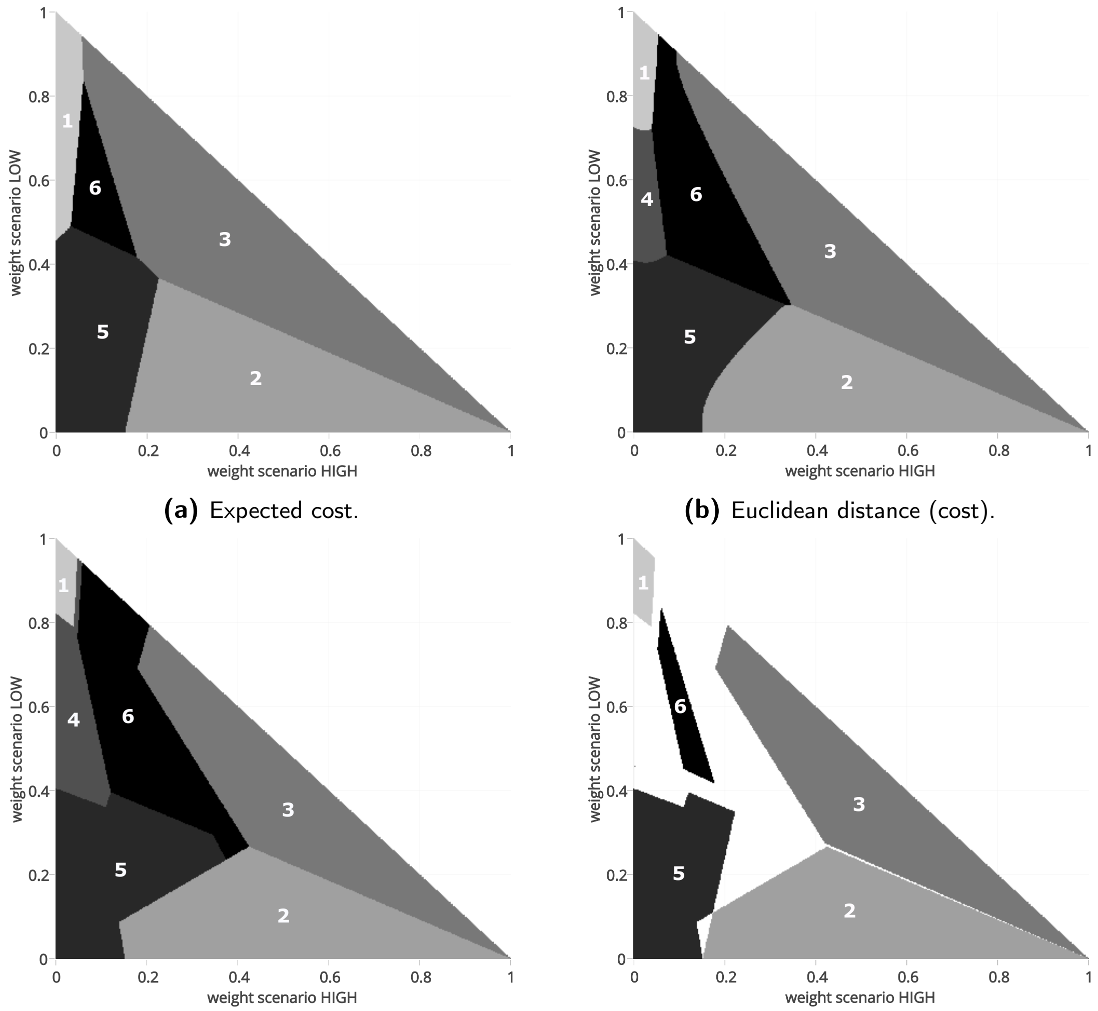

(a) Expected cost.

(b) Euclidean distance (cost).

(c) Least worst weighted regret.

(d) Stability regions.

Figure 4.10 Optimal strategies for weighted scenarios and different metrics

superposing the charts for the expected cost approach (Figure 4.10a) and the one associated to LWWR (Figure 4.10c) it is possible to find what can be defined as *decision-stability* regions, namely those regions characterised by a combination of weights within which the selection of the optimal strategy would be the same regardless of the metric used to calculate it.

As each decision-stability region is defined for a range of weights for each scenario, this allows us to potentially select a strategy from the stable regions which is independent of the metric used and can also cope with "uncertainty" in the determination of the probability of each scenario. For example, if the LOW and HIGH scenarios were to be considered low probability scenarios (e.g. ca. 10% each), the strategy selected would be number 5 regardless of the metric used; this would be true even if the scenario HIGH would change its weight between 0 and 15%, scenario LOW in the 0 to 35% range and the scenario MEDIUM between 50 and 100%. Decision-stability regions can thus be a powerful tool to test the robustness of given solutions to uncertain scenario probability assignment or the plausibility of given scenarios.

Another interesting aspect worth highlighting from the results presented in Figure

4.10 is that there exists a relationship between the location of the reinforcement and the geometry of the areas. Strategies 1 and 4 correspond to the expansion of line 1, strategies 2 and 5 to line 2, and strategies 3 and 6 to line 3. It can be seen that lines 2 and 3 hedge the system much better than line 1 for all the metrics as seen in Figures 4.10a, 4.10b and 4.10c.

It is also interesting to point out that, as discussed above, the "classical" (apparently "unweighted") LWR approach would correspond to an equal weight combination for the three scenarios. Such LWR (that is, a LWWR with equal probability weights) could be compared with the results from the probabilistic assessment with the same 33.3%-33.3%-33.3% combination of weights. It is clear from visual inspection that in this specific case study, the classical approach does not yield decision-stable solutions across different metrics, hinting that further analysis may be worthwhile. This is discussed further below.

It is important to highlight that for applications with more than three scenarios (e.g. the four scenarios considered in NGESO's Network Options Assessment (NOA) process or the five scenarios considered by AEMO in the context of the ISP), the same graphical representation could still be obtained by varying the probability weights of two scenarios, for example, the ones that are expected to perform "worst" and "best", and by assuming that the other two (more "central") scenarios are equally probable. Also, a four-scenario case can be represented through a 3D heatmap with specific values assigned to each scenario probability.

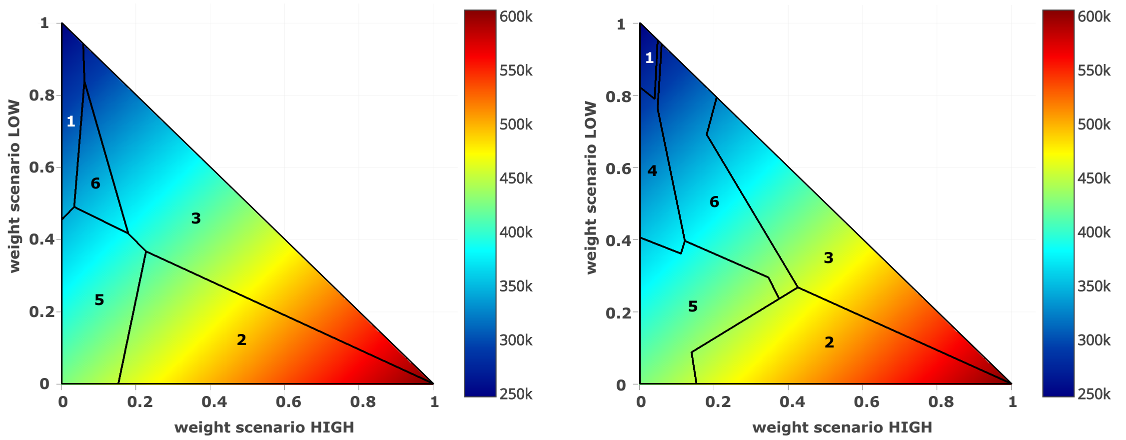

(a) Probabilistic. **(b)** Least worst weighted regret.

Figure 4.11 Expected cost for the optimal decisions in the probabilistic and LWWR cases.

Figure 4.11 illustrates the distribution of expected costs and Figure 4.12 the maximum regrets within each of the areas for the selected strategies using the probabilistic and LWWR approaches. To understand how the regrets push the boundaries of the areas to become what they are in Figure 4.10c, Figure 4.12 shows that the optimal areas found by the LWWR metric naturally reduce the greatest regrets that can be experienced compared to the probabilistic case in Figure 4.12a. The probabilistic metric is applied to minimise the weighted average costs across scenarios, resulting in strategy spaces that have been optimised without considering the corresponding regrets.

In general, by performing this kind of expected costs and expected regrets analyses for different methodologies, all the implications of using different approaches, risk-aversion degrees, and scenario weights may be clearly assessed, potentially leading to developing an enhanced decision-making framework where the performance of the proposed investment solutions are much more transparent in terms of including costs and risks and robust to different uncertainties.

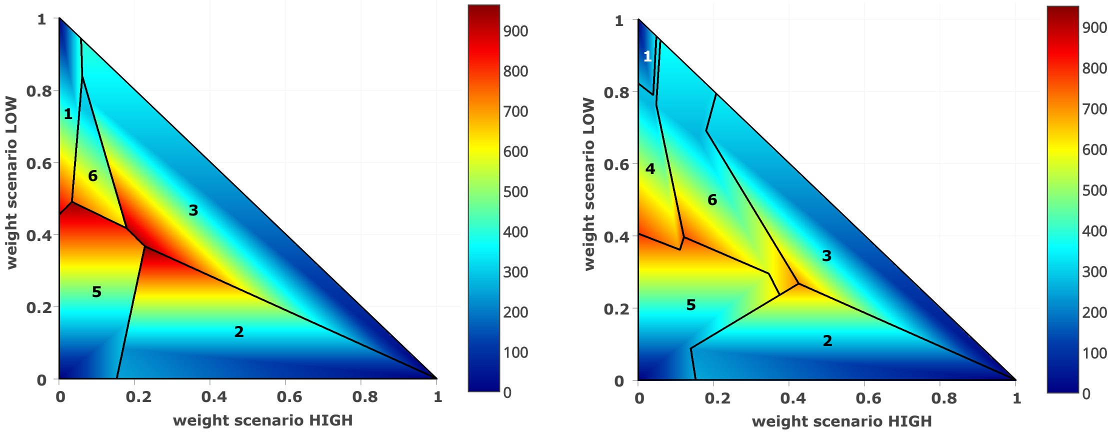

(a) Probabilistic. **(b)** Least worst weighted regret.

Figure 4.12 Weighted regrets for the optimal decisions in the probabilistic and LWWR cases.

Appendix B presents an application of LWWR in the context of the planning process of National Grid Electricity System Operator. The aim of the case study is to explain how LWWR analysis can be used to support the decision-making in the context of the methodology applied by said system operator.

4.3 Seeking investment flexibility

Flexibility in an investment problem is affected by aspects that can be gathered under two main categories, both being closely connected with the way the problem is modelled. These categories are information accessibility and information use. To understand them, it may be convenient to provide some examples.

From the perspective of increased **accessibility to information**, the decision-maker can consider larger sets of investment options (technical characteristics, costs, etc.), a more detailed description of each investment option or, among other things, a more extensive set of information about the characteristic of future scenarios to model the operation as detailed as possible. A larger set of investment options will provide flexibility by simply giving more solution alternatives and potential paths; more information about each investment option will create flexibility by enabling actions within a project that before were not described; a bigger data set to describe the operation in each scenario will potentially allow capturing more value from each investment option. Each of these options will unlock flexibility, but this naturally will come at the cost of dealing with a larger problem.

On the other hand, there is the **information use** aspect. Considering that the information sets are fixed for a given problem, the way in which the decision-maker structures the decision process will impact how the selected investment options will hedge against the future. Considering independent deterministic scenarios to drive decisions will produce fundamentally different solutions compared to strategies that combine the view of the future across scenarios to make decisions. Also, the latter approach is not unique; there is always a possibility to make the decision less often or consider different degrees of uncertainty as deeper into the future a given decision is. The more often a decision can be made, or the more complex the structure of uncertainty and the decision-making problem are, the heavier a problem will result.

These two information-related aspects interact in different ways depending on the selected **methodology** (e.g., deterministic vs stochastic, risk awareness, etc.). The methodologies are structured as algorithms that make decisions based on different decision indicators (e.g., costs, regrets) and metrics (Manhattan, Euclidean, Chebyshev, etc.); each methodology will use the accessible information in different ways.

In general, the main idea behind the concept of investment flexibility is to find solutions whose characteristics can produce/capture value in a broad range of scenarios, hence hedging more effectively against an uncertain future. Although both information categories are relevant, the impact of the accessibility aspect is more natural to understand than the usage aspect; in the following sections, the focus is put on explaining the methodological aspects of improved information usage in the transmission expansion problem.

From a deterministic point of view, it is relatively straightforward to understand the process of finding a set of candidate investments whose impact in relieving system constraints is such that the cost savings will balance out the associated investment costs. If this process is repeated for each independent scenario, the decision-maker can use the information to select a unique investment set that will guarantee a certain behaviour across scenarios given a certain rule. This approach can be improved by finding compromise solutions that will hedge better against the different uncertain scenarios under consideration.

The example in Section 4.1.1 shows how certain reinforcements can act as compromise solutions. While these reinforcements can be overlooked due to their relatively higher costs or their low NPV performance in a deterministic context, they exhibit the capacity to capture value in multiple scenarios, which is precisely what a flexible investment option is. On the other hand, some of these options may not be present in the decision set coming from the deterministic solutions pool.

Figure 4.13 presents the fundamental aspects that interact and impact the capacity to capture flexibility when making investment decisions.

Representation of the system operation refers to the level of details in the operation of the system that is being captured to drive the evaluation of the investment alternatives. Some elements are captured by the information used to represent the system

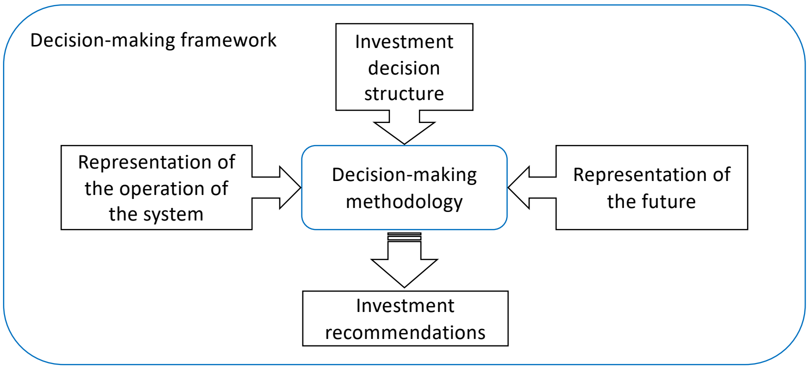

Figure 4.13 Factors influencing investment flexibility

within the decision-making framework, for instance, the refinement of the sampling of demand and renewable energy availability. This aspect was covered in Chapter 3 with the introduction of the security-constrained UC and the description of the unit commitment and security constraints. In general, the principle behind the representation of the operation is simple: higher precision in the representation of the operation (e.g. security constraints) will help to harness more value when adding different investment options (e.g. synchronous condensers, BESS).

Decision-making methodology corresponds to the set of metrics, indicators, risk measures, algorithms and processes used to incorporate all the information about the system behaviour, representation of the future and decisions structure to determine what investments to proceed. The discussion about methodological aspects was presented in Section 4.2.

Investment decisions structure includes all the decision stages associated with the process of deploying a new asset and the set that results from combining all the reinforcement options and their associated decisions. It allows departing from the idea of modelling a single decision of the type build/not build towards a real options-like approach that considers project deferrals, resizing, etc. [99, 118]. This approach naturally provides more flexibility to the decision-making process because it allows modifying the nature of the project dynamically as uncertainty unfolds. It, however, imposes challenges from the point of view of information accessibility and modelling.

Representation of the future refers to how the future and uncertainties are represented/considered in order to identify the optimal development path for the system. The central task in this regard corresponds to identifying the relevant uncertain variables in the longterm and build a representation of the future; to keep all the relevant correlations within the system adequately represented, the usual approach corresponds to define a finite set of scenarios to describe the possible futures. The uncertainty set will then interact with the methodological considerations and the decisions structure, yielding different stages of decisions (e.g. decision tree for stochastic optimisation) depending on the assumption about how uncertainty can unfold as time passes.

The following sections address three topics that influence the flexibility that each investment option can provide in an evolving environment characterised by high uncertainties. First, the concepts associated with the structure of investment decisions in transmission are discussed, and the focus is put on discussing aspects associated with the representation of the future.

4.3.1 Investment decisions structure

In general, the decision process behind the deployment of new assets in transmission focuses on incorporating lots of detail on the operation representation and some information associated with future scenarios. This already represents a substantial challenge, so many simplifications are done regarding how projects are implemented and managed, and how risk is incorporated. As described in [118] the decision-making process can be modelled under one of the following approaches:

- **Deterministic approach**: The discounted cash flows are used to determine what to do with an investment option considering a binary decision on the execution of the project. The project will continue to exist even if it is reporting negative cash flow in the future, and the risks are incorporated in the discount rates used to value future income and expenditures.
- **Scenario approach**: The uncertain variables that can have a substantial effect on the behaviour of the system are used to create structured accounts of possible futures of operation of the system/market, also known as scenarios. These scenarios are then explored through different approaches to assess the value of the different investment options and drive decisions considering their performance across possible futures. The approaches include sensitivity analysis, probabilistic assessment, application of risk measures, and decisions analyses which can consider decision trees and more elaborate metrics and indicators to join the information of multiple scenarios and produce a single decision on each candidate that maximises expected benefits.
- **Real options approach**: Real Options theory was developed in the context of financial options pricing and was specifically tailored to deal with uncertainty when evaluating investment options; its purpose is to assess the viability of engineering projects like transmission assets. This approach can be advantageous in power system development as it enables identifying possible flexible investment strategies to cope with uncertainties. Its value resides in developing adaptive paths of investment decisions that minimise the exposure to risk by exploiting the fact that decision-makers will incorporate new information as uncertainty unfolds and take actions accordingly. However, Real Options theory was created in the context of financial theory, and the underlying assumptions to work with analytical solutions are often not entirely or at all applicable when dealing with engineering problems. The application of this theory in the context of transmission investment should then aim to "mimic" the optionality concept through mathematical programming

techniques that can be applied to engineering problems; this should be done in order to develop flexibility in the decisions for each investment project so that its development can be "optimally" (flexibly) adjusted as uncertainty unfolds. From the perspective of centralised transmission planning, this approach can represent an information access/management challenge because the planner needs to have access to all the options and associated costs faced by the transmission owners.

The real options faced by an engineering project are: defer, time to build, alter operating scale, abandon, switch, growth, and multiple interacting options. A summary of each RO as introduced by [118] is presented below.

- Defer: This is the most common RO found in the literature. It is related to the alternative of delaying investment decisions with the objective of gathering additional information to assess the projects better.
- Time to build: This is the alternative to build a project in stages; each stage involving a small investment and the reassessment of the project. This provides an option to abandon the project before the whole capital needed to build it has been used.
- Alter operating scale: This is the alternative to expand the project in favourable scenarios and reduce or abandon it in negative scenarios. These ROs usually involve supplementary investments in additional capacity or the sale of franchises and infrastructure.
- Abandon: This is the option to abandon a project and sell its infrastructure if the project is resulting in significant losses.
- Switch: This is the alternative to change the technology or size of the project.
- Growth: Growth options involve the alternative to invest in an R&D or pilot project meant to secure resources or provide information about the project's environment. These assets can facilitate investment decisions in additional interrelated projects. In other words, the growth option begins investments with a small project that can grow into one or more larger projects.
- Multiple interacting options: This is the alternative of analysing several ROs in combination instead of assessing each RO independently. In practice, projects might possess several available ROs that affect each other. In other words, in real-world applications, the combined value of the RO might defer from the sum of each option assessed in isolation. Accordingly, assessing RO and their interactions is deemed convenient for most projects in real-world applications.

It is relevant to highlight that the theory usually used to conduct real options valuation of financial assets cannot be directly applied to the assessment of options in transmission project [99, 118]; in this context, the real options aspect corresponds to the design flexibility that is considered and represented within the decision framework.

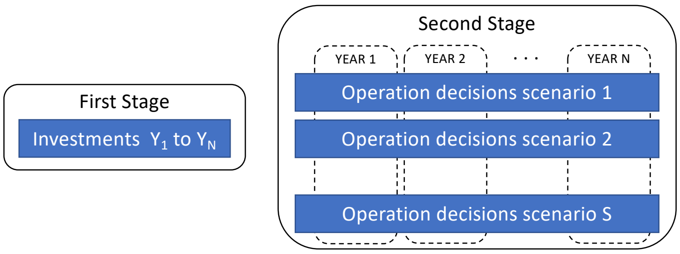

Figure 4.14 Two-stage investment problem.

The issue lies in the effective identification of real options in an engineering project at every point in time; the set of options can be effectively not countable which renders the theory not applicable.

When the set of decisions associated with each reinforcement option has been defined, the actual set of decisions that the decision-maker faces corresponds to the combination of all decisions for all projects in each time step when a decision can be made. This set is very relevant because it corresponds to the foundation of the different decision spaces presented in Figure 4.1. Reducing the decision space in any way can reduce the capacity of the underlying methodology to find the most flexible investment path.

4.3.2 Representation of the future

The discussion on how much information and how to use information is paramount to understand investment flexibility. Both aspects enter in direct conflict with the time and resources necessary to account for them, so it is essential to identify the necessary information to decide how to utilise it to reduce costs and risks.

The previous section presented ways to achieve more flexibility in the investment problem by expanding the number of decisions associated with each reinforcement under consideration. This section discusses how to structure the decision process under uncertainty to identify solutions that provide the most investment flexibility.

The theory of decision-making under uncertainty [102] divides the set of decisions into two groups. There are several decisions taken before uncertainty unfolds (also known as here-and-now decisions), called first-stage decisions; there are also decisions that have to be taken after uncertainty unfolds which correspond to the second-stage decisions (or wait-and-see decisions). These different variables are clearly represented in the example of Section 4.1.1, with investment decisions being the first stage decisions, and the operation of the system (generator outputs, line flows, load shedding) correspond to second-stage decisions (one independent set of decisions for each scenario). The stages represent states of uncertainty, and they have nothing to do with the periods that are being considered within the problem. For instance, first-stage decisions can cover many different periods (for instance, years) that are all included in the second stage, as presented in Figure 4.14.

The two-stage approach can be adequate to represent decisions facing uncertainty,

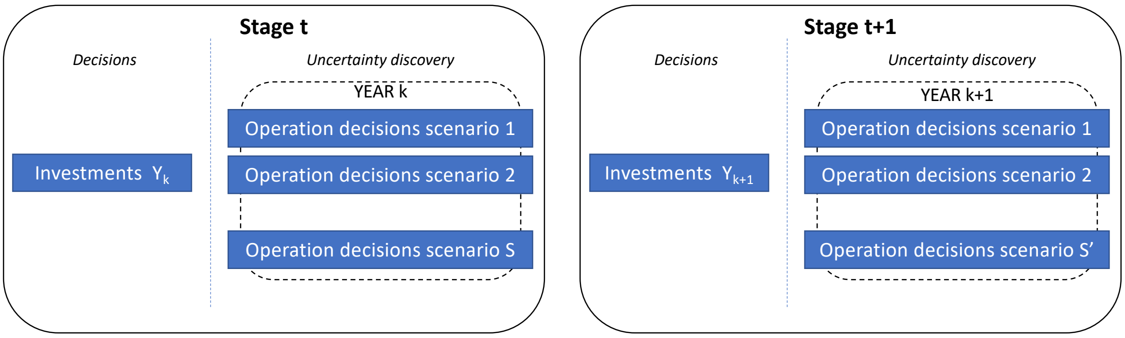

Figure 4.15 Multi-stage approach.

but it can be insufficient to capture all the investment flexibilities that exist in a real problem like the TEP with the consideration of real options, where the future can unfold in different paths not only at the beginning of the problem but also at different points in the future. For instance, considering the methodology used by NGESO in the context of the NOA study presented in Appendix B, it considers the single-year proceed/delay decisions for the subset of reinforcements that are permuted as the here-and-now decisions. All other decisions coming from the deterministic assessment are wait-and-see decisions that are made assuming that the uncertainty has already unfolded.

It is relevant to highlight that the two-stage approach supports making decisions for multiple years, which is something that the NOA CBA methodology could readily incorporate to make the decisions more flexible. Considering more scenarios in the two-stage approach would also help identify a different set of solutions that can better adapt to a broader range of operational conditions. Despite that, the two-stage approach cannot incorporate the reality that these decisions will be updated as the future evolves.

In order to increase the flexibility of an investment option, the model has to incorporate the reality that decisions will be updated as the future unfolds; this is achieved by incorporating several decision stages, each of them assuming certainty of the path followed up to the point where decisions are updated and also modelling the future ahead at that point. The two-stage model can therefore be extended to a so-called multi-stage decision process; such an approach will allow explicit implementation of further levels of decision (e.g. real options) as uncertainty unfolds to capture the investment flexibility of different projects (e.g. stop one project and implement another option which can compromise the uncertainty seen at that point). Figure 4.15 shows a graphical representation of the chain of stages and investment decisions, where the stages of uncertainty coincide with each year under analysis.

A multi-stage representation leads naturally to a more complex problem representation, given the fact that the decisions made in stage $t + 1$ will depend on the scenario realisation in stage t. This structure may seem to isolate the decisions of each stage, but, in reality, they are all strictly interrelated. Modelling flexibility in the future can substantially impact the decisions that are being made today because of the potential to modify them as uncertainty unfolds.

This difference in the modelling approach (two-stage vs multi-stage) is paramount

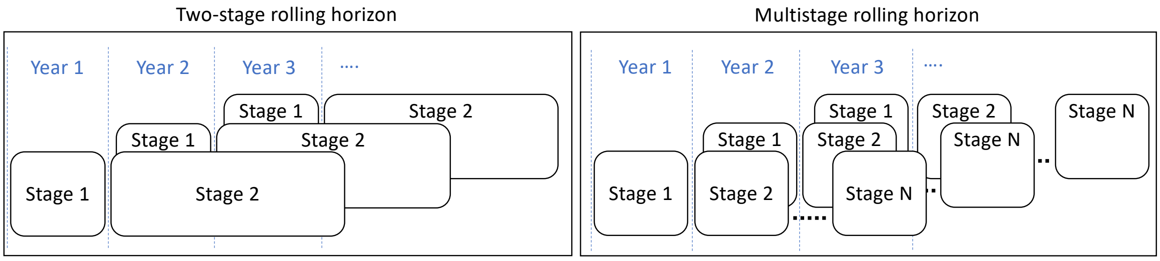

Figure 4.16 Conceptual application of rolling horizon in two-stage and multi-stage decision approaches.

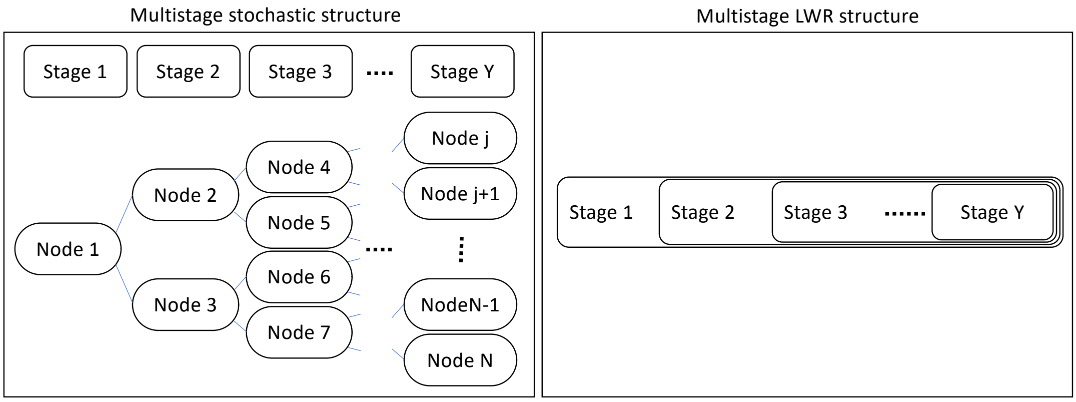

Figure 4.17 Structure of multi-stage decision approaches.

to develop the system efficiently. It could be argued that the investment flexibility provided by the multi-stage approach could be achieved by the two-stage approach by repeating the investment exercise as often as possible (rolling horizon). However, this is incorrect in the sense that, although the rolling horizon is effective in correcting the investment strategy as uncertainty unfolds, the two-stage approach might be blind to future compromise solutions that could be found if the future is modelled as it would reveal itself sequentially in multiple stages; in turn, this will affect the decisions made in each rolling period[16]. As a matter of fact, the multi-stage approach can also be used in the context of a rolling horizon exercise, as shown in Figure 4.16.

A multi-stage representation generally creates challenges from the point of view of the size of the problem. This can render infeasible any approach relying on exhaustive analysis of investment combinations.

Among the options to make decisions in the context of a multi-stage setup (to capture more flexibility), the two natural options to consider are the multi-stage stochastic decision approach and the multi-stage LWR approach, as presented in Figure 4.17.

The multi-stage stochastic approach has been widely used in the context of power system expansion, and its solution methods are well-known. Since in every stage a minimisation problem is solved, it is possible to find solution strategies that scale well for

[16]The concept could also be expressed as follows. Even if the decisions were adjusted systematically through the rolling horizon, modelling with a two-stage approach would only capture a reduced amount of investment flexibility simply because after the first stage everything else would become wait-and-see decisions associated with each scenario. That is, the loss of flexibility comes from assuming that the future is set after stage 1. Of course, this is not strictly a problem of the two-stage approach, but rather a more general implication of how the future is modelled.

large problems, through decomposition approaches [102]; also, adequate risk measures can be included in the formulation with the aim to search for solutions that keep the downside risk limited to fit the risk aversion requirements [112].

The corresponding multi-stage problem using the LWR approach is a rather complex problem [100]. As seen in Figure 4.17, the resulting multi-stage problem yields a nested structure, which stems from the subsequent min-max problems that have to be solved in each stage. There are solution strategies that have been proposed for this problem, typically based on dynamic programming. However, the issue lies with the classic shortcoming of dynamic programming, the so-called curse of dimensionality, which is activated by the number of reinforcements being considered and the different decisions that can be made for each reinforcement.

In this work, the preferred approach is the multi-stage expected cost minimisation due to the advantages it presents to address large problems with the uncertainty structured as large scenario trees[17].

4.4 Chapter summary

This chapter discussed the foundations of decision-making under uncertainty in the context of power system expansion planning. The core concept covered in the chapter was investment flexibility, a characteristic associated with assets (e.g. transmission lines, BESS) that can adapt and provide value across different scenarios. In order to identify such investment options, it is necessary to use an adequate stochastic methodology, which can identify value across scenarios; on top of this, the representation of the future has to represent all potential scenarios that can unfold and the structure of the decisions behind each investment option has to be as detailed as possible in order to grant the model the capacity to produce an adaptable investment strategy.

[17]Scenario trees also provide the flexibility to model high-impact low-probability events. They can be included in the scenario tree using the corresponding probability and the description of the event through the input data for the specific node in the scenario tree.

CHAPTER 5

Expansion planning of low-inertia power systems

5.1 Introduction

This work presents an expansion planning model that makes decisions on new transmission infrastructure, storage units and generation units, with the consideration of frequency security constraints and the representation of long-term uncertainty. The underlying features necessary to assemble this novel expansion model include the development of the security constraints presented in Chapter 3 and the development of an expansion model capable of embedding these constraints and model uncertainty through a scenario tree. In general, the possibility to represent the expansion of the system under uncertainty through a monolithic or deterministic equivalent problem is limited due to the large number of competing investment options, uncertain variables, and the need of representing the operation of the system with high levels of detail. Despite the significant advances in off-the-shelf optimisation software and high-performance computing, the computational requirements of this problem impose the need to use decomposition techniques to address the challenge. In this section, the state of the art in these topics is presented.

In the previous chapter, the concepts behind investment flexibility were presented, focusing on how to adequately represent the uncertainty and investment decisions to capture that flexibility. One fundamental aspect of capturing investment flexibility is representing the operational flexibility of the different assets, either existing or candidate assets. Flexibility in operation can only be assessed if the underlying operational model is able to represent the limitations and strengths of the different units, in particular thermal synchronous units with specific technical constraints. Understanding the impact of different models of operational flexibility in the expansion planning model has been addressed by multiple authors in the past. References [119, 120] investigate the impact of operational flexibility in the design of a generation portfolio, and various works [121–125] also aim to describe the appropriateness of investing in transmission and storage assets. It is clear that in an attempt to capture more operation flexibility, a price is paid in computational burden due to the need to have a more detailed operation of the assets (more constraints) and a denser representation of the operation (more variables). Schwele et al. [126] utilise multi-cut Benders' decomposition to assess the impact of UC constraints in a two-stage generation expansion problem. Reference [127] presents a generation expansion model that includes UC constraints and a convex relaxation to address the computational challenges. Various reviews [128–131] on expansion planning highlight multiple works that describe -among other things- different approaches to account for operational flexibility in generation and transmission expansion modelling.

This work's main contribution lies in the analysis of expansion planning of storage, transmission and generation assets with the consideration of frequency security constraints that can differentiate among frequency response resources (inertia, FFR, PFR, SFR, etc.). A review of the literature shows that a model featuring these characteristics has not been presented before. Inzunza et al. [132] introduce a generation expansion model that considers the effect of inertia and PFR to limit frequency nadir. The model does not consider the effect of the natural frequency response coming from demand or the effect of FFR in the allocation of frequency response resources. In [133] the demand damping factor is considered in the frequency response constraints including inertia and PFR in the context of a generation expansion planning. Recently, [134] proposed a generation expansion model that considers unit commitment constraints, a second-order cone approximation of the AC optimal power flow, and introduces inertia requirements via ROCOF. A model capable of expanding generation considering a generalised $n-1$ security criterion is presented in [135], which allocates droop-controlled response, but it fails to consider inertia which limits the capacity to account for frequency extrema requirements. As seen here, it is possible to say that the expansion planning of low-carbon power systems with consideration of fast frequency response resources remains broadly unexplored.

Including frequency response constraints in a highly detailed model of the system's operation, in the context of the expansion planning under uncertainty, creates a very large monolithic problem. Different works on stochastic planning models have relied on advanced decomposition techniques to overcome the intractability of large MILP models. Recent work on Dantzig–Wolfe decomposition and column generation-based algorithms have provided an approach to handle the size of this problem. A multi-stage stochastic capacity problem is solved by applying a "variable splitting" technique in the column generation algorithm [136]. Flores et al. [101], UC constraints have been incorporated in the operational problem for solving a generation expansion problem, in [137] the same is done for the expansion of transmission and storage assets, and in [138] gas networks have been integrated into a stochastic planning problem. In [97], authors ensure that developing computationally efficient methods to address non-convexities when considering high operational details in planning is an important research avenue to be able to fully capture the benefits of smart grid technologies in real-size planning problems.

Although effective in dealing with the size challenges, the column generation algorithm usually displays three critical issues: slow convergence during the final iterations, commonly known as the tailing-off effect; the plateau effect, which describes the process in which the master problem solution value remains relatively constant for several iterations, and the bang-bang effect, a source of instability in the convergence process, where the dual solutions jump from one extreme to another, slowing down convergence [139]. Different methods [140–142] have been applied to tackle these effects, which in general involve restricting or relaxing the master problem.

In the following sections, a novel security-constrained expansion problem is presented, whose performance is tested on the Australian power system in the context of its recent long-term expansion review [9]. Transmission, storage and generation investment candidates are considered in the planning problem, for instance, new lines, BESS and synchronous condensers. The performance of the column generation algorithm against the solution of the deterministic equivalent problem is compared. The use of distributed computing is applied in the column generation algorithm to show the advantages in the speed of resolution it enables. The benefits of combined storage and transmission investments to deal with future uncertainty are shown, also considering the potential development of large pumped-hydro storage projects. Investment flexibility is assessed through the consideration of different scenario trees representing the future developments of the system.

5.2 Expansion planning model

The security-constrained expansion planning of the system is a problem that requires a high degree of operational detail to represent the subtleties of the allocation of FR resources and, at the same time, imposes all the challenges associated with the expansion of power systems under deep uncertainties. Considering the current state-of-the-art in expansion planning models, this work focuses on the use of Dantzig-Wolfe (DW) decomposition to divide the large deterministic-equivalent problem (expected cost minimisation), and a column generation algorithm is applied to find a solution for the decomposed model.

The stochastic nature of some parameters (load, renewable energy availability, decommission of synchronous units, investment costs and operation costs, among others) within the expansion model is represented through a scenario tree. Scenarios have the capacity to represent uncertain variables while preserving all the relevant interactions between the elements of the system. As usual on this type of problem, the nodes of the tree are organised in epochs (for instance, different years in the planning horizon), as seen in Figure 5.1. That example displays three scenarios, each of them including the nodes that cover the operation from the beginning to the end of the horizon

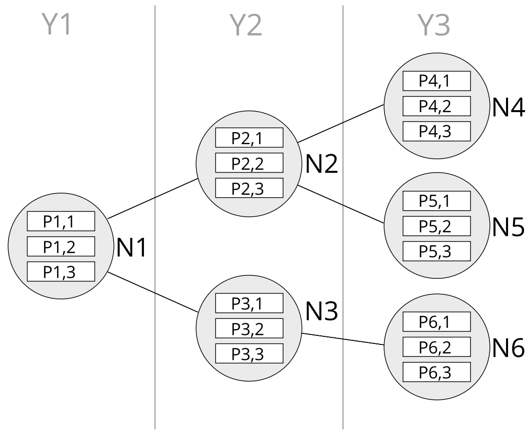

Figure 5.1 Scenario tree representing 3 yearly stages through six nodes, each of them containing 3 representative weeks.

($N1 - N2 - N4$, $N1 - N2 - N5$ and $N1 - N3 - N6$). Each node in the tree represents the operation and investment in a particular year for the corresponding values of the stochastic variables. The system's operation is represented through a set of representative days, weeks or months (or any other period defined for the study), which are assumed to be independent; in this work, the operation is modelled through representative weeks. Investment decisions on new candidate assets are made for each node of the tree, considering specific models for each element of the system, that will be introduced in the coming sections.

Naturally, the stochastic tree can be represented as a monolithic optimisation problem, known in the literature as the deterministic equivalent problem. For some expansion planning case study applications where the tree's size and the operation's representation do not yield an extremely large problem, the associated monolithic problem can be promptly solved using off-the-shelf mixed-integer linear programming solvers. Larger problems resulting from the consideration of various stochastic parameters, greater detail in the modelling of the operation and, especially, a large number of scenarios, will render the monolithic approach impractical due to high memory requirements and slow convergence of the underlying branch-and-cut algorithm used to solve MILPs.

The use of decomposition methods can considerably increase the size of the problems that can be effectively solved. As presented in [97, 101, 143], reformulating the problem using DW approach [144] can make the problem solvable by column generation-based algorithms, which can obtain optimal solutions for the original problem via the iterative resolution of multiple smaller problems known as the restricted master problem (RMP) and the pricing subproblems SP. The RMP decides the optimal investment for all nodes of the scenario tree considering the optimal operational solutions found through the SPs. The details about the decomposition and solution algorithm are presented in the following sections.

5.2.1 Monolithic expansion planning problem

This section describes the main components of the underlying mathematical problem that describes the expansion planning problem under uncertainty. The objective here is to show the structure of the problem and not to describe the specific modelling features of the operation, hence the model presented in Chapter 3 (3.3.1)-(3.3.54) is represented through the following compact notation:

$$\min_{x,z} \; OP_{m,w} = c^{\intercal}_{m,w} x_{m,w} + h^{\intercal}_{m,w} z_{m,w} \tag{5.2.1}$$

subject to:

$$A_{m,w} x_{m,w} + G_{m,w} z_{m,w} \leq b_{m,w} \tag{5.2.2}$$

$$x_{m,w} \geq 0, \;\; x_{m,w} \in \mathbb{R}^{\nu} \tag{5.2.3}$$

$$z_{m,w} \geq 0, \;\; z_{m,w} \in \mathbb{Z}^{\eta} \tag{5.2.4}$$

The model (5.2.1)-(5.2.4) represents the operation of a specific week w for a given node m in the scenario tree, as depicted in Figure 5.1. $x_{m,w}$ and $z_{m,w}$ are vectors of real and integer variables for node m and week w, respectively, and $c_{m,w}$ and $h_{m,w}$ are the corresponding vectors of costs associated to those variables. $A_{m,w}$ and $G_{m,w}$ are matrices and $b_{m,w}$ is a vector describing the constraints associated to the operation.

Then, a simplified version of the monolithic problem can be described as follows:

$$\min_{y,x,z} \sum_{m \in M} \frac{\rho_m}{(1+RT)^{Y_m - Y_R}} \left(IC^{\intercal}_m y_m + \sum_{w \in W_m} \omega_{m,w} OP_{m,w}(x_{m,w}, z_{m,w}) \right) \tag{5.2.5}$$

subject to:

$$\tilde{A}_{m,w} x_{m,w} + \tilde{G}_{m,w} z_{m,w} + I_m y_m \leq \tilde{b}_{m,w} \quad \forall m, w \in W_m \tag{5.2.6}$$

$$y_m \geq y_{P(m)} \quad \forall m \tag{5.2.7}$$

$$x_{m,w} \geq 0 \quad \forall m, w \in W_m \tag{5.2.8}$$

$$z_{m,w} \geq 0 \quad \forall m, w \in W_m \tag{5.2.9}$$

$$y_m \geq 0 \quad \forall m, w \in W_m \tag{5.2.10}$$

$$x_{m,w} \in \mathbb{R}^{\tilde{\nu}} \tag{5.2.11}$$

$$z_{m,w} \in \mathbb{Z}^{\tilde{\eta}} \tag{5.2.12}$$

$$y_m \in \mathbb{Z}^{\mu} \tag{5.2.13}$$

The objective function of problem (5.2.5)-(5.2.13) adds up all the investment $IC^{\intercal}_m y_m$ (IC_m corresponds to a vector of investment costs) and operation $OP_{m,w}(x_{m,w}, z_{m,w})$ costs of the set M of nodes (and associated representative weeks) in the scenario tree. Note that the operation of each representative week is multiplied by a factor $\omega_{m,w}$ to reflect the weight of that representative week in the operation of the year associated with node m. These costs are discounted from year Y_m for each node m using a rate of return RT to a reference year Y_R. Also, since the approach considers expected cost minimisation, each node is weighted by its probability of occurrence ρ_m. Constraint (5.2.6) describes the operation of each week w within the set of representative weeks W_m of node m. This constraint has been modified to represent the operation of the set of investment candidates in each node m, which is why matrices $A_{m,w}$ and $G_{m,w}$, and vector $b_{m,w}$ from problem (5.2.1)-(5.2.4) are represented by $\tilde{A}_{m,w}$ and $\tilde{G}_{m,w}$, and $\tilde{b}_{m,w}$, respectively. The activation of the expansion modules is controlled through the vector y_m that contains the variables to determine new investments in node m and the interaction of the investment decisions with the corresponding operation constraints is represented through matrix I_m. The consistency of the investment decisions (if a new asset is deployed in the present, it as to be active in the future) is imposed by means of constraint (5.2.7), where $P(m)$ represents the preceding node to node m (e.g. in Figure 5.1, $P(N2) = N1$). In this simplified formulation no lead times are specifically considered; in the following section, more detail is provided regarding the specific modelling considerations for the investment in each asset type.

Problem (5.2.5)-(5.2.13) is very modular, displaying a block-diagonal structure, characteristic that can be exploited to divide the problem into smaller pieces through the application of DW decomposition and a delayed column generation solution approach. Each operation problem can be isolated, creating a small investment problem that considers only the information of that specific week to make the optimal investment decision for the operation in that period. Each of these small problems is usually referred to as the pricing subproblem (SP). (5.2.6) corresponds to a complicating constraint that links the results among SPs, which is why that constraint is placed in what is called the master problem; in the context of the column generation algorithm, the master problem is often called restricted master problem (RMP) because it solves an incomplete version of the problem in each iteration, only using the partial information about the operation and investment found in the SPs in the previous iterations. The RMP and the set of SPs interact through the transfer of information found in each of them, a process that is presented in Section 5.2.4.

The following section presents the structure of the RMP highlighting the different assets that can be considered in the expansion of the system (lines, storage, generators) and the corresponding investment modelling. Then in Section 5.2.3, the structure of the SPs is presented, focusing on the changes to the model (3.3.1)-(3.3.54) to enable the activation of new assets through investment variables and the modification of the objective function to include the information obtained from the RMP.

5.2.2 Restricted Master Problem

The restricted master problem is in charge of dealing with the high-level cost-benefit analysis. This means that the RMP "sees" the information about investing in different assets and the related costs of operating the system with them. It does not, however, make any low-level operation decision; this information is contained in vectors of information that have been obtained from the successive solution of the SPs. These vectors are called *columns*, and they contain an investment profile in a given SP and the associated costs of operating the system with those new assets.

The objective function of the RMP (5.2.14) is very similar to the one presented for the monolithic expansion problem. In this case, the vector notation is dropped and the investment costs in different investment types (storage systems are specified using superindex S and candidate set S^C, lines with super index L and candidate set L^C, and generators with superindex G and candidate set G^C) are explicitly shown. At any given point of the iteration process, there will be a set $K_{m,w}$ of available columns representing the operation of the problem representing week w in node m. Each of the columns p contains the information of the total cost of operation of that week $\widehat{OP}^p_{m,w}$ and the associated investment decision results ($\hat{i}^{S,p}_{m,w,j}\ \forall\ j$, $\hat{i}^{L,p}_{m,w,l}\ \forall\ l$ and $\hat{i}^{G,p}_{m,w,g}\ \forall\ g$) made within the operation problem.

$$\begin{aligned}\min_{y^S_{m,j},y^L_{m,l},y^G_{m,k},\lambda^p_m} Z^{IP}_{RMP} : \sum_{m\in M} \frac{\rho_m}{(1+RT)^{Y_m-Y_R}} \Bigg(& \sum_{j\in S^C} IC^S_{m,j} y^S_{m,j} + \sum_{l\in L^C} IC^L_{m,l} y^L_{m,l} \\ & + \sum_{k\in G^C} IC^G_{m,k} y^G_{m,k} + \sum_{w=1}^{W_m} \sum_{p\in K_{m,w}} \omega_{m,w} \widehat{OP}^p_{m,w} \lambda^p_{m,w} \Bigg)\end{aligned} \tag{5.2.14}$$

subject to:

$$\sum_{p\in K_{m,w}} \hat{i}^{S,p}_{m,w,j} \lambda^p_{m,w} \leq \sum_{\mu\in\Psi_m} y^S_{\mu,j} \qquad \forall m, w\in W_m, j\in S^C \qquad \left[\pi^S_{m,w,j}\right] \tag{5.2.15}$$

$$\sum_{p\in K_{m,w}} \hat{i}^{L,p}_{m,w,l} \lambda^p_{m,w} \leq \sum_{\mu\in\Psi_m} y^L_{\mu,l} \qquad \forall m, w\in W_m, l\in L^C \qquad \left[\pi^L_{m,w,l}\right] \tag{5.2.16}$$

$$\sum_{p\in K_{m,w}} \hat{i}^{G,p}_{m,w,k} \lambda^p_{m,w} \leq \sum_{\mu\in\Psi_m} y^G_{\mu,k} \qquad \forall m, w\in W_m, k\in G^C \qquad \left[\pi^G_{m,w,k}\right] \tag{5.2.17}$$

$$\sum_{p\in K_{m,w}} \lambda^p_{m,w} = 1 \qquad \forall m, w\in W_m \qquad [\sigma_{m,w}] \tag{5.2.18}$$

$$y^S_{m,j}, y^L_{m,l}, y^G_{m,k} \in \mathbb{Z}_{\geq 0} \qquad \forall m, j, l, k \tag{5.2.19}$$

$$\lambda^p_{m,w} \in \{0,1\} \qquad \forall m, w\in W_m, p\in K_m \tag{5.2.20}$$

If a given column is selected by making the corresponding binary variable $\lambda^p_{m,w} = 1$ this pushes the right-hand side expressions in (5.2.15)-(5.2.17) to take the value of the subproblem's investment results. The right-hand side expression corresponds to the sum of all the new investments y done in the set of nodes Ψ_m preceding and including node m. In turn, the restricted master problem investment variables y are valued at the corresponding investment costs in the objective function. The so-called convexity constraints are imposed to force the RMP to choose one and only one column among the available options for each week in each node. These constraints require solving the RMP with at least one feasible column (which has implications in the initialisation of the algorithm, as described in the following sections). The RMP investment variables are integer and the column selection variables λ are binary.

If the integer and binary variables in problem (5.2.14)-(5.2.20) are relaxed, the resulting linear problem allows for the construction of the dual linear problem, which enables the calculation of the dual variables associated to constraints (5.2.15)-(5.2.18). These dual variables contain the information regarding the global value of deploying an extra asset in any of the nodes, which is then used to value the investment in new assets within each of the pricing subproblems[18]. If the integrality constraints are relaxed, the value of the objective function is labelled Z^{LP}_{RMP} as opposed to Z^{IP}_{RMP} when integer variables are used.

Model (5.2.14)-(5.2.20) does not exactly represent the RMP used in this work. It was presented because it highlights the model's core elements and enables a relatively easy description of its structure. However, the model as was presented will experience *end of horizon* issues, where the investment in new assets (variables y) in nodes close to the end of the horizon will be valued at the total cost of the investment, which will not be balanced out by the long-term benefits in operation, creating the wrong investment decisions. Also, the model presented before does not consider the lead-time of some investments, which can have a substantial effect on the decisions.

[18]As it will be seen in the description of the algorithm to solve the problem, the relaxed RMP is used to explore the search space until the corresponding relaxed criterion to stop is met, at which point the integer RMP will be used to determine the optimal solution of the problem.

$$\min_{y^S_{m,j},y^L_{m,l},y^G_{m,k},\lambda^p_m} Z^{IP}_{RMP} : \sum_{m\in M} \frac{\rho_m}{(1+RT)^{Y_m-Y_R}} \Bigg(\sum_{l\in L^C} IC^{AL}_{m,l} d^L_{m,l} + \sum_{j\in S^C}\sum_{\mu\in\Psi_m} IC^{AS}_{\mu,j} y^S_{\mu,j}$$
$$+ \sum_{l\in L^C}\sum_{\mu\in\Psi_m} IC^{AL}_{\mu,l} y^L_{\mu,l} + \sum_{k\in G^C}\sum_{\mu\in\Psi_m} IC^{AG}_{\mu,k} y^G_{\mu,k} + \sum_{w=1}^{W_m}\sum_{p\in K_{m,w}} \omega_{m,w}\widehat{OP}^p_{m,w}\lambda^p_{m,w} \Bigg) \tag{5.2.21}$$

subject to:

$$d^L_{P(m),l} = y^L_{m,l} \qquad \forall m, m\neq 1, l\in L^C \tag{5.2.22}$$

$$\sum_{p\in K_{m,w}} \hat{i}^{S,p}_{m,w,j}\lambda^p_{m,w} \leq \sum_{\mu\in\Psi_m} y^S_{\mu,j} \qquad \forall m, w\in W_m, j\in S^C \qquad \left[\pi^S_{m,w,j}\right] \tag{5.2.23}$$

$$\sum_{p\in K_{m,w}} \hat{i}^{L,p}_{m,w,l}\lambda^p_{m,w} \leq \sum_{\mu\in\Psi_m} y^L_{\mu,l} \qquad \forall m, w\in W_m, l\in L^C \qquad \left[\pi^L_{m,w,l}\right] \tag{5.2.24}$$

$$\sum_{p\in K_{m,w}} \hat{i}^{G,p}_{m,w,k}\lambda^p_{m,w} \leq \sum_{\mu\in\Psi_m} y^G_{\mu,k} \qquad \forall m, w\in W_m, k\in G^C \qquad \left[\pi^G_{m,w,k}\right] \tag{5.2.25}$$

$$\sum_{p\in K_{m,w}} \lambda^p_{m,w} = 1 \qquad \forall m, w\in W_m \qquad [\sigma_{m,w}] \tag{5.2.26}$$

$$y^S_{m,j}, y^L_{m,l}, y^G_{m,k}, d^L_{m,l} \in \mathbb{Z}_{\geq 0} \qquad \forall m, j, l, k \tag{5.2.27}$$

$$\lambda^p_{m,w} \in \{0,1\} \qquad \forall m, w\in W_m, p\in K_m \tag{5.2.28}$$

Model (5.2.21)-(5.2.28) addresses the two issues pointed out before. To solve the *end of horizon* problem, the solution is to use annualised investment costs (denoted, for example, $IC^{AL}_{m,l}$ for lines) to account for the cost of investment in the different nodes. In a given node m the total amount to be paid -for example- for a given storage asset j corresponds to $\sum_{\mu\in\Psi_m} IC^{AS}_{\mu,j} y^S_{\mu,j}$. This corresponds to the new modules invested in node m plus the investment in new modules in each of the previous nodes μ multiplied by the annuity calculated in the node μ. This approach not only solves the *end of horizon* issues but also accounts for the reduction in the investment costs for a given technology as time evolves.

Although all investment options can potentially have a lead time, for the sake of conciseness, model (5.2.21)-(5.2.28) only presents the feature for investment in new lines assuming a lead-time of one epoch. To achieve this, the auxiliary variable $d^L_{P(m),l}$ describing the decision to build is defined, which is added to the objective function multiplied by the corresponding annualised investment. The moment the decision to build is made (5.2.22), it triggers the activation of the asset in all the succeeding nodes, which can also be labelled as a non-anticipativity constraint. This modelling approach has the advantage to explicitly account for investment costs incurred before the asset becomes available.

5.2.3 Pricing subproblem

In this section, the adjustments to model (3.3.1)-(3.3.54) are described so that it can be used in the context of the column generation algorithm. Only subsets of constraints are affected to incorporate investment decisions, so only those specific constraints are presented here.

One of the most important changes occurs in the objective function (3.3.1). OP_w denotes the function of all the costs directly associated with the operation as presented in (3.3.1); to keep all the balances referred to the original monolithic problem, the total operation costs are weighted by the probability of the node, the weight of the week and the corresponding discount factor for node m, $df_m = 1/(1+RT)^{Y_m - Y_R}$. The pricing subproblem models the operation over a week w in the node m, and receives the dual values found in the RMP that correspond to the investments in node m and week w ($\widehat{\pi}^S_{m,w,j}$, $\widehat{\pi}^L_{m,w,l}$, $\widehat{\pi}^G_{m,w,k}$, $\widehat{\sigma}_{m,w}$). These dual values are used to price the new investments in the objective function, which creates the feedback loop necessary for the pricing subproblem to find the right investment level in the context of the original problem. The value of the objective function of the pricing subproblem is labelled $Z_{SP_{m,w}}$ for future reference.

$$\min_{\vec{x},\vec{y}} \rho_m \omega_{m,w} df_m OP_w - \sum_{j \in S^C} \widehat{\pi}^S_{m,w,j} i^S_{m,w,j} - \sum_{l \in L^C} \widehat{\pi}^L_{m,w,l} i^L_{m,w,l} - \sum_{k \in G^C} \widehat{\pi}^G_{m,w,k} i^G_{m,w,k} - \widehat{\sigma}_{m,w} \quad (5.2.29)$$

Let us review the changes to the constraints associated with the new investment candidates. Given the formulation of (3.3.1)-(3.3.54), adding new generators is straightforward. By simply taking the commitment variable n, it is possible to impose the following additional condition:

$$n_{k,t} \leq i^G_{m,w,k} \quad \forall k \in G^C, t \quad (5.2.30)$$

This approach allows to include the candidate generators as any other generator and by adding (5.2.30) the investment in new assets is reflected in the operation (in the context of the case study application presented in this chapter, synchronous condensers are used as candidate investment options, which are modelled as a generator that cannot inject energy or reserves). Investment in new transmission lines with a transport model only (no DC power flow constraints) is straightforward. Using (3.3.4) and (3.3.5) it is possible to model the effect of investing in new lines in a similar fashion to (5.2.30).

$$-F^{rev}_{l,t} i^L_{m,w,l} \leq fl_{l,t} \leq F^{fwd}_{l,t} i^L_{m,w,l} \quad \forall l \in L^C, t \quad (5.2.31)$$

$$fl_{l,t} + fp_{l,t} = F^{fwd}_{l,t} i^L_{m,w,l} \text{ and } fl_{l,t} + fn_{l,t} = -F^{rev}_{l,t} i^L_{m,w,l} \quad \forall l \in L^C, t \quad (5.2.32)$$

Finally, the modelling for new storage assets is presented. The approach, in this case, is not as straightforward as before because of the variable $u_{j,t}$ controlling the charging and discharging mode. The direct approach would be to include the investment variables $i^S_{m,w,j}$ in (5.2.33) and (5.2.34), however, this would result in bilinear terms. To deal with these constraints (5.2.33) and (5.2.34) are modified to include the maximum number NS^{max}_j of investment modules that can be installed (or any large number for that matter).

$$ch_{j,t} \leq \left(1 - u_{j,t}\right) \cdot CH^{max}_j \cdot NS^{max}_j \quad \forall j \in S^C, t \tag{5.2.33}$$

$$dch_{j,t} \leq u_{j,t} \cdot DCH^{max}_j \cdot NS^{max}_j \quad \forall j \in S^C, t \tag{5.2.34}$$

Then, the investment variables are used to determine the charging, discharging, maximum reserve provision and energy storage capacity.

$$ffr^{up}_{j,t} + sfr^{up}_{j,t} \leq DCH^{max}_j \cdot i^S_{m,w,j} - dch_{j,t} + ch_{j,t} \quad \forall j \in S^C, t \tag{5.2.35}$$

$$ffr^{dw}_{j,t} + sfr^{dw}_{j,t} \leq CH^{max}_j \cdot i^S_{m,w,j} + dch_{j,t} - ch_{j,t} \quad \forall j \in S^C, t \tag{5.2.36}$$

$$ffr^{dw}_{j,t}, ffr^{up}_{j,t} \leq FFR^{max}_j \cdot i^S_{m,w,j} \quad \forall j \in S^C, t \tag{5.2.37}$$

$$E^{\min}_j \cdot i^S_{m,w,j} \leq e_{j,t} \leq E^{\max}_j \cdot i^S_{m,w,j} \quad \forall j \in S^C, t \tag{5.2.38}$$

The variables in the pricing subproblem are the same as in shown in (3.3.53) and (3.3.54), considering also one integer investment variable per investment option ($i^S_{m,w,j}$ $\forall j$, $i^L_{m,w,l}$ $\forall l$, $i^G_{m,w,k}$ $\forall k$). The following section describes the different steps of the column generation algorithm used to perform the systematic search of the optimal solution based on the RMP and SPs.

5.2.4 Column generation algorithm

Sections 5.2.2 and 5.2.3 described the restricted master problem and pricing subproblem formulations. In the case of the restricted master problem $\widehat{OP}^p_{m,w}$, $\hat{i}^{S,p}_{m,w,j}$, $\hat{i}^{L,p}_{m,w,l}$, $\hat{i}^{G,p}_{m,w,k}$ are known values obtained from all the feasible/optimal solutions of the SPs in each iteration. The pricing subproblem associated to node m, week w, denoted $SP_{m,w}$, considers the values $\widehat{\pi}_{m,w,j}$, $\widehat{\pi}_{m,w,l}$, $\widehat{\pi}_{m,w,k}$, $\widehat{\mu}_{m,w}$ obtained in the latest solution of the RMP. If the value of the objective function value $Z_{SP_{m,w}}$ of a slave problem (also known as reduced cost) is negative, then the introduction of this (promising) new column in the RMP can eventually reduce the overall cost. The RMP is, therefore, updated by adding all promising columns found in the SPs. The interdependency between RMP and SPs creates an iterative process that ends when a given stopping criterion is met or, naturally, when no new promising columns are found in the SPs. At this point, the current solution is optimal for the linear programming relaxation of the RMP, which is the condition needed to obtain the dual values needed in the pricing subproblem. In order to obtain a feasible integer solution, one can simply reimpose integrality constraints (5.2.27) and (5.2.28), and solve the resulting MILP. Figure 5.2 depicts the procedure. In order to determine when the algorithm has converged, it is necessary to calculate the upper and lower bounds for the problem. The RMP can be solved as an integer problem or as a relaxed linear problem; the associated optimal value of (5.2.21) is used to define the integer upper bound Z^{IP}_{RMP} or a linear upper bound Z^{LP}_{MP}, respectively.

$$LB := Z^{LP}_{RMP} + \sum_{m}\sum_{w} \min\left\{0, Z_{SP^*_{m,w}}\right\} \tag{5.2.39}$$

$$gap_L = \frac{(Z^{LP}_{RMP} - LB)}{LB} \tag{5.2.40}$$

$$gap_I = \frac{(Z^{IP}_{RMP} - LB)}{LB} \tag{5.2.41}$$

The LB (5.2.39) is used both when calculating the linear gap gap_L or the integer gap gap_I, as shown in (5.2.40) and (5.2.41), respectively. The previous definition for the lower bound is valid only if the reduced costs $Z_{SP_{m,w}}$ used in the calculation are a result of the SPs reaching optimality. In the case that any of the pricing subproblems have not reached optimality, the corresponding reduced cost has to be ignored for the calculation of LB, hence obtaining a worse LB but avoiding the potential overestimation of the LB that can come from using suboptimal reduced costs. This procedure of adding columns to the RMP will continually improve its objective, thereby reducing the upper bound. As it can be seen in the definition of the LB, as soon as the reduced costs of all the columns is zero, the LB will arrive at the value of the upper bound, which is the value of the RMP. More details about the column generation algorithm can be found in [101, 136, 143]. Algorithm 5.1 provides a pseudo-code representation of the steps described here and in Figure 5.2, highlighting some of the steps where distributed computing can be applied to accelerate the convergence of the algorithm.

The column generation algorithm can exploit the benefits of distributed computing, in particular in the stage where the SPs are solved. In Algorithm 5.1 the double loop that iterates over all the nodes and solves the operation for all week in each node contains optimisation problems that are entirely independent of each other. This feature allows to create a pool of problems that can be sent to adequate computation environments (see Appendix A) to solve them simultaneously instead of sequentially, which can significantly accelerate the solution process. This characteristic becomes critical for very large problems, because as it will be seen in the next section, the larger the problem, the heavier the search. This behaviour becomes especially problematic when trying to solve the monolithic problem, which can consume prohibitive levels of memory to perform the search. By breaking the original problem into smaller pieces through the decomposition, solving the SPs is less demanding on computational resources, which enables to solve substantially larger problems than the monolithic approach.

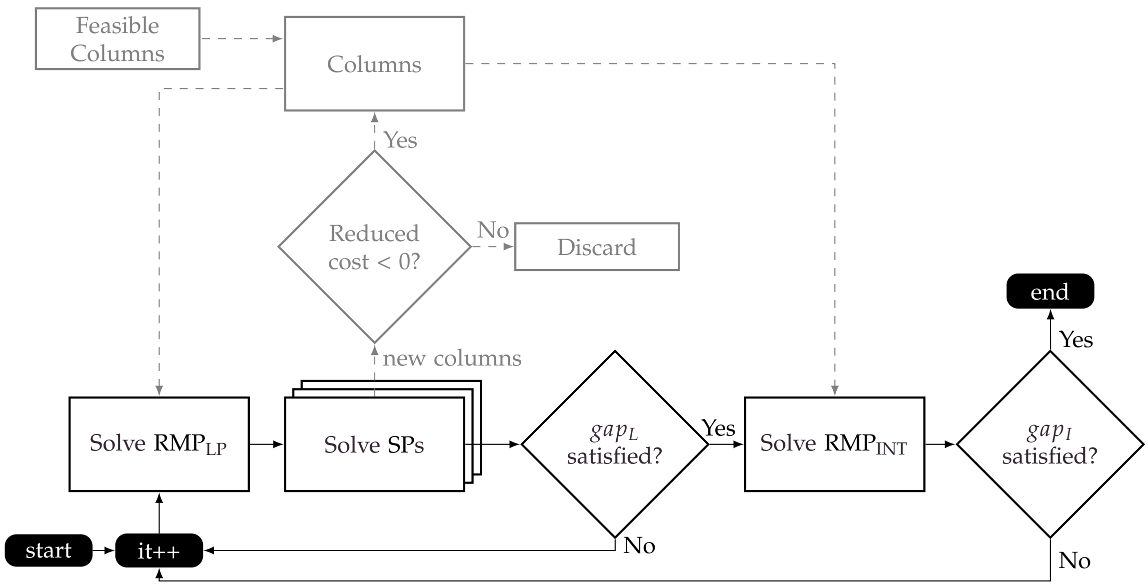

Figure 5.2 Algorithm for updating the time limit and column selection.

Algorithm 5.1: Column generation algorithm.

Data: System and scenarios data, initial feasible columns, target gap Δ
Init: $LB = -\infty$, $UP = \infty$, $gap_L = \infty$, $gap_I = \infty$
Result: Optimal values for RMP variables (5.2.28) $y^S_{m,j}, y^L_{m,l}, y^G_{m,k}, d^L_{m,l}\ \forall m, j, l, k$
while *integer gap (5.2.41)* $gap_I > \Delta$ **do**
  while *linear gap (5.2.41)* $gap_L > \Delta$ **do**
    $it = it + 1$;
    Solve the linear relaxation of the RMP (5.2.21)-(5.2.28);
    Store values of dual variables $\widehat{\pi}_{m,w,j}$, $\widehat{\pi}_{m,w,l}$, $\widehat{\pi}_{m,w,k}$, $\widehat{\mu}_{m,w}$ $\forall m, w, j, l, k$;
    $UB = Z^{LP*}_{RMP}$;
    for $m \in M$ **do**
      for $w \in W_m$ **do**
        Solve $SP_{m,w}$ with dual variables $\widehat{\pi}_{m,w,j}$, $\widehat{\pi}_{m,w,l}$, $\widehat{\pi}_{m,w,k}$, $\widehat{\mu}_{m,w}$ $\forall j, l, k$;
        Obtain $\widehat{OP}_{m,w}$, $\hat{i}^S_{m,w,j}$, $\hat{i}^L_{m,w,l}$, $\hat{i}^G_{m,w,k}$ $\forall j, l, k$;
        if $Z^*_{SP_{m,w}} < 0$ **then**
          Add column $\widehat{OP}_{m,w}$, $\hat{i}^S_{m,w,j}$, $\hat{i}^L_{m,w,l}$, $\hat{i}^G_{m,w,k}$ $\forall j, l, k$ to RMP;
        end
      end
    end
    Calculate $LB = Z^{LP*}_{RMP} + \sum_m \sum_w \min\left\{0, Z^*_{SP_{m,w}}\right\}$;
    Calculate $gap_L = (Z^{LP*}_{RMP} - LB)/LB$;
  end
  Solve RMP (5.2.21)-(5.2.28);
  Calculate $gap_I = (Z^{IP*}_{RMP} - LB)/LB$;
end

5.3 Case study applications

The different studies on expansion planning presented in this section use the information presented in the 2020 Integrated System Plan (ISP) [9]. Even though the expansion methodology presented in this chapter is fundamentally different from the ISP methodology, it is relevant to describe it to understand the input data of the study. Then, the input data used in the case study applications is introduced, along with the description of the representation of the future and uncertainty. The expansion planning model introduced in Section 5.2 is validated against its deterministic equivalent problem, and several tests are performed to determine the speed of the solution algorithm. Then the model is used to find the optimal expansion plan for the NEM for two different representations of the uncertainty in the system.

5.3.1 Integrated System Plan 2020 methodolgy

AEMO's ISP process covers a decision horizon of 20 years and includes the effect of distributed energy resources (DER), virtual power plant (VPP), grid-scale generation, energy storage systems (ESS), high voltage transmission, the gas system, hydro resources and the electrification of transport. ISP 2020 did not consider the effects of the emerging global hydrogen economy and the potential development of nuclear energy in Australia.

The ISP addresses the power system needs for reliability, security, public policy objectives and their supporting system standards. The transmission expansion decisions necessary to leverage the transition from a coal-fired generation dominated system to a low-carbon, low-inertia system dominated by VRES and DER are made using a least-cost and least-regret approach.

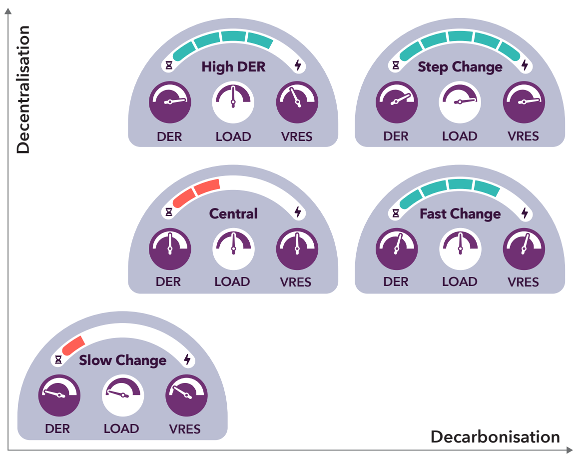

Figure 5.3 ISP scenarios (Source [9]).

In order to determine the optimal transition path for the system, the ISP models the future through a set of scenarios (see Figure 5.3) that are characterised by varying load

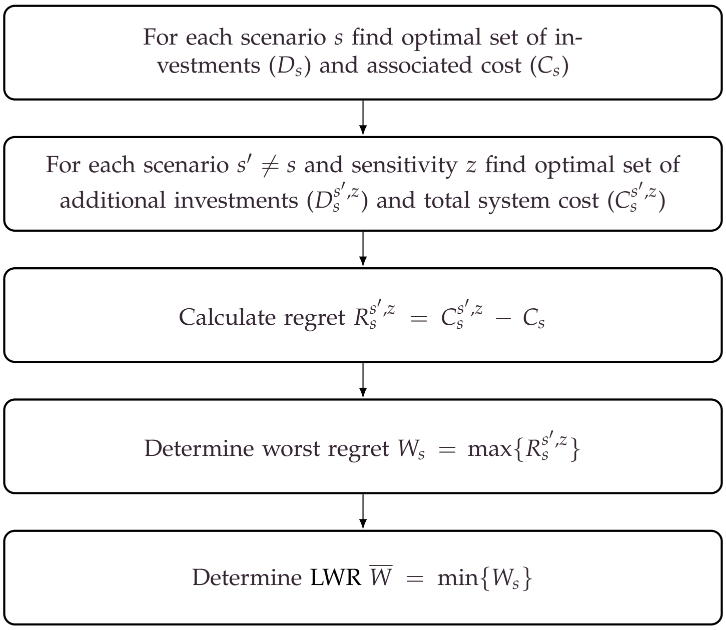

Figure 5.4 Steps for the calculation of the least-regret path in ISP.

levels (LOAD) and supply profiles (VRES and DER), energy storage parameters and investment costs, the behaviour of the gas and electricity markets, etc. Figure 5.3 allows to understand how each scenario balances the decentralisation and decarbonisation objectives by indicating the level of DER, load, and VRES. On top of the five scenarios, the methodology considers additional sensitivities on relevant system projects, like earlier retirement of generators, delays in large PSS, closure of large industrial loads (smelters), etc.

The methodology aims to find the least cost development path for each scenario and sensitivities separately. Each deterministic least cost development path is determined using a generation and transmission expansion model resulting in hourly dispatch outcomes that are then tested for security criteria (fault levels, dynamics, voltage compliance, etc.) using electromagnetic transient analysis software. Then, using those results, it determines the least-regret development path across all scenarios, as described in Figure 5.4.

AEMO states that LWR is preferred over the expected cost minimisation since it inherently considers the adapted plans (modified investment $D_s^{s',z}$) rather than locking a single view of the future for each scenario. The ISP report [9] also highlights the fact that the LWR does not need to ascribe probabilities to the corresponding scenarios.

All the information necessary to run the steps described above is available to the public, including the partial results of each step of the methodology. This work uses the information associated with the generation plan in each scenario, the demand data (which already considers the effect of electric vehicles and behind-the-meter storage), transmission and storage investment options and associated capital costs. The following section describes the details about the input data describing each of the scenarios.

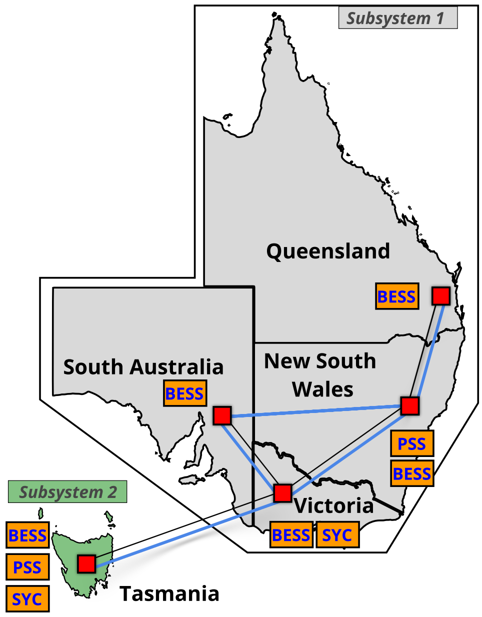

Figure 5.5 NEM system highlighting candidate investment options.

5.3.2 Input data

The system under consideration for this case study application corresponds to the Australian NEM as defined in the input assumptions database associated to Integrated System Plan (ISP) 2020 [9]. Figure 5.5 depicts the inertial areas under consideration for the expansion planning exercise, highlighting the candidate lines (blue segments) and the candidate technologies including battery energy storage systems (BESS), pumped-hydro storage systems (PSS) and synchronous condensers (SYC).

5.3.2.1 Initial system and trends

To reduce the computational burden, the existing generating units are clustered into one or two equivalent generators per technology in each bus; Table 5.1 presents the techno-economic parameters for the clusters of units in the system in year the 2020. A total of 28 clusters of synchronous units are considered; QLD is represented through 7 clusters and NSW through 6 clusters, with both states including the four types of synchronous units. Victoria's synchronous units are organised in 6 clusters including coal, hydro and OCGT units. Tasmania includes hydro, OCGT and CCGT organised in 3 clusters and South Australia synchronous generation units include only gas-fuelled technologies organised in 5 clusters. The evolution of the installed capacity of synchronous units is presented in Figure 5.6 highlighting the values by state and scenario. This evolution in the installed capacity by technology is included in the model through a time series associated with the maximum number of units in each clusters, which varies by cluster and scenario.

Table 5.1 Techno-economic parameters for clustered synchronous units available in 2020.

Technology	Coal	Hydro	OCGT	CCGT
Number of units	48	110	93	10
Variable cost [$/MWh]	12 – 42	7.3	95 – 490	65 – 79
Start-up costs [k$]	46 – 93	–	0.4 – 6.5	12 – 46
Rated Power [MW]	354 – 744	25 – 127	33 – 500	180 – 644
Forced outage rate	0.77 – 0.87	0.975	0.88 – 0.98	0.98
MSG [MW]	141 – 300	5 – 25	8 – 165	44 – 190
Ramp rate [MW/min]	3.5 – 6	–	3	2 – 10
Inertia constant [s]	4	2.5	4	4
Min up time[h]	8 – 16	–	–	4 – 6
Max PR headroom	10%	10%	10%	10%
PR slope factor	0.3	0.6	0.6	0.4

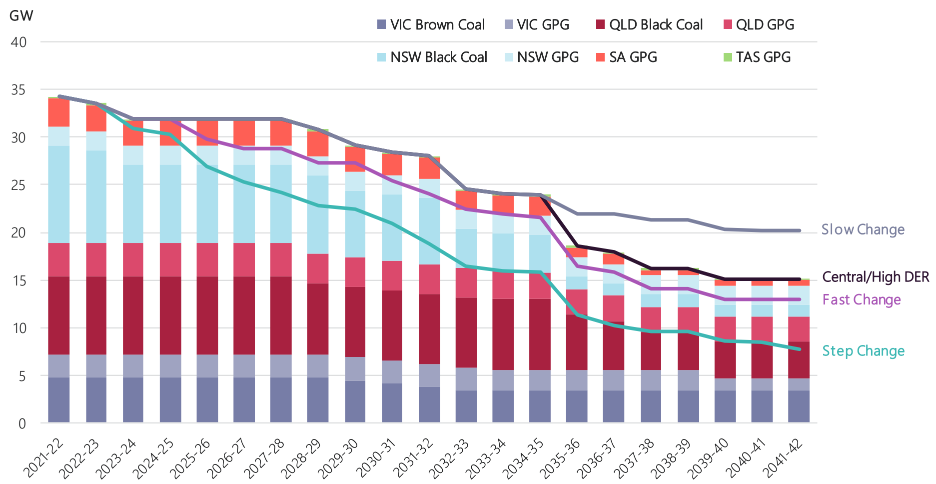

Figure 5.6 Synchronous capacity retirement by scenario (Source [9]).

Non-synchronous generation is split into large scale wind, large scale solar PV and rooftop solar PV, represented each as a single unit in each state. In order to have access to the most precise information about demand in the system (to account for its natural response after frequency changes), rooftop solar PV is modelled as a separate unit hence avoiding the need to subtract it from the gross demand for each state. The installed capacity of wind and solar technologies by scenario is depicted in Figure 5.7 alongside the capacities for other technologies.

The transmission system considers six existing links between the different states, whose forward and reverse ratings are specified in Table 5.2. Although Kirchoff's voltage law is active, the current transfers between states are radial. Basslink is an HVDC link, which produces the split of the system into two inertial subsystems, which are constrained independently for ROCOF and frequency extrema.

AEMO models 4 different types of storage systems: behind-the-meter storage, controllable distributed storage, and both BESS and PSS with different charging depths. The effect of behind-the-meter storage is included in the demand profiles. Controllable distributed storage is handled as a virtual power plant (VPP) with the capacity

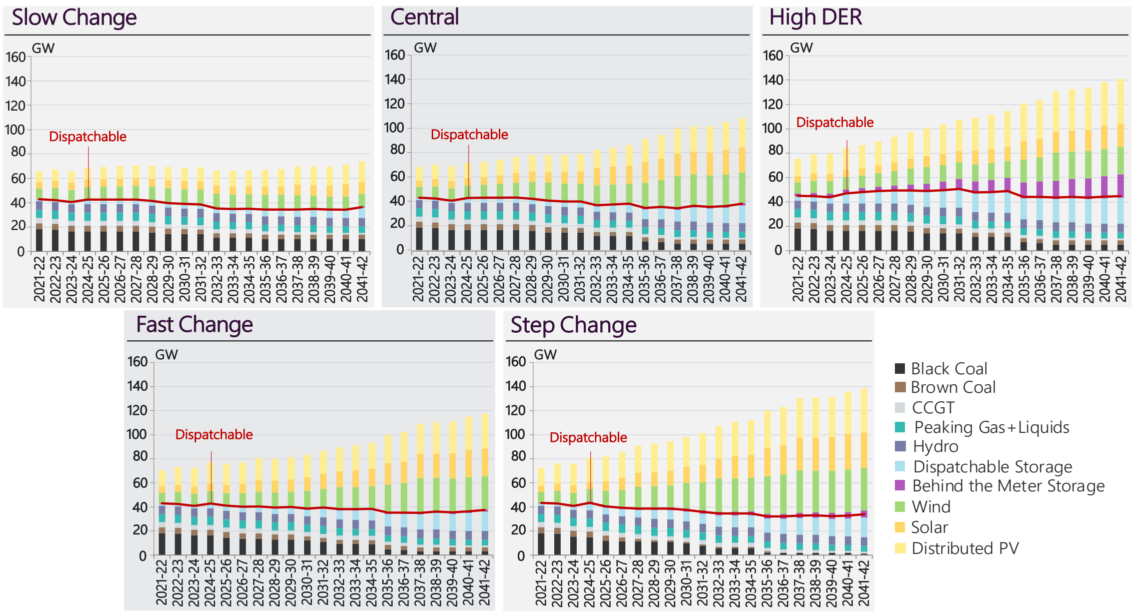

Figure 5.7 Installed capacity by technology by scenario (Source [9]).

Table 5.2 Description of existing transmission links under consideration.

Interconnector	Technology	State A	State B	Rating A to B (MW)	Rating B to A (MW)
Heywood	HVAC	VIC	SA	650	650
Murraylink	HVDC	VIC	SA	220	200
QNI	HVAC	NSW	QLD	565	1145
Terranora	HVDC	NSW	QLD	50	150
Basslink	HVDC	TAS	VIC	478	478
VNI	HVAC	VIC	NSW	700	400

to only perform arbitrage in the system (no provision of frequency response). In 2020, utility-scale BESS is present in SA (140 MW with 140 MWh storage capacity) and VIC (75.33 MW with 114 MWh storage capacity); PSS is available in NSW (Shoalhaven and Snowy) and QLD (Wivenhoe). In general, for existing and new BESS, the round-trip efficiency is considered 81%, while for existing and new PSS the round-trip efficiency is 70% and 75%, respectively. In Figure 5.7 it is possible to see the optimal storage capacity (dispatchable and behind-the-meter) determined by AEMO in each scenario. The dispatchable storage capacity is not imposed as an input in this work; only the existing capacity in 2020 is considered and then the expansion planning model is run considering storage assets as investment options.

From the point of view of frequency security, the model allocates FFR, PFR, SFR and inertia to comply with a ROCOF limit of 1 Hz/s in both directions, QSSF of 49.5 Hz in low-frequency events and 50.5 Hz in high-frequency events; SFR is allocated to bring frequency back inside the frequency dead-band 49.85 to 50.15 Hz. When applying frequency extrema constraints in each inertial subsystem, this case study application only focuses on frequency nadir (49 Hz), since it considers that the system will remain intact after contingency.

Demand in the system is obtained from the database associated with [9]. The information is presented in hourly periods, with two levels of demand available, 10% and 50% probability of exceedance (POE)[19]. In this case study application, a 10% POE is used, and, as pointed out before, it includes the effect of electric vehicle uptake and behind-the-meter non-controllable storage in each scenario.

5.3.2.2 Investment options

Investment options include transmission lines, BESS, PSS and synchronous condensers. All investment related cash flows manipulations (annuities, discounting, etc.) are calculated using a rate of return of 6.3%, following [9].

Although this model has the capacity to model real transmission options (sets of mutually exclusive projects), the approach taken here for some reinforcements is to determine the transmission capacity needed between states, which leads to introduce one reinforcement option between pairs of adjacent states (Figure 5.5, SA-VIC, VIC-NSW, and NSW-QLD) and then determine a unitary investment value based on the capital costs presented in the ISP for the reinforcement alternatives considered in that specific boundary. For the link between TAS-VIC, known as *Marinus Link*, and the link between SA-NSW, known as project *EnergyConnect*, the real reinforcement projects are used, due to the particular characteristics of those projects; *Marinus Link* is an underwater HVDC transmission link that considers two transfer capacity levels and *EnergyConnect* is a very long ($\sim$1000 km) transmission line that would create the first interconnection between SA-NSW. To understand the transfer capacity requirements between boundaries, the new links are not subject to Kirchhoff's voltage law (transport model only). Table 5.3 presents the parameters for the different network reinforcement options. All reinforcement options consider a lifetime of 50 years and a lead time of 5 years. The investment costs presented in Table 5.3 correspond to overnight capital costs, and it is assumed these costs do not change in the future. The column presenting the so-called "expansion modules" refers to the maximum number of investment decisions that can be made for each investment option; for example, the line VIC_NSW_I can be expanded up to 40 times, reaching a total rating of 8 GW if the model decides to deploy all the modules.

Table 5.3 Investment options in transmission lines.

Interconnector	State A	State B	Rating (MW)		Investment cost (M$/MW)	Expansion modules
			A to B	B to A		
NSW_QLD_I	NSW	QLD	200	200	1.7044	40
VIC_NSW_I	VIC	NSW	200	200	1.9473	40
VIC_SA_I	VIC	SA	200	200	1.8716	40
Marinus Link	TAS	VIC	750	750	2.3438	2
EnergyConnect	SA	NSW	800	800	2.3442	1

The investment in energy storage systems is modelled in a similar fashion. To keep

[19] POE is the chance a maximum demand forecast will be surpassed. For example, a 50% POE maximum demand forecast is expected to be exceeded, on average, 5 years in 10.

thing relatively simple this case study application considers only BESS units with 2 hours storage capacity. Each state can expand BESS independently; on top of this, NSW and TAS can invest in large PSS projects representing Snowy 2.0 [145] and Battery of the Nation (BOTN) [146], respectively. The investment parameters for storage projects are presented in Tables 5.4. All BESS in the system (existing and new) are assumed to provide the same type of FFR (400 ms activation delay, 20 ms response speed, up to 70% maximum capacity) and PSS provide only PFR. The investment costs for BESS reduces in time and depends on the scenario, as seen on Table 5.5. All the details about these assumptions can be found in the input assumptions database associated to [9], except the investment costs for the large PSS which are found in [145, 146].

Table 5.4 Investment options in energy storage systems.

ESS	State	Tech	Charging capacity (MW)	Energy storage (MWh)	Investment cost (M$/MW)	Life time (years)	Expansion modules
BESS_I	ALL	BESS	100	200	1.3780	20	200
Snowy2.0	NSW	PSS	2000	336000	2.7045	50	1
BOTN	TAS	PSS	1700	36720	1.5508	50	1

Table 5.5 Investment cost evolution for BESS.

Scenarios	State	Tech	Investment cost by year (M$/MW)			
			2020	2025	2030	2035
Slow change - Central	ALL	BESS	1.378	1.0870	0.9712	0.9691
Fast change - High DER	ALL	BESS	1.378	1.1643	1.0322	1.0180
Step change	ALL	BESS	1.378	1.1842	1.0119	1.0078

The investment in synchronous condensers (SYC) is modelled as the addition of a new synchronous generation that does not inject any energy capable of balancing out the demand in the system. The approach, in this case, is also modular, following steps of 100 MW. The inertia constant for the synchronous condensers is assumed to be 2s. The cost of running each 100 MW module is assumed to be \$10/h[20], which are added to the objective function through the commitment variable associated with the operation of the unit. The investment cost associated with this technology[21] is assumed to be 0.2143 M$/MW following the figures presented in [147].

5.3.2.3 Operational data selection

Although off-the-shelf state-of-the-art MILP solvers can efficiently handle extremely large problems, the larger the problem, the slower the search process will be. Since the

[20]The assumption behind the operational cost of synchronous condensers is that it corresponds to 1-2% of the cost of running a cheap synchronous technology.

[21]The option of investing in the conversion of decommissioned units into synchronous condensers was also considered. This option set is straightforward to implement from a modelling perspective, assuming that the decommissioning dates of existing units are known. However, this avenue was not explored due to the lack of trustworthy information regarding the investment costs and lead time associated with the conversion.

column generation algorithm presented in Section 5.2.4 relies on multiple iterations to find the solution, it is desirable to have SP that solve as fast as possible. To help to reduce the computation time, each year under analysis is represented by a subset of representative weeks selected among the 52 available weeks. The selection of the input data is critical to ensure adequate representation of the system's operation [148], which can have a substantial impact on the investment decisions derived from the long-term operation model.

For each of the years selected to sample the scenarios, the following steps were taken to identify the subset of weeks closest to represent the operation of the 52 weeks: first, select the year and split all the corresponding data series into 52 weeks. Then, between 3 and 5 weeks are preselected to represent the periods with maximum demand within the year at both system and state levels. The remaining weeks are clustered using k-means, based on the following parameters representing the times series in each week: maximum, minimum, mean, standard deviation, skewness, kurtosis, root mean square, and minimum and maximum slopes. For each year, a total of 12 representative weeks are selected, yielding the following root mean square errors [149]: 1.32%, 1.78%, 2.28% and 2.04%, for years 2020, 2025, 2030 and 2035, respectively (average error across scenarios). Each representative week has a specific weight ($\omega_{m,w}$) within the representation of the operation of the year.

5.3.3 Scenario trees

The case study applications under analysis consider two representations of future uncertainty. The first scenario tree aims to represent the modelling approach of the ISP, where five main scenarios are considered. These five scenarios are arranged in a two-stage scenario tree, as presented in Figure 5.8a. The root node represents the investment and operation in 2020, which in the ISP corresponds to the Central scenario; from that node, the tree spreads into the five different scenarios, with each node representing the system in 2025 and equal probabilities for each transition between the root node and the nodes in the second epoch. This tree assumes that the moment a scenario starts developing, the system will stay in that development path. Each of the scenarios models the system up to the year 2035 (included). This scenario tree will be referred to as ST16 since it contains 16 decision nodes.

As discussed in the previous chapter, a two-stage approach will overlook opportunities to build flexible investment options by assuming that the future will not unfold following more intricate paths. In order to study the differences that a more complex scenario tree can introduce, a second scenario tree is presented. Figure 5.8b shows the structure of the multi-stage modelling approach, which was built using the same nodes used in tree ST16 but arranged in a way that they will emulate the potential "incremental" transitions in Figure 5.3. Incremental refers to transitions to scenarios that have higher decarbonisation or decentralisation profiles, for instance, if the system is in the

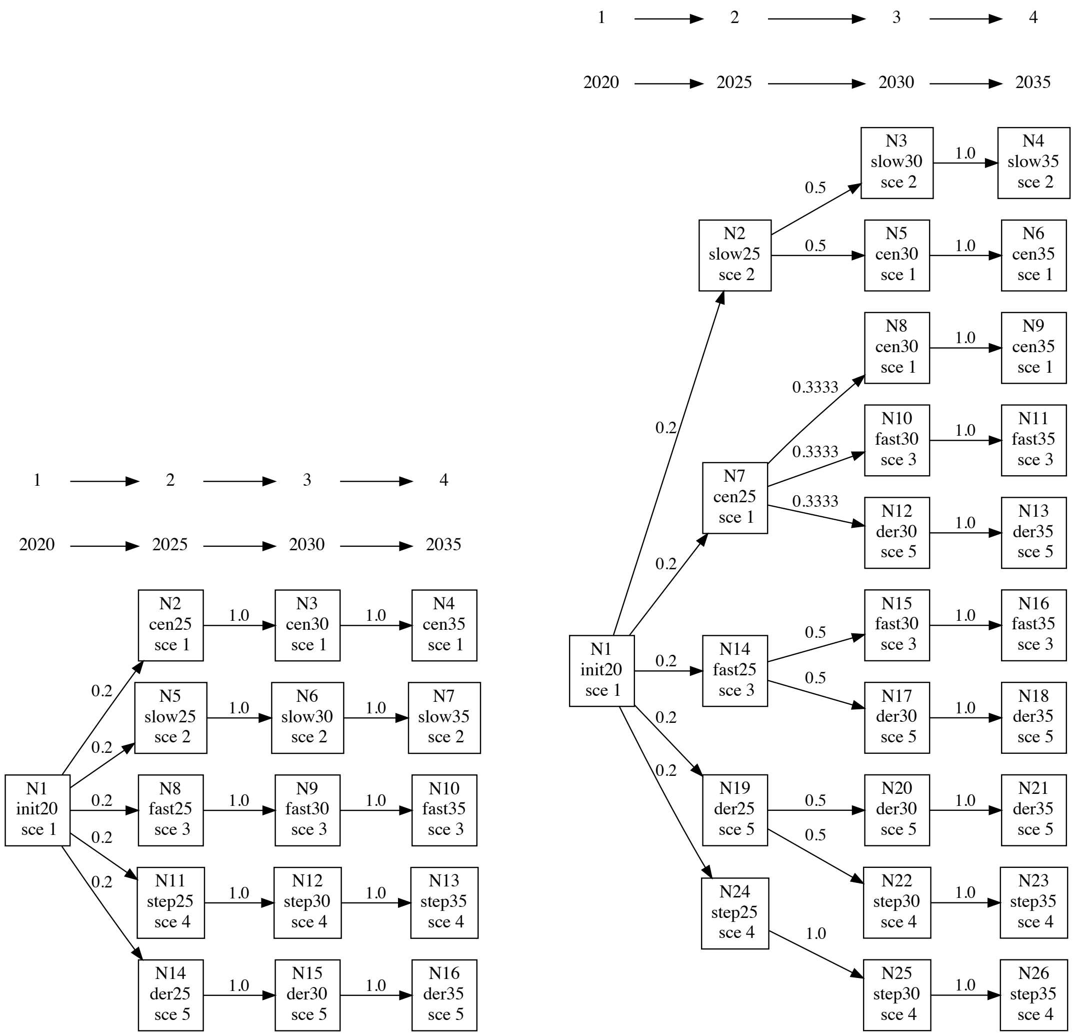

(a) Two-stage scenario tree (ST16). **(b)** Multi-stage scenario tree (ST26).

Figure 5.8 Representation of the future.

Slow scenario in a given node, in the succeeding epoch, it can stay in that scenario or transition to the Central scenario; if the system conditions are described by the Central scenario, in the next epoch it can stay in the Central scenario or transition to the High DER or the Fast scenarios. All transitions are assumed to be equiprobable. The resulting tree is labelled ST26.

In general, the term scenario refers to one of the paths connecting the root node (2020) to any of the leaf nodes representing the conditions of the system for 2035. ST16 contains five scenarios and ST26 considers 10 of them. It is interesting to highlight that the construction of the multi-stage tree contains all the scenarios available in ST16.

5.3.4 Monolithic vs Dantzig-Wolfe decomposition

This section compares the results and performance observed when solving the deterministic equivalent problem (monolithic) and the decomposed problem using the column generation algorithm. The tests are conducted on the two-stage scenario tree (ST16) using a different number of representative weeks for all the nodes in the tree to measure the performance of both approaches as the problem grows. The comparison between the results of both approaches is conducted using one representative week per node since the only objective of this comparison is to check that the results are consistent between both solution strategies.

All tests presented in this section include unit-commitment constraints considering linearised commitment variables, fixed contingency size, ROCOF and QSSF constraints for both high- and low-frequency events, and all basic power system constraints (power balances, transmission limits, etc.). Unless otherwise said, the frequency response requirement considers ROCOF limited to ± 1 Hz/s, QSSF of 49.5 and 50.5 Hz for low- and high-frequency events, respectively (and SFR allocation to bring the frequency back to the frequency dead-band 49.85-50.15 Hz), and frequency nadir of maximum 49 Hz. In this case study, frequency zenith constraints are not applied because the system is assumed to remain intact and load contingencies are relatively small; under those assumptions, frequency zenith does not represent a binding constraint in the allocation of resources.

Due to the high memory requirements of the monolithic approach, all the studies presented in this section were run in the high-performance computing facility at the University of Melbourne (see Appendix A for more information on the hardware and software used in this work). The target gap across studies is set to 0.5% both in the monolithic and decomposition approaches.

5.3.4.1 Results

Presenting results about expansion planning is a challenging task due to the long list of investment options and the size of the scenario tree since in each node of the tree a decision is made for each investment option. The first comparison is conducted on the same instance of the problem, considering that the operation in each node in the scenario tree ST16 is characterised using only one representative week (WN1).

The results presented in Table 5.6 for the monolithic approach and in Table 5.7 for the decomposition approach should not be used to derive any conclusion about the optimal development for the system because the use of only one representative week per node poorly reflects the operation of the system. The reason to conduct the comparison with only one week per node is twofold: first, it allows to accomplish the objective of this section, which is to show that both approaches yield quasi-equal results; second, it provides a reference to the quality of the decisions based on an incomplete representation of the operation (the following sections present results for the same case with a denser representation of the operation).

The case studies here only consider the ROCOF and QSSF constraints, which will be referred to as the base case. An important factor in the slight differences observed in the two approaches (highlighted in grey in Table 5.7) is the fact that BESS investment costs are the same for all the states; this creates some degree of degeneracy in the results, with the total number of new modules across states being almost the same.

Table 5.6 Investment results monolithic model, ST16-WN1.

Tree		Scenario	Central				Slow			Fast			Step			High DER		
		Node	1	2	3	4	5	6	7	8	9	10	11	12	13	14	15	16
		Year	20	25	30	35	25	30	35	25	30	35	25	30	35	25	30	35
LINE	NSW-QLD	(200)	0	0	2	15	0	0	9	0	0	0	0	5	5	0	8	8
	VIC-NSW	(200)	0	2	5	5	2	2	2	2	5	8	2	2	3	2	2	14
	VIC-SA	(200)	0	0	0	0	0	0	0	0	0	0	0	0	0	0	0	0
	TAS-VIC	(750)	0	0	0	0	0	0	0	0	0	1	0	1	1	0	0	2
	SA-NSW	(800)	0	0	0	0	0	0	0	0	0	0	0	0	0	0	0	0
SYC	VIC	(100)	0	0	0	0	0	0	0	0	0	0	0	0	0	0	0	0
	TAS	(100)	0	1	1	1	1	1	1	1	1	1	1	1	1	1	1	1
BESS	QLD	(100)	0	0	0	87	0	0	0	0	0	0	0	18	18	0	0	0
	NSW	(100)	0	0	0	32	0	0	11	0	0	0	0	0	0	0	0	0
	VIC	(100)	0	0	0	17	0	0	5	0	0	0	0	0	0	0	0	0
	TAS	(100)	0	0	0	1	0	0	0	0	0	0	0	0	0	0	0	0
	SA	(100)	0	0	0	15	0	0	4	0	0	0	0	0	0	0	0	0
PSS	NSW	(2000)	0	0	0	1	0	0	0	0	0	0	0	1	1	0	0	0
	TAS	(1700)	0	0	0	0	0	0	0	0	0	0	0	0	0	0	0	0

Table 5.7 Investment results decomposed model, ST16-WN1.

Tree		Scenario	Central				Slow			Fast			Step			High DER		
		Node	1	2	3	4	5	6	7	8	9	10	11	12	13	14	15	16
		Year	20	25	30	35	25	30	35	25	30	35	25	30	35	25	30	35
LINE	NSW-QLD	(200)	0	0	2	15	0	0	9	0	0	0	0	5	5	0	8	8
	VIC-NSW	(200)	0	2	5	5	2	2	2	2	5	8	2	2	2	2	2	14
	VIC-SA	(200)	0	0	0	0	0	0	0	0	0	0	0	0	0	0	0	0
	TAS-VIC	(750)	0	0	0	0	0	0	0	0	0	1	0	1	1	0	0	2
	SA-NSW	(800)	0	0	0	0	0	0	0	0	0	0	0	0	0	0	0	0
SYC	VIC	(100)	0	0	0	0	0	0	0	0	0	0	0	0	0	0	0	0
	TAS	(100)	0	1	1	1	1	1	1	1	1	1	1	1	1	1	1	1
BESS	QLD	(100)	0	0	0	87	0	0	0	0	0	0	0	16	17	0	0	0
	NSW	(100)	0	0	0	32	0	0	11	0	0	0	0	0	0	0	0	0
	VIC	(100)	0	0	0	13	0	0	4	0	0	0	0	2	2	0	0	0
	TAS	(100)	0	0	0	1	0	0	0	0	0	0	0	0	0	0	0	0
	SA	(100)	0	0	0	20	0	0	4	0	0	0	0	0	0	0	0	0
PSS	NSW	(2000)	0	0	0	1	0	0	0	0	0	0	0	1	1	0	0	0
	TAS	(1700)	0	0	0	0	0	0	0	0	0	0	0	0	0	0	0	0

The differences between the case studies are explained by the gap applied both in the context of the branch and cut for the monolithic case and the gap used to determine the convergence in the case of the column generation algorithm (5.2.41). The discounted total expected cost (operation and investment) of the monolithic case is $8901.1 million with a gap of 0.18%, and the column generation algorithm found a solution resulting in an expected cost of $8910.5 million (with a gap of 0.44%).

5.3.4.2 Performance

Considering that both the monolithic and the decomposed problems display very similar results, this provides confidence that the decomposition and solution algorithm were successfully implemented (smaller test cases show matching solutions when solved to optimality). The focus is put now on the performance of both approaches. Since some off-the-shelf MILP solvers are displaying an impressive capacity to deal with very large problems, it is interesting to explore the speed of convergence of both approaches for different levels of computational burden. However, speed is not the only factor in play here; the size of resources that each solution approach needs can become the real limitation for their application. The latter is probably the main reason to use the DW decomposition, because the search for the optimal solution in the monolithic model involves exploring the branch-and-cut tree based on a very large model. Depending on the problem characteristics, this search can be very demanding on physical memory. To test performance, the problem solved in the previous section, for ST16 with the operation represented by one week, is solved here with progressively more weeks representing the operation of each node.

Table 5.8 Monolithic problem dimensions (ST16).

Label	Weeks per node	Total weeks	N rows	N variables	N non-zeros	N continuous variables	N integer variables
WN1	1	16	1.79×10^6	1.11×10^6	5.37×10^6	1.07×10^6	3.80×10^4
WN2	2	32	3.58×10^6	2.21×10^6	1.07×10^7	2.13×10^6	7.56×10^4
WN3	3	48	5.38×10^6	3.31×10^6	1.61×10^7	3.20×10^6	1.13×10^5
WN4	4	64	7.17×10^6	4.42×10^6	2.15×10^7	4.27×10^6	1.51×10^5
WN6	6	96	1.08×10^7	6.63×10^6	3.22×10^7	6.40×10^6	2.26×10^5
WN7	7	112	1.25×10^7	7.73×10^6	3.76×10^7	7.47×10^6	2.64×10^5
WN8	8	128	1.43×10^7	8.84×10^6	4.29×10^7	8.54×10^6	3.01×10^5
WN9	9	144	1.61×10^7	9.94×10^6	4.83×10^7	9.60×10^6	3.39×10^5
WN12	12	192	2.15×10^7	1.33×10^7	6.44×10^7	1.28×10^7	4.52×10^5

Table 5.8 displays the dimensions of the problems that will be tested. Given the nature of the problem, increasing the number of weeks increases the dimensions of the underlying matrices linearly. The tests are performed using 16 CPUs[22] with an ample RAM limit so that the problems will not stop due to memory limits. It is important to highlight that the pricing subproblems in the column generation approach require less than 1 GB of RAM to solve the weekly UC with expansion decisions with a time limit of 60 seconds. Although memory limit was intentionally set at a very large number for the monolithic approach, in the process of testing and determining the correct memory limit, the large monolithic instances were run with a memory limit of 400 GB (25 GB

[22] It is important to highlight that both the monolithic and distributed approaches will reduce resolution time by increasing the number of CPUs. For the monolithic case, Gurobi implements parallelism to explore more nodes of the branch-and-bound tree; hence more CPUs will increase the capacity of Gurobi to explore the tree faster, potentially finding the solution in less time (but also increasing memory use). In the case of the distributed algorithm, more CPUs translate directly into the capacity to solve more slave problems in parallel, which will speed up the convergence process.

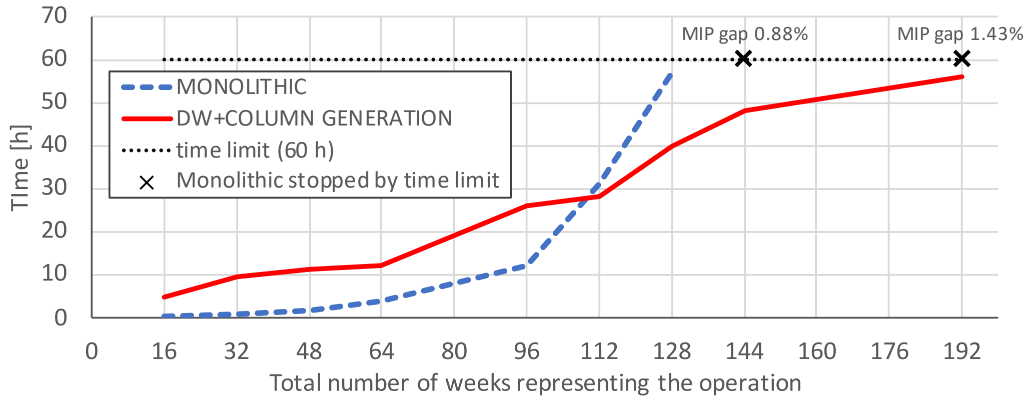

Figure 5.9 Performance of Monolithic vs Column generation approaches (16 CPUs).

per CPU). Also, a time limit was set at 60 hours[23], which was determined by solving the largest instance using the column generation algorithm and adding some headroom to determine if the monolithic approach would solve the problem in a shorter or longer period.

Figure 5.9 presents the results of the performance test. The monolithic approach displays an exponential trend in the solution time as the representation of the operation becomes more detailed. The performance of the MILP solver (Gurobi [150]) to address the monolithic problem is far superior to the decomposition (which also uses Gurobi to solve the RMP and SP) for instances of the problem with up to 7 weeks representing each node or 112 weeks in total. It is at around this size of the problem where the solution of the monolithic problem starts taking substantially longer to solve compared to the column generation counterpart, consuming significant amounts of memory in the process of exploring the MILP solution tree. Figure 5.9 also indicates the status of the MIP gap when problems ST16-WN9 and ST16-WN12 were stopped due to the time limit; it is worth pointing out that the convergence process in each case had been stuck at that MIP gap for several hours at the time of termination.

The solver tackling the monolithic approach can use the 16 CPUs to explore the MILP tree in parallel. The column generation algorithm used to solve the DW decomposition utilises 1 CPU to solve one pricing subproblem at the time, which allows solving 16 problems in parallel. If the total number (pool) of problems is larger than the number of CPUs, as soon as the solution of one SP is found, the next problem in the pool starts processing. Each subproblem has a time limit of 60 seconds to search for a feasible solution[24] that would satisfy a MIP gap of 0.5%.

The conditions described before for the solution of the pricing subproblems can explain the behaviour of the red performance curve in Figure 5.9. The performance of

[23]Requests sent to high-performance computing facilities usually require the definition of CPUs and memory needs, and also the definition of a time limit for the process. Based on those parameters, it can allocate and prioritise the resources.

[24]To provide a reference to the times involved in the solution process of the subproblems, case ST16-WN12 solution results can be presented: 375 iterations were necessary to narrow down the gap below 0.5%, which involved solving 72000 pricing subproblems. 26163 of those problems were stopped due to the pre-imposed time limit.

the column generation algorithm as the problem grows larger follows a linear trend. However, between consecutive tests, it is possible to appreciate that sometimes the solution time does not increase proportionally with the number of representative weeks (e.g. WN2 to WN4); there is a point where additional operational information substantially increase the time necessary to find a solution (e.g. WN4 to WN6). This is connected with the fact that most of the new problems reach the desired gap very quickly; it is the problems that reach the time limit that drive the total time of convergence of the column generation algorithm.

As shown in this section, the decomposition approach is strictly necessary to solve the expansion planning problem with a high degree of operational resolution to capture the value of new investments with the consideration of deep uncertainties represented through complex scenario trees. The times presented in Figure 5.9 are only referential because they are achieved through the use of only 16 CPUs.

5.3.5 Impact of the frequency nadir constraint

Problem ST16-WN12 is used to study further the solution set when the nadir constraints are embedded in the problem for both inertial subsystems (the subsystems are assumed to share all frequency response resources except inertia). The first step is to present the solution for problem ST16-WN12 without the nadir constraints. Table 5.9 presents the results for case ST16-WN12 following the same structure as Table 5.6 for ST16-WN1. The inspection of both decision sets shows how relevant is the inclusion of more representative weeks for the operation. Just by adding more operational resolution, there is a substantial increase (in some scenarios and years, a slight reduction is also seen) in investment in transmission capacity between QLD and NSW, and VIC and NSW. Investment in BESS also increases, in particular in early epochs (the fast scenario displays the biggest change, with no investment whatsoever in ST16-WN1 and close to 6 GW in 2030), and PSS also appears in the Fast scenario in 2030 and 2035. The Step scenario displays additional investment in synchronous condensers by considering more operational resolution, which indicates ROCOF issues due to the extensive penetration in VRES by 2035. Both case study applications show a low investment in storage in the High DER scenario, which stems from the substantial penetration of controllable distributed storage (VPP), with almost 15 GW (compared, for instance, to 0.9 GW in the Central scenario). VPPs are modelled as regular storage that cannot provide reserves. This source of flexibility not only avoids investment in new storage but also allows to adapt the operation so as to allow synchronous units to become online when needed to provide inertia, thus avoiding investment in synchronous condensers. The inclusion of higher operational resolution substantially increases investment since this approach dominates over the option of not investing and incurring higher operation costs. The

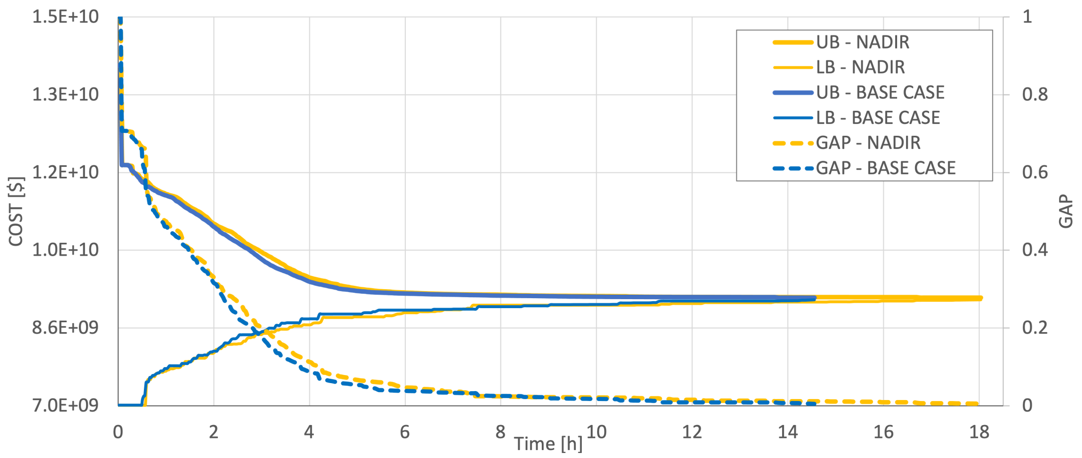

Figure 5.10 Convergence for ST16-WN12 base case and case with nadir constraints.

total expected costs for ST16-WN12 are \$9270.3 million[25] with a gap 0.46%, which is ∼4% increase with respect to the already reported \$8910.4 million for ST16-WN1.

Adding nadir constraints to both inertial subsystems in case ST16-WN12 induces a slower convergence of the column generation algorithm, as depicted in Figure 5.10[26]. The burden associated to the nadir constraints is non-negligible considering the nadir constraints have to be added to every single period in every week: let assume each nadir function is approximated by 10 hyperplanes for each hourly time step, this means that there are 192 weeks $\times$ 168 hours $\times$ 2 subsystems $\times$ 10 hyperplanes $=$ 645120 new constraints in the monolithic approach, a 3% increase in constraints (rows) in the problem. This results in a 24% increase in computation time (14.55 to 18.03 hours), with bounds and gap following a very similar trajectory but with a longer tailing-off period for the case with frequency nadir constraints. The expected costs of this case study application are \$9291.1 million (gap of 0.47%), an increase of 0.2% due to the addition of nadir constraints to ST16-WN12. In the context of a 0.47% gap, a 0.2% increase in the objective function is not significant, which does not allow to discriminate the source of the change. For example, it can originate from small changes in operation decisions associated with the new constraints or entirely different feasible solutions available within the convergence gap.

Before analysing the changes in the investment decisions due to the addition of the frequency response constraints, let us analyse their effect in a randomly selected pricing subproblem to show how the operation behaves when investment decisions are included along with the nadir constraints. By extracting the solution of the subproblem (this is, all operational decisions, including those of selected candidate assets), it is possible to show that decisions in new BESS are made, which naturally will be dependant on the

[25]The total cost of investment and operation is very close to the value reported by AEMO in the ISP report. The amounts reported in this work correspond to a sampling of the horizon; by using each of the samples to represent five consecutive years, it is possible to calculate, for instance, that the total cost for the Central scenario resulting from the application of the model is \$47.74 billion, compared to the ca. \$49 billion reported for the same scenario in the ISP.

[26]These problems were solved using 46 independent tasks, each of them using 4 CPUs and 8 GB RAM, see Appendix A for the description of the infrastructure of HPC Hendrix.

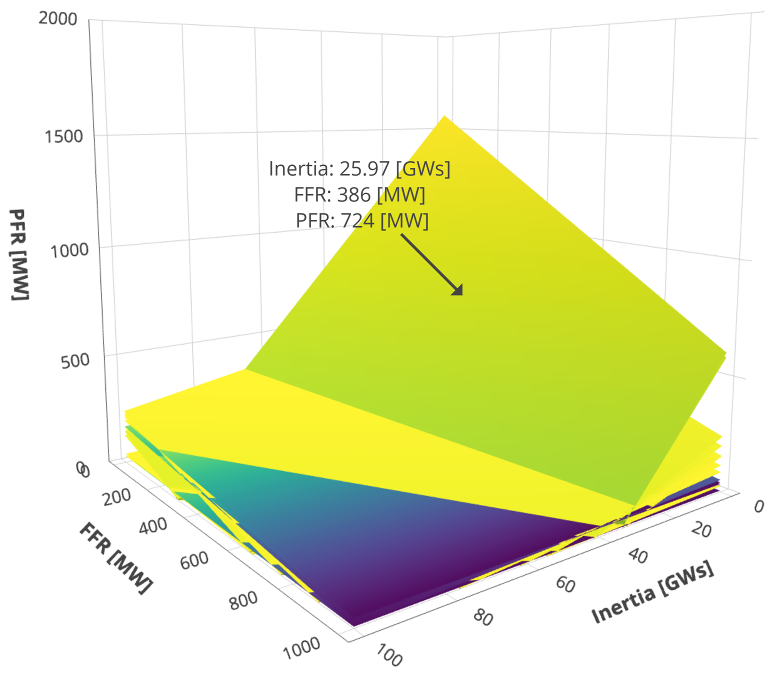

Figure 5.11 Frequency nadir constraint for period 153 in the pricing subproblem.

corresponding duals obtained from the RMP (signalling the overall value of investing in new BESS in that subproblem, for the current iteration). The frequency nadir constraint connects the three FR resources as presented in Figure 5.11, which corresponds to a specific period (hour 153) in one of the weekly scheduling problems representing the operation for Node 14 in ST16-WN12.

As seen in Figure 5.12, this particular period displays a very low inertia level, which pushes up the requirement on PFR and/or FFR. Under the assumption that BESS can offer up to 70% of their capacity in the contingency reserve market, the existing FFR capacity is close to 150 MW. As it can be seen in Figure 5.12c[27], the aggregated upward response coming from BESS is 386 MW, which takes into consideration the response that can be delivered by the investment candidates that have been selected in the particular week under consideration, in the particular iteration (it = 103) under analysis. Figure 5.12b shows the allocation of PFR and FFR for the system over the week, highlighting period 153, with amounts consistent with the active nadir hyperplane for the amount of available inertia for that period as depicted in Figure 5.12a. The increased requirement of FR resources when inertia goes down can leverage the investment of new BESS if this avoids additional costs of running more synchronous units to provide inertia and PFR, plus the potential benefits coming from additional arbitrage capacity in the system.

[27] Another interesting fact that can be deduced from the aggregated behaviour of BESS is that only allowing the expansion of storage systems with 2-hour storage capacity might yield sub-optimal results. The total energy (10+ GWh) stored in the candidate batteries selected in this iteration is much larger than the capacity used to discharge (2+ GW) and charge (2.5+ GW) the batteries. This allows us to conjecture that the level of investment in batteries is driven by the need for energy storage rather than flexible capacity coming from BESS.

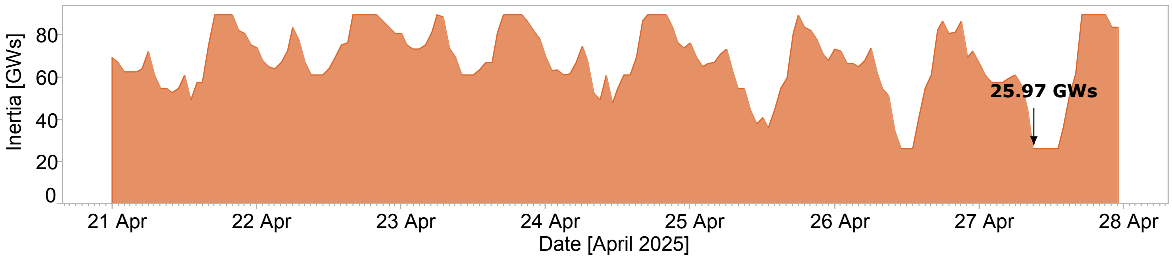

(a) Inertia dispatch.

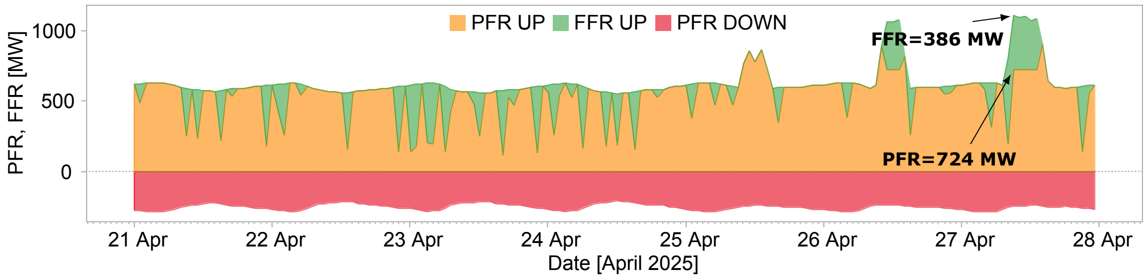

(b) PFR and FFR dispatch.

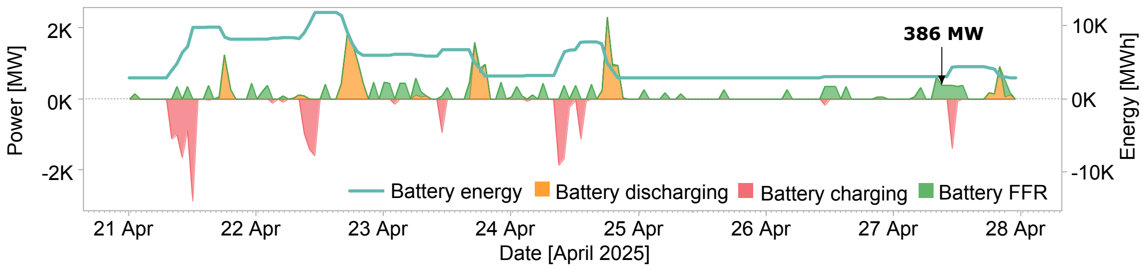

(c) BESS dispatch.

Figure 5.12 Optimal results for a representative week in node 14 (ST16 - High DER scenario).

Table 5.9 Results for ST16-WN12 base case.

Tree		Scenario	Central				Slow			Fast			Step			High DER		
		Node	1	2	3	4	5	6	7	8	9	10	11	12	13	14	15	16
		Year	20	25	30	35	25	30	35	25	30	35	25	30	35	25	30	35
LINE	NSW-QLD	(200)	0	3	8	14	3	3	9	3	4	4	3	3	4	3	8	10
	VIC-NSW	(200)	0	5	5	5	5	5	5	5	7	7	5	5	5	5	5	10
	VIC-SA	(200)	0	0	0	0	0	0	0	0	0	0	0	0	0	0	0	0
	TAS-VIC	(750)	0	0	0	0	0	0	0	0	0	1	0	1	1	0	0	1
	SA-NSW	(800)	0	0	0	0	0	0	0	0	0	0	0	0	1	0	0	0
SYC	VIC	(100)	0	0	0	0	0	0	0	0	0	0	0	0	1	0	0	0
	TAS	(100)	1	1	1	1	1	1	1	1	1	1	1	1	1	1	1	1
BESS	QLD	(100)	0	0	0	76	0	0	0	0	0	9	0	13	81	0	0	0
	NSW	(100)	0	0	5	33	0	0	22	3	6	39	0	0	44	0	0	7
	VIC	(100)	0	0	0	18	0	0	0	0	0	5	0	5	30	0	0	0
	TAS	(100)	0	0	0	2	0	0	0	0	0	0	0	0	0	0	0	0
	SA	(100)	0	0	0	38	0	0	2	0	0	5	0	0	15	0	0	0
PSS	NSW	(2000)	0	0	0	1	0	0	0	0	1	1	0	1	1	0	0	0
	TAS	(1700)	0	0	0	0	0	0	0	0	0	0	0	0	0	0	0	0

Table 5.10 presents the results for the case study with nadir constraints. It can be compared field by field with the results of the base case presented in Table 5.9. The investment decisions that are straightforward to justify due to the inclusion of nadir constraints are the additional synchronous condensers installed in TAS. This constraint can be satisfied by different combinations of PFR, FFR and inertia; among the available investment options, adding new PFR would involve investing in any of the two PSS projects, inertia can be increased by installing synchronous condensers or PSS, and additional FFR can be deployed by installing new BESS. Since the ROCOF constraint did not change between case studies, the only justification for investing to increase inertia in the system is the fact that the nadir constraint is pushing the needs for PFR and FFR to the point that a synchronous condenser is more cost-effective than a new battery or a large PSS project. Of course, this neglects other benefits that a synchronous condenser brings to the system, like system strength and voltage support, which, if considered, are likely to increase the installation of these devices.

The critical change in this case study is the increase of FFR in years 2025 in the Central and Slow scenarios (both scenarios display very low penetration of VPPs). The new storage capacity can provide both flexibility to accommodate more inertia and FFR. This capacity is deployed in NSW.

The expansion in transmission after the nadir constraints are considered also changes: one additional expansion module is used to reinforce more the interconnection between VIC-NSW instead of the link NSW-QLD. This change impacts all scenarios due to the lead-time of the decision, which in turn allows reducing the overall installation of BESS in the Central and Fast scenarios in 2030, and the Slow and Fast scenarios in 2035.

The Step and High DER scenarios do not see investment in storage in early epochs because the large capacity of distributed, controllable storage in those scenarios provides the flexibility to comply with the nadir constraints through the management of synchronous resources to provide inertia and PFR.

Table 5.10 Results for ST16-WN12 with nadir constraints.

Tree		Scenario	Central				Slow			Fast			Step			High DER		
		Node	1	2	3	4	5	6	7	8	9	10	11	12	13	14	15	16
		Year	20	25	30	35	25	30	35	25	30	35	25	30	35	25	30	35
LINE	NSW-QLD	(200)	0	2	8	14	2	2	9	2	4	4	2	4	4	2	7	10
	VIC-NSW	(200)	0	6	6	6	6	6	6	6	7	7	6	6	6	6	6	10
	VIC-SA	(200)	0	0	0	0	0	0	0	0	0	0	0	0	0	0	0	0
	TAS-VIC	(750)	0	0	0	0	0	0	0	0	0	1	0	1	1	0	0	1
	SA-NSW	(800)	0	0	0	0	0	0	0	0	0	0	0	0	1	0	0	0
SYC	VIC	(100)	0	0	0	0	0	0	0	0	0	0	0	0	1	0	0	0
	TAS	(100)	1	1	1	1	1	2	2	1	1	1	1	1	1	1	1	1
BESS	QLD	(100)	0	0	0	81	0	0	0	0	0	8	0	15	83	0	0	0
	NSW	(100)	0	2	2	30	3	3	19	3	3	41	0	0	36	0	0	7
	VIC	(100)	0	0	0	17	0	0	0	0	0	5	0	3	41	0	0	0
	TAS	(100)	0	0	0	1	0	0	0	0	0	0	0	0	5	0	0	0
	SA	(100)	0	0	0	38	0	0	3	0	0	4	0	0	3	0	0	0
PSS	NSW	(2000)	0	0	0	1	0	0	0	0	1	1	0	1	1	0	0	0
	TAS	(1700)	0	0	0	0	0	0	0	0	0	0	0	0	0	0	0	0

To visually understand the solution set presented in Table 5.10, Figure 5.13 shows the deployment of transmission lines, storage systems and synchronous condensers on a section of the map of Australia.

5.3.6 Multi-stage scenario tree

The final case study application that is presented in this chapter corresponds to the application of the expansion model without nadir constraints on the multi-stage scenario tree ST26 (see Figure 5.8b), with 12 representatives weeks per node (ST26-WN12). The results for this case are presented in Table 5.11; it took almost 22 hours to solve (compared to 14.5 hours for case ST16-WN12 without nadir constraints) with total expected costs of \$9434.3 million (\$163.7 million or 1.76% increase with respect to ST16-WN12 without nadir constraints). The increase in cost is expected because the new branches added to the tree in 2030 represent, in general, more challenging scenarios than the original ones. Table 5.11 is organised similarly to the previous investment result tables, except for the rows describing the scenarios: the first row aggregates all the nodes that are attached to the main scenario (also referred to as the main branch) whose name is specified in that row, and the second row specifies the different branches that are attached to the main scenario. By comparing the main scenarios of ST26-WN12 and ST16-WN12 (Table 5.9), it is possible to see the effects of the addition of branches in 2030 to represent uncertainty. In general, the consideration of the multi-stage tree introduces earlier or additional investment in transmission. The link between NSW and QLD is expanded in one additional module in 2025 (decision made in 2020, hence affecting all the main branches of the tree); this represents a significant difference because it is an early investment whose annuity is paid in all nodes of the tree (a discounted total of \$60.4 millions), which leads to the conclusion that the flexibility provided by this

(a) Central 2025

(b) Central 2030

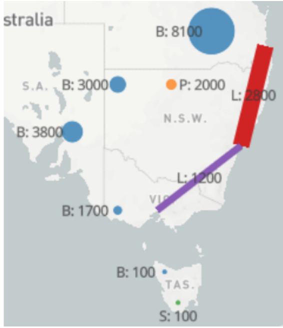

(c) Central 2035

(d) Slow 2025

(e) Slow 2030

(f) Slow 2035

(g) Fast 2025

(h) Fast 2030

(i) Fast 2035

(j) Step 2025

(k) Step 2030

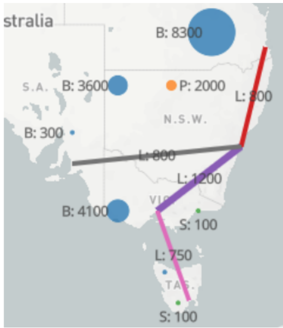

(l) Step 2035

(m) High DER 2025

(n) High DER 2030

(o) High DER 2035

Figure 5.13 Expansion trajectory maps by scenario ST16-WN12 with nadir constraints.

link helps capturing value across the branches in the scenario tree under analysis. Also, in 2030 (another stage of uncertainty in all branches except the Step scenario), there are changes in transmission: the Slow, Central and Fast scenarios see the expansion of NSW-QLD compared with the two-stage scenario tree. The aggregated storage capacity does not change in the main branches of the Slow and High DER scenarios; the Central scenario sees an increase in 2035, in the Fast scenario an increase in 2030 and a decrease in 2035, and the step scenario also has an increase in storage capacity in 2030 and 2035. The resulting expansion plan is better prepared to face a future where uncertainty can unfold not only between 2020 and 2025 but also in the period 2025 and 2030; although the resulting expansion plan is more expensive, the system with those assets is better prepared to face not only the five scenarios associated to ST16 but the ten scenarios included in ST26. This means that the expansion plan associated with ST16 tested against any of the extra five scenarios included in ST26 would yield additional costs that justify the investment plan found using ST26.

Table 5.11 Results for ST26-WN12 with nadir constraints.

Tree		Main scenario	Central	Slow					Central							Fast					DER					Step		
		Branch	Central	Slow			Central		Central			Fast		DER		Fast			DER		DER			Step		Step		
		Node	1	2	3	4	5	6	7	8	9	10	11	12	13	14	15	16	17	18	19	20	21	22	23	24	25	26
		Year	20	25	30	35	30	35	25	30	35	30	35	30	35	25	30	35	30	35	25	30	35	30	35	25	30	35
LINE	NSW-QLD	(200)	0	4	6	9	6	13	4	9	13	9	9	9	10	4	6	6	6	10	4	5	10	5	5	4	4	4
	VIC-NSW	(200)	0	5	5	5	5	5	5	5	5	5	6	5	10	5	6	6	6	10	5	5	10	5	5	5	5	5
	VIC-SA	(200)	0	0	0	0	0	0	0	0	0	0	0	0	0	0	0	0	0	0	0	0	0	0	0	0	0	0
	TAS-VIC	(750)	0	0	0	0	0	0	0	0	0	0	1	0	1	0	0	1	0	1	0	1	1	1	1	0	1	1
	SA-NSW	(800)	0	0	0	0	0	0	0	0	0	0	0	0	0	0	0	0	0	0	0	0	0	0	1	0	0	1
SYC	VIC	(100)	0	0	0	0	0	0	0	0	0	0	0	0	0	0	0	0	0	0	0	0	0	0	1	0	0	1
	TAS	(100)	1	1	1	1	1	1	1	1	1	1	1	1	1	1	1	1	1	1	1	1	1	1	1	1	1	1
BESS	QLD	(100)	0	0	0	0	0	75	0	0	82	0	24	0	0	0	0	17	0	0	0	0	0	39	86	0	13	84
	NSW	(100)	0	0	0	20	9	37	0	5	30	11	19	0	7	3	14	28	3	7	0	0	7	42	42	0	0	34
	VIC	(100)	0	0	0	0	0	17	0	0	19	0	0	0	0	0	0	0	0	0	0	0	0	8	41	0	6	41
	TAS	(100)	0	0	0	0	1	1	0	0	1	0	0	0	0	0	0	1	0	0	0	0	0	0	1	0	0	0
	SA	(100)	0	0	0	4	0	39	0	0	38	0	5	0	0	0	0	4	0	0	0	0	0	2	11	0	0	15
PSS	NSW	(2000)	0	0	0	0	0	1	0	0	1	0	1	0	0	0	0	1	0	0	0	0	0	0	1	0	1	1
	TAS	(1700)	0	0	0	0	0	0	0	0	0	0	0	0	0	0	0	0	0	0	0	0	0	0	0	0	0	0

5.4 Chapter summary

This chapter presented a novel expansion planning model that includes frequency response constraints, in particular a set of linear expressions representing the relationship between FR resources and the compliance with frequency nadir target. The expansion model was introduced as a deterministic equivalent problem (monolithic approach) and a Dantzig-Wolfe decomposition strategy was applied to divide the problem into smaller problems to avoid scalability issues. The solution to the decomposed problem is found using a column generation approach. The performance of the original problem and its decomposed counterpart were tested in an instance of the Australian power system. Further case study applications were developed to understand how the frequency response constraints and the representation of the uncertainty determine the optimal expansion decisions in the system.

CHAPTER 6

Conclusions

This thesis has developed models to represent the operation and expansion planning of electrical networks facing an accelerated reduction in the levels of synchronous inertia. The motivation for the work is set by the need for a power system expansion planning model which is successfully able to model frequency security constraints; this feature guarantees that the investment decisions made by the expansion model will lead to the frequency secure operation of the system in future low-inertia operation conditions under consideration. The core of the work revolved around developing a scheduling model capable of embedding constraints that ensure compliance with the standard frequency event metrics in power systems for both low- and high-frequency events: rate of change of frequency, quasi-steady-state frequency and frequency nadir/zenith. The frequency security model was derived from first principles and allows the consideration of multiple services for the provision of frequency response, on top of including the role of the natural response of demand to frequency changes, the consideration of the size of the contingency and the account of available inertia in the system after a contingency occurs. The frequency response model has been used in modelling developed to analyse several aspects of low-inertia power systems, including the impact of decreasing inertia in specific areas of the system, separation events, the role of fast frequency response, etc.

Weakly interconnected low-inertia power systems are seeing an increased risk of splitting due to cascading frequency events. To address this issue, a frequency security-constrained multi-area unit-commitment model is introduced to optimally allocate frequency response resources that will prevent frequency violations even when specific areas of the system become isolated. This scheduling model features the capacity to co-optimise the contingency size (generation, load, transmission) and consider the beneficial effect of fast frequency response to containing frequency events.

The case study applications for the security-constrained scheduling models showed that the supply of inertia and fast frequency response is becoming critical to contain frequency events in low-inertia systems. From a system architecture perspective, this should push the penetration of technologies capable of providing these services; the optimal quantity of each of these technologies will depend on the other benefits these technologies will bring to the system in a wide range of operation conditions. From a private perspective, the provision of frequency response services can represent relevant revenue streams for the different technologies providing them (if adequate market arrangements are in place to value them). Consequently, either from a centralised or competitive perspective, in order to fully identify the value of specific technologies in low-inertia power systems, a security-constrained expansion planning model becomes necessary.

The sheer size of such a planning problem is challenging, both because of the level of detail necessary to model operation flexibility (including frequency security) in low-inertia power systems and the need to represent future deep uncertainty through large scenario trees. The foundations behind the available methodologies for selecting the optimal mix of technologies to address the needs of the system across possible development scenarios were presented. Following an expected cost minimisation approach, a state-of-the-art security-constrained transmission, generation, and storage expansion model cast as a mixed-integer linear problem was introduced. Such a model allows for the application of Dantzig-Wolfe decomposition used to reduce it to a set of smaller, more manageable problems. The interaction of these problems through a column generation algorithm enables the search for a globally optimal solution. The expansion model was used to investigate the optimal expansion of storage, transmission and synchronous condensers in an instance of the Australian power system following the guidelines of AEMO's integrated system plan.

System operators around the world are already using many of the elements developed in this thesis. In the following sections, as the research novelty and contributions are described, the specific real-world applications of this research project are also identified.

6.1 Research novelty and contributions

The research performed in this thesis has presented several novel contributions beyond the state of the art in security-constrained operation and expansion of low-inertia power systems. The following summarises the primary novelty of the work.

(i) A framework for assessing multi-service frequency response adequacy in low-inertia power systems which can be translated into frequency security constraints to be used in operation scheduling and expansion planning.

(ii) The development of a comprehensive multi-area security-constrained cost minimisation unit commitment model capable of controlling the size of the potential generation, load and transmission contingencies and allocate the necessary frequency response resources to guarantee compliance with frequency requirements.

(iii) The presentation of a framework to compare expansion methodologies and to assess the value of investment flexibility and risk in low-inertia power systems.

(iv) This work presents the first power system expansion planning model capable of making decisions on new generation, transmission and storage assets, considering frequency security constraints and fast frequency response resources.

(v) The expansion planning model is applied to a real instance representing the Australian power system as described in the Integrated System Plan presented in 2020. The instance considers information on the evolution of the system in 5 different scenarios, including the availability and technical characteristics of synchronous units, renewable energy sources, electric vehicles uptake, controllable distributed storage, among many other details.

(vi) A power system modelling tool that integrates operation and expansion models to conduct studies in low-inertia power systems. The tool has been designed to handle large data sets and facilitate the analysis of results through proprietary and open-source visualisation tools.

Each of these points will be reviewed in more detail below, where conclusions and recommendations which may be drawn are presented.

6.1.1 Frequency response adequacy

Power systems experiencing a rapid decrease of synchronous inertia due to the massive penetration of variable renewable energy sources and the decommissioning of coal-fired power plants will experience a decrease in frequency response adequacy. In order to contribute to providing more clarity on this problem, this work has presented a first-principles approach to frequency response adequacy analysis for generation, load and transmission contingencies.

Key contributions from the application of the multi-service frequency response model developed in this work can be summarised as follows:

(i) The interaction of the three standard metrics to describe frequency events allows to define what qualifies as a low-inertia power system: when the frequency response resources necessary to comply with frequency standards are defined by the quasi-steady-state frequency requirements, the system will be labelled as a "high-inertia power system". On the other hand, when the frequency response needs of the system are defined by either the rate of change of frequency or the frequency nadir/zenith requirements, the system will be defined as a "low-inertia power system".

(ii) The natural response to frequency changes coming from demand substantially affects the requirements for frequency response resources. Currently, the sensitivity of demand to frequency changes is still relevant and it should not be neglected if the system is expected to operate efficiently. It is possible to envision that in the next 10 to 20 years, this contribution will decrease substantially, which will increase the need for contingency reserves to address frequency events. If the response coming from demand becomes negligible, there is a silver lining: the process of modelling frequency security constraints would be greatly simplified.

(iii) Fast frequency response has an enormous effect on the amount of primary frequency response resources needed to contain frequency events. In Australia, under low-inertia conditions, 100 MW of fast frequency response can replace 600+ MW of primary frequency response.

(iv) Although generally neglected due to the small size of the originating contingency, high-frequency events need to be considered in power systems facing a probability of splitting. The sudden loss of exports can have devastating effects on light power systems.

(v) The frequency response adequacy model has been used to analyse the frequency security of future energy scenarios in Australia in the context of the *Independent Review into the Future Security of the National Electricity Market* conducted by Australia's Chief Scientist in 2017.

(vi) The frequency response security maps derived from the frequency adequacy model has been used by the Australian Energy Market Operator to analyse the frequency behaviour of the South West Interconnected System in Western Australia in 2019.

6.1.2 Optimal allocation of frequency response resources

Inertia, primary frequency response and fast frequency response are quasi-independent resources that compete economically to provide frequency support after a contingency event of a given size. Determining the efficient amount of each of those resources is a complex problem because it interacts with the other constraints commanding the scheduling of the system to comply with other power system requirements. This work presented a deterministic security-constrained unit commitment model capable of making the standard unit-commitment decisions with the addition of frequency response constraints, with a particular interest in the non-convex frequency nadir/zenith constraints. The main conclusions obtained from the application of this model are summarised below:

(i) Co-optimising the contingency size that defines the frequency control ancillary services requirements exhibits relevant effects on the resulting dispatches and costs of the system. In low-inertia power systems with limited response capability, it allows finding feasible dispatch points that enable an operation within frequency control boundaries. The transition to low-inertia power systems will include the development of multiple strategies and further investment to deal with the security requirements. For those systems that are experiencing a rapid penetration of non-synchronous technologies, controlling the contingency size[28] might be the most straightforward and efficient way to operate the system economically and securely.

(ii) In a similar fashion, the co-optimisation of power flows across interconnectors, along with inertia and contingency reserves, can help preserve frequency stability after a system split occurs, thus enhancing system resilience. The model allows guaranteeing that post-contingency conditions in each subsystem comply with requirements on the rate of change of frequency, quasi-steady-state frequency, and frequency nadir and zenith. In particular, the model proves effective in controlling pre- and post-contingency control variables hence reducing overall system costs and guaranteeing resilience to extreme separation events.

(iii) The linearised model for the representation of frequency nadir/zenith requirements allows applying this approach in dispatch engines used to coordinate the operation of the energy and frequency control ancillary service markets, which usually are limited to linear constraints. Since the model has been built based on the sampling of different system conditions, the generation of linear constraints can be plugged into any dynamic model or data set capable of providing information about system inertia, frequency response service allocation, contingency size and the associated frequency nadir/zenith experienced by the system under those conditions.

(iv) The tests for the Australian power system show that if the system has sufficient fast frequency response capacity, it will, in general, be able to comply with the nadir/zenith constraint based on the aggregated reserve capacity needed to comply with the quasi-steady-state requirement.

6.1.3 Investment flexibility in low-carbon power systems

The framework used to evaluate flexible investment decisions in power systems can have relevant effects not only on the decisions themselves but also on the limitations that the associated mathematical modelling can impose on the feasibility to find a solution. The main conclusions drawn in this regard include:

(i) There are investment options/strategies that can better adapt to the deep uncertainties associated with the power system transition. Without a suitable stochastic

[28] In many markets implementing such measure is not straightforward because it goes against the basic principle of economic merit behind the energy product and it might impact the economics of cheap, large units operating as baseload. For instance, the market rules in Australia provide the capability to the market operator to reduce the contingency size in case the supply of frequency control ancillary services is below the requirement for a given level of contingency, but it does not allow the market operator to reduce the contingency size based on cost minimisation arguments. Other markets organised as centralised pools aiming to minimise overall operation costs based on the incremental cost of operation of each unit might be able to implement such a mechanism in a more straightforward manner.

methodology, it is impossible to effectively discriminate the best investment plan from an investment flexibility point of view.

(ii) Contrary to popular belief, the least worst regret approach is not independent of the use of scenario probabilities. The apparent independence from probabilities only conceals an underlying assumption of equiprobable scenarios.

(iii) Least worst regret inherently hedges against extreme negative outcomes due to the use of regrets as the indicator of value. A similar behaviour can be achieved by means of coherent risk metrics like conditional value at risk when using expected cost minimisation.

(iv) Although in theory both least worst regret and expected cost minimisation with an adequate risk metric could hedge the system against adverse outcomes, in practice, expected cost minimisation has better mathematical properties than least worst regret. This enables to solve more complex problems with a better representation of the uncertainty and the structure of the decisions, which make expected cost minimisation a superior framework to solve power system expansion planning problems.

(v) In 2020, UK's National Grid Electricity System Operator started applying a new framework to evaluate investment decisions in new transmission assets based on the least worst weighted regret approach presented in this work.

6.1.4 Security-constrained expansion planning

Power systems are increasingly relying on variable renewable energy sources to cover their energy needs both because they are competitive alternatives and they replace the use of fossil fuel power plants, which directly translates into a reduction of greenhouse gas emissions. However, this trend is also resulting in the reduction of system inertia, which negatively impacts frequency security. The irruption of battery storage and its capacity to provide fast frequency response and also to defer investments in transmission are expanding the set of available investment strategies when evaluating the best development path for low-inertia power systems, which results in a more difficult search for the optimal solution.

The expansion model introduced here draws the operational structure from the security-constrained unit commitment model presented in this work. It is built as a decomposed expected cost minimisation problem, which enables the representation of very large scenario trees with a dense representation of the operation conditions of the system in each scenario. The model is broken down into the master and slave problems, and it is solved by means of a column generation approach.

The key contributions of this work in the context of power system expansion planning are summarised below:

(i) To the best of the author's knowledge, this is the first stochastic expansion planning model that includes frequency nadir/zenith constraints and the consideration of fast frequency response resources as an alternative to comply with the frequency response requirements.

(ii) Depending on the degree of details considered to model the operation and the long term uncertainty, the sheer size of the resulting expansion problem is such that the monolithic approach cannot be solved even by the best commercial mixed-integer linear solvers available today. The use of decomposition is then necessary to enable the consideration of large scenario trees and sufficient operational details including, unit-commitment and frequency security constraints. Under the conditions represented in the case study application for the Australian power system, it is possible to see that for a 16 node scenario three, modelling the operation with more than seven representative weeks per year renders the monolithic approach slower than the decomposition approach when compared using the same computational infrastructure.

(iii) By considering synchronous condensers among the investment options, it is possible to see that both the rate of change of frequency and the frequency nadir requirements push for the investment in this technology. This happens even when the other benefits of this technology (i.e. system strength support) are not considered in the operational model.

(iv) Including the nadir constraint in the context of the expansion planning of the Australian power system produces an increment of 0.2% of the expected total costs of investment and operation, and introduces changes in the optimal investment decisions. It drives the deployment of synchronous condensers and battery storage in early epochs of the planning horizon, with changes in the deployment of transmission, as a response to the increased storage capacity. However, since the increase in costs falls within the target gap (0.5%), it is not possible to assert that the frequency nadir constraint is the only one responsible for these changes.

6.2 Future work and open questions

Although recently there have been developments in the realm of security-constrained operation and expansion planning of low-inertia power systems, there remain many open questions. Here several topics are discussed for which there remain the potential to apply and improve the models presented in this work.

6.2.1 Risk aversion in security-constrained expansion planning

Future scenarios displaying extreme conditions can yield high operational costs (for instance, as a result of loss of load) if adequate assets are not placed in the system in a timely manner. These costs can have a substantial impact on the final consumer, and they need to be hedged against starting with the investment decisions being made today. However, if decisions are made only based on an expected cost minimisation basis, they might be exposing the system to extremely adverse outcomes that get balanced out by very positive ones. In order to deal with this, the expansion planning model presented here can be readily modified to embed adequate risk metrics to balance out the cost minimisation through the simultaneous minimisation of the worst negative outcomes. Although this has been done in multiple expansion planning models preceding this work, the effect of different risk aversion profiles has never been tested in an expansion planning model that explicitly embeds frequency security considerations, which might have a substantial impact on the outcomes of very low-inertia scenarios.

6.2.2 Demand side response

Demand plays a vital role in the development of future power systems since its inherent flexibility can solve many of the problems faced by the power system today and envisioned for the power system in the future. In order to assess the full value of demand response in the system, its underlying operation has to be adequately included in the scheduling model of the system by, for instance, considering its willingness to pay to consume or its capacity to provide frequency response. The resulting operational model can then be used in expansion planning to determine the value of demand response in different future operating conditions. A excellent example of an interesting future source of demand response is water electrolysers for the production of hydrogen, which might become ubiquitous in renewable energy dominated power systems.

6.2.3 Integration of system strength constraints in operation scheduling and expansion planning

Low-inertia systems are displaying system strength issues, with voltage deviating substantially after faults and disturbances occur in the system. Since synchronous condensers also contribute to support system strength, it would be of value to proceed in a similar way as with the frequency response model, to attempt to include expressions that can link short circuit strength supplied by different technologies and the requirements of the grid in different areas. This way, assessing the value behind the investment in synchronous condensers would be fairer than just considering inertia provision (as it was done in this work). This would also help identify convenient locations to deploy synchronous generators (e.g., OCGT) in some locations if this helps with the provision of energy, inertia and system strength.

6.2.4 Coupling power and gas investment decisions

Recent developments on linear models to represent the operation of the natural gas system can allow its integration in the security-constrained operation and expansion planning models presented in this work. This approach opens an avenue to explore different aspects of the interaction between the power and gas systems: the gas network can represent a reliability liability for the operation of the power system in periods where too many gas-fired units are needed to support the operation of the system. Also, the gas system spans through the territory transferring big blocks of energy and alleviating the operation of the power network; in turn, this complementarity between pipelines and the grid, and the corresponding investment decisions in each of them, could be analysed in the context of a joint expansion of the systems with security considerations.

6.2.5 Global emissions constraints

Although the expansion planning model presented in this work has the capacity to make decisions on generation assets, this capability was only used to model synchronous condensers; the generation mix available in the system by scenario was taken as an input from the integrated system plan. In order to fully understand the optimal balance between different generation, transmission and storage assets to cover demand with frequency security constraints, the best approach would be to also make investment decisions on new synchronous and variable renewable energy assets. However, any decision on new generation assets must comply with the global environmental targets that the country under analysis has in place. Including these constraints in the context of the decomposed expansion problem presented in this work is not a trivial task and represents an area that has not been explored yet.

This page intentionally left blank.

References

[1] A. Finkel, K. Moses, C. Munro, T. Effeney, and M. O'Kane, "Independent Review Into the Future Security of the National Electricity Market," tech. rep., 2017.

[2] H. Gu, R. Yan, and T. K. Saha, "Minimum Synchronous Inertia Requirement of Renewable Power Systems," *IEEE Transactions on Power Systems*, vol. 33, no. 2, pp. 1533–1543, 2017.

[3] A. Boston, G. Bongers, S. Byrom, and I. Staffell, "Managing Flexibility Whilst Decarbonising Electricity - The Australian NEM is changing," tech. rep., 2017.

[4] AEMO, "Black System South Australia 28-09-2016," tech. rep., 2017.

[5] P. Mancarella, S. Püschel-Løvengreen, L. Zhang, H. Wang, M. Brear, T. Jones, M. Jeppesen, R. Batterham, R. Evans, and I. Mareels, "Power system security assessment of the future National Electricity Market," Tech. Rep. June, 2017.

[6] AEMO, "Initial Operation of the Hornsdale Power Reserve Battery Energy Storage System," Tech. Rep. April, 2018.

[7] AEMO, "2020 System Strength and Inertia Report," Tech. Rep. December, 2020.

[8] AEMO, *Ancillary Services Payments and Recovery*. Web page: https://aemo.com.au/en/energy-systems/electricity/national-electricity-market-nem/data-nem/ancillary-services-data/ancillary-services-payments-and-recovery.

[9] AEMO, "2020 Integrated System Plan," tech. rep., 2020.

[10] National Grid ESO, "Network Options Assessment Methodology," tech. rep., 2020.

[11] S. Pfenninger and J. Keirstead, "Renewables, nuclear, or fossil fuels? Scenarios for Great Britain's power system considering costs, emissions and energy security," *Applied Energy*, vol. 152, pp. 83–93, 2015.

[12] N. Al-Masood, R. Yan, and T. K. Saha, "A new tool to estimate maximum wind power penetration level: In perspective of frequency response adequacy," *Applied Energy*, vol. 154, pp. 209–220, 2015.

[13] L. Mehigan, D. Al Kez, S. Collins, A. Foley, B. Ó'Gallachóir, and P. Deane, "Renewables in the European power system and the impact on system rotational inertia," *Energy*, vol. 203, 2020.

[14] N. Miller, D. Lew, R. Piwko, L. Hannett, S. Achilles, J. Macdowell, M. R. Douglas, D. Wilson, and M. Adamiak, "Technology Capabilities for Fast Frequency Response," tech. rep., General Electric, 2017.

[15] B. Elliston, M. Diesendorf, and I. MacGill, "Simulations of scenarios with 100% renewable electricity in the Australian National Electricity Market," *Energy Policy*, vol. 45, pp. 606–613, 2012.

[16] B. Elliston, I. MacGill, and M. Diesendorf, "Least cost 100% renewable electricity scenarios in the Australian National Electricity Market," *Energy Policy*, vol. 59, pp. 270–282, 2013.

[17] M. Wright and P. Hearps, "Zero Carbon Australia Stationary Energy Plan," tech. rep., 2010.

[18] N. Al-Masood, N. Modi, T. K. Saha, and R. Yan, "Investigation of non-synchronous penetration level and its impact on frequency response in a wind dominated power system," *IEEE Power and Energy Society General Meeting*, 2016.

[19] R. Yan, T. K. Saha, N. Modi, N.-A. Masood, and M. Mosadeghy, "The combined effects of high penetration of wind and PV on power system frequency response," *Applied Energy*, vol. 145, pp. 320–330, 2015.

[20] H. Marzooghi, D. J. Hill, and G. Verbic, "Performance and Stability Assessment of Future Grid Scenarios for the Australian NEM," in *2014 Australasian Universities Power Engineering Conference (AUPEC)*, pp. 1–6, 2014.

[21] S. Riaz, G. Verbič, and A. C. Chapman, "Computationally efficient market simulation tool for future grid scenario analysis," *IEEE Transactions on Smart Grid*, vol. 10, no. 2, pp. 1405–1416, 2019.

[22] A. S. Ahmadyar, S. Riaz, G. Verbic, J. Riesz, and A. Chapman, "Assessment of minimum inertia requirement for system frequency stability," *2016 IEEE International Conference on Power System Technology, POWERCON 2016*, pp. 1–6, 2016.

[23] J. Riesz, J. Gilmore, and I. MacGill, "Frequency control ancillary service market design: Insights from the australian national electricity market," *Electricity Journal*, vol. 28, no. 3, pp. 86–99, 2015.

[24] O. Agranat, I. Macgill, and A. Bruce, "Fast Frequency Markets under High Penetrations of Renewable Energy in the Australian National Electricity Market," *Proceedings of the Asia-Pacific Solar Research Conference*, 2015.

[25] F. Teng, V. Trovato, and G. Strbac, "Stochastic Scheduling With Inertia-Dependent Fast Frequency Response Requirements," *IEEE Transactions on Power System*, vol. 31, no. 2, pp. 1557 – 1566, 2016.

[26] L. Zhang, Y. Zhou, D. Flynn, J. Mutale, and P. Mancarella, "System-Level Operational and Adequacy Impact Assessment of PV and Distributed Energy Storage, with Consideration of Inertial Constraints, Dynamic Reserve and Interconnection Flexibility," *Energies*, vol. 10, no. 989, pp. 1–40, 2017.

[27] P. Kundur, N. J. Balu, and M. G. Lauby, *Power system stability and control*. EPRI power system engineering series, McGraw-Hill, 1994.

[28] Y. Bian, H. Wyman-Pain, F. Li, R. Bhakar, S. Mishra, and N. P. Padhy, "Demand Side Contributions for System Inertia in the GB Power System," *IEEE Transactions on Power Systems*, vol. 33, no. 4, pp. 3521–3530, 2018.

[29] S. Püschel-Løvengreen, M. Ghazavi Dozein, S. Low, and P. Mancarella, "Separation event-constrained optimal power flow to enhance resilience in low-inertia power systems," *Electric Power Systems Research*, vol. 189, pp. 1–8, 2020.

[30] S. Püschel-Løvengreen and P. Mancarella, "Frequency response constrained economic dispatch with consideration of generation contingency size," in *20th Power Systems Computation Conference, PSCC 2018*, 2018.

[31] Arthur R. Bergen and Vijay Vittal, *Power systems analysis*. Prentice Hall, 2nd ed., 2000.

[32] F. Paganini and E. Mallada, "Global Analysis of Synchronization Performance for Power Systems: Bridging the Theory-Practice Gap," *IEEE Transactions on Automatic Control*, vol. 65, no. 7, pp. 3007–3022, 2020.

[33] AEMO, "Contingency Frequency Response in the South West Interconnected System (SWIS)," tech. rep., 2019.

[34] M. Rezkalla, M. Pertl, and M. Marinelli, "Electric power system inertia: requirements, challenges and solutions," *Electrical Engineering*, vol. 100, no. 4, pp. 2677–2693, 2018.

[35] S. Püschel-Løvengreen and P. Mancarella, "Mapping the Frequency Response Adequacy of the Australian National Electricity Market," in *Proceedings of the Australasian Universities Power Engineering Conference*, 2017.

[36] AEMO, "National Electricity Market Fact Sheet," tech. rep., 2017.

[37] AEMO, "South Australian Fuel and Technology Report," Tech. Rep. January, 2017.

[38] D. Hagan and K. Massie, "Australian Electricity Regulation," tech. rep., Getting the Deal Through, 2016.

[39] AEMO, "Guide to ancillary services in the National Electricity Market," tech. rep., 2015.

[40] AEMO, "FCAS model in NEMDE," tech. rep., 2017.

[41] AEMO, "Constraint Formulation Guidelines," Tech. Rep. December, 2013.

[42] AEMO, "National Transmission Network Development Plan," tech. rep., 2016.

[43] Q. Hong, M. Nedd, S. Norris, I. Abdulhadi, M. Karimi, V. Terzija, B. Marshall, K. Bell, and C. Booth, "Fast frequency response for effective frequency control in power systems with low inertia," *The Journal of Engineering*, vol. 2019, no. 16, pp. 1696–1702, 2019.

[44] EirGrid and SONI, "RoCoF Alternative & Complementary Solutions Project," Tech. Rep. March, 2016.

[45] AEMO, "Final Report – Queensland and South Australia system separation on 25 August 2018," tech. rep., 2019.

[46] AEMO, "Frequency control ancillary services," tech. rep., 2012.

[47] National Grid ESO, "Operating a Low Inertia System - A System Operability Framework document," tech. rep., 2020.

[48] J. O'Sullivan and M. O'Malley, "A New Methodology for the Provision of Reserve in an Isolated Power System," *IEEE Transactions on Power Systems, vel*, vol. 14, no. 2, p. 519, 1999.

[49] J. F. Restrepo and F. D. Galiana, "Unit commitment with primary frequency regulation constraints," *IEEE Transactions on Power Systems*, vol. 20, no. 4, pp. 1836–1842, 2005.

[50] W. Winter, K. Elkington, G. Bareux, and J. Kostevc, "Pushing the limits: Europe's new grid: Innovative tools to combat transmission bottlenecks and reduced inertia," *IEEE Power and Energy Magazine*, vol. 13, no. 1, pp. 60–74, 2015.

[51] P. Tielens and D. Van Hertem, "The relevance of inertia in power systems," *Renewable and Sustainable Energy Reviews*, vol. 55, pp. 999–1009, 2016.

[52] F. Milano, F. Dorfler, G. Hug, D. J. Hill, and G. Verbič, "Foundations and challenges of low-inertia systems (Invited Paper)," in *20th Power Systems Computation Conference, PSCC 2018*, 2018.

[53] P. Daly, D. Flynn, and N. Cunniffe, "Inertia considerations within unit commitment and economic dispatch for systems with high non-synchronous penetrations," in *2015 IEEE Eindhoven PowerTech*, pp. 1–6, IEEE, 2015.

[54] J. H. Eto, J. Undrill, P. Mackin, R. Daschmans, B. Williams, B. Haney, R. Hunt, J. Ellis, H. Illian, C. Martinez, M. O'Malley, K. Coughlin, and K. H. LaCommare, "Use of Frequency Response Metrics to Assess the Planning and Operating Requirements for Reliable Integration of Variable Renewable Generation," tech. rep., 2010.

[55] R. Doherty, G. Lalor, and M. O. Malley, "Frequency Control in Competitive Electricity Market Dispatch," *IEEE Transactions on Power Systems*, vol. 20, no. 3, pp. 1588–1596, 2005.

[56] R. Bhana and T. J. Overbye, "The Commitment of Interruptible Load to Ensure Adequate System Primary Frequency Response," *IEEE Transactions on Power Systems*, vol. 31, no. 3, pp. 2055–2063, 2016.

[57] A. S. Ahmadyar, S. Riaz, G. Verbic, A. Chapman, and D. J. Hill, "A Framework for Assessing Renewable Integration Limits with Respect to Frequency Performance," *IEEE Transactions on Power Systems*, vol. 33, no. 4, pp. 4444–4453, 2018.

[58] H. Chavez, R. Baldick, and S. Sharma, "Governor Rate-Constrained OPF for Primary Frequency Control Adequacy," *IEEE Transactions on Power Systems*, vol. 29, no. 3, pp. 1473–1479, 2014.

[59] Y. Y. Lee and R. Baldick, "A frequency-constrained stochastic economic dispatch model," *IEEE Transactions on Power Systems*, vol. 28, no. 3, pp. 2301–2312, 2013.

[60] H. Ahmadi and H. Ghasemi, "Security-Constrained Unit Commitment With Linearized System Frequency Limit Constraints," *IEEE Transactions on Power Systems*, vol. 29, no. 4, pp. 1536–1545, 2014.

[61] C. Cardozo, W. van Ackooij, and L. Capely, "Cutting plane approaches for frequency constrained economic dispatch problems," *Electric Power Systems Research*, vol. 156, pp. 54–63, 2018.

[62] M. Paturet, U. Markovic, S. Delikaraoglou, E. Vrettos, P. Aristidou, and G. Hug, "Stochastic unit commitment in low-inertia grids," *IEEE Transactions on Power Systems*, vol. 35, no. 5, pp. 3448–3458, 2020.

[63] I. Pavić, T. Capuder, and I. Kuzle, "Low carbon technologies as providers of operational flexibility in future power systems," *Applied Energy*, vol. 168, pp. 724–738, 2016.

[64] F. Teng, Y. Mu, H. Jia, J. Wu, P. Zeng, and G. Strbac, "Challenges on primary frequency control and potential solution from EVs in the future GB electricity system," *Applied Energy*, vol. 194, pp. 353–362, 2017.

[65] F. Teng, M. Aunedi, and G. Strbac, "Benefits of flexibility from smart electrified transportation and heating in the future UK electricity system," *Applied Energy*, vol. 167, pp. 420–431, 2016.

[66] F. Teng and G. Strbac, "Business cases for energy storage with multiple service provision," *Journal of Modern Power Systems and Clean Energy*, vol. 4, no. 4, pp. 615–625, 2016.

[67] V. Trovato, A. Bialecki, and A. Dallagi, "Unit Commitment with Inertia-Dependent and Multispeed Allocation of Frequency Response Services," *IEEE Transactions on Power Systems*, vol. 34, no. 2, pp. 1537–1548, 2019.

[68] L. Badesa, F. Teng, and G. Strbac, "Simultaneous Scheduling of Multiple Frequency Services in Stochastic Unit Commitment," *IEEE Transactions on Power Systems*, vol. 34, no. 5, pp. 3858–3868, 2019.

[69] L. E. Sokoler, P. Vinter, R. Baerentsen, K. Edlund, and J. B. Jorgensen, "Contingency-Constrained Unit Commitment in Meshed Isolated Power Systems," *IEEE Transactions on Power Systems*, vol. 31, no. 5, pp. 3516–3526, 2016.

[70] L. Badesa, F. Teng, and G. Strbac, "Optimal Portfolio of Distinct Frequency Response Services in Low-Inertia Systems," *IEEE Transactions on Power Systems*, vol. 35, no. 6, pp. 4459–4469, 2020.

[71] A. Jalali, G. Dozein, and P. Mancarella, "Frequency Stability Provision From Battery Energy Storage System Considering Cascading Failures, with Applications to Separation Events in Australia," in *2019 IEEE Milan PowerTech*, pp. 1–6, 2019.

[72] A. Kannan, M. Nuschke, B. P. Dobrin, and D. Strauß-Mincu, "Frequency stability analysis for inverter dominated grids during system split," *Electric Power Systems Research*, vol. 188, 2020.

[73] X. Cao, I. Abdulhadi, A. Emhemed, C. Booth, and G. Burt, "Evaluation of the impact of variable system inertia on the performance of frequency based protection," in *12th IET International Conference on Developments in Power System Protection (DPSP 2014)*, (Copenhagen, Denmark), pp. 1–6, 2014.

[74] A. Adrees, J. V. Milanović, and P. Mancarella, "Effect of inertia heterogeneity on frequency dynamics of low-inertia power systems," *IET Generation, Transmission and Distribution*, vol. 13, no. 14, pp. 2951–2958, 2019.

[75] F. Conte, S. Massucco, M. Paolone, G. P. Schiapparelli, F. Silvestro, and Y. Zuo, "Frequency stability assessment of modern power systems: Models definition and parameters identification," *Sustainable Energy, Grids and Networks*, vol. 23, 2020.

[76] L. Badesa, F. Teng, and G. Strbac, "Conditions for Regional Frequency Stability in Power Systems – Part I: Theory," *arXiv e-prints*, 2020.

[77] L. Badesa, F. Teng, and G. Strbac, "Conditions for Regional Frequency Stability in Power Systems – Part II: Applications," *arXiv e-prints*, 2020.

[78] C. B. Barber, D. P. Dobkin, and H. Huhdanpaa, "The Quickhull Algorithm for Convex Hulls," *ACM Transactions on Mathematical Software*, vol. 22, no. 4, pp. 469–483, 1996.

[79] L. Zhang, T. Capuder, and P. Mancarella, "Unified Unit Commitment Formulation and Fast Multi-Service LP Model for Flexibility Evaluation in Sustainable Power Systems," *IEEE Transactions on Sustainable Energy*, vol. 7, no. 2, pp. 658–671, 2016.

[80] T. Feehally, A. Forsyth, R. Todd, M. Foster, D. Gladwin, D. Stone, and D. Strickland, "Battery energy storage systems for the electricity grid: UK research facilities," in *8th IET International Conference on Power Electronics, Machines and Drives (PEMD 2016)*, 2016.

[81] M. Carrion and J. M. Arroyo, "A computationally efficient mixed-integer linear formulation for the thermal unit commitment problem," *IEEE Transactions on Power Systems*, vol. 21, no. 3, pp. 1371–1378, 2006.

[82] National Grid, "Long-term Market and and Network Constraint Modelling," Tech. Rep. January, 2017.

[83] Jacobs Group, "Modelling illustrative electricity sector emissions reduction policies Climate Change Authority," Tech. Rep. June, 2016.

[84] Australian Energy Regulator, "State of the Energy Market," Tech. Rep. May, 2017.

[85] AEMO, "NEM - Market Event Report – High FCAS Prices in South Australia," Tech. Rep. November, AEMO, 2015.

[86] AEMO, *Generation Information Page*. Web page: https://www.aemo.com.au/energy-systems/electricity/national-electricity-market-nem/nem-forecasting-and-planning/forecasting-and-planning-data/generation-information.

[87] Australian Photovoltaic Institue, *Mapping Australian Photovoltaic installations*. Web page: https://pv-map.apvi.org.au/historical.

[88] AEMO, "Interconnector Capabilities for the National Electricity Market," tech. rep., 2017.

[89] AEMO, "Integrated System Plan For the National Electricity Market 2018," tech. rep., 2018.

[90] S. K. Yee, J. V. Milanović, and F. M. Hughes, "Overview and comparative analysis of gas turbine models for system stability studies," *IEEE Transactions on Power Systems*, vol. 23, no. 1, pp. 108–118, 2008.

[91] AEMO, "Review of NEM load relief," Tech. Rep. September, 2019.

[92] A. Street, F. Oliveira, and J. M. Arroyo, "Contingency-constrained unit commitment with n-K security criterion: A robust optimization approach," *IEEE Transactions on Power Systems*, vol. 26, no. 3, pp. 1581–1590, 2011.

[93] P. Mancarella, S. Püschel-Løvengreen, L. Zhang, and C. Bas-Domenech, "Study of advanced modelling for network planning under uncertainty Part 1: Review of frameworks and industrial practices for decision-making in transmission network planning Report prepared for National Grid Electricity System Operator," tech. rep., 2020.

[94] P. Mancarella, L. Zhang, and S. Püschel-Løvengreen, "Study of advanced modelling for network planning under uncertainty Part 2: Review of power transfer capability assessment and investment flexibility in transmission network planning Report prepared for National Grid Electricity System Operator," tech. rep., 2020.

[95] National Grid ESO, "Network Options Assessment Methodology," tech. rep., 2020.

[96] National Grid ESO, "Network Options Assessment #NOA2021," tech. rep., 2021.

[97] R. Moreno, A. Street, J. M. Arroyo, and P. Mancarella, "Planning low-carbon electricity systems under uncertainty considering operational flexibility and smart grid technologies," *Philosophical Transactions of the Royal Society A: Mathematical, Physical and Engineering Sciences*, vol. 375, no. 2100, 2017.

[98] I. Konstantelos and G. Strbac, "Valuation of flexible transmission investment options under uncertainty," *IEEE Transactions on Power Systems*, vol. 30, no. 2, pp. 1047–1055, 2015.

[99] J. A. Schachter and P. Mancarella, "A critical review of Real Options thinking for valuing investment flexibility in Smart Grids and low carbon energy systems," *Renewable and Sustainable Energy Reviews*, vol. 56, pp. 261–271, 2016.

[100] E. Delage and D. Iancu, "Robust Multistage Decision Making," in *INFORMS TutORials in Operations Research*, pp. 20–46, 2015.

[101] A. Flores-Quiroz, R. Palma-Behnke, G. Zakeri, and R. Moreno, "A column generation approach for solving generation expansion planning problems with high renewable energy penetration," *Electric Power Systems Research*, vol. 136, pp. 232–241, 2016.

[102] J. Birge and F. Louveaux, "Introduction to Stochastic Programming," *Springer Series in Operations Research*, p. 421, 1997.

[103] S. Park, Q. Xu, and B. F. Hobbs, "Comparing scenario reduction methods for stochastic transmission planning," *IET Generation, Transmission & Distribution*, vol. 13, no. 7, pp. 1005–1013, 2019.

[104] W. B. Powell and S. Meisel, "Tutorial on Stochastic Optimization in Energy - Part I: Modeling and Policies," *IEEE Transactions on Power Systems*, vol. 31, no. 2, pp. 1459–1467, 2016.

[105] W. B. Powell and S. Meisel, "Tutorial on Stochastic Optimization in Energy - Part II: An Energy Storage Illustration," *IEEE Transactions on Power Systems*, vol. 31, no. 2, pp. 1468–1475, 2016.

[106] V. Miranda and L. M. Proença, "Probabilistic choice vs. risk analysis-conflicts and synthesis in power system planning," *IEEE Transactions on Power Systems*, vol. 13, no. 3, pp. 1038–1043, 1998.

[107] V. Miranda and L. M. Proença, "Why risk analysis outperforms probabilistic choice as the effective decision support paradigm for power system planning," *IEEE Transactions on Power Systems*, vol. 13, no. 2, pp. 643–648, 1998.

[108] J. M. Arroyo, N. Alguacil, and M. Carrión, "A risk-based approach for transmission network expansion planning under deliberate outages," *IEEE Transactions on Power Systems*, vol. 25, no. 3, pp. 1759–1766, 2010.

[109] D. E. Bell, "Regret in Decision Making under Uncertainty," *Operations Research*, vol. 30, no. 5, pp. 961–981, 1982.

[110] G. Loomes and R. Sugden, "Regret Theory: An Alternative Theory of Rational Choice Under Uncertainty," *The Economic Journal*, vol. 92, pp. 805–824, 1982.

[111] A. K. Dixit and R. S. Pindyck, *Investment under Uncertainty*. Princeton University Press, 1994.

[112] A. J. Conejo, M. Carrion, and J. M. Morales, *Decision Making Under Uncertainty in Electricity Markets*. New York: Springer, 2010.

[113] J. Kisiala, *Conditional Value-at-Risk: Theory and Applications*. PhD thesis, 2015.

[114] M. K. Starr and M. Zeleny, *Multiple Criteria Decision Making*. North-Holland Publishing Company, 1977.

[115] A. M. Geoffrion, *A Parametric Programming Solution to the Vector Maximum Problem with Applications to Decisions Under Uncertainty*. Stanford University, 1965.

[116] E. Crousillat, P. Dorfner, P. Alvarado, and H. Merrill, "Conflicting objectives and risk in power system planning," *IEEE Transactions on Power System*, vol. 8, no. 3, pp. 887–893, 1993.

[117] National Grid ESO, "Network Options Assessment Report Methodology v5.1," Tech. Rep. January, 2020.

[118] E. Martinez-Cesena, *Real Options Theory Applied to Renewable Energy Generation Projects Planning*. PhD thesis, 2012.

[119] J. Ma, V. Silva, R. Belhomme, D. S. Kirschen, and L. F. Ochoa, "Evaluating and planning flexibility in sustainable power systems," *IEEE Transactions on Sustainable Energy*, vol. 4, no. 1, pp. 200–209, 2013.

[120] B. S. Palmintier and M. D. Webster, "Impact of Operational Flexibility on Electricity Generation Planning with Renewable and Carbon Targets," *IEEE Transactions on Sustainable Energy*, vol. 7, no. 2, pp. 672–684, 2016.

[121] K. Poncelet, E. Delarue, and W. D'haeseleer, "Unit commitment constraints in long-term planning models: Relevance, pitfalls and the role of assumptions on flexibility," *Applied Energy*, vol. 258, p. 113843, 2020.

[122] N. Helistö, J. Kiviluoma, H. Holttinen, J. D. Lara, and B. M. Hodge, "Including operational aspects in the planning of power systems with large amounts of variable generation: A review of modeling approaches," *Wiley Interdisciplinary Reviews: Energy and Environment*, vol. 8, no. 5, 2019.

[123] Y. Dvorkin, F. B. Ricardo, Y. Wang, B. Xu, D. S. Kirschen, H. Pandžić, J. P. Watson, and A. S. M. Cesar, "Co-planning of investments in transmission and merchant energy storage," *IEEE Transactions on Power Systems*, vol. 33, no. 1, pp. 245–256, 2018.

[124] G. Diaz, A. Inzunza, and R. Moreno, "The importance of time resolution, operational flexibility and risk aversion in quantifying the value of energy storage in long-term energy planning studies," *Renewable and Sustainable Energy Reviews*, vol. 112, pp. 797–812, 2019.

[125] M. Kristiansen, M. Korpås, H. Farahmand, I. Graabak, and P. Härtel, "Introducing system flexibility to a multinational transmission expansion planning model," in *19th Power Systems Computation Conference, PSCC 2016*, IEEE, 2016.

[126] A. Schwele, J. Kazempour, and P. Pinson, "Do unit commitment constraints affect generation expansion planning? A scalable stochastic model," *Energy Systems*, vol. 11, no. 2, pp. 247–282, 2020.

[127] B. Hua, R. Baldick, and J. Wang, "Representing Operational Flexibility in Generation Expansion Planning Through Convex Relaxation of Unit Commitment," *IEEE Transactions on Power Systems*, vol. 33, no. 2, pp. 2272–2281, 2018.

[128] V. Oree, S. Z. Sayed Hassen, and P. J. Fleming, "Generation expansion planning optimisation with renewable energy integration: A review," *Renewable and Sustainable Energy Reviews*, vol. 69, pp. 790–803, 2017.

[129] N. E. Koltsaklis and A. S. Dagoumas, "State-of-the-art generation expansion planning: A review," *Applied Energy*, vol. 230, pp. 563–589, 2018.

[130] P. V. Gomes and J. T. Saraiva, "State-of-the-art of transmission expansion planning: A survey from restructuring to renewable and distributed electricity markets,"

International Journal of Electrical Power and Energy Systems, vol. 111, pp. 411–424, 2019.

[131] L. Gacitua, P. Gallegos, R. Henriquez-Auba, Lorca, M. Negrete-Pincetic, D. Olivares, A. Valenzuela, and G. Wenzel, "A comprehensive review on expansion planning: Models and tools for energy policy analysis," *Renewable and Sustainable Energy Reviews*, vol. 98, pp. 346–360, 2018.

[132] A. Inzunza, R. Moreno, A. Bernales, and H. Rudnick, "CVaR constrained planning of renewable generation with consideration of system inertial response, reserve services and demand participation," *Energy Economics*, vol. 59, pp. 104–117, 2016.

[133] Z. Wang, J. Wang, G. Li, and M. Zhou, "Generation-expansion planning with linearized primary frequency response constraints," *Global Energy Interconnection*, vol. 3, no. 4, pp. 346–354, 2020.

[134] S. Wogrin, D. Tejada-Arango, S. Delikaraoglou, and A. Botterud, "Assessing the impact of inertia and reactive power constraints in generation expansion planning," *Applied Energy*, vol. 280, 2020.

[135] M. Carrion, Y. Dvorkin, and H. Pandzic, "Primary Frequency Response in Capacity Expansion with Energy Storage," *IEEE Transactions on Power Systems*, vol. 33, no. 2, pp. 1824–1835, 2018.

[136] K. J. Singh, A. B. Philpott, and R. K. Wood, "Dantzig-Wolfe Decomposition for Solving Multistage Stochastic Capacity-Planning Problems," *Operations Research*, vol. 57, no. 5, pp. 1271–1286, 2009.

[137] H. Otarola, "Co-optimising network and storage systems investments through stochastic optimisation via column generation algorithms," *Master's Thesis*, 2019.

[138] C. Saldarriaga-Cortés, H. Salazar, R. Moreno, and G. Jiménez-Estévez, "Stochastic planning of electricity and gas networks: An asynchronous column generation approach," *Applied Energy*, vol. 233-234, pp. 1065–1077, 2019.

[139] F. Vanderbeck, "Implementing Mixed Integer Column Generation," in *Column Generation* (G. Desaulniers, J. Desrosiers, and M. M. Solomon, eds.), vol. 5, Springer Science & Business Media, 2006.

[140] M. E. Lübbecke and J. Desrosiers, "Selected topics in column generation," *Operations Research*, vol. 53, no. 6, pp. 1007–1023, 2005.

[141] L. M. Rousseau, M. Gendreau, and D. Feillet, "Interior point stabilization for column generation," *Operations Research Letters*, vol. 35, no. 5, pp. 660–668, 2007.

[142] O. Du Merle, D. Villeneuve, J. Desrosiers, and P. Hansen, "Stabilized column generation," *Discrete Mathematics*, vol. 194, no. 1-3, pp. 229–237, 1999.

[143] A. Downward, R. Baucke, and A. B. Philpott, "JuDGE.jl: a Julia package for optimizing capacity expansion," tech. rep., Engineering Science, University of Auckland, 2020.

[144] G. B. Dantzig and P. Wolfe, "Decomposition principle for linear programs," *Operations Research*, vol. 8, no. 1, pp. 101–111, 1960.

[145] N. West, "Battery of the Nation - Pumped Hydro Energy Storage Projects," tech. rep., HydroTasmania, 2019.

[146] N. West, P. Williams, and C. Potter, "Pumped-hydro cost modelling," tech. rep., Entura, 2018.

[147] L. Patterson, "Investigation into intervention mechanisms and system strength in the national electricity market (epr0070): consultation paper," 2019.

[148] I. J. Scott, P. M. Carvalho, A. Botterud, and C. A. Silva, "Clustering representative days for power systems generation expansion planning: Capturing the effects of variable renewables and energy storage," *Applied Energy*, vol. 253, 2019.

[149] F. J. De Sisternes and M. D. Webster, "Optimal Selection of Sample Weeks for Approximating the Net Load in Generation Planning Problems," tech. rep., MIT, 2013.

[150] Gurobi Optimization LLC, "Gurobi Optimizer Reference Manual," 2021.

[151] J. Bezanson, A. Edelman, S. Karpinski, and V. B. Shah, "Julia: A fresh approach to numerical computing," *SIAM Review*, vol. 59, no. 1, pp. 65–98, 2017.

[152] I. Dunning, J. Huchette, and M. Lubin, "JuMP: A modeling language for mathematical optimization," *SIAM Review*, vol. 59, no. 2, pp. 295–320, 2017.

[153] L. Lafayette and B. Wiebelt, "Spartan and NEMO: Two HPC-cloud hybrid implementations," in *Proceedings - 13th IEEE International Conference on eScience, eScience 2017*, pp. 458–459, Institute of Electrical and Electronics Engineers Inc., 11 2017.

[154] K. W. Schulz, C. R. Baird, D. Brayford, Y. Georgiou, G. M. Kurtzer, D. Simmel, T. Sterling, N. Sundararajan, and E. van Hensbergen, "Cluster Computing with OpenHPC," in *HPC Systems Professionals Workshop*, pp. 1–6, MAICS, 2016.

[155] National Grid ESO, "Future Energy Scenarios," tech. rep., 2020.

APPENDIX A

Modelling environment and computational infrastructure

When discussing the expansion of generation and transmission of power systems, particularly when uncertainty plays a relevant role in the future conditions of the system, scalability of the mathematical and data models is of the essence. The main considerations to define the development environment for this project are listed below:

- Programming language and database software have to be open-source. They need to be capable of seamlessly connecting with open source and proprietary optimisation software.
- Data model has to allow escalation of the number of elements, time frames and scenarios. Also, data storage has to be secure, not prone to data corruption, and be on the cloud so multiple instances can access the same data source to run different studies.
- The user should be capable of modifying input data, and output data has to be organised so that it will allow for the use of visualisation software to conduct systematic analysis.

In order to address these requirements, a modelling environment based on Julia programming language [151] and its modelling language for mathematical optimisation package JuMP [152] is used. Julia-JuMP complies with being open source and allows the integration of multiple optimisation solvers. To store input and output data, a relational database is used (MySQL), which is embedded in the software through Julia's DBInterface package, which allows it to connect to different proprietary and open source databases seamlessly. This choice is based on the fact that MySQL is a very common choice within the set of relational databases, it is easily installed across platforms, and it allows to run a data server in the cloud to access the system information from multiple computational environments without the risk of facing data inconsistency across computational platforms.

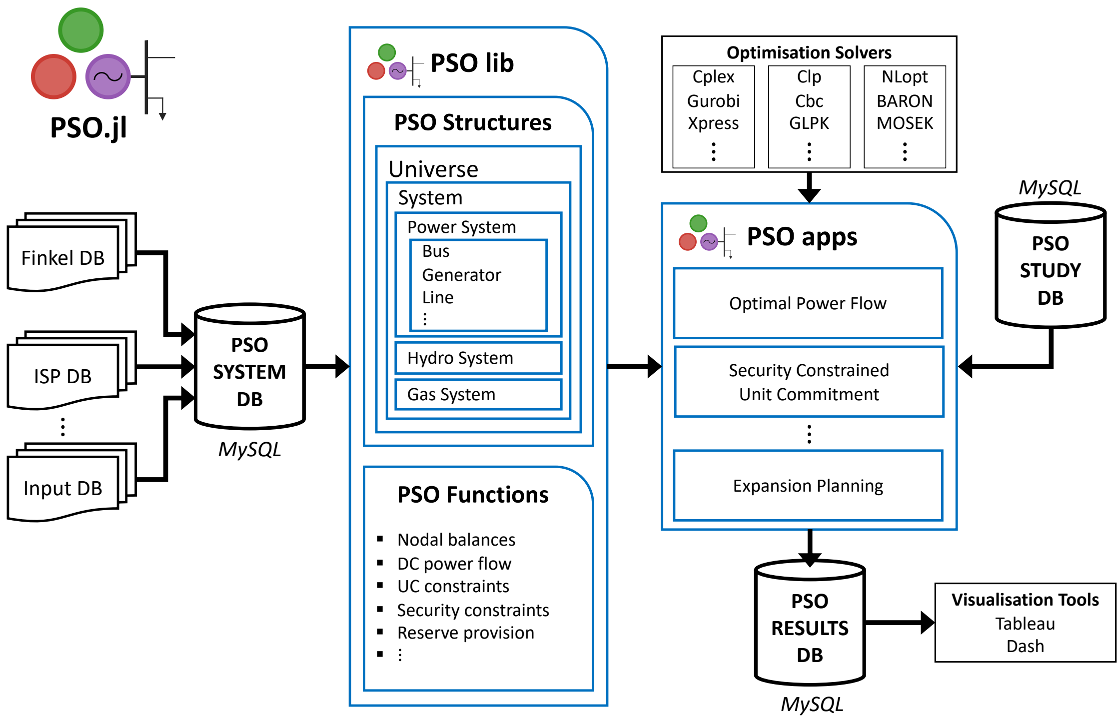

Figure A.1 Structure of the modelling environment "Power System Optimisation" based on Julia programming language and MySQL DB

Using the tools described before, it is possible to create the Power System Optimisation (PSO) library, which has data structures (PSO Structures) that allows defining a complex system, such as Australia's NEM, with multiple subsystems, complex electrical interconnections, several water basins, etc. Based on the PSO Structures, a set of functions is defined, which are the building blocks of various power system optimisation applications, such as unit-commitment, economic dispatch and expansion planning models.

Figure A.1 presents the interaction of the PSO library, I/O of data using MySQL databases and external open source and proprietary software for linear, mixed-integer and non-linear optimisation. Also, the figure highlights three databases (DB): the input database (PSO SYSTEM DB), the study database (PSO STUDY DB) and the results database (PSO RESULTS DB). PSO SYSTEM DB stores the data about the system under analysis with the corresponding time series data with temporal information, like wind and solar output profiles, activation schedules of elements, etc. PSO STUDY DB stores the data necessary to define the case study applications based on the system data in PSO SYSTEM DB, defining the number of cases, duration, start dates, initial conditions, scenarios (or scenario trees), etc. PSO RESULTS DB stores the values for the decision variables of the corresponding application.

Since all the information is kept in consistent databases, it is possible to standardise the visualisation of results through proprietary (Tableau) and open source (Dash) software. This allows to readily analyse the results of the different PSO applications through user-friendly, interactive interfaces.

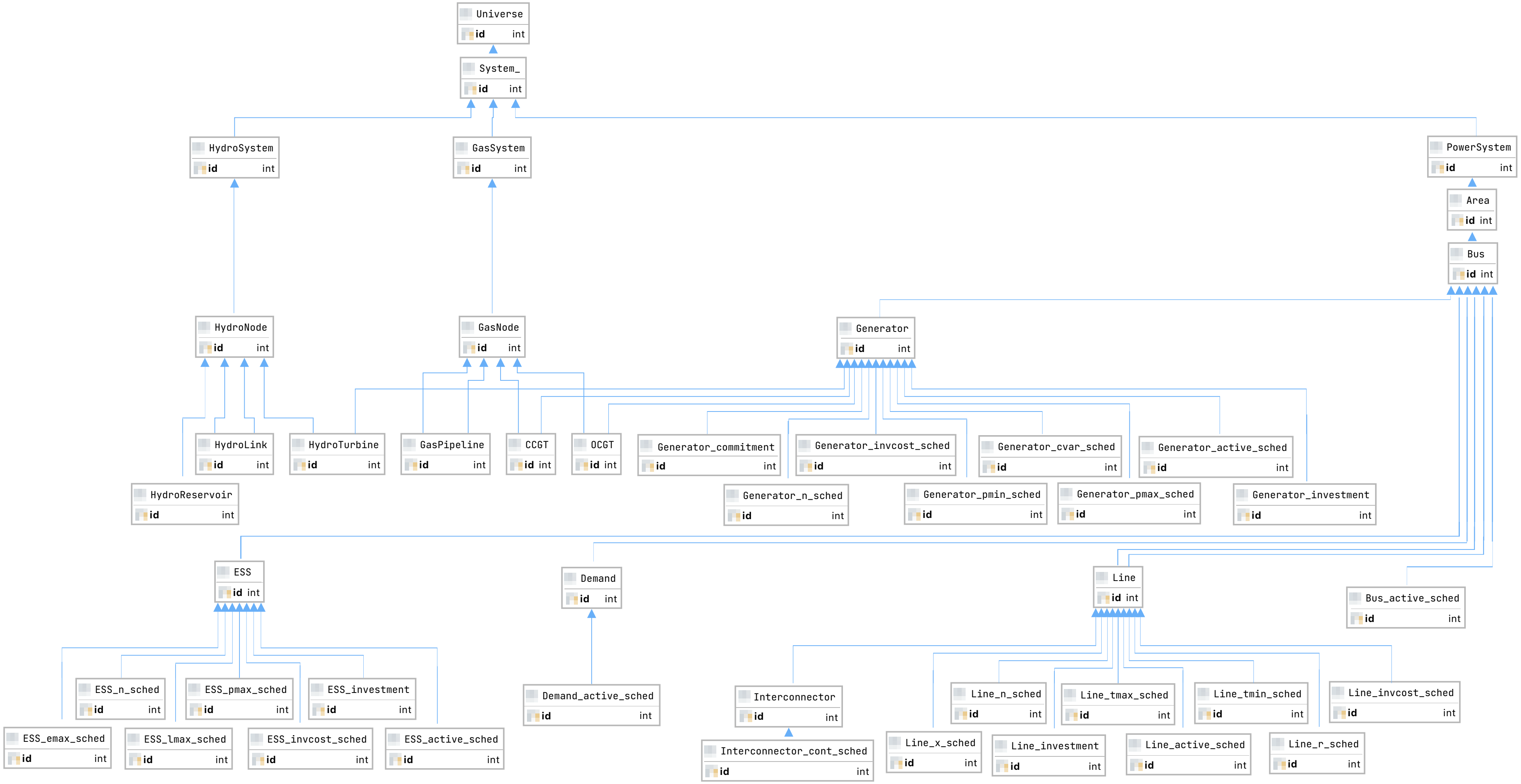

Figure A.2 Structure of data model in the PSO library

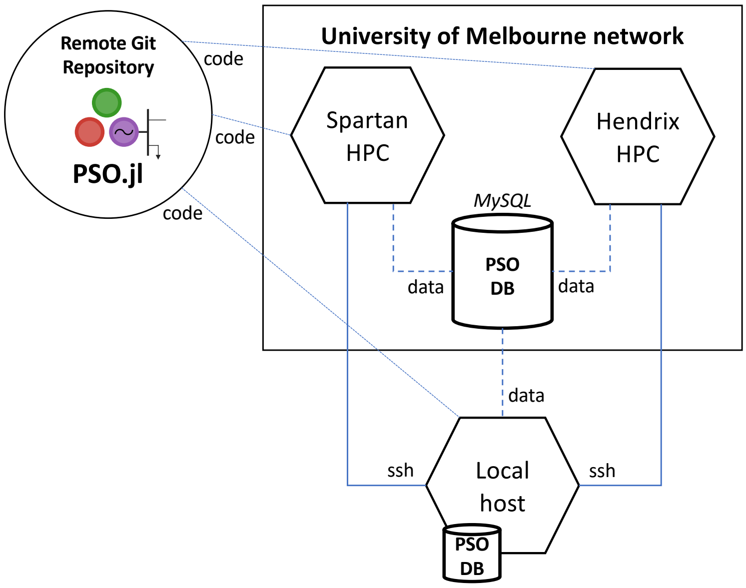

Figure A.3 Computational infrastructure used in the context of this work

Regarding the details of the data model of the PSO structure, Figure A.2 presents a summary of the elements that are included in the PSO SYSTEM DB. So far, the main focus has been put on the element power system and its dependants. Let us look at the element *Generator*: its relation to the power system is established through the *Bus* element, which represents the nodes in the network. In turn, each generator has internal parameters (not showing in the figure for the sake of conciseness) and also dependant sets of data, for instance, the parameters describing the behaviour of generation units with unit commitment constraints and the times series for the maximum output capacity (*Generator_pmax_sched*), number of available units (*Generator_n_sched*), investment information (*Generator_investment*), etc. The scaffolding for the Hydro and Gas System was implemented but it has not yet been applied in studies.

Based on the data structure, it is possible to apply this model to any system, country or set of countries. In particular, for the Australian case, the Universe corresponds to Australia, which is composed of several systems, like the NEM and the South West Interconnected System in Western Australia. Then, a system like the NEM is split into its balancing areas (QLD, NSW, VIC, SA and TAS). Each area can contain many buses representing the internal transmission network, and so on according to the data dependency presented in Figure A.2. PSO was conceived to simplify the production of studies, so it is possible to activate and deactivate elements on the PSO SYSTEM DB, which is consistently reflected on the corresponding study; this enables, for instance, to activate only one balance area and run a specific study on a specific state without the need to duplicate the input DBs.

When it comes to computational infrastructure, this project relied on three sources to process case study applications, one development and testing machine (localhost) and two high performance computing (HPC) servers within the University of Melbourne network:

- **Localhost**: MacBook Pro (16-inch, 2016) - 2.9 GHz Quad-Core Intel Core i7 - 16 GB 2133 MHz LPDDR3
- **Spartan HPC**: 41 Nodes each with 72 Intel Xeon Gold 6254 CPU @ 3.10GHz and 745 GB RAM
- **Hendrix HPC**: 23 Nodes each with 3.4-3.6 GHz Quad-Core Intel Core i7 and 16 GB 2133 MHz DDR3 (total: 92 physical CPUs and 368 GB RAM)

All these resources interact as presented in Figure A.3, which highlights the fact that a MySQL server is run within the University's network to handle input and output data associated with the PSO applications. All the computation machines keep an up-to-date version of the PSO library by means of the use of a remote Git repository.

Spartan HPC [153] is an extremely powerful shared resource within the University; however, the scheduling system (SLURM) within Spartan reduces the priority of a user based on the amount of resources the user has been using. This introduces a progressively large delay (up to 5 days) in allocating resources, which hinders the capacity to run a batch of studies.

This limitation triggered the need to develop an exclusive HPC server to cope with the computational requirements of the project. Using openHPC [154] it was possible to assemble a set of 23 desktop computers that enabled permanent access to sufficient computational capacity to process an expansion case study application in less than 36 hours.

This page intentionally left blank.

APPENDIX B

Least worst weighted regret case study application

In its most recent Network Options Assessment (NOA) study [96], National Grid Electricity System Operator (NGESO) has introduced the use of LWWR to further study reinforcement options and define if they are selected or not to be deployed in the system. In [93] a detailed description of the NOA process is presented; here only the main components are presented to introduce the use of LWWR.

The NOA process is run every year with the objective to provide recommendations to the transmission operators on what projects to execute, based on a set of candidate transmission reinforcements proposed by each transmission owner in the country. The possible recommendations fall within different categories, which include starting a new reinforcement, continuing or putting on hold the works of a project under construction, or stopping the development of a reinforcement altogether.

To complete this task, the NOA process starts by finding the optimal set of reinforcements in the system (from a cost-benefit point of view) for each of the scenarios which describe different future conditions for the system (the scenarios are described in the Future Energy Scenarios (FES) report [155]). The set of optimal reinforcements for each scenario is a subset of a total of over 170 projects (for the 2020-2021 NOA process) presented by the transmission operators.

The proposed reinforcements are studied to determine how much transfer capacity they add to the system when they become available. Each reinforcement is studied individually, and groups of reinforcements are studied together to determine the effect on transfer capability of operating them simultaneously. The studies include several security-related assessments to determine the safe amount of power to transfer when the reinforcements (and groups of reinforcements) are in place. With this information and the model of the system in each scenario based on the information available in the FES report, NGESO proceeds to determine the optimal development path for the system, using a cost-benefit approach, as described in Figure B.1.

The process is split into three main parts or phases. Phase I considers the determi-

Figure B.1 NOA cost-benefit analysis (CBA) process

nation of the optimal deployment path by progressively assessing the costs of operating the system with subsets of reinforcements; this is done for each FES scenario. Phase II takes the path found in phase I and checks if the outages associated with the construction of different reinforcements in the path do not produce clashes that can make the path infeasible. If clashes are detected, the entry year of the reinforcements creating the problem is changed until a feasible path is found.

When all the feasible paths have been determined for each scenario, a LWR approach is used to make decisions on what reinforcements need to be deployed in the current year. This part is referred to as the *logic* phase, or phase III. At this point, the focus is put on the reinforcements whose lead time is binding, that is, if the works for those reinforcements (referred to as critical) are not started now, they will not be ready by the time they should be operational according to phases I and II. All other reinforcements for the different scenarios are fixed at the entry time resulting from the analysis conducted in phase II. The problem is then reduced to the decision of proceeding or delaying the critical reinforcements.

To achieve this, the decision variables associated with each reinforcement option in the LWR correspond to proceeding today or delaying the works, which lead to a permutation exercise, where all the critical reinforcements have to be considered simultaneously. Each permutation corresponds to an investment strategy. To exemplify this, let us consider a case with two critical reinforcements, A and B. This leads to four investment strategies, delay both reinforcements, proceed both of them, proceed A and delay B, and vice versa. For each investment strategy, the corresponding deterministic costs are calculated in all the scenarios. The next step consists in finding the least-cost strategy in each scenario, which then enables the calculation of the regrets for each strategy in each scenario. The next step consists in finding the least-cost strategy in each scenario, which then enables the calculation of the regrets for each strategy in each scenario. The final step corresponds to finding the worst regret for each strategy and then selecting the strategy with the least worst regret. This decision is then presented as the recommendation to the transmission owners (and the system stakeholders) on what projects to proceed.

The previous set of steps makes no reference to scenario probabilities, which is precisely why the LWR approach is believed to be independent of scenario weights. However, as discussed and illustrated before, it is now clear that the underlying assumption is that the scenarios are equiprobable. With the same information about costs and regrets, it is possible to apply probabilities to each scenario and analyse how the optimal strategy changes.

Figure B.2 contain the LWWR maps built based on a set of costs and regrets similar to

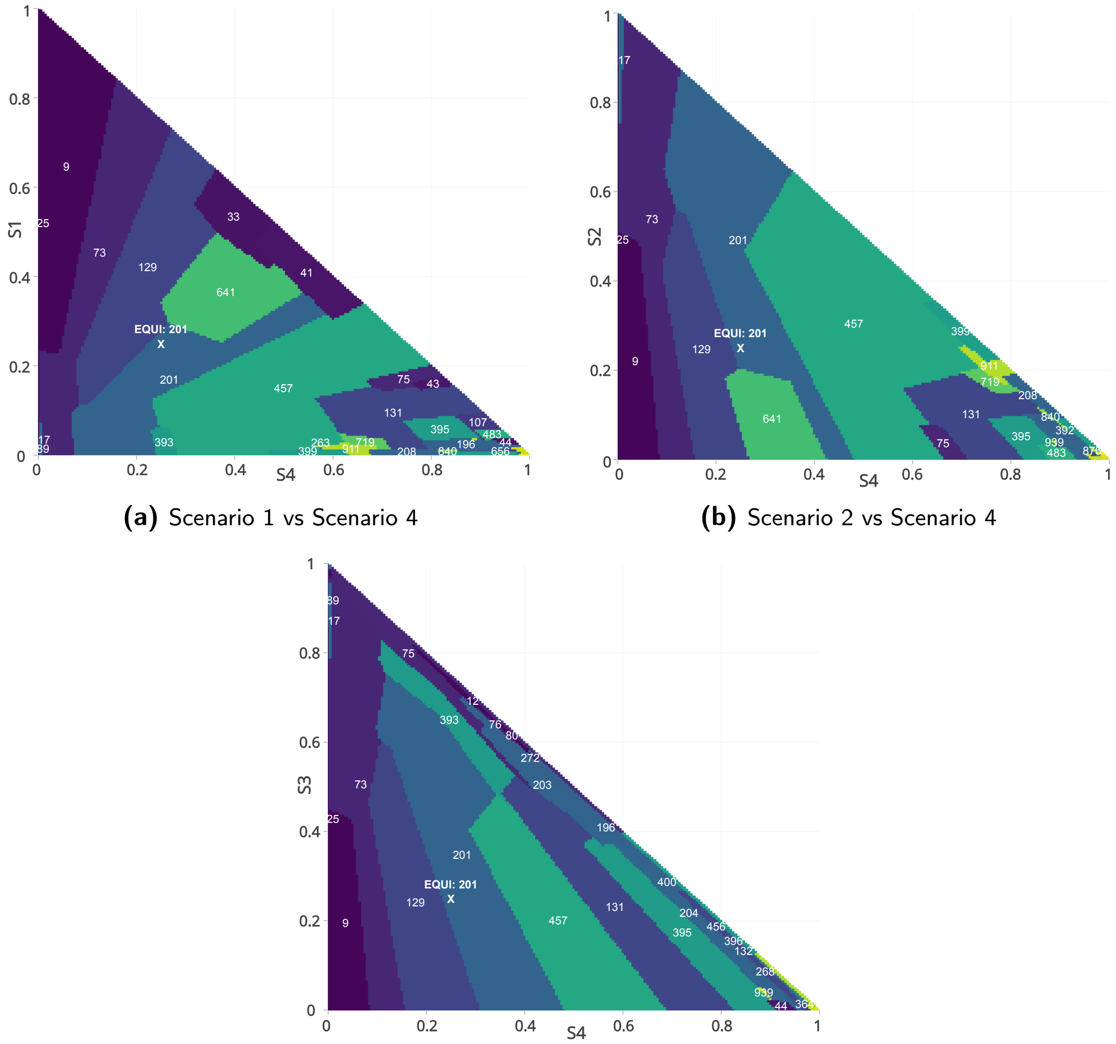

(a) Scenario 1 vs Scenario 4

(b) Scenario 2 vs Scenario 4

(c) Scenario 3 vs Scenario 4

Figure B.2 LWWR analysis for Scenario 4 highlighting active and equiprobable strategies

those obtained after Phase II during the NOA, which have been modified to comply with confidentiality, but whose LWWR maps closely represents those calculated by NGESO . The set of investment options contains 10 reinforcements, which yields $2^{10} = 1024$ investment strategies to analyse. Following the structure of the NOA process, this case study considers four scenarios.

Having to analyse a case with four or more scenarios makes the task harder than the case with three scenarios (as seen in Section 4.2.8). Four scenarios allow to use a three dimensional representation of the LWWR graphical representation, however, such a chart is impractical to conduct any analysis here. The approach taken corresponds to plot two scenarios simultaneously, considering that the implicit probabilities associated with the remaining two scenarios are split into equal parts. This approach has the advantage that the resulting cross-section always contains the equiprobable point (labelled as *EQUI* in each cross-section).

In this case, the standard LWR result (equiprobable scenarios) is to select investment strategy 201, as highlighted in Figure B.2. Out of the 1024 investment strategies, only

34 become active in the LWWR, a few of which are extremely close to the equiprobable solution. The underlying assumption is that, even though the equiprobable solution is theoretically acceptable, it is possible that committing to that solution might not be strategic due to the lack of knowledge regarding the real probability of the underlying scenarios.

When the equiprobable strategy includes decisions on specific reinforcements that are contested by the expert panel in charge of the assessment of the final solution, the LWWR can shed light on the behaviour of such reinforcement in neighbouring strategies. For instance, considering the closeness (less than 5%) of strategies 129 and 641, it is relevant to assess the reinforcements that swing between proceed and delay decisions for those strategies. Also, if one of the scenarios is considered extreme compared to others, special attention can be put in the strategies that appear when that scenario is very likely or very unlikely to occur. Using the same approach as before, these strategies can be compared with the equiprobable strategy to analyse the reinforcements decisions that swing, hence enabling to choose a strategy that proceeds reinforcements that might not be substantially more expensive but that can provide hedging against extreme scenarios.